Investigating Structure-Function Relationships in Ion Channels Using Unnatural Amino Acids

Thesis by

Amy Lynn Eastwood

In Partial Fulfillment of the Requirements for
the Degree of Doctor of Philosophy

Division of Chemistry and Chemical Engineering

California Institute of Technology
Pasadena, CA

2009

(Defended October 31, 2008)

This thesis is dedicated to my family

DAD, MOM, *and* BARRETT

for their constant support
and tireless ability to listen.

ACKNOWLEDGEMENTS

"Without deep reflection,
one knows from daily life that
one exists for other people."
~ Albert Einstein

This thesis was possible because I had a strong network of support during my graduate career, and I owe a great deal of thanks to those people that contributed to the work included herein and to my graduate experience as a whole. First and foremost, I must thank my advisor, Professor Dennis Dougherty. I cannot imagine having a better mentor during these past six years. His guidance through each of the projects described in this thesis and through my education as a scientist has been invaluable. Thanks largely to the opportunities that he afforded me, I am leaving his laboratory confident in my ability as an independent researcher and in my future in academia.

I next must thank Professor Henry Lester, who was essentially my unofficial coadvisor here at Caltech. He was always willing to listen and offer advice, no matter if the setting were a meeting or an accidental run in near the Red Door Cafe. I hope to keep with me his lessons on maintaining professionalism and providing clear data when presenting results.

I also owe much thanks to my thesis committee for their support and encouragement over these past many years. Professor Harry Gray's suggestions in my candidacy examination concerning selenium's potential for oxidation were critical to interpreting the initial photolysis results in the SNIPP model system. Professor Peter Dervan's focus and drive are admirable, and I thank him for always asking the most pertinent questions to keep me headed in the right direction. Professor Linda Hsieh-Wilson's support of my *O*-GlcNAc

yeast three-hybrid design during my proposal examination was a highlight in my graduate career. I hope to thank her for her encouragement by seeing that project through to fruition.

I am thankful to have had so many successful collaborative projects during my graduate career. First, I cannot thank Chris Ahern enough for initiating the collaboration between the Institute of Hyperexcitability at the Jefferson Medical College in Philadelphia and our laboratory. Chris's passion for science was infectious, and I hope to emulate his success during my postdoctoral career. Professor Richard Horn and Vincent Santarelli were also crucial to that collaboration, and I thank them for the time they put into teaching me about the Na^+ channel. Second, I owe a tremendous amount of thanks to Niki Zacharias and Angela Blum, past and present members of the Dougherty laboratory, for all of the work they did on the SNIPP project. Niki's initial efforts provided a sturdy framework that I relied on during the many years that I worked on this project, and Angela's help at the end was paramount to the ultimate success of the model system.

I also thank the other members of the Dougherty laboratory who were around when I joined, Don Elmore, Sarah May, Darren Beene, David Dahan, James Petersson, Tingwei Mu, Amanda Cashin, Steve Spronk, and Lori Lee, not only for introducing me to the methods and techniques used in nonsense suppression, but also for their friendship. The openness of the laboratory meant that I had full access to the knowledge and experience that each of them had to offer. I enjoyed watching them get their PhDs and branch out to many different career paths.

I owe special thanks to the members of the Dougherty laboratory who started around the same time as I did: Michael Torrice, Erik Rodriguez, and Xinan (Joanne) Xiu. It was exceptionally helpful for me to go through important graduate milestones such as candidacy with them. Joanne's work ethic was astounding and something I hope to take with me as I move to Stanford. Michael's combination of humor and skepticism provided me with a welcome perspective to my typical idealism and will undoubtedly ensure him success in science writing. Erik's passion for science was always evident, and I hope that one day he is able to accept a position as an assistant chemistry professor at some famous university.

I also must thank the other members of the Dougherty laboratory that joined after me, Kiowa Bower, Katie McMenimen, Ariele Hanek, Jinti Wang, Kristin Gleitsman, Walrati (Kay) Limapichat, Sean Kedrowski, Jai Shanata, Nyssa Puskar, Shawna Frazier, Noah Duffy, and Darren Nakamura, for everything that they taught me and for all of their friendships. It was through conversations with them about their goals and interests that I was empowered to focus on my own, and I thank them for encouraging me to follow my own path towards the nematode *C. elegans*. I know Kiowa wants his own paragraph, but if I were to give each person their due credit, these acknowledgements would be ten pages long!

There are many other people in the Chemistry Division here at Caltech that deserve thanks for their support during my years as a graduate student. I would like to specifically thank Linda Syme, Joe Drew, Mona Shahgholi, Scott Ross, Tom Dunn, Rick Gerhart, Paul Carroad, Anne Penney, Chris Smith, Steve Gould, Lillian Kremar, Dian Buchness, Laura Howe, and Agnes Tong.

One of the best decisions that I made during my graduate career was becoming the Resident Associate for Ricketts Hovse. During my two years in this position, I met some very extraordinary students, had a wonderful set of bosses, got to know a variety of administrators, and gained an appreciation for the inner workings of this school. This experience profoundly shaped my graduate career and my future ambitions. There are far too many people that need to be thanked for me to list them here, but I hope they already know how appreciative I am of my interactions with them.

I owe a great deal of gratitude to all of my friends and family who have impacted this thesis through their unconditional support over the past six plus years. I thank my college friends for all of their phone calls and for getting married at intervals that allowed for frequent reunions. I thank my running friends for their companionship through long runs, workouts, and races, and for the welcome reprieve from science that they provided. Though I have not listed names, I hope these people know who they are. I also must thank Alex Gagnon for his constant championing of my work and my abilities and for his love and support. Finally, I thank my family—my parents, Ken and Bonnye Eastwood; my brother Barrett Eastwood and his wife Amy Caroline Eastwood; and all of my extended family—for their unconditional love and encouragement and for understanding my choice to move 3,000 miles away from them in pursuit of the best PhD possible.

Lastly, I think the National Institute of Health Predoctoral National Research Service Award (5-T32-GM07616) for funding a portion of my graduate work.

ABSTRACT

Ion channels are proteins that traverse the cell membrane and form gated pores that open and close in response to various stimuli. In order to experimentally probe aspects of ion channel functionality, we performed subtle structure-function studies using the *in vivo* nonsense-suppression method, which allows for the incorporation of synthetically accessible unnatural amino acids and hydroxy acids into an ion channel at a site of interest.

Fluorinated aromatic amino acids are good probes for a cation-π interaction because fluorine substituents reduce the binding affinity of the aromatic for a cation in a linear, step-wise fashion. In collaboration with Professor Richard Horn at the Thomas Jefferson University, we substituted a series of fluorinated-phenylalanines for important tyrosines in the Shaker B K^+ channel and experimentally determined that TEA was binding to the residues through a cation-π interaction. We also determined that Ca^{2+} binds to and blocks the $Na_V1.4$ channel through a cation-π interaction with a tyrosine at the top of the pore of this channel. We found that tetrodotoxin, another channel blocker, also binds to this same residue through a cation-π interaction. Finally, we proved that lidocaine and other local anesthetics bind to a phenylalanine at the bottom of the pore of this channel through a cation-π interaction.

An important aspect of our work is the development of unnatural amino acids that can be used in the study of ion channels through the *in vivo* nonsense-suppression methodology. We determined that D-amino acids could not be incorporated into ion channels using this method. We synthesized several novel fluorescent-MTS reagents to be used in FRET

studies. We probed the sterics around phenylalanines using the unnatural amino acid 3,5-dimethylphenylalanine. We also attempted to incorporate 4-amino-phenylalanine, but, unfortunately, we never saw the enhanced binding of a cationic ligand that was our expected phenotype.

Finally, we also designed and synthesized two α-hydroxy acids capable of site-specific proteolysis upon UV irradiation. We used a tripeptide model system to isolate and characterize the cleavage fragments, proving that these two residues are indeed capable of site-specific proteolysis through the predicted mechanism.

TABLE OF CONTENTS

LIST OF FIGURES

LIST OF TABLES

LIST OF SCHEMES

C h a p t e r I

SUMMARY

I like nonsense, it wakes up the brain cells.
~ Dr. Seuss

While Theodore Seuss Geisel, more commonly known as Dr. Seuss, was referring to his affection for fantasy, this quote has a slightly different meaning for this thesis: it humorously merges the crucial methodology described herein, nonsense suppression, with this thesis's overarching interest in understanding the intricacies of the brain. Applying the *in vivo* nonsense-suppression methodology to neurobiology "wakes up" studies on proteins important to learning, memory, addiction, and disease by moving beyond the twenty natural amino acids and into a realm of amino acids that is limited only by imagination and, of course, the ribosome.

Introduction

The human brain is made up of approximately 100 billion neurons, and each neuron makes approximately 10,000 synaptic connections to other neurons. This complex

neuronal network uses both electrical and chemical signals to rapidly pass information from one neuron to the next. A signal in one neuron is propagated through that neuron in the form of an electrical current, which culminates in the release of small molecules, called neurotransmitters, upon reaching the end of the axon. These neurotransmitters diffuse across the synapse until they connect with the postsynaptic neuron (figure 1.1). To encode the thoughts, sounds, smells, and more that occur to a human brain, the specificity of the wiring of the neurons and the precise patterns of signals are thought to be crucial. To begin to explore this complexity, our studies focus on one type of protein, the ion channel, which is found across the surface of the neuron and is immensely important to neuronal communication. Voltage-gated ion channels propagate the electrical impulse that flows through a neuron, and ligand-gated ion channels located across the synapse translate the chemical message of the neurotransmitters sent by the presynaptic neuron into an electrical signal in the postsynaptic neuron.

Ion channels are dynamic proteins found in the membranes of not only neurons but also all other types of cells. These proteins allow their namesake, ions, to pass into and out of cellular compartments, essentially creating an electrical current (figure 1.2).[1] They function by remaining closed until triggered by an external stimulus, such as the binding of a small molecule, a change in membrane voltage, or the tensing of the membrane, which alters the protein structure in such a way as to open the channel. The resulting pore in the membrane is not a featureless hole. Instead, it is rich in structure and can select for the passage of certain ions over others down their chemical gradient. There exist K^+-selective channels, Na^+-selective channels, channels that select for a wider range of cations, and Cl^--selective channels, all of which will be discussed in this thesis.

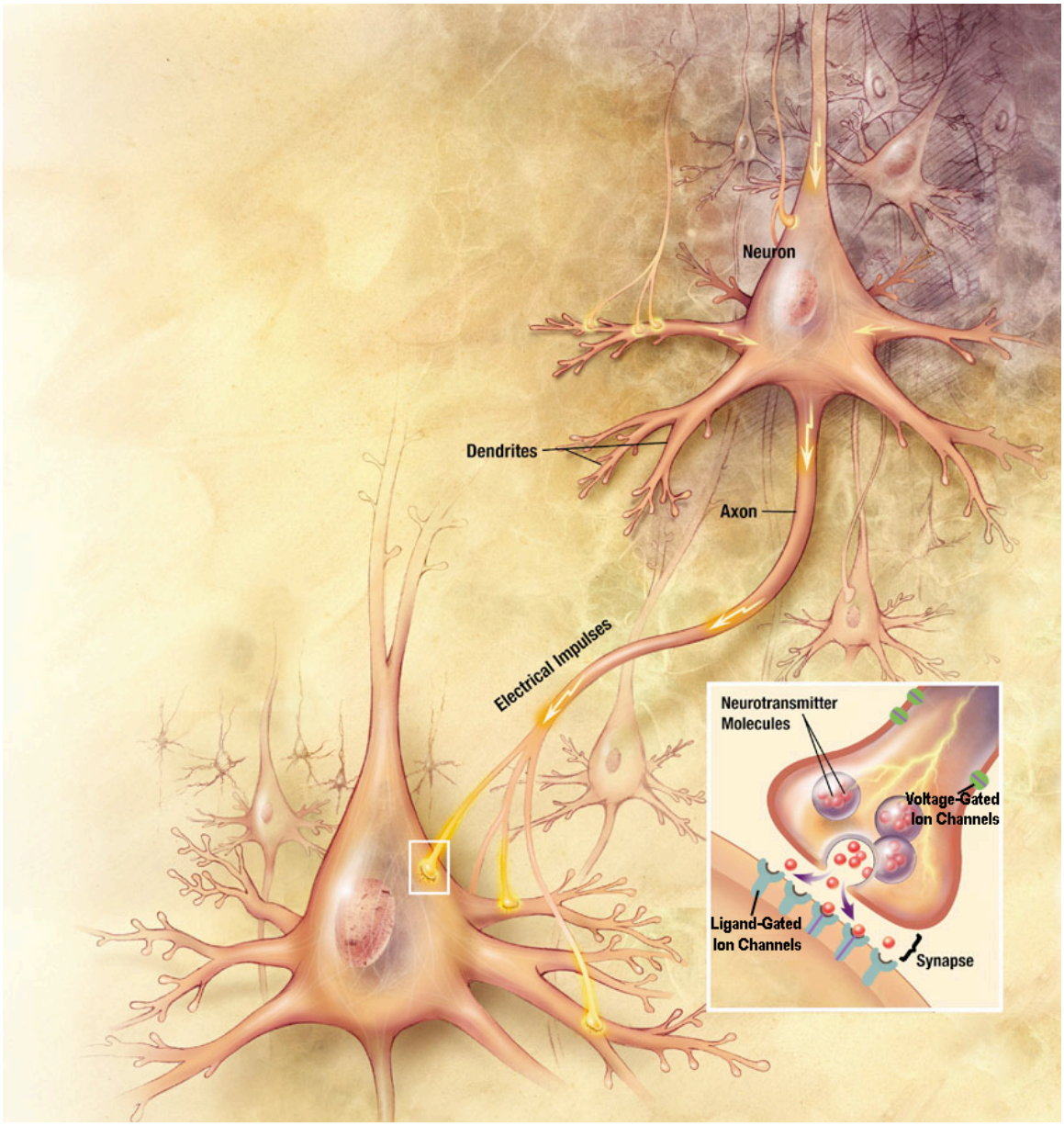

Figure 1.1. An illustration of signals traveling through nerve cells in the brain.

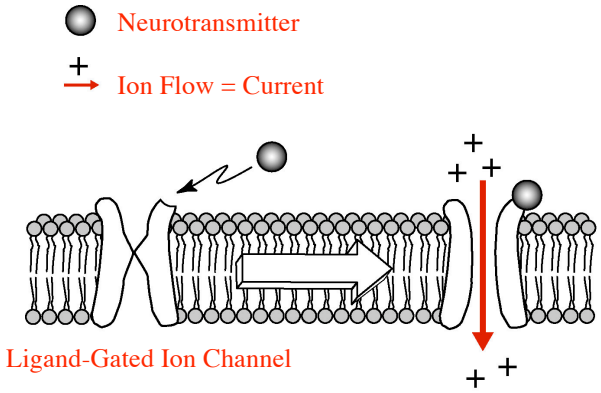

Figure 1.2. An illustration of the current produced by an ion channel upon the binding of neurotransmitters.

A Brief Introduction to Four Ion Channels

Shaker B K^+ Channel

The first ion channel studied in this thesis is the voltage-gated K^+ channel Shaker B (ShB). This channel appears in chapters 2, 6, 7, and 8. ShB is a homotetramer that has a long intracellular N-terminus, six transmembrane domains with a pore loop between the fifth and sixth transmembrane domains, and a short intracellular C-terminus (figure 1.3). The fourth transmembrane helix of this channel contains several positively charged arginines that allow it to sense changes in the voltage across the membrane of the cell. The movement of this helix is thought to pull the channel open when the cell becomes depolarized. By responding to changes in voltage, K^+ channels can control the action potential, the electrical impulse that travels down an axon.

As revealed upon the publication of the crystal structure of the bacterial K^+ channel KcsA,[2] this channel and others in its family select for K^+ because of the ordered framework of amino acids located in the pore loop; specifically, the conserved GYG residues position their backbone carbonyls into the pore, and when aligned together with the other subunits, the carbonyls mimic the hydration shell that typically surrounds a K^+ ion. Another characteristic feature more specific to ShB is rapid N-type inactivation, which is the blocking of the channel by the N-terminus of one of its subunits almost immediately upon channel activation (figure 1.3). The first twenty amino acids of the N-terminus make up a "ball" that is connected through a "chain" of amino acids to the channel. N-type channel inactivation occurs when one of the four balls of the homotetrameric channel swings up and plugs the channel.[3-6] Removal of the N-terminus region of the protein eliminates this N-type inactivation.

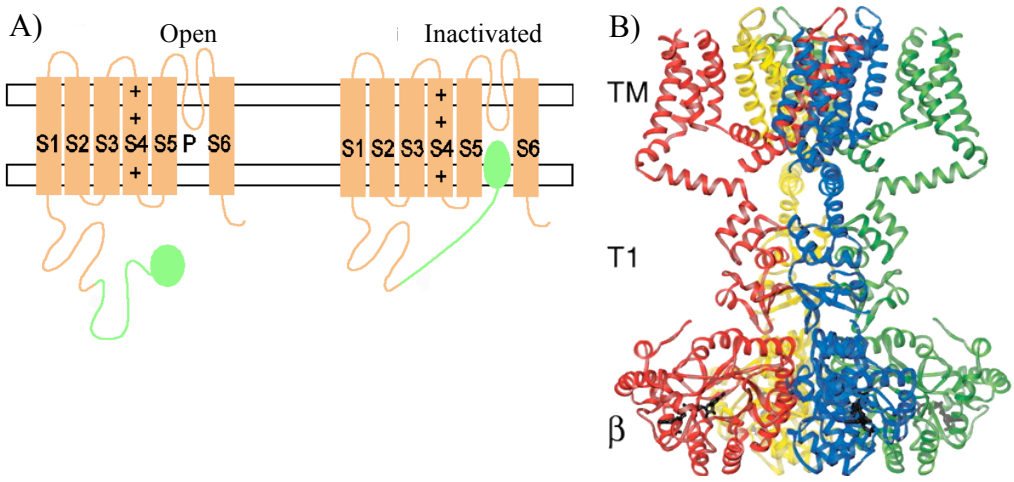

Figure 1.3. Views of the K^+ channel. A) Schematic of one subunit of ShB. The S4 domain is voltage-sensing component of the channel. C) Representation of the K^+ channel Kv1.2, which is similar in structure to ShB, adapted from Long *et al.*[7] TM = Transmembrane domain, T1 = N-terminal intracellular domain, β = β subunit.

$Na_V1.4$ Na^+ Channel

The voltage-gated Na^+ channel $Na_V1.4$ is the second channel that is explored in this thesis; it is found in chapters 3, 4, and 5 and makes a brief appearance in chapter 7. While this specific channel is closely associated with skeletal muscle, Na^+ channels are also involved in the rise of the action potential in a neuron. The structure of this channel is similar to that of a K^+ channel except that this channel is composed of only one subunit with 24 transmembrane domains (figure 1.4). The protein is divided into four domains (D1-D4), and each resembles a K^+ channel subunit with six transmembrane helices and a reentrant pore loop. A crystal structure of the Na^+ channel has not yet been published, but Lipkind and Fozzard have made a model of the transmembrane helices nearest the pore (S5-P-S6 for all four domains) using the crystal structure of the K^+ channel KcsA (figure 1.4B, C).[8] Highlighted in figure 1.4C are the four residues thought to make the most important contributions to the selectivity of this channel for Na^+: aspartate, glutamate, lysine, and alanine, from D1, D2, D3, and D4, respectively.

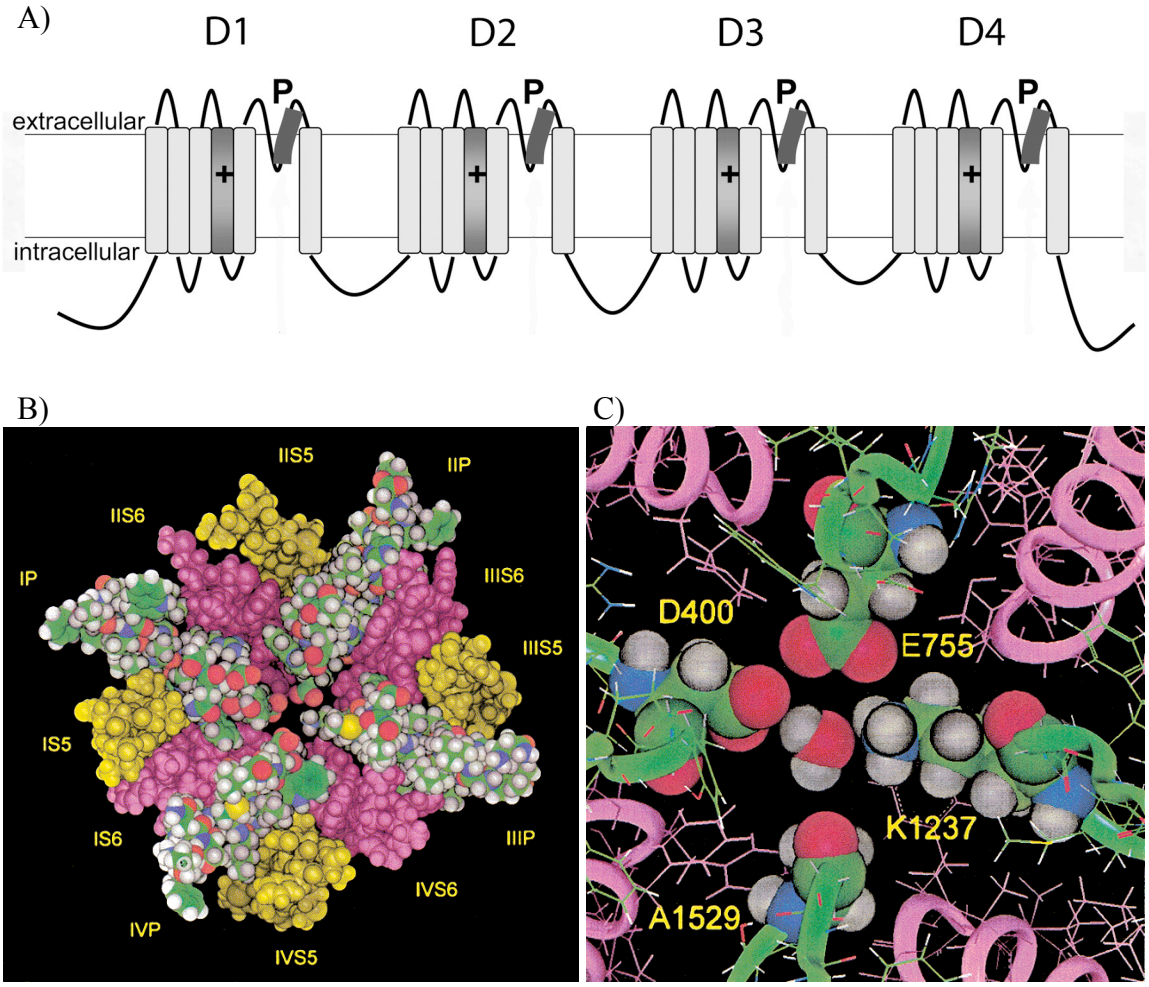

Figure 1.4. Views of the Na^+ channel. A) Topology of a voltage-gated Na^+ channel. Na^+ channels are composed of four domains (D1-D4), each with six transmembrane segments. The + labels the primary component of the voltage-sensor, and the P labels the reentrant pore loop. B) Space-filling model of the $Na_V1.4$ as published by Lipkind and Fozzard.[8] C) A close-up view of the DEKA selectivity filter as published by Lipkind and Fozzard.[8]

Nicotinic Acetylcholine Receptor

The nicotinic acetylcholine receptor (nAChR) is the prototypical ligand-gated ion channel and is explored in chapters 6, 7, and 8. Unlike the two channels introduced above, it

allows for a range of cations to pass through its pore, it has a large extracellular domain that has evolved to bind acetylcholine, and it is made up of a pentagonal array of subunits. In humans there are 17 nAChR subunits, α1-10, β1-4, δ, γ, and ε. The nAChR used in this study is found in muscle fibers and made up of two α1 subunits, a β1 subunit, a δ subunit, and a γ subunit.[9] The muscle nAChR serves as a model for neuronal nAChRs, which is important for gaining insight into synaptic ACh signaling between neurons, nicotine addition (nicotine mimics ACh in the extracellular binding site of this protein), and mental disorders such as schizophrenia, attention deficit hyperactivity disorder, Alzheimer's disease, Parkinson's disease, and more.

Each subunit has a large N-terminal domain and four transmembrane domains. The α subunits are characterized by a loop formed by a disulfide bond between two cysteines in the N-terminal domain of the protein, appropriately named the Cys loop. Each α subunit (yellow in figure 1.5) can also provide four of the five aromatic amino acids that make up the binding site for acetylcholine (circled in figure 1.5C). The fifth aromatic amino acid in the binding site is provided by the neighboring subunit (blue in figure 1.5), which can be either an α or a non-α subunit. The second transmembrane domain (TM2) of each nAChR subunit predominantly lines the pore of the channel. A ring of leucines, one from each TM2, forms part of the hydrophobic band that occludes the pore of the channel when closed (highlighted with a red arrow in figure 1.5). This leucine is called Leu9'. The association of acetylcholine in the binding site created by the five aromatic amino acids in the extracellular domain results in a conformational change in the protein that ultimately widens this band of leucines enough to allow cations to flow through the channel.

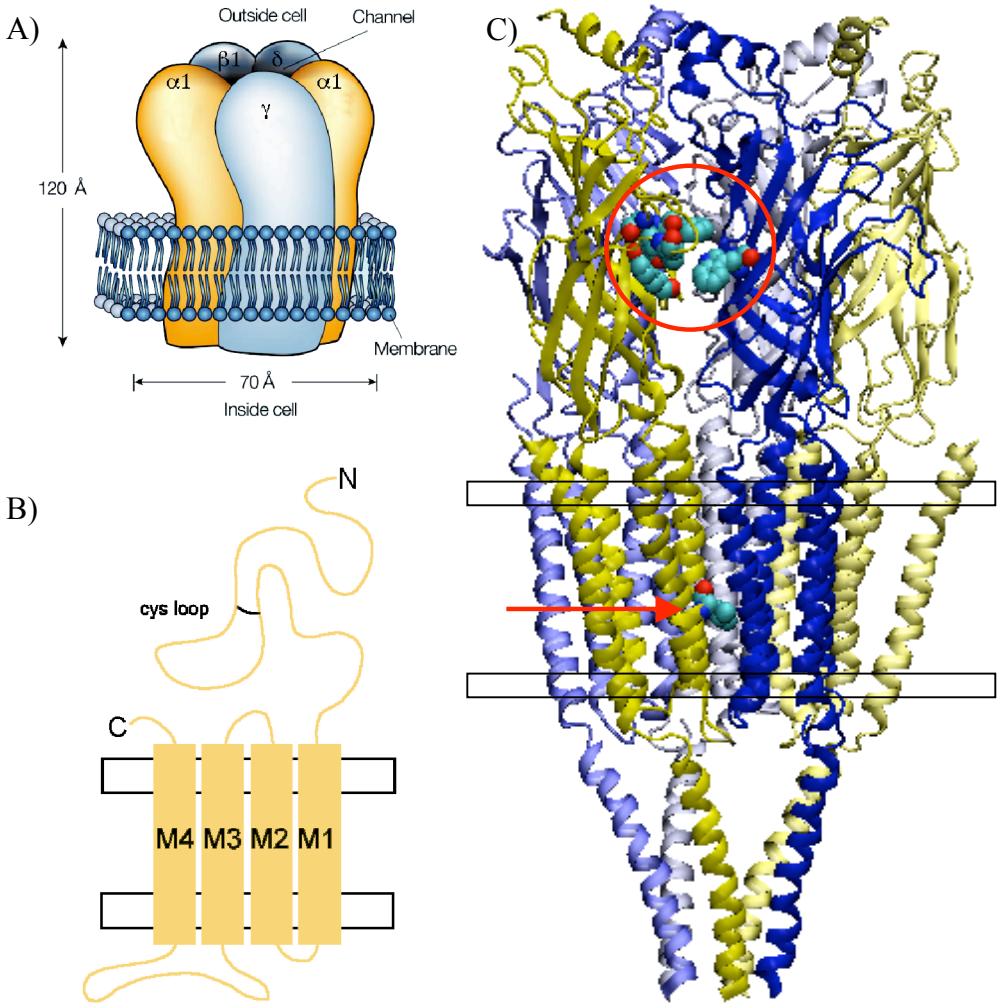

Figure 1.5. Views of the nAChR. A) An illustration of the pentameric channel. B) Each subunit has a large extracellular domain and four transmembrane domains. The α subunit is characterized by the Cys loop. C) Representation of a nAChR from PDB 2BG9.[10] The binding box (top circle) and a pore lining leucine (Leu9', bottom arrow) are highlighted.

$GABA_C$ Receptor

Ionotropic GABA receptors are the dominant inhibitory channels in the brain, though the specific type of GABA receptor studied in chapter 7, the $GABA_C$ receptor, is primarily

associated with the retina. These channels are so named because they bind and open in response to the neurotransmitter γ-aminobutyric acid (GABA). Since GABA receptors are in the Cys-loop superfamily with nAChRs,[11] they are very similar in structure to the channels described immediately above, but they specifically select for Cl^- ions instead of cations. Like nAChRs, these channels are made up of a pentagonal array of subunits, and the specific channel studied in this thesis is a homopentamer of ρ1 subunits. Also like nAChRs, the large extracellular domain of this channel has a ligand-binding site that consists of aromatic amino acids.

The Power of Unnatural Amino Acids

Ion channels are dynamic proteins. Therefore, while the structures shown above provide an extensive amount of information about the structure of these proteins, they are static pictures capturing only a moment in the life of the active protein and can only provide predictions on how the protein functions *in vivo*. To truly understand how structure relates to function in a channel, the channel needs to be studied while opening, closing, and going through all of the other states in its natural gating pathway.

The traditional method for exploring structure-function relationships in ion channels is through conventional mutagenesis, where the DNA for the protein of interest is altered so that it encodes a sequence that contains amino acid changes at known sites. For instance, if the importance of a phenylalanine was being explored, then the side chain could be ablated by mutating the residue to alanine, or the global importance of having a generic aromatic amid acid at this site could be explored by mutating the residue to one of the

other natural aromatic amino acids, tyrosine or tryptophan (figure 1.6). Each of these mutations alters many of the features of the phenylalanine though, so only global information can be gained. If the limits imposed by the 20 natural amino acids are lifted, then chemical-scale explorations into the importance of the aromaticity of the ring could begin with the replacement of the aromatic ring with a cyclohexyl ring, creating cyclohexylalanine. As shown in figure 1.6, cyclohexylalanine is similar in size and shape to phenylalanine. Because of the more subtle change with a phenylalanine to cyclohexylalanine mutation, any difference in the function of an ion channel could be interpreted as due to the direct loss of the aromatic nature of that specific residue. To gradually reduce the aromatic character of the phenylalanine instead of simply removing it, fluorine atoms could be substituted for the hydrogen atoms on the aromatic ring. Since fluorine atoms are electronegative, they will pull a small amount of electron density away from the ring. The electrostatic potential surfaces of benzene and the various fluorinated benzenes in figure 1.6 show that as the number of fluorine substituents on the ring is increased, the negative potential (red) on the surface of the ring is reduced. These examples are just the beginning of the chemical-scale structure-function questions that can be addressed using unnatural amino acids.

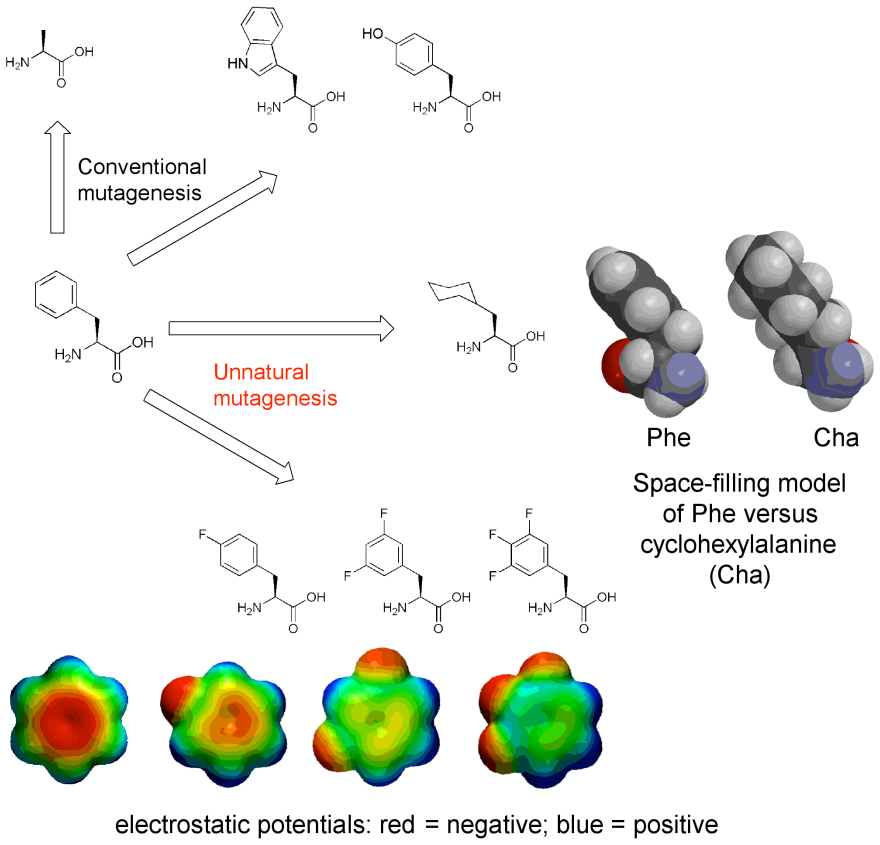

Figure 1.6. Unnatural mutagenesis allows for more subtle alteration in the structure of an amino acid such as phenylalanine than conventional mutagenesis.

The *In Vivo* Nonsense-Suppression Method

The *in vivo* nonsense-suppression method was developed as an extension of conventional mutagenesis for the purpose that was described above: probing specific structure-function relationships in ion channels.[12] It offers a highly sensitive assay that allows for site-specific control over the structure of ion channels while they function in a membrane. The technology is similar to conventional mutagenesis, but instead of mutating the amino acid of interest to one of the twenty coded amino acids, almost any unnatural amino acid

or α-hydroxy acid can be selected. This versatility is due to the hijacking of the translational system. In the nonsense-suppression method the codon for the amino acid of interest has been converted to a blank codon, either a stop codon (typically UAG) or a four-base codon (typically GGGU), which is not recognized by a natural tRNA (figure 1.7). A combination of chemical synthesis and molecular biology allow the blank codon to instead be recognized by an orthogonal suppressor tRNA acylated with the desired unnatural amino acid.[13,14] The development of this method followed the work of Schultz and co-workers, who first reported a general procedure for the incorporation of unnatural amino acids *in vitro* using the *E. coli* translational system.[15,16] Nonsense suppression was adapted for use *in vivo* with the heterologous expression system *Xenopus laevis* oocytes by former members of the Dougherty laboratory in order to functionally study ion channels.[12,17] The specific advantages of the *Xenopus* oocyte include the ease of injection; the few endogenous channels; and the stores of enzymes, organelles, and proteins that efficiently produce foreign protein.[18,19]

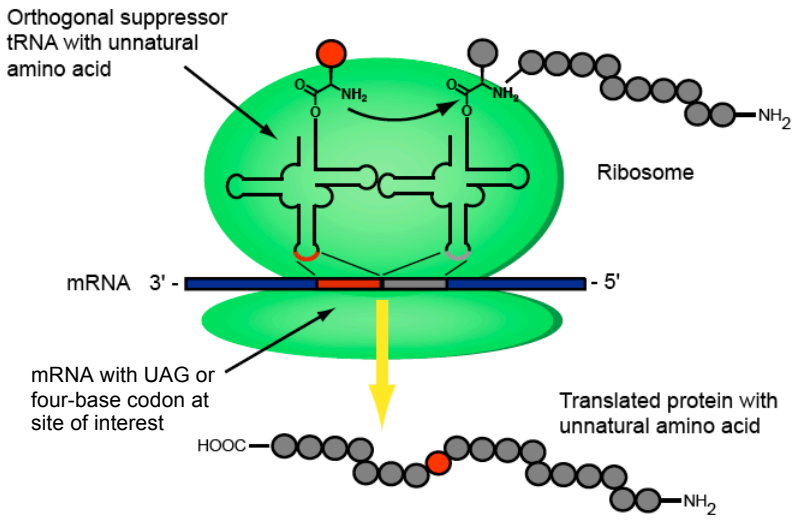

Figure 1.7. The hijacking of the translation machinery that occurs in nonsense suppression.

The specifics of the *in vivo* nonsense-suppression method as used in this thesis are outlined below (figure 1.8). First, either the nonsense codon TAG or the four-base codon GGGT are inserted at the site of interest in the DNA that encodes the ion channel being studied. The DNA is then converted to mRNA using *in vitro* methodology, giving mRNA with a UAG or a GGGU codon at the site of interest (①, figure 1.8). Second, the desired unnatural amino acid is protected on its amine, activated as an ester, and then coupled to a dinucleotide that mimicks the 3' end of tRNA, dCA (the 2' hydroxyl of cytosine is removed since it is not necessary for translation and since its deletion increases the specificity of aminoacylation). The acylated dinucleotide is then ligated to a suppressor tRNA (either THG73 with its CUA anticodon or YFaFs with its ACCC anticodon) using T4 RNA ligase (②, figure 1.8). Third, the mRNA and the tRNA are coinjected into a *Xenopus* oocyte (③, figure 1.8) where protein synthesis, processing, assembly, and transportation to the surface are carried out by the *Xenopus* translation system (④, figure 1.8).[20] Finally, the functional consequences of the mutagenesis can be studied using established two-electrode voltage clamp techniques (⑤, figure 1.8). It should be noted that the amount of protein synthesized by the *Xenopus* oocyte is limited by the amount of tRNA added to the system since the tRNA cannot be reaminoacylated by the cell. This drawback restricts the widespread use of this technique, since not all protein function assays are as sensitive as electrophysiology.

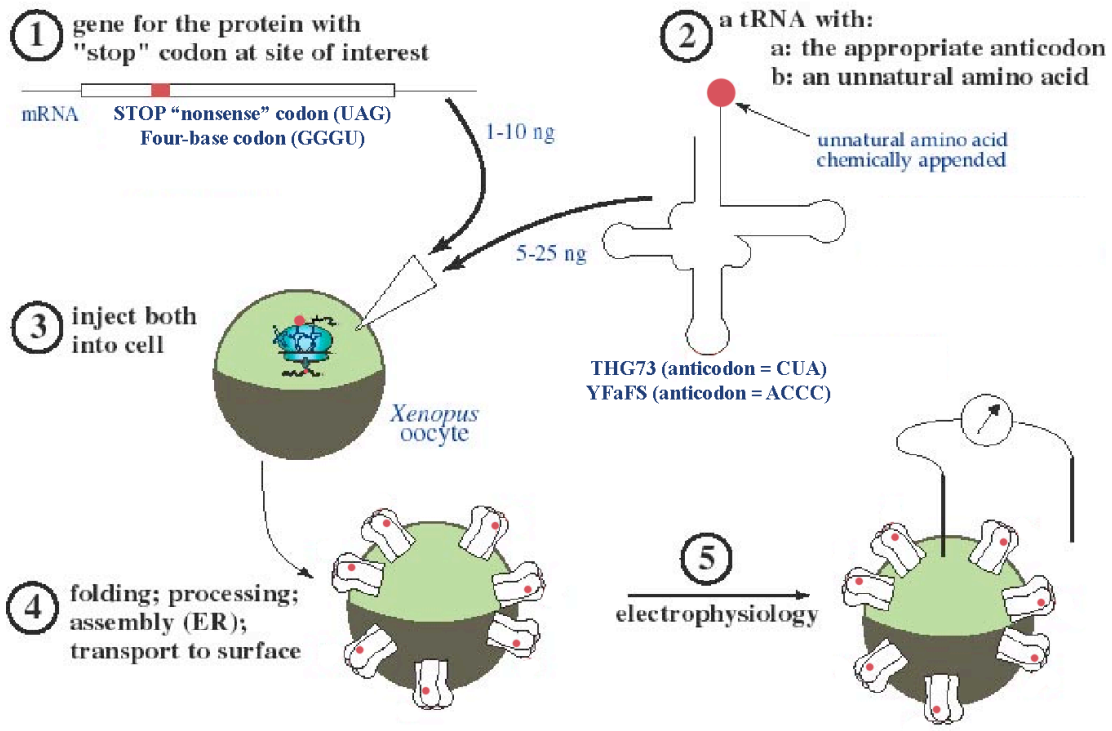

Figure 1.8. An outline of the experimental steps for *in vivo* nonsense suppression.

Exploiting the Scope of Nonsense Suppression

The work in this thesis takes advantage of many different unnatural amino acids to explore many different proteins. In the first half of this thesis, the fluorinated phenylalanine derivatives and cyclohexylalanine introduced above in figure 1.6 were used to explore four different hypothesized cation-π interactions between the voltage-gated channels ShB and $Na_V1.4$ and several cationic small molecules known to selectively block these channels. Only when a small aromatic is perched at the top of the pore in ShB can TEA can block this channel.[21-23] Early work suggested that a cation-π interaction was important,[22] but more recently published crystal structures rejected this

proposal. The experimental work discussed in chapter 2 proves that a cation-π interaction is important for the association of this blocker to the channel.[24] Chapters 3 through 5 represent the first examples of *in vivo* nonsense suppression on $Na_V1.4$. The first studies in this channel targeted an important tyrosine in $Na_V1.4$ that is located in the pore just above the aspartate in the DEKA selectivity filter. This tyrosine, Tyr401, was found to bind two of its known channel blockers, Ca^{2+} and tetrodotoxin, through a cation-π interaction, as discussed in chapter 3 and 4.[25,26] Several aromatic residues at the bottom of the pore of $Na_V1.4$ have been linked to anesthetic block of this channel.[27,28] The work in chapter 5 shows that only one, Phe1579, binds lidocaine and other cationic anesthetics through a cation-π interaction.[29]

The second half of this thesis serves to enhance and explore the variety of unnatural amino acids that can be incorporated by nonsense suppression. This technique has been used to incorporate over 100 amino acids and α-hydroxy acids (figure 1.9), and this number will expand as novel unnatural amino acids are designed to probe new and specific structure-function relationships in ion channels.[30] This thesis describes several such novel unnatural amino acids and α-hydroxy acids, their syntheses, and their incorporation (or attempts at incorporation) in the four ion channels introduced above. D-amino acids were targeted for their ability to achieve backbone peptide bond angles that are rare for natural L-amino acids. Unfortunately, as seen in chapter 6, D-amino acids were not compatible with nonsense suppression. In chapter 7 a variety of aromatic unnatural amino acids were studied, each for its unique properties. First, a set of fluorophore tags was synthesized for the purpose of making fluorescent amino acids *in situ*. Next, 3,5-dimethylphenylalanine was designed to probe the sterics around the *meta*

position of important phenylalanines. Finally, 4-amino-phenylalanine was incorporated into several known cation-π interaction sites in the anticipation that it would enhance the binding of the small molecule to the channel. Unfortunately, the expected functional enhancement was not seen in ShB, $GABA_C$, or nAChR. In chapter 8, the last chapter of this thesis, the synthesis is described of two novel unnatural α-hydroxy acids that were designed to site-specifically cleave the backbone of a protein upon irradiation with UV light.[31] Much of the chapter is devoted to the work that went into the design and optimization of the model system that was used to prove that both α-hydroxy acids were capable of proteolysis. Though successful in the model system, their success *in vivo* has yet to be seen.

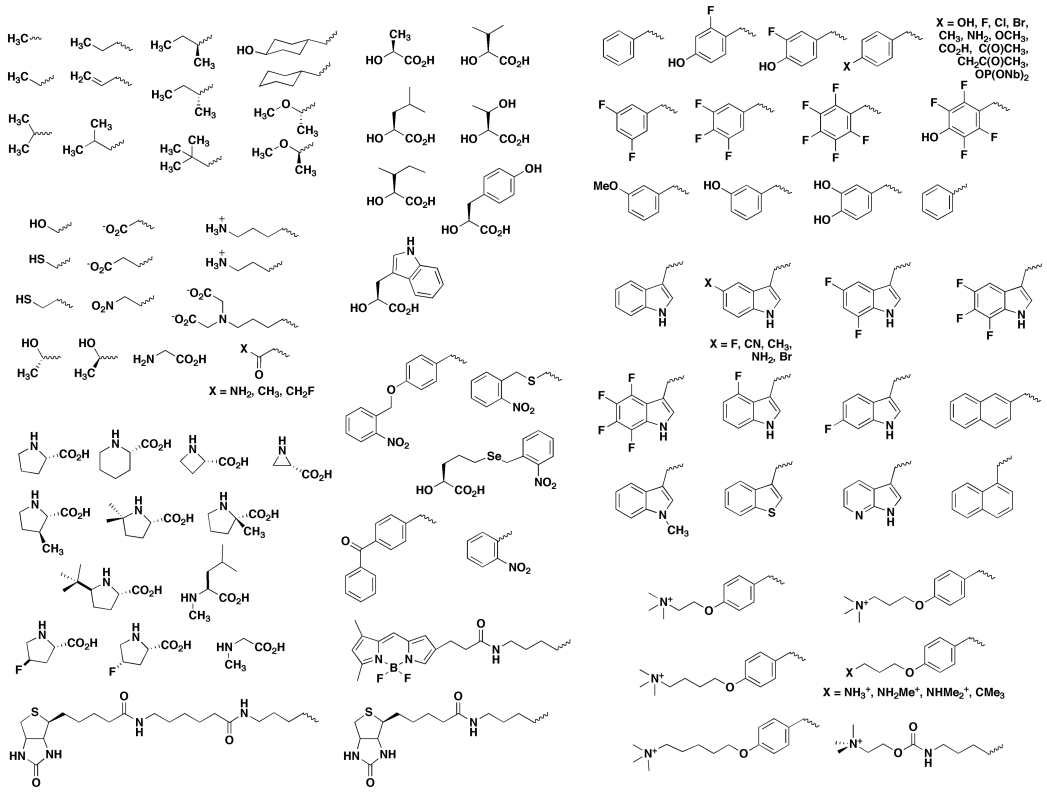

Figure 1.9. Examples of unnatural amino acids and α-hydroxy acids that have been incorporated into proteins using *in vivo* nonsense suppression.

Conclusion

The work included in this thesis focuses on understanding chemical-scale features of important proteins relevant to the nervous system through the use of the *in vivo* nonsense-suppression technique. Proving that TEA binds to the aromatic at the top of the pore of ShB through a cation-π interaction dispels the controversy created upon the introduction of the K^+ channel crystal structure. Understanding how tetrodotoxin and lidocaine bind to $Na_V1.4$ not only provides structural information as to how these blockers function but also aids in the mapping of the still mysterious Na^+ channel pore.

This thesis also serves to expand the limits of the nonsense-suppression methodology by testing its boundaries and adding more unnatural amino acids to its library. The development of novel unnatural amino acids is important to expand the scope structure-function relationships investigated. The design and synthesis of 3,5-dimethylphenylalanine added another dimension to the study of the sterics around phenylalanines. Because of it, interesting functional maps can be created that would have otherwise been missed. The two novel α-hydroxy acids capable of cleaving the peptide backbone upon photolysis provide another means for exploring the importance of covalent connections in these and other dynamic proteins. Together, the many different avenues of exploration taken in this thesis all were directed toward enhancing the understanding of the brain, the proteins that encourage neuronal communication, and an important technique used to study those types of proteins.

References

(1) Hille, B. *Ionic Channels of Exictable Membranes*; Sunderland, MA: Sinauer Associates, Inc., 1992.

(2) Doyle, D. A.; Morais Cabral, J.; Pfuetzner, R. A.; Kuo, A.; Gulbis, J. M.; Cohen, S. L.; Chait, B. T.; MacKinnon, R. *Science* **1998**, *280*, 69-77.

(3) Hoshi, T.; Zagotta, W. N.; Aldrich, R. W. *Science* **1990**, *250*, 533-538.

(4) Zagotta, W. N.; Hoshi, T.; Aldrich, R. W. *Science* **1990**, *250*, 568-571.

(5) Demo, S. D.; Yellen, G. *Neuron* **1991**, *7*, 743-753.

(6) Mackinnon, R.; Aldrich, R. W.; Lee, A. W. *Science* **1993**, *262*, 757-759.

(7) Long, S. B.; Campbell, E. B.; Mackinnon, R. *Science* **2005**, *309*, 897-903.

(8) Lipkind, G. M.; Fozzard, H. A. *Biochemistry* **2000**, *39*, 8161-70.

(9) Karlin, A. *Nat. Rev. Neurosci.* **2002**, *3*, 102-114.

(10) Unwin, N. *J. Mol. Biol.* **2005**, *346*, 967-89.

(11) Lester, H. A.; Dibas, M. I.; Dahan, D. S.; Leite, J. F.; Dougherty, D. A. *Trends Neurosci.* **2004**, *27*, 329-36.

(12) Nowak, M. W.; Kearney, P. C.; Sampson, J. R.; Saks, M. E.; Labarca, C. G.; Silverman, S. K.; Zhong, W.; Thorson, J.; Abelson, J. N.; Davidson, N.; Schultz, P. G.; Dougherty, D. A.; Lester, H. A. *Science* **1995**, *268*, 439-442.

(13) Nowak, M. W.; Gallivan, J. P.; Silverman, S. K.; Labarca, C. G.; Dougherty, D. A.; Lester, H. A. *Methods Enzymol.* **1998**, *293*, 504-29.

(14) Rodriguez, E. A.; Lester, H. A.; Dougherty, D. A. *Proc. Natl. Acad. Sci. USA* **2006**, *103*, 8650-5.

(15) Noren, C. J.; Anthonycahill, S. J.; Griffith, M. C.; Schultz, P. G. *Science* **1989**, *244*, 182-188.

(16) Cornish, V. W.; Schultz, P. G. *Curr. Opin. Struct. Biol.* **1994**, *4*, 601-607.

(17) Nowak, M. W.; Gallivan, J. P.; Silverman, S. K.; Labarca, C. G.; Dougherty, D. A.; Lester, H. A. In *Ion Channels, Pt B* 1998; Vol. 293, p 504-529.

(18) Gundersen, C. B.; Miledi, R.; Parker, I. *Proc. R. Soc. Lond. Ser. B-Biol. Sci.* **1983**, *219*, 103-109.

(19) Miller, A. J.; Zhou, J. J. *Biochimica et Biophysica Acta (BBA)-Biomembranes* **2000**, *1465*, 343-358.

(20) Beene, D. L.; Dougherty, D. A.; Lester, H. A. *Curr. Opin. Neurobio.* **2003**, *13*, 264-270.

(21) MacKinnon, R.; Yellen, G. *Science* **1990**, *250*, 276-9.

(22) Heginbotham, L.; MacKinnon, R. *Neuron* **1992**, *8*, 483-91.

(23) Kavanaugh, M. P.; Varnum, M. D.; Osborne, P. B.; Christie, M. J.; Busch, A. E.; Adelman, J. P.; North, R. A. *J. Biol. Chem.* **1991**, *266*, 7583-7.

(24) Ahern, C. A.; Eastwood, A. L.; Lester, H. A.; Dougherty, D. A.; Horn, R. *J. Gen. Physiol.* **2006**, *128*, 649-57.

(25) Santarelli, V. P.; Eastwood, A. L.; Dougherty, D. A.; Ahern, C. A.; Horn, R. *Biophys. J.* **2007**, *93*, 2341-9.

(26) Santarelli, V. P.; Eastwood, A. L.; Dougherty, D. A.; Horn, R.; Ahern, C. A. *J. Biol. Chem.* **2007**, *282*, 8044-51.

(27) Ragsdale, D. S.; McPhee, J. C.; Scheuer, T.; Catterall, W. A. *Science* **1994**, *265*, 1724-8.

(28) Nau, C.; Wang, G. K. *J. Membr. Biol.* **2004**, *201*, 1-8.

(29) Ahern, C. A.; Eastwood, A. L.; Dougherty, D. A.; Horn, R. *Circ. Res.* **2008**, *102*, 86-94.

(30) England, P. M. *Biochemistry* **2004**, *43*, 11623-9.

(31) Eastwood, A. L.; Blum, A. P.; Zacharias, N. M.; Dougherty, D. A. *unpublished manuscript*.

Chapter II

A CATION-π INTERACTION BETWEEN EXTRACELLULAR TEA AND AN AROMATIC RESIDUE IN POTASSIUM CHANNELS

Open-channel blockers such as tetraethylammonium (TEA) have a long history as probes of the permeation pathway of ion channels. High-affinity blockade by extracellular TEA requires the presence of an aromatic amino acid at a position that sits at the external entrance of the permeation pathway (residue 449 in the eukaryotic voltage-gated K^+ channel Shaker B (ShB)). The importance of a cation-π interaction between TEA and such an aromatic residue to TEA block was investigated using the *in vivo* nonsense-suppression method to incorporate a series of increasingly fluorinated-phenylalanine side chains at position 449. Fluorination, which is known to decrease the cation-π binding ability of an aromatic ring, progressively increased the inhibitory constant K_i for TEA block of ShB. A larger increase in K_i was observed when the benzene ring of Phe449 was substituted by nonaromatic cyclohexane. These results support a strong cation-π component to the TEA block. The data provide an empirical basis for choosing between ShB models that are based on two classes of reported crystal structures for the bacterial channel KcsA, showing residue Tyr82 in orientations either compatible or incompatible with a cation-π mechanism. We propose that the aromatic residue at this position in ShB is favorably oriented for a cation-π interaction with the permeation pathway. This choice

is supported by high-level *ab initio* calculations of the predicted effects of phenylalanine modifications on TEA binding energy.

Introduction

It is exactly a decade since the ion channel field was electrified by the first atomic-resolution images of a K^+-selective ion channel, the KcsA channel from the bacterium *Streptomyces lividans.*[1] Since then, a number of important K^+ channel structures have appeared, all but one imaging a channel of bacterial origin. The KcsA structure (and subsequent structures of other K^+ channels) was consistent with and rationalized a wide range of biochemical and biophysical studies of K^+ channels, clearly establishing its relevance to mammalian K^+ channels—including the location of a residue associated with blockade of K^+ channels by the external application of the cation TEA. For many years open-channel blockers such as TEA have been exploited to gain insights into the processes of gating and permeation.[2-13] Tyr82 of KcsA is positioned at the mouth of the channel in a location that appears well suited to binding extracellular TEA. This KcsA residue aligns with Thr449 in the eukaryotic ShB, and early work established its critical role for external TEA blockade. In particular, high-affinity blockade by TEA requires an aromatic amino acid (tyrosine or phenylalanine) at this site;[4,6,14] the ShB mutants Thr449Tyr and Thr449Phe have high TEA affinity, as do other K^+ channels that naturally have a tyrosine or phenylalanine at the aligned site.[4,15,16] Aromaticity is critical, as nonaromatic amino acids either more hydrophobic, such as leucine, isoleucine, and valine, or more hydrophilic, such as serine, threonine, glutamate or lysine, lead to low-

affinity block by extracellular TEA.[6,17] The unique requirement of an aromatic amino acid at position 449 led Heginbotham and MacKinnon to propose that a cation-π interaction was critical to the high-affinity binding of TEA.[6] An optimal cation-π interaction is supported only if the cation, in this case TEA, interacts with the face, not the edge, of the aromatic ring, an arrangement that will be referred to as *en face*.

Reported crystal structures of KcsA actually show two orientations for residue Tyr82. In support of the cation-π hypothesis, a recent crystal structure of a noninactivating mutant of KcsA shows an *en face* orientation of Tyr82 (orange side chain, figure 2.1B),[18] suggesting that this orientation might be obtained in eukaryotic K^+ channels. However, other reported KcsA structures pose a possible problem. Specifically, the side chain of Tyr82 in many published structures of KcsA (e.g., 1BL8,[1] 1K4C,[19] 1R3J,[20] 2A9H,[21] and 1ZWI[18] in the Protein Data Bank, www.rcsb.org/pdb/) is aligned such that a TEA positioned to block the channel would not interact with the face of the aromatic ring (blue side chains in figure 2.1). Furthermore, several molecular dynamics studies of KcsA complexed with TEA support this nonoptimal geometry at Tyr82, such that the edges of the tyrosine rings point toward the blocker.[22-25] Indeed, a subsequent crystal structure of KcsA complexed with the TEA analogue tetraethylarsonium (TEAs) also has this *edge-on* conformation.[26] It was thus concluded that a cation-π interaction was not involved in binding TEA to KcsA, but rather the crucial tyrosine influenced the local hydration structure of the binding site.

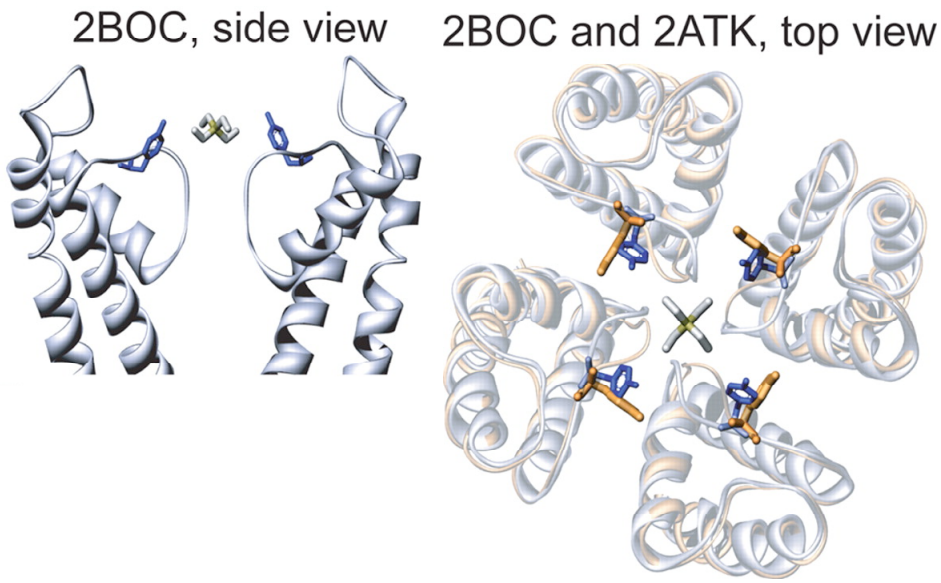

Figure 2.1. Two orientations of Tyr82 residues of KcsA. The atomic coordinates (2BOC and 2ATK) were obtained from the Protein Data Bank. 2BOC (blue) is wild-type KcsA cocrystallized with TEAs.[26] 2ATK (orange) is one of two crystal forms of the E71A mutant.[18] The first is a side view of two opposing subunits of 2BOC with TEAs, and the second is the top view of 2BOC aligned with 2ATK, showing the approximate *en face* orientation of Tyr82 in 2ATK.

There is, therefore, support both for and against a cation-π interaction at the aromatic residue at the entrance to K^+ channels. Simulation studies of the *edge-on* KcsA channel argue against a cation-π interaction, but the binding studies of TEA to eukaryotic K^+ channels, and the recent *en face* KcsA structure, allow for such an interaction. Here a cation-π mechanism in ShB will be directly assessed using a definitive probe developed for functional ion channels and receptors. Modifying the side chain of an aromatic amino acid with fluorine substantially diminishes the cation-π binding ability of the aromatic ring, and multiple substitutions produce additive effects.[27-30] Such substitutions in ShB are achieved using the nonsense-suppression methodology for unnatural amino acid

incorporation.[31] This methodology has numerous advantages, making it ideal for probing potential cation-π interactions. In comparison to conventional mutagenesis, the steric perturbation introduced by fluorine substitution is universally considered to be minimal. Also, fluorine substitution does not substantially alter the hydrophobicity of the ring. For example, benzene and hexafluorobenzene have nearly identical logP (water/octanol partition) values.[32] Therefore, induced affinity shifts in cation binding cannot be attributed solely to effects of hydrophobicity. This fluorination strategy has been successfully used to probe cation binding sites in the nicotinic acetylcholine receptor (nAChR),[33] the 5-HT_3 receptor,[34,35] the $GABA_C$ receptor,[36] the $GABA_A$ receptor,[37] the NMDA receptor,[38] and more.

In this study a choice between the *edge-on* and *en face* orientations is provided by applying the side chain fluorination approach to position 449 of ShB. A compelling correlation is found between degree of fluorination of the phenylalanine suppressed at Thr449 and loss of TEA affinity. The correlation is supported by *ab initio* quantum mechanical calculations of the two disparate models of the TEA binding site. Therefore, there is, indeed, a significant cation-π interaction involved in the binding of TEA to ShB, suggesting that an aromatic residue at this position adopts an *en face* orientation.

Results

Synthesis of Fluorinated Phenylalanine-tRNA

To fully explore the importance of the potential cation-π interaction between TEA and the aromatic residues at position 449 in ShB using *in vivo* nonsense-suppression technology, tRNAs aminoacylated with threonine, which is identical to the wild-type residue; with successively fluorinated phenylalanines, which increasingly reduce the negative electrostatic potential on the face of the aromatic ring; and with cyclohexylalanine, which completely abolishes the aromatic nature while mimicking the sterics of phenylalanine, were necessary. The synthesis of phenylalanine-tRNA is shown in scheme 2.1.[31,39,40] The amine was first protected with the nitroveratryloxycarbonyl (NVOC) photolabile protecting group.[41] Next, the acid was activated as a cyanomethyl ester. This compound was then coupled to the tetrabutylammonium salt of dCA. At this point, the amino acid can be attached to either the 2' or the 3' hydroxyl of dCA since it is thought to rapidly sample both sites. Finally, the aminoacylated dCA was ligated to THG-73 using T4 RNA ligase.

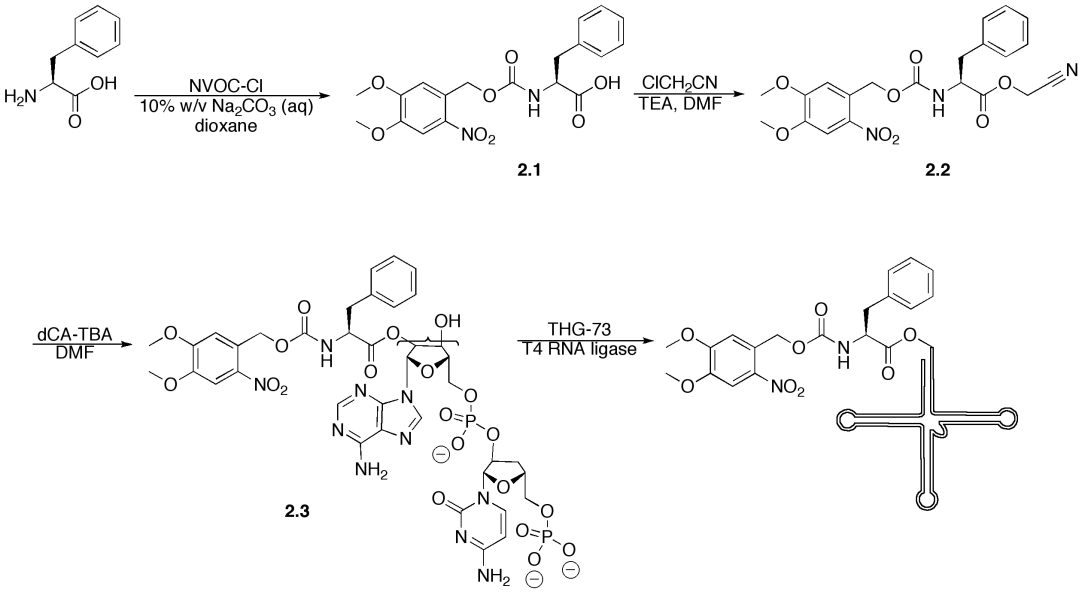

Scheme 2.1. Synthesis of phenylalanine-tRNA.

The synthesis of 3,5-F_2-phenylalanine-dCA was attempted, but while the protection of the amine and the activation of the acid were successful, the coupling of the compound to dCA was never productive (scheme 2.2). Therefore, 3,5-F_2-phenylalanine-dCA was obtained from Dr. Niki Zacharias, a former graduate student in the Dougherty laboratory. 4-F-Phenylalanine-dCA, 3,4,5-F_3-phenylalanine-dCA, cyclohexylalanine-dCA, and threonine-dCA were also acquired thanks to the synthetic efforts of Dr. Tingwei Mu, Dr. Wenge Zhong, and other former members of the Dougherty laboratory.

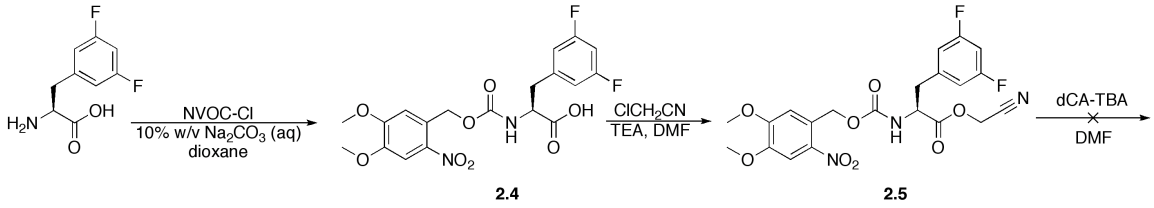

Scheme 2.2. Attempt to synthesize 3,5-F_2-phenylalanine-tRNA.

Evaluating the Role of the Cation-π Interaction

To test for the role of a cation-π interaction between extracellular TEA and an aromatic residue at position 449 of ShB, the phenylalanine analogs described above, were incorporated at this site. Figure 2.2 shows examples of inactivation-removed ShB currents obtained with this method. In all cases the cRNA encoding for ShB was identical, containing a UAG codon at position 449. This cRNA was coinjected into oocytes with one of six different constructs of suppressor tRNAs, each containing the anticodon CUA and all but one synthetically acylated with an amino acid. Figure 2.2A-D show families of K^+ currents in which the tRNAs were acylated with phenylalanine and three of its fluorinated derivatives. Inserts show color-coded electrostatic potential surfaces, determined by *ab initio* calculations, of benzene and these fluorinated derivatives. On this color scale, red indicates negative electrostatic and blue positive electrostatic potential. As shown, successive substitution of fluorine atoms for hydrogen atoms on a benzene ring produces a successive decrease in the negative electrostatic potential on the face of the aromatic ring, leading to a monotonic decrease in intrinsic cation binding ability.[27,28] Figure 2.2E shows currents from the mutant cyclohexylalanine (Cha) in which the benzene ring of phenylalanine was replaced by cyclohexane. In general the currents in all of the mutants examined had similar kinetics and voltage dependence. Figure 2.2F shows the absence of current from an oocyte coinjected with ShB Thr449UAG and a suppressor tRNA that had not been charged with an amino acid (dCA-tRNA). This control ensures that the suppressor tRNA is not reaminoacylated by the cell with a natural amino acid, which could then get incorporated into the channel protein. To control for read through, namely the possibility that another tRNA species

can incorrectly recognize the UAG codon and attach its amino acid at position 449, cRNA for ShB Thr449UAG alone was injected. This control was performed routinely for every experiment and also produced no detectable K^+ currents, ruling out read through.

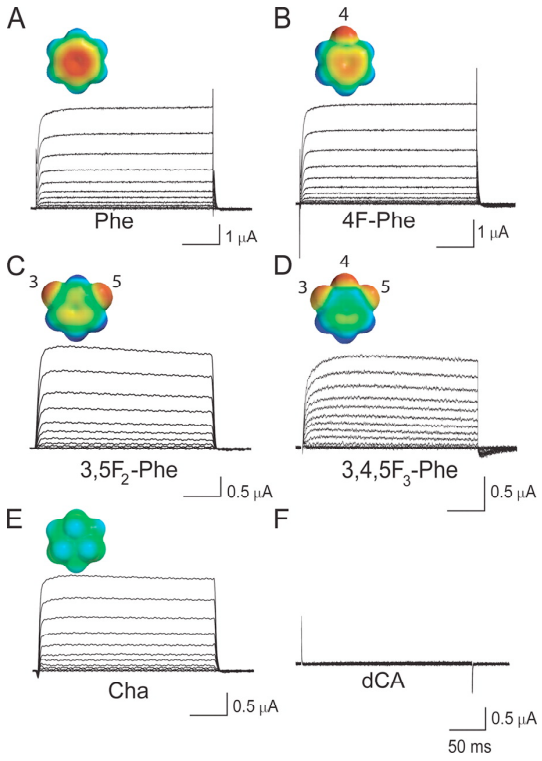

Figure 2.2. Functional expression of unnatural amino acids in ShB at position 449. A-E) Representative families of K^+ currents elicited by test depolarizations for 10 mV increments between −60 mV and +50 mV, from a holding potential of −80 mV. Leak and capacitance currents were subtracted online with a –P/8 protocol. The label beneath each panel indicates the introduced amino acid. In each case, the inset shows the 6-31G** electrostatic potential surface of benzene derivatives, with red and blue corresponding to −20 and +20 kcal/mol, respectively.[27,28] The numbered positions of the fluorine atoms are shown with respect to the δ-carbon of phenylalanine. F) Lack of K^+ currents originating from cellular tRNA acylation when ShB Thr449UAG mRNA was coinjected with an uncharged tRNA.

The block of extracellular TEA in channels containing six different residues at position 449 were measured. These residues included phenylalanine, threonine (wild type), the three fluorinated derivatives of phenylalanine, and cyclohexylalanine. In all cases the block was rapid, as typically observed for extracellular TEA.[42] That is, the blocker reduced the macroscopic current amplitude with no effect on gating kinetics (e.g., figure 2.3A, B). Figure 2.3C plots the fraction of unblocked channels at +50 mV versus the extracellular TEA concentration, and table 2.1 lists the concentrations producing half block (K_i) based on fits of dose-response curves in figure 2.3C. The pivotal role of the residue at position 449 is evident in this figure and in table 2.1. The absolute magnitudes and relative K_i values for phenylalanine and the native threonine residue at this position in ShB agree with a previous study.[6] The affinities differ by nearly two orders of magnitude between these two natural amino acid residues, supporting the hypothesis that an aromatic residue plays a critical role in TEA binding.

Table 2.1 Inhibitory constants for TEA block.*

T449X, where X=	K_i (mM)	$\Delta\Delta G$ (kcal/mol)
Phe (n = 10)	0.39 ± 0.04	0
Thr (n = 7)	33.5 ± 8.9	2.58
4-F-Phe (n = 5)	3.3 ± 0.6	1.23
3,5-F_2-Phe (n = 7)	47.6 ± 5.9	2.78
3,4,5-F_3-Phe (n = 7)	175.2 ± 36.2	3.54
Cha (n = 3)	249.2 ± 20.1	3.75

* K_i values given as mean ± sem. Free energy ($\Delta\Delta G$) is calculated as $\Delta\Delta G = RT \ln(K_{i,X} / K_{i,Phe})$, where RT is 0.58 kcal/mol at room temperature.

The potency of TEAs as a blocker for ShB was measured for a comparison to the study of TEAs cocrystallized with KcsA.[26] A crude sample of TEAs was obtained from Dr. Adrian Gross,[26] and its concentration was determined by NMR, using glycine as a standard. TEAs was found to make up 70% of the crude mixture. Taking this offset into account, TEAs was found to be a weaker blocker than TEA by a factor of 25 in ShB Thr449Phe.

One of the distinctions between aromatic and nonaromatic residues at position 449 is the voltage dependence of TEA block. TEA apparently senses 19% of the transmembrane electric field for Thr449 and only 4% for Tyr449.[6] This difference suggests that TEA blocks at a more superficial site when an aromatic residue at 449 creates a high-affinity binding site. Because fluorination of phenylalanine reduces TEA affinity, it might also allow TEA to bind at a deeper location in the electric field. However, the voltage dependence of block was found to be shallow (2%-8%) for all fluorinated derivatives of Phe449 (figure 2.4), supporting the idea that the blocking site for TEA is the same for all of these derivatives. Note that the measured voltage dependence from the plots in figure 2.4 could be due to the distribution of K^+ ions within the selectivity filter rather than to the position of TEA within the electric field.[43]

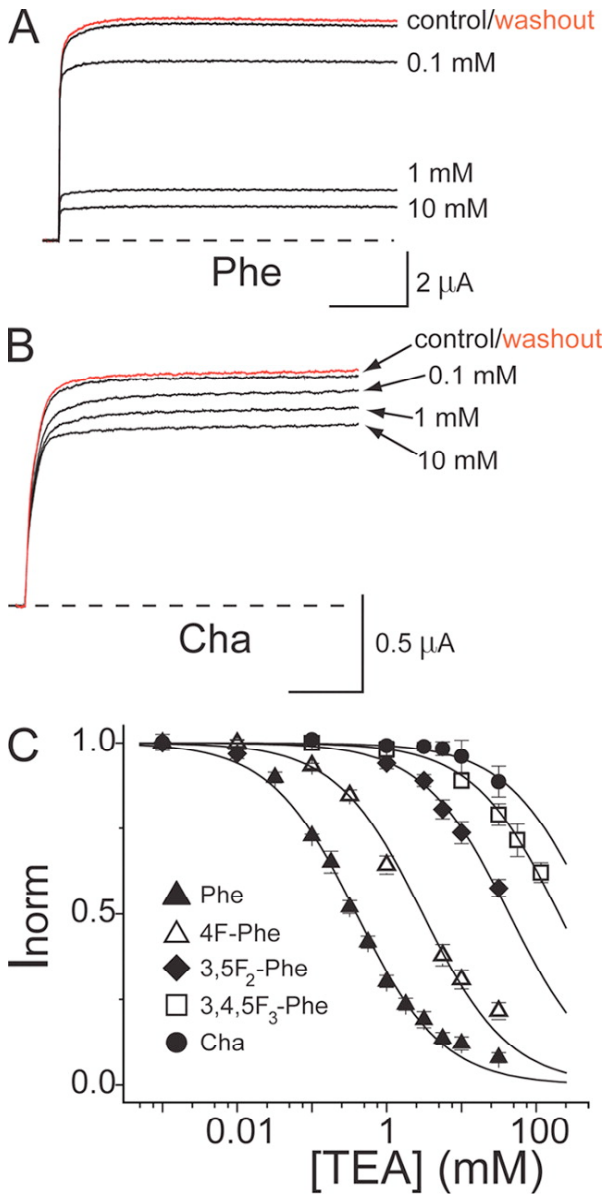

Figure 2.3. Evidence for a cation-π interaction in TEA block. A-B) Reversible TEA inhibition for phenylalanine and cyclohexylalanine currents at +50 mV. C) TEA inhibition plots for ShB channels containing the indicated residue at position 449. Curves are standard binding isotherms fitted to the data. Increased fluorination monotonically increases the dissociation constant K_i (table 2.1). Cyclohexylalanine, which is devoid of aromatic character, renders the channel nearly insensitive to TEA.

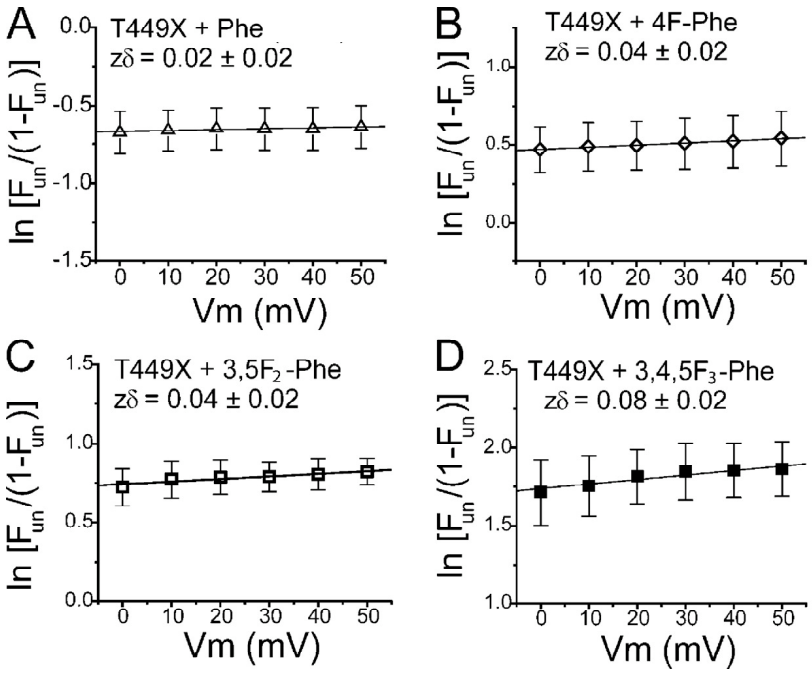

Figure 2.4. Voltage dependence of block is similar for all fluorinated derivatives. A-D) Natural logarithm of the relative fraction of unblocked channels (F_{un}) versus blocked channels is plotted against membrane potential. [TEA] = 1 mM, 1 mM, 10 mM, and 10 mM for Phe (n = 10), 4-F-Phe (n = 4), 3,5-F_2-Phe (n = 7), and 3,4,5-F_3-Phe (n = 8), respectively.

If an electrostatic component of TEA binding were due to a cation-π interaction involving the aromatic side chain at residue 449, then one would expect increasing substitution of fluorine atoms to decrease the binding affinity monotonically.[27,28] This trend is exactly what was observed (figure 2.3C and table 2.1). In other systems such a trend has been interpreted as compelling evidence for a sizable cation-π interaction involving the site undergoing substitution.[33-36] The first such conclusion, the cation-π interaction between acetylcholine and the tryptophan residue at position 149 in the α1 subunit of the muscle nAChR,[33] was subsequently confirmed by X-ray crystallography.[44]

The largest effect on TEA affinity, 640-fold, occurs with the nonaromatic residue cyclohexylalanine. As discussed below, this observation provides further support for a cation-π interaction in TEA binding and contributes valuable information on proposed alternative models underlying TEA affinity.

Discussion

Our data argue that high-affinity TEA blockade results in part from a significant cation-π interaction between TEA and an aromatic amino acid at position 449 in ShB. As in other studies of this type, it is not a single mutation that leads to this conclusion, but rather a consistent trend across a systematic series of subtle mutations. Figure 2.5A plots the change in free energy of TEA binding (open squares) for the phenylalanine derivatives against the effect on the energy of Na^+ ion binding to comparable derivatives of benzene. Na^+ binding energy in the gas phase was determined by *ab initio* calculations. The monotonic, nearly linear relationship for ShB establishes a cation-π contribution to TEA block. Moreover, previous studies show that fluorination has little effect on "nonelectrostatic" energetic components of cation binding to a benzene ring (e.g., donor-acceptor, charge-transfer, and induced dipoles in the aromatic[30]).

To estimate the energetic contribution of the cation-π interaction, a comparison of phenylalanine and 3,4,5-F_3-phenylalanine is useful. Examination of the electrostatic potential surfaces of figure 2.2 shows that three fluorine atoms effectively erase the electrostatic attractiveness of the aromatic ring to the cation, and earlier studies showed that trifluorobenzene is a good model for an aromatic that has little or no electrostatic

binding ability.[27,28,45] From this perspective, the $\Delta\Delta G$ values of table 2.1 suggest that the cation-π interaction is the dominant factor in distinguishing strong from weak TEA binders, in that the energetic consequence of the phenylalanine to 3,4,5-F_3-phenylalanine mutation (3.5 kcal/mol) is comparable with that of the phenylalanine to threonine mutation (2.6 kcal/mol).

The biggest decrease in TEA affinity is seen for the phenylalanine to cyclohexylalanine mutation (3.8 kcal/mol). This decrease is consistent with both theoretical and experimental studies showing that cyclohexane binds cations more poorly than any of the aromatics considered here.[27,28,46] Note that the side chains of phenylalanine and cyclohexylalanine, modeled here as benzene and cyclohexane, respectively, are similar in size, shape, and hydrophobicity (figure 2.2). The most noticeable difference, in the context of noncovalent binding interactions, is that the negative electrostatic potential that leads to cation binding in benzene disappears in cyclohexane. The phenylalanine to cyclohexylalanine mutation thus further confirms that the π character and its associated negative electrostatic potential dominate strong TEA binding when phenylalanine is present at position 449. Note also that cyclohexane is considerably more polarizable than benzene,[47] ruling out any special role for an induced dipole in the binding of TEA by phenylalanine and its derivatives.

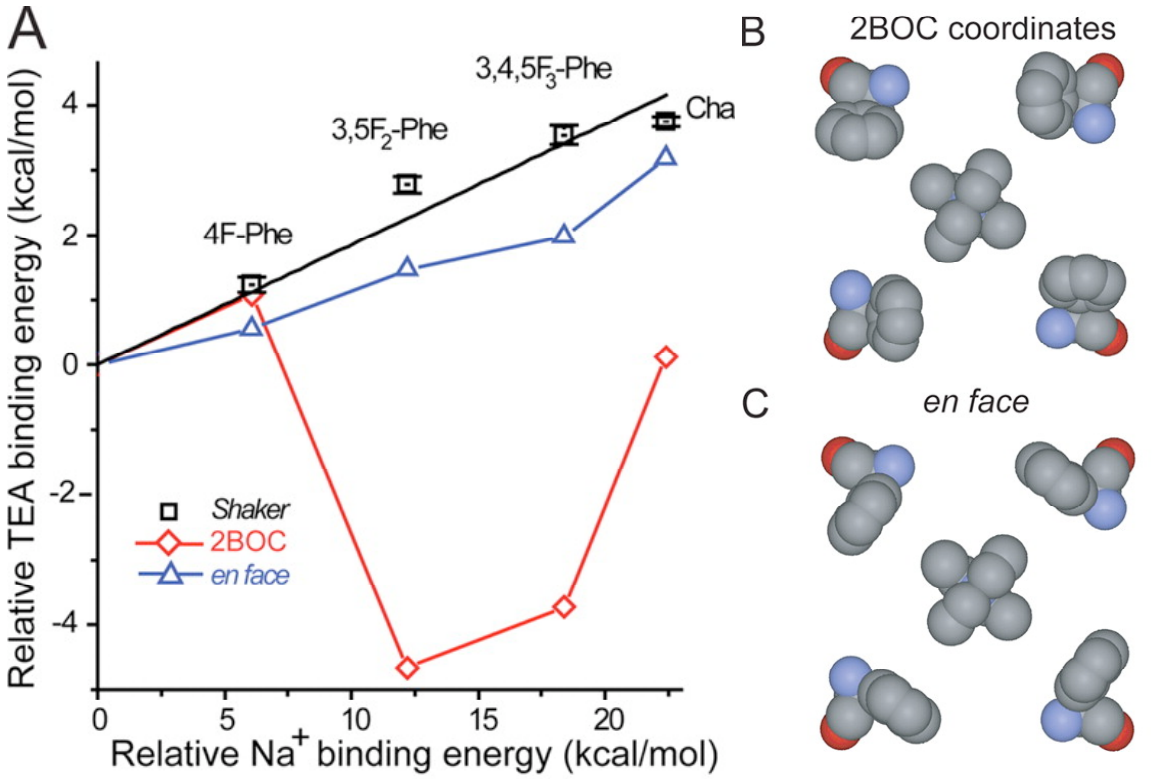

Figure 2.5. Thermodynamic and *ab initio* calculations support an *en face* model of TEA binding to ShB. A) Relative binding energy of TEA to phenylalanine derivatives plotted against that calculated for Na^+ binding to benzene derivatives. Data obtained experimentally for ShB, black squares, display a linear change (black line, slope = 0.19 ± 0.01, R^2 = 0.88) in binding energy as π electrons are withdrawn by fluorine substitutions. *Ab initio* calculations for the binding energetics of a reduced system comprised of four aromatics and a single TEA molecule are shown on the same plot for comparison. B) The reduced system (minus hydrogen atoms) based on the coordinates of KcsA and TEAs.[26] These coordinates predict enhanced binding (red diamonds in A)) as π electrons are removed from the aromatic face, a trend inconsistent with experimental data. Conversely, a 60° rotation displayed in C) qualitatively reproduces (blue triangles in A)) the trend of TEA binding energetics obtained experimentally from ShB.

Previous computational studies of the KcsA channel are based on structures with Tyr82 in the *edge-on* orientation and have led others to conclude that the cation-π interaction does not contribute substantially to external TEA blockade. These studies instead emphasize local hydration structure as a crucial component of the energetics of TEA binding,[22-25] although electrostatic stabilization by the backbone carbonyls of Tyr78 and Gly79 (in KcsA) may also play a role.[24] The distribution of K^+ ions within the selectivity filter also appears to affect TEA binding energy,[22-24] another possible source of electrostatic energy. Energetic contributions of local hydration include both electrostatic and hydrophobic forces. However, an essential role of attractive hydrophobic forces between TEA and its binding site is contradicted by earlier data from ShB, where relatively hydrophobic residues at site 449 are not in general better at binding TEA.[6] Comparison of the essentially isosteric residues valine and threonine, for example, shows that polar threonine is associated with a higher TEA affinity.[6] Also, leucine, isoleucine, and valine are all substantially more hydrophobic than phenylalanine,[48] yet produce weak TEA binding sites. The phenylalanine/cyclohexylalanine pair described here presents another isosteric comparison, and again hydrophobics do not explain the results. Also, the size, but not hydrophobicity, of the alkylammonium blocker appears to be a critical factor in binding affinity.[6,49] Furthermore, examination of the temperature dependence of TEA block shows that enthalpy rather than entropy largely accounts for the free energy of binding,[6] again arguing against a fundamental role of hydrophobic forces in TEA binding.

Computational Examination of the TEA-Channel Interaction

To investigate the evidence for a cation-π mechanism further, the TEA-side chain interaction was modeled computationally. One constraint was the necessity to use KcsA structures for the computational modeling, because KcsA is the only crystallized K^+ channel with an aromatic residue (Tyr82) at this position. The structure 2BOC, a cocrystal of KcsA and TEAs (blue side chain in figure 2.1),[26] was the initial starting point. KcsA is highly homologous to voltage-gated K^+ channels in this region of the protein. In the vicinity of the selectivity filter, KcsA has the sequence TTVGYGDL**Y**, whereas in $K_V1.2$ it is TTVGYGDM**V**. In addition, the crystallographic distances across the tetramer between the α-carbons of these residues agree within 1 Å when comparing KcsA structures to the mammalian $K_V1.2$ (2A79). With respect to a cation-π mechanism, the majority of published structures of KcsA display an unfavorable orientation of the Tyr82 aromatic rings. Moreover, the closest carbon-carbon distance between the blocker and the aromatic side chains (4.1 Å) is larger than typically observed for simple cation-π interactions (e.g., 2.4 Å between Na^+ and the center of a benzene ring[29,30]). To examine the energetic consequences of withdrawing π electrons by fluorinating the aromatic ring of this residue, a reduced molecular model of TEA and its four coordinating phenylalanine residues was constructed, based on the 2BOC structure.[26] In this reduced system (117 atoms; figure 2.5B) high-level *ab initio* quantum mechanical calculations of the binding energy of TEA were performed. Instead of decreasing the binding, as was observed experimentally (black squares in figure 2.5A), successively fluorinating these phenylalanine residues *in silico* had a nonmonotonic effect on TEA binding energy (red

diamonds in figure 2.5A), the main effect being a substantial *increase* of TEA affinity in the difluorinated and trifluorinated derivatives.

Our *ab initio* calculations can be rationalized as follows. The cationic blocker is directed more towards the edge than the face of the aromatic ring (figure 2.5B). The electrostatic potential along the edge of a simple aromatic ring is positive (e.g., insert in figure 2.2A), and would therefore electrostatically repel TEA. Fluorination, however, introduces negative electrostatic potential to the edge of the ring via the fluorines (figure 2.2), and this would tend to attract TEA, especially in the 3 or 5 position of the aromatic ring (figures 2.1, 2.5B). In fact, the 3,5-F_2- and 3,4,5-F_3-derivatives of phenylalanine show the most dramatic increases in TEA affinity in the *ab initio* calculations.

Because these self-consistent theoretical results disagree with our experimental data, the possibility that the aromatic rings were rotated to face the central axis of the pore was considered (figure 2.5C), as proposed before the crystal structures of KcsA were available.[6,50] In this *en face* orientation TEA would be attracted to the negative electrostatic potential on the face of the aromatic rings. Fluorination would then decrease the negative electrostatic potential presented to TEA and destabilize its binding, a prediction consistent with our experimental data. To quantify this idea, the energetic consequences of fluorinating the aromatic rings of Phe82 on TEA binding in this conformation were calculated. The only modification of the structure of figure 2.5B was a 60° rotation of the aromatic rings, maintaining all other coordinates of the four Phe residues. With this single change, the results of the *ab initio* calculations now resemble our experimental results, showing a monotonic destabilization of TEA binding as the aromatic rings are increasingly fluorinated (blue triangles in figure 2.5A). Moreover, the

rotation itself enhanced TEA affinity by 3 kcal/mol. Although the optimal dihedral angle was not examined in detail, rotations of 40° or 80° were less effective at replicating our experimental data. Given the crudeness of this model, and the fact that it is based on a crystal structure of KcsA rather than a eukaryotic voltage-gated K^+ channel, the agreement is quite acceptable. Even the larger perturbation associated with the nonaromatic cyclohexylalanine residue is reproduced by the calculations.

Although the 144° χ_2 dihedral angle in our *en face* model is unusual for both tyrosine and phenylalanine residues in known protein structures,[51] an *en face* orientation of Tyr82 was reported for one of the crystal structures of the functional Glu71Ala mutant of KcsA.[18] Figure 2.1B shows this structure (2ATK, orange Tyr82 side chains) aligned with that of KcsA cocrystallized with TEAs (blue Tyr82 side chains). The similarity to our *en face* model (figure 2.5C) is apparent. There are other subtle structural changes in this region of the 2ATK structure that enable *en face* geometry. Of note, the selectivity filter has conformational variants in wild-type KcsA, depending on the concentration of permeant ions,[19] supporting the possibility that the functional conformation of ShB is compatible with an *en face* orientation of Phe449 residues. It also raises the possibility that the open states of K^+ channels in general have conformational flexibility including the orientation of an aromatic residue at this position.

The slope of the experimental fluorination plot as shown in figure 2.5A is considered a crude indication of the energetic magnitude of the cation-π interaction. The slope of this plot (0.19) is comparable to those seen in studies of agonists such as GABA and 5-HT_3 binding to neuroreceptors.[34,36] However, the receptor studies measure the binding of an

$R\text{-}NH_3^+$ ion to a *single* aromatic residue. Here, four aromatic residues are simultaneously being modified. Thus, the slope in the present case suggests that any single TEA-aromatic interaction is not very strong, which is consistent with the low affinity of TEA and the fact that TEA is a very diffuse cation, and so it is expected to experience a weaker cation-π interaction than more focused cations such as $R\text{-}NH_3^+$. The energetic magnitude of the cation-π interaction taken from the slope may also reflect the fact that TEA cannot make van der Waals contact with all four rings at once, in either of the *en face* conformations that were considered (figures 2.1B, 2.5C), which should weaken the cation-π interaction. Nevertheless, the magnitude of the cation-π interaction does not fall off steeply with distance,[29] and therefore four nonoptimal interactions can combine to create a moderate effect. It is worth noting that a closer approach of the aromatic side chains to the blocker may be impossible if the open channel structure is maintained, because this residue is only two amino acids downstream from the TVGYGD signature sequence of the selectivity filter. Functional data argue against a large-scale collapse of the aromatics onto the blocker, because TEA has no effect on open dwell times of single channels.[42]

Not considering all possible energetic factors in the described calculations was intentional. Our calculations primarily evaluate one component of the binding interaction—the electrostatic attraction between a cation and the side–chain. The fact that binding energies correlate so nicely with this term establishes an important role for electrostatic attractions in the binding. Additional effects such as hydrophobics are neither ruled out nor ruled in; the data simply show that electrostatics must be important. The functional data on eukaryotic K^+ channels shows that while there may well be a

hydrophobic contribution to binding, it is not the factor that discriminates among residues. Another factor that might contribute to TEA binding in these experiments is the possibility that the electronegative fluorine atoms could influence the local structure of water molecules in the vicinity of the blocker. However, it is not clear how this effect would produce the systematic destabilization of TEA binding that was observed (figures 2.3C, 2.5A). To explore this possibility the Gibbs free energy of TEA binding in our reduced *edge-on* model was estimated, accounting both for the gas-phase *ab initio* energies, as well as the energies of hydration, using a self-consistent reaction field method with the Poisson-Boltzmann solver in the program Jaguar (http://www.schrodinger.com/). As in the gas-phase calculations of figure 2.5A, difluorinating the phenylalanine residue in this conformation enhanced TEA binding (by 2.3 kcal/mol), again inconsistent with our experimental results.

How are our conclusions resolved with earlier works disputing a role for a cation-π mechanism? As noted, previous simulations were based on analysis of two *edge-on* crystallographic structures (1BL8 and 2BOC) of the bacterial channel KcsA, rather than on a eukaryotic, voltage-gated K^+ channel or on the *en face* structure of a KcsA mutant (2ATK). Note that even though KcsA contains an aromatic residue at the aligned position (Tyr82), it does not bind TEA strongly. Its K_i for TEA block is 3.2 mM,[52] almost tenfold higher than for ShB Thr449Phe. Also, KcsA Tyr82Thr shows a TEA blocking constant of 143 mM, significantly higher than obtained in ShB with its wild-type Thr449. Finally, the TEA analogue TEAs used for the 2BOC crystal structure shown in figure 2.1 has a 25-fold larger inhibitory constant than TEA in ShB Thr449Phe, allowing for the possibility that the structure may not be representative of TEA in its

binding site. Thus, inherent but unknown aspects of the KcsA channel, perhaps including a nonoptimal arrangement of Tyr82 residues, underlie a relatively weak TEA binding site.

Conclusion

In conclusion, this chapter shows that a cation-π interaction makes a substantial contribution to high-affinity blockade by extracellular TEA in voltage-gated K^+ channels. Evidently, the orientation of an aromatic residue at this position is favorable for a cation-π mechanism. This hypothesis is supported by our experimental and theoretical results, and it provides a simple explanation of the longstanding observation that aromatics at position 449 are necessary and sufficient for high-affinity, external TEA blockade in voltage-gated K^+ channels. The (presumably subtle) conditions that govern crystallization of KcsA in one state or the other are not yet understood, but the functional form relevant to ShB in this region is apparently the *en face* orientation.

Methods

The work in this chapter was a collaborative effort that included important contributions from Dr. Chris Ahern and Dr. Richard Horn of the Jefferson Medical College in Philadelphia, PA. Detailed methods for the experiments discussed in this chapter that were not performed by the author can be found in Ahern *et al.*[53]

Synthesis

All reactions were performed at ambient temperature and pressure unless otherwise noted. All reactions involving potentially air-sensitive compounds were conducted under an inert atmosphere using Schlenk techniques. Solvents were purified by passage through alumina.[54] Unless otherwise noted, all chemicals and reagents were used as received without further purification. Flash chromatography was performed using EMD (Gibbstown, NJ) silica gel 60 (particle size 0.040-0.063 mm). Thin-layer chromatography (TLC) was performed using EMD (Gibbstown, NJ) silica gel 60 F_{254} precoated plates (0.25 mm) and visualized by UV and potassium permanganate. Nuclear magnetic resonance spectroscopy (NMR) was preformed on a Varian (Palo Alto, CA) Mercury 300 instrument, and NMR resonances are reported relative to Me_4Si (δ 0.0), CD_3OD (δ 3.31), or D_2O (δ 4.79). Data for ^1H NMR spectra are reported as follows: chemical shift (δ ppm), integration, multiplicity, and coupling constant (Hz). Mass spectroscopy (MS) spectra were obtained from the Caltech Mass Spectrometry Lab. Electrospray ionization mass spectrometry (ESI-MS) was preformed on an LCQ Classic ion trap (ThermoFinnigan, Waltham, MA) in direct infusion mode. HPLC was preformed using Waters (Milford, MA) equipment and software (510 HPLC pumps and 996 Photodiode Array Detector) and reverse-phase Nova-Pak® ^{18}C columns (3.9 × 150 mm analytical column, 7.8 × 300 mm preparatory column).

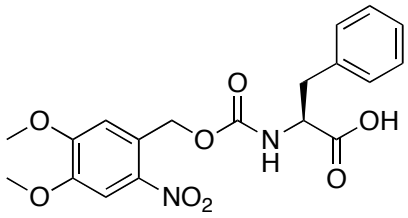

2.1

NVOC-L-phenylalanine **2.1**: L-Phenylalanine (0.297 g, 1.8 mmol, 1 eq) was added to a round-bottom flask and dissolved in 10% (w/v) sodium carbonate in water (7 mL). To this solution was added dioxane (7 mL). The mixture was stirred in an ice bath and nitroveratryloxycarbonyl chloride (0.50 g, 1.9 mmol, 1.1 eq) was added slowly. The mixture was allowed to warm to room temperature while stirring for 4 hours. The mixture was then poured into distilled water and washed with ether (3x). Under vigorous stirring, the aqueous solution was adjusted to pH 2 by slowly adding 5 M HCl. The yellow precipitate that formed was filtered to afford NVOC-L-phenylalanine **2.1** as a yellow solid. ^{1}H NMR (300 MHz, CD_3OD, 298 K) δ 7.63 (1H, s), 7.15 (5H, s), 6.98 (1H, s), 5.31 (2H, d, J = 10.5 Hz), 4.31 (1H, m), 3.79 (3H, s), 3.76 (3H, s), 3.11 (1H, m), 2.83 (1H, m).

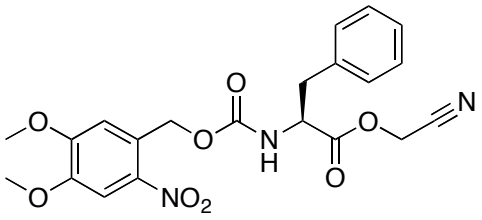

2.2

NVOC-L-phenylalanine cyanomethyl ester **2.2**: NVOC-L-phenylalanine **2.1** (0.254 g, 0.63 mmol) was added to a round-bottom flask under Ar (g) and dissolved in DMF (2 mL). Chloroacetonitrile (2 mL) and then triethylamine (0.25 mL) were added to the

solution. The mixture was stirred at room temperature for 75 minutes and then the solvent was removed under vacuum. The crude product was purified by flash column chromatography (CH_2Cl_2, then 5% EtOAc in CH_2Cl_2 once the yellow product started eluting) to afford NVOC-L-phenylalanine cyanomethyl ester **2.2** as pale yellow crystals. ^{1}H NMR (300 MHz, $CDCl_3$, 298 K) δ 7.72 (1H, s), 7.33 (3H, m), 7.16 (2H, d, J = 6.3 Hz), 6.93 (1H, s), 5.53 (2H, q, J = 15 Hz), 5.26 (1H, d, J = 8.4 Hz), 4.77 (2H, m), 3.96 (3H, s), 3.95 (3H, s), 3.18 (2H, t, J = 5.1 Hz).

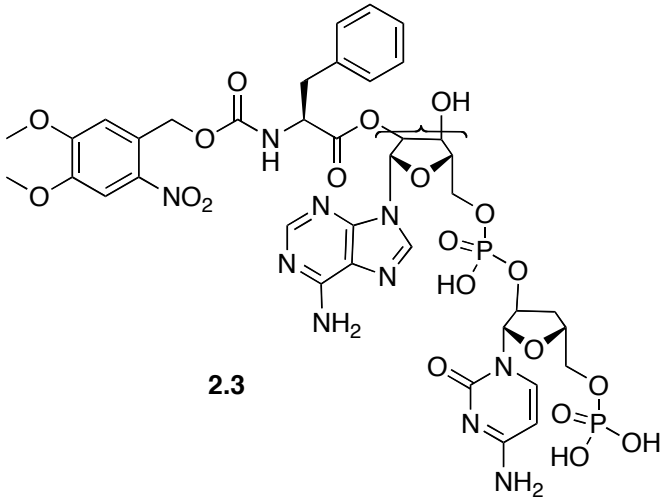

2.3

NVOC-L-phenylalanine-dCA **2.3**: NVOC-L-phenylalanine cyanomethyl ester **2.2** (0.011 g, 0.025 mmol, 3.4 eq) was added to a round-bottom flask under Ar (g) and dissolved in DMF (0.5 mL). This solution was transferred to another round-bottom flask under Ar (g), which contained dCA (0.020 g, 0.017 mmol, 1 eq) as a tetrabutylammonium salt (2.4 eq). The reaction was stirred at room temperature for 18 hours while being monitored by reverse-phase analytical HPLC with a linear solvent gradient from 5% acetonitrile in 25 mM NH_4OAc buffer pH 4.5 to 100% acetonitrile. The crude product was purified using reverse-phase semipreparative HPLC with the same linear solvent gradient. The fractions

containing the NVOC-L-phenylalanine-dCA **2.3** were combined, and the solvent was removed by lyophilization. The solid was redissolved in 10 mM acetic acid and reconcentrated via lyophilization (3x) to afford NVOC-L-phenylalanine-dCA **2.3** as a white powder (0.0016 g, 0.0015 mmol, 19% yield). ESI-MS *m/z* calc'd for $C_{38}H_{44}N_{10}O_{20}P_2$ [M-H]: 1021.2; found: 1021.4.

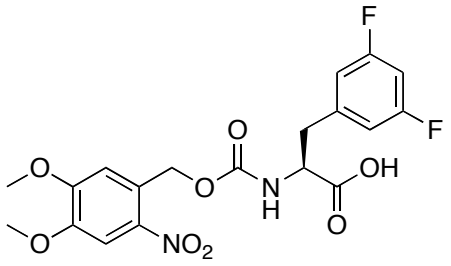

2.4

NVOC-L-3,5-F_2-phenylalanine **2.4**: The procedure described above for **2.1** was repeated using L-3,5-F_2-phenylalanine (0.72 g, 3.6 mmol, 1 eq) to afford NVOC-L-3,5-F_2-phenylalanine **2.4** (1.3 g, 2.9 mmol, 80% yield). R_f = 0.62 (100% EtOAc); ^{1}H NMR (300 MHz, CD_3OD, 298 K) δ 7.64 (1H, s), 7.02 (1H, s), 6.78 (2H, dd, *J* = 8.6, 2.1 Hz), 6.69 (1H, tt, *J* = 9.3, 2.4 Hz), 5.33 (2H, q, *J* = 15 Hz), 4.33 (1H, m), 3.81 (3H, s), 3.80 (3H, s), 3.16 (1H, m), 2.86 (1H, m).

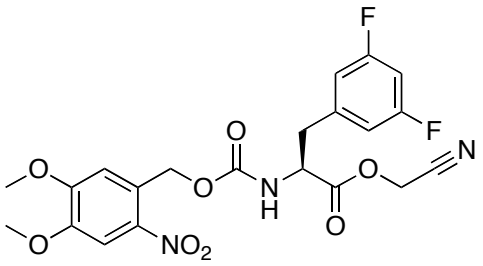

2.5

NVOC-L-3,5-F_2-phenylalanine cyanomethyl ester **2.5**: The procedure described above for **2.2** was repeated using NVOC-L-3,5-F_2-phenylalanine **2.4** (0.264 g, 0.60 mmol). The crude product was purified by trituration with CH_2Cl_2 to afford NVOC-L-3,5-F_2-phenylalanine cyanomethyl ester **2.5**. R_f = 0.54 (17% EtOAc in CH_2Cl_2); ^{1}H NMR (300 MHz, d_6DMSO, 298 K) δ 8.2 (1H, d), 7.7 (1H, s), 7.1 (1H, s), 7.0 (3H, m), 5.3 (2H, d), 5.0 (2H, s), 4.5 (1H, m), 3.8 (3H, s), 3.8 (3H, s), 3.0 (2H, m).

Molecular Biology

The aminoacylated dinucleotides for the amino acids used in this chapter were ligated to a modified tRNA from *Tetrahymena thermophila*, THG73, using T4 RNA ligase (New England Biolabs, Ipswich, MA).[31,39]

Determining the Concentration of TEAs

Glycine (0.0035 g, 0.047 mmol, 1 eq) was placed in an NMR tube and dissolved in D_2O (0.5 mL). ^{1}H NMR (300 MHz, D_2O, 298 K) δ 3.53 (2H, s). To this solution was added a crude mixture containing an unknown amount of tetraethylarsonium (0.0041 g, ~0.018

mmol, ~0.38 g). ^{1}H NMR (300 MHz, D_2O, 298 K) δ 3.53 (2H, s), 2.36 (2.1H, q, J = 7.8 Hz), 1.29 (2.8H, b). Analysis of the NMR resonance integrations, tetraethylarsonium was found to constitute 70% of the mass of the crude tetraethylarsonium mixture (0.0041 g, 0.013 mmol, 0.29 eq).

Acknowledgements

We thank Benoit Roux for extensive discussions and advice about Poisson-Boltzmann calculations, Carol Deutsch for comments on the manuscript, Adrian Gross for the gift of a sample of TEAs-Cl, and Stephanie Huang, Purnima Deshpande, and Lindsey Ingleby for help with the oocytes. This research was sponsored by grants from the NIH (GM079427, NS11756, and NS34407).

References

(1) Doyle, D. A.; Morais Cabral, J.; Pfuetzner, R. A.; Kuo, A.; Gulbis, J. M.; Cohen, S. L.; Chait, B. T.; MacKinnon, R. *Science* **1998**, *280*, 69-77.

(2) Armstrong, C. M. *J. Gen. Physiol.* **1971**, *58*, 413-37.

(3) Miller, C. *J. Gen. Physiol.* **1982**, *79*, 869-91.

(4) MacKinnon, R.; Yellen, G. *Science* **1990**, *250*, 276-9.

(5) Choi, K. L.; Aldrich, R. W.; Yellen, G. *Proc. Natl. Acad. Sci. USA* **1991**, *88*, 5092-5.

(6) Heginbotham, L.; MacKinnon, R. *Neuron* **1992**, *8*, 483-91.

(7) Hidalgo, P.; MacKinnon, R. *Science* **1995**, *268*, 307-10.

(8) Ikeda, S. R.; Korn, S. J. *J. Physiol.* **1995**, *486 (Pt 2)*, 267-72.

(9) Bretschneider, F.; Wrisch, A.; Lehmann-Horn, F.; Grissmer, S. *Biophys. J.* **1999**, *76*, 2351-60.

(10) Jiang, Y.; MacKinnon, R. *J. Gen. Physiol.* **2000**, *115*, 269-72.

(11) Thompson, J.; Begenisich, T. *J. Gen. Physiol.* **2003**, *122*, 239-46.

(12) Andalib, P.; Consiglio, J. F.; Trapani, J. G.; Korn, S. J. *Biophys. J.* **2004**, *87*, 3148-61.

(13) Chatelain, F. C.; Alagem, N.; Xu, Q.; Pancaroglu, R.; Reuveny, E.; Minor, D. L., Jr. *Neuron* **2005**, *47*, 833-43.

(14) Kavanaugh, M. P.; Varnum, M. D.; Osborne, P. B.; Christie, M. J.; Busch, A. E.; Adelman, J. P.; North, R. A. *J. Biol. Chem.* **1991**, *266*, 7583-7.

(15) Frech, G. C.; VanDongen, A. M.; Schuster, G.; Brown, A. M.; Joho, R. H. *Nature* **1989**, *340*, 642-5.

(16) Stuhmer, W.; Ruppersberg, J. P.; Schroter, K. H.; Sakmann, B.; Stocker, M.; Giese, K. P.; Perschke, A.; Baumann, A.; Pongs, O. *EMBO J.* **1989**, *8*, 3235-44.

(17) Molina, A.; Castellano, A. G.; Lopez-Barneo, J. *J. Physiol.* **1997**, *499 (Pt. 2)*, 361-7.

(18) Cordero-Morales, J. F.; Cuello, L. G.; Zhao, Y.; Jogini, V.; Cortes, D. M.; Roux, B.; Perozo, E. *Nat. Struct. Mol. Biol.* **2006**, *13*, 311-8.

(19) Zhou, Y.; Morais-Cabral, J. H.; Kaufman, A.; MacKinnon, R. *Nature* **2001**, *414*, 43-8.

(20) Zhou, Y.; MacKinnon, R. *J. Mol. Biol.* **2003**, *333*, 965-75.

(21) Yu, L.; Sun, C.; Song, D.; Shen, J.; Xu, N.; Gunasekera, A.; Hajduk, P. J.; Olejniczak, E. T. *Biochemistry* **2005**, *44*, 15834-41.

(22) Crouzy, S.; Berneche, S.; Roux, B. *J. Gen. Physiol.* **2001**, *118*, 207-18.

(23) Luzhkov, V. B.; Aqvist, J. *FEBS Lett.* **2001**, *495*, 191-6.

(24) Guidoni, L.; Carloni, P. *J. Recept. Signal Transduct. Res.* **2002**, *22*, 315-31.

(25) Luzhkov, V. B.; Osterberg, F.; Aqvist, J. *FEBS Lett.* **2003**, *554*, 159-64.

(26) Lenaeus, M. J.; Vamvouka, M.; Focia, P. J.; Gross, A. *Nat. Struct. Mol. Biol.* **2005**, *12*, 454-9.

(27) Mecozzi, S.; West, A. P., Jr.; Dougherty, D. A. *Proc. Natl. Acad. Sci. USA* **1996**, *93*, 10566-71.

(28) Mecozzi, S.; West, A. P., Jr.; Dougherty, D. A. *J. Am. Chem. Soc.* **1996**, *118*, 2307-2308.

(29) Dougherty, D. A. *Science* **1996**, *271*, 163-8.

(30) Ma, J. C.; Dougherty, D. A. *Chem. Rev.* **1997**, *97*, 1303-1324.

(31) Nowak, M. W.; Kearney, P. C.; Sampson, J. R.; Saks, M. E.; Labarca, C. G.; Silverman, S. K.; Zhong, W.; Thorson, J.; Abelson, J. N.; Davidson, N.; *et al*. *Science* **1995**, *268*, 439-42.

(32) Leo, A.; Hansch, C.; Elkins, D. *Chemical Reviews* **1971**, *71*, 525-616.

(33) Zhong, W.; Gallivan, J. P.; Zhang, Y.; Li, L.; Lester, H. A.; Dougherty, D. A. *Proc. Natl. Acad. Sci. USA* **1998**, *95*, 12088-93.

(34) Beene, D. L.; Brandt, G. S.; Zhong, W.; Zacharias, N. M.; Lester, H. A.; Dougherty, D. A. *Biochemistry* **2002**, *41*, 10262-9.

(35) Mu, T. W.; Lester, H. A.; Dougherty, D. A. *J. Am. Chem. Soc.* **2003**, *125*, 6850-1.

(36) Lummis, S. C.; D, L. B.; Harrison, N. J.; Lester, H. A.; Dougherty, D. A. *Chem. Biol.* **2005**, *12*, 993-7.

(37) Padgett, C. L.; Hanek, A. P.; Lester, H. A.; Dougherty, D. A.; Lummis, S. C. *J. Neurosci.* **2007**, *27*, 886-92.

(38) McMenimen, K. A.; Petersson, E. J.; Lester, H. A.; Dougherty, D. A. *ACS Chem. Biol.* **2006**, *1*, 227-34.

(39) Nowak, M. W.; Gallivan, J. P.; Silverman, S. K.; Labarca, C. G.; Dougherty, D. A.; Lester, H. A. *Methods Enzymol.* **1998**, *293*, 504-29.

(40) Li, L.; Zhong, W.; Zacharias, N.; Gibbs, C.; Lester, H. A.; Dougherty, D. A. *Chem. Biol.* **2001**, *8*, 47-58.

(41) Vossmeyer, T.; Jia, S.; Delonno, E.; Diehl, M. R.; Kim, S. H.; Peng, X.; Alivisatos, A. P.; Heath, J. R. *J. Appl. Phys.* **1998**, *84*, 3664-3670.

(42) Spruce, A. E.; Standen, N. B.; Stanfield, P. R. *J. Physiol.* **1987**, *393*, 467-78.

(43) Spassova, M.; Lu, Z. *J. Gen. Physiol.* **1998**, *112*, 211-21.

(44) Brejc, K.; van Dijk, W. J.; Klaassen, R. V.; Schuurmans, M.; van der Oost, J.; Smit, A. B.; Sixma, T. K. *Nature* **2001**, *411*, 269-76.

(45) Williams, J. H. *Accounts Chem. Res.* **1993**, *26*, 593-598.

(46) Shepodd, T. J.; Petti, M. A.; Dougherty, D. A. *J. Am. Chem. Soc.* **1988**, *110*, 1983-1985.

(47) Craven, I. E.; Hesling, M. R.; Laver, D. R.; B., L. P.; Ritchie, G. L. D.; Vrbancich, J. *J. Phys. Chem.* **1989**, *93*, 627-631.

(48) Radzicka, A.; Pedersen, L.; Wolfenden, R. *Biochemistry* **1988**, *27*, 4538-41.

(49) Hille, B. *J. Gen. Physiol.* **1967**, *50*, 1287-302.

(50) Kumpf, R. A.; Dougherty, D. A. *Science* **1993**, *261*, 1708-10.

(51) Dunbrack, R. L., Jr.; Cohen, F. E. *Protein Sci.* **1997**, *6*, 1661-81.

(52) Heginbotham, L.; LeMasurier, M.; Kolmakova-Partensky, L.; Miller, C. *J. Gen. Physiol.* **1999**, *114*, 551-60.

(53) Ahern, C. A.; Eastwood, A. L.; Lester, H. A.; Dougherty, D. A.; Horn, R. *J. Gen. Physiol.* **2006**, *128*, 649-57.

(54) Pangborn, A. B.; Giardell, M. A.; Grubbs, R. H.; Rosen, R. K.; Timmers, F. J. *Organometallics* **1996**, *15*, 1518-1520.

Chapter III

CALCIUM BLOCK OF SINGLE SODIUM CHANNELS: ROLE OF A PORE-LINING AROMATIC RESIDUE

Extracellular Ca^{2+} ions cause a rapid block of voltage-gated Na^+ channels, manifest as an apparent reduction of the amplitude of single-channel currents. Here the influence on both single-channel conductance and Ca^{2+} block of Tyr401 in the Na^+ channel isoform $Na_V1.4$ from rat was examined. One possible explanation for the link between Ca^{2+} block and this tyrosine is that the cationic blocker and the aromatic residue interface through a cation-π interaction. To test this hypothesis the attraction between small metal cations (Na^+ and Ca^{2+}) and this residue was explored using a series of fluorinated derivatives of phenylalanine incorporated at this position. As described in chapter 2, increasing fluorination decreases the strength of the possible cation-π interaction, which would be evidenced by reduced single-channel conductance or pore block. The results show a monotonic decrease in Ca^{2+} block as the aromatic ring is increasingly fluorinated, a result in accord with a cation-π interaction between Ca^{2+} and the aromatic ring. This decrease occurred without a change of single-channel conductance, consistent with a greater electrostatic effect of the π system on divalent than on monovalent cations. High-level quantum mechanical calculations show that Ca^{2+} ions likely do not bind directly to the aromatic ring because of the substantial energetic penalty of dehydrating a Ca^{2+} ion. However, the complex of a Ca^{2+} ion with its inner hydration shell, $Ca^{2+}(H_2O)_6$, interacts

electrostatically with the aromatic ring in a way that affects the local concentration of Ca^{2+} ions in the extracellular vestibule.

Introduction

Voltage-gated Na^+ channels are transmembrane proteins involved critically in a variety of physiological functions, including muscle contraction, generation of action potentials in neurons, and secretion of neurotransmitters and hormones. These channels control the diffusion of Na^+ ions across the cell membrane in response to changes of transmembrane potential. When open, ion channels allow high-ionic fluxes while discriminating among ions based on charge and size. Understanding the basis of Na^+ permeation requires the identification of amino acids that form the selectivity filter, a narrow region of the pore where ions are partially dehydrated. As in structurally similar K^+ and Ca^{2+} channels, Na^+ channels have a pore or "P" region, a reentrant loop between the fifth and sixth transmembrane spanning segments in each of four homologous domains (figure 3.1). This P region houses the selectivity filter. In Na^+ channels there are four key residues responsible for determining the selectivity of Na^+ over other cations (boxed in figure 3.1). These resides, one from each domain (D), are aspartate in D1, glutamate in D2, lysine in D3, and alanine in D4. This sequence is referred to as DEKA [1]. Mutation of any of these residues alters the channel's selectivity.

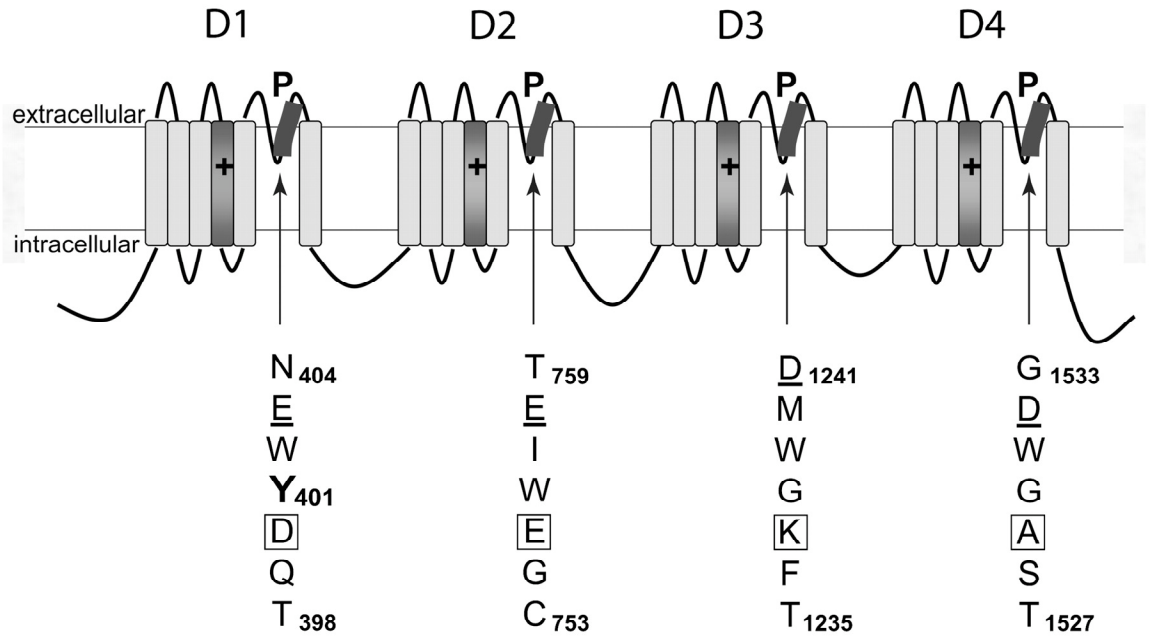

Figure 3.1. Topology of a voltage-gated Na^+ channel. Na^+ channels are composed of four domains (D1-D4), each with six transmembrane segments (S1-S6). S4 is the primary component of the voltage sensor (**+**), and the loop between S5-S6 is the pore (P) region. The amino acid sequence of the highlighted portion of the pore is shown below each domain. The DEKA ring is outlined in blocks, the outer negative ring underlined. Tyr401 (bold) in D1 is one residue above the DEKA ring.

The side chain of lysine (D3) is perhaps the most important player of DEKA. Changing from DEKA to DEAA eliminates selectivity among monovalent cations (Li^+, Na^+, K^+, Rb^+, Cs^+) and enhances permeability to divalent cations (Mg^{2+}, Ca^{2+}, Ba^{2+}) [1-5]. Enhanced Ca^{2+} permeation is obtained for all charge-altering substitutions of lysine (D3), but not by substitution with a charge-preserving arginine [2]. By contrast, wild-type Na^+ channels are typically blocked by extracellular Ca^{2+} ions. The apparent blocking affinity is strongly correlated with the overall negative charge of residues at the DEKA positions, establishing an important role of electrostatics [3]. The close relationship between

selectivity and block in these studies suggests that external Ca^{2+} block occurs at or near the DEKA ring [5].

Single-channel measurements have shown that block by extracellular Ca^{2+} is voltage-dependent and fast, manifest as an apparent reduction of single-channel current amplitude. Estimates of the inhibition constant range between 10 and 35 mM, with the blocking site apparently located 20% to 30% of the way into the transmembrane electric field [3,6-11]. A separate effect of changing external Ca^{2+} concentration ($[Ca^{2+}]$) is a shift in the activation gating range for Na^+ channels. This phenomenon has been ascribed to Ca^{2+} ions screening and/or binding to negative surface charges that influence the voltage-sensing mechanism [12].

Charge-altering mutations involving either DEKA or a more extracellular ring of negatively charged residues (underlined residues EEDD in figure 3.1) strongly reduce block by the guanidinium toxins tetrodotoxin (TTX) and saxitoxin (STX). Mutations of residues adjacent to these two charged rings typically have smaller effects, if any, on toxin block. These experiments suggest that the charged rings create part of the extracellular mouth or pore wall of the Na^+ channel [13]. In addition, neutralizing any negative residue causes a decrease in single-channel conductance, consistent with the idea that the negative charges act to concentrate cations in the extracellular vestibule of the pore [13]. Nevertheless, the influence of charged vestibule residues on Na^+ permeation cannot be explained entirely by the charges of these residues [2,14,15].

Charged residues are not the only determinants of permeation and pore block. An aromatic residue in D1, either tyrosine or phenylalanine, is found exclusively in Na^+

channels that have nanomolar affinity for TTX block [16-20]. This residue, Tyr401 in $Na_V1.4$, is located between the charged rings in the primary sequence (figure 3.1). Mutating this residue to cysteine, its homolog in the TTX-resistant cardiac channel $Na_V1.5$, results in a decrease in TTX sensitivity as well as in single-channel conductance [16,17]. The lowered conductance is similar in magnitude to that found in human $Na_V1.5$ [16,17]. Interestingly, the converse mutation in human $Na_V1.5$ (Cys374Tyr) produces no change in single-channel conductance [17]. This residue also affects Ca^{2+} block. Single-channel recording shows that $Na_V1.4$ is more sensitive to Ca^{2+} block than $Na_V1.5$ [21,22]; however see Ravindran, Schild, and Moczydlowski and Sheets and Hanck for an alternative interpretation [8,9]. This observation leads naturally to the question of how a hydrophobic aromatic residue could enhance the pore block of a small metal cation. One possibility is an electrostatic attraction between the π electrons of the aromatic ring and the cationic blocker.

The intention of the work presented in this chapter is not to explore the isoform differences that might affect permeation or Ca^{2+} block. Rather the focus is on residue 401 of rat $Na_V1.4$ and asking (i) whether a cation-π interaction is a contributing factor, based on experimental data, and (ii) whether such an interaction between a metal cation and an aromatic ring can be rationalized theoretically in an aqueous environment.

Results

Outside-out patches from oocytes were used to measure single-channel Na^+ currents. Figure 3.2A shows representative single-channel currents of the mutant Tyr401Phe in

response to a depolarization to −50 mV (arrow), using an extracellular solution containing 2 mM Ca^{2+}. This mutant was created by standard mutagenesis and serves as our control for unnatural amino acid substitutions. The data in figure 3.2A were converted into an amplitude histogram that was fit by a sum of two Gaussian functions (figure 3.2B). Notice the slight excess of points between the two prominent peaks, largely a consequence of a single opening at a subconductance level. The mean current level was estimated as the difference between the means of each Gaussian function, −1.9 pA at this membrane potential. The prolonged open durations in our experiments are a consequence of internal modification by fenvalerate, which does not affect the single-channel conductance [23]. In agreement with this, figure 3.2C shows indistinguishable amplitudes of single-channel currents of wild-type $Na_V1.4$ recorded without (open squares) and with (triangles) 20 μM fenvalerate added to the pipette, in this case in the absence of added Ca^{2+}.

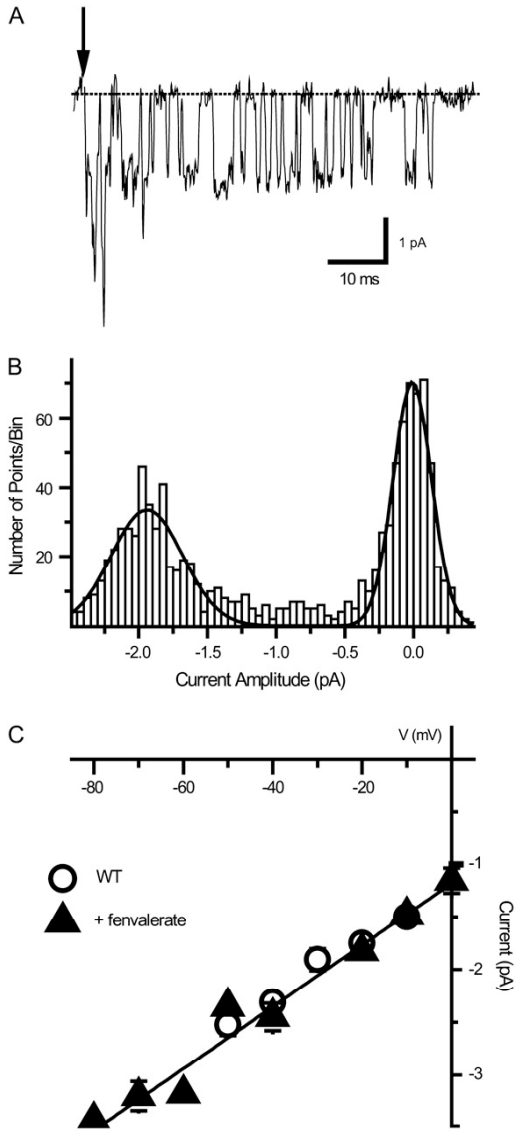

Figure 3.2. Representative single-channel recording, histogram analysis, and current-voltage relationship. A) Single-channel currents of Tyr401Phe, with 2 mM Ca^{2+} in response to a 30 ms depolarization (arrow) to −50 mV. Prolonged open durations are due to the effects of 10 μM intracellular fenvalerate. B) Data from figure 3.2A converted to an amplitude histogram and fit by a sum of two Gaussian functions. The single-channel current amplitude is −1.9 pA at this membrane potential. C) Single-channel amplitude versus voltage of wild-type rat $Na_V1.4$ recorded without (open squares) and with (triangles) 10 μM internal fenvalerate; 0 mM Ca^{2+}. Data from 2-5 patches at each membrane potential. Fenvalerate shifts the activation range in the hyperpolarizing direction but does not change the single-channel current amplitude. The regression line was from the fit to the data for fenvalerate.

Figure 3.3 shows representative single-channel openings at −60 mV, in either 0.1 (below) or 10 mM external Ca^{2+} (above). Raising the external [Ca^{2+}] reduces the amplitude of single-channel currents with phenylalanine incorporated at position 401 (figure 3.3A) due to Ca^{2+} block [3,6-8,11,21,22]. Figure 3.3B shows that Ca^{2+} also blocks when the trifluorinated mutant 3,4,5-F_3-phenylalanine is incorporated at this site, although less effectively (arrow/dashed line shows current amplitude for the Tyr401Phe mutant in panel 3.3A). Trifluorination approximately abolishes the negative electrostatic potential of an aromatic ring [24,25] without significantly affecting hydrophobicity, polarizability, or shape, suggesting that the change in electrostatics is responsible for the relief of Ca^{2+} block in this experiment. Insets show color-coded electrostatic potential surfaces of benzene and the trifluorinated derivative. On this color scale red, blue, and green indicate negative, positive, and zero electrostatic potential, respectively. By contrast to the effect on Ca^{2+} block, the single-channel conductance in 0.1 mM extracellular Ca^{2+} was not significantly different among the fluorinated variants of phenylalanine at position 401, ranging between 23.2 ± 2.2 pS for 4-F_1-phenylalanine and 25.9 ± 1.6 pS for 3,5-F_2-phenylalanine (legend for figure 3.4). This result is consistent with a greater effect of the negative electrostatic potential on the local concentration of Ca^{2+} ions than on that of Na^+ ions at the entrance of the selectivity filter.

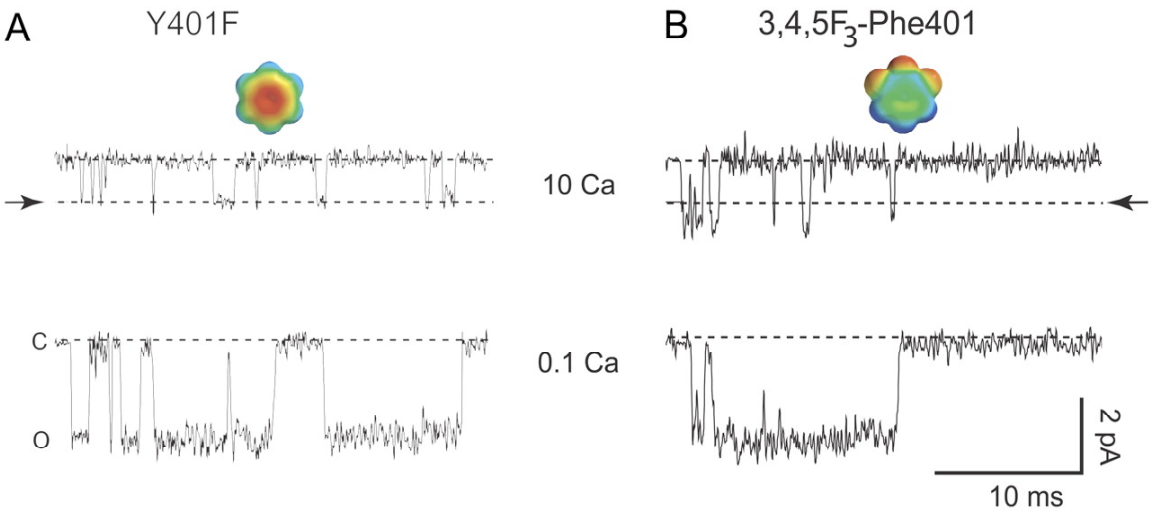

Figure 3.3. Fluorination of phenylalanine at position 401 reduces sensitivity of the channel to Ca^{2+} block. Single-channel currents in response to a depolarization to −60 mV in either 10 or 0.1 external Ca^{2+}. Openings are downward. A) Single-channel recordings of the mutant Tyr401Phe. Raising the external [Ca^{2+}] from 0.1 to 10 mM Ca^{2+} reduces the amplitude of the single-channel current. B) Currents of the mutant 3,4,5-F_3-phenylalanine. The two channel constructs have similar current amplitudes in 0.1 mM Ca^{2+}. However, fluorination of phenylalanine at position 401 relieves Ca^{2+} block. Arrow shows the current amplitude of Tyr401Phe in 10 mM Ca^{2+} (mean of 4 patches). Insets show color-coded electrostatic surfaces of benzene and 3,4,5-F_3-benzene (blue is +20 kcal/mol, red is −20 kcal/mol).

Single-channel current-voltage relationships for phenylalanine at position 401 and three fluorinated mutants are shown in figure 3.4 at three different Ca^{2+} concentrations, 0.1 mM (open circles), 2 mM (filled squares) and 10 mM (open triangles). Because the patches tended to be unstable in the absence of added Ca^{2+} and because the amplitudes of single-channel currents were indistinguishable between 0 and 0.1 mM Ca^{2+}, 0.1 mM Ca^{2+} was used as the unblocked control. The single-channel current-voltage relationships in

0.1 mM extracellular Ca^{2+} were fit by straight lines, and the fractional block at higher $[Ca^{2+}]$ is represented as

$$\frac{I([Ca^{2+}],V)}{I([Ca^{2+}]=0.1\,\mathrm{mM},V)}=\frac{K(V)}{K(V)+[Ca^{2+}]}.$$

The voltage-dependent inhibition constant $K(V)$, based on a simple Woodhull-type model,[26] is defined as

$$K(V)=K_j(0)\exp(\frac{\delta zFV}{RT}),$$

where V is the membrane potential, $K_j(0)$ is the inhibition constant at 0 mV for a mutant containing j fluorine atoms (j = 0, 1, 2, 3) on the phenylalanine incorporated at position 401, δ is the effective fraction through the electric field for a blocker with valence z, and RT/F = 25 mV at room temperature. For the least squares fit, the value of δ was constrained to be identical for all mutants in this study. The monotonic effect of fluorination on Ca^{2+} block is evident from the block observed at 2 mM Ca^{2+} and from the estimated values of $K_j(0)$ (legend of figure 3.4 and figure 3.5). The curvature of the current-voltage relationship, most obvious at 10 mM Ca^{2+}, is indicative of the voltage dependence of the block. The estimated value of δ was 0.18 ± 0.03, comparable to previous estimates for Ca^{2+} block of single Na^{+} channels.[8,9,11] The curvature of the current-voltage relationship is noticeably muted in the trifluorinated mutant (figure 3.4D). Although only speculation can be drawn on this observation, it suggests either that the blocking site is more superficial in this mutant or that trifluorination reduces the local

concentration of cations (see discussion) whose distribution might be affected by membrane potential.

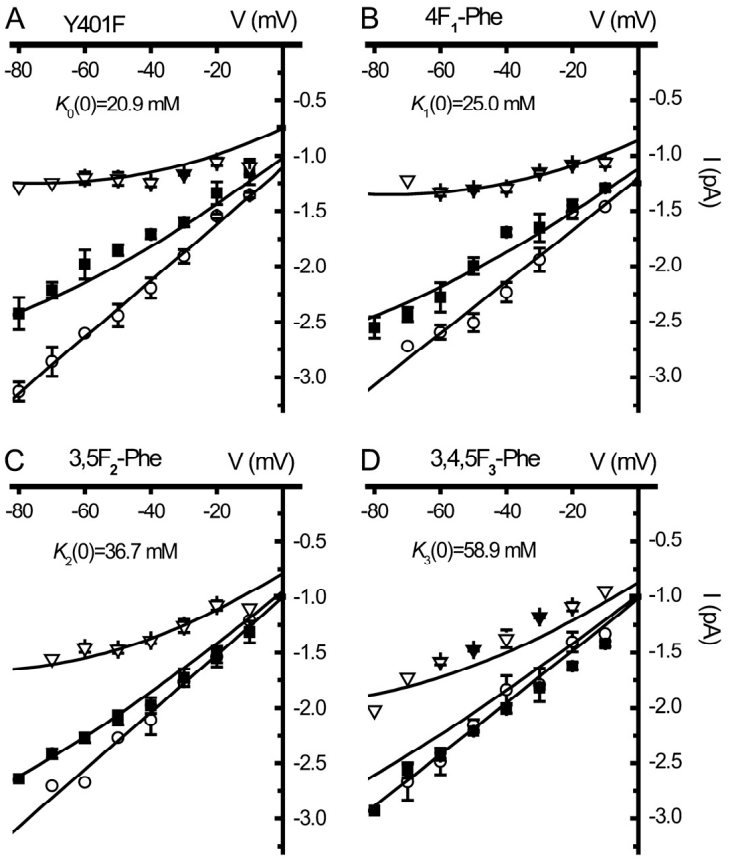

Figure 3.4. Single-channel current-voltage relationships of the phenylalanine mutants at position 401. Ca^{2+} concentrations are 0.1 mM (open circles), 2 mM (filled squares), and 10 mM Ca^{2+} (open triangles). Each symbol represents data from 2-8 patches. Data for 0.1 mM Ca^{2+} were fit by straight lines (slopes: 25.3 ± 0.8, 23.2 ± 2.2, 25.9 ± 1.6, 23.4 ± 1.6 pS, for Tyr401Phe, 4-F-Phe, 3,5-F_2-Phe, and 3,4,5-F_3-Phe, respectively) while fractional block at higher [Ca^{2+}] was fit by a Woodhull model (see results). The curvature of the current-voltage relationship illustrates the voltage-dependent block. The effective fraction through the electric field (δ) for Ca^{2+} block, constrained to be the same for each Phe variant, was 0.18 ± 0.03. Note the decrease in Ca^{2+} block with increased fluorination. The estimates of inhibition constants were $K_0(0)$ = 20.9 ± 2.8 mM, $K_1(0)$ = 25.0 ± 3.2 mM, $K_2(0)$ = 36.7 ± 5.1 mM, and $K_3(0)$ = 58.9 ± 9.2 mM.

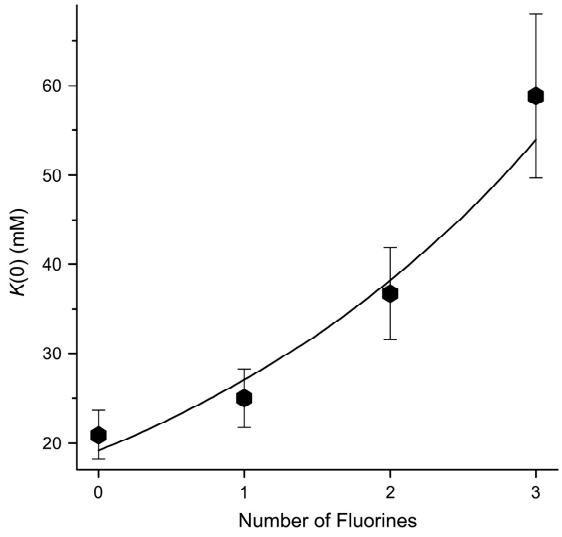

Figure 3.5. Exponential effect of fluorination on the inhibition constant for Ca^{2+} block. The data points are the estimates (± standard error) of the inhibition constants at 0 mV, i.e., $K_j(0)$, from figure 3.4 (j is the number of fluorines). The best-fit theoretical curve is $K_j(0) = 19.2\exp(0.344\,j)$ mM.

Discussion

The side chains of amino acids that line the extracellular aqueous vestibule of a Na^+ channel pore could affect permeation in a variety of ways, primarily by consequences on the local concentration or hydration of permeant ions and blockers. Amino acid side chains may, for example, interact directly (i.e., within the range of van der Waals forces) with ions in the vestibule. For permeant ions, such contacts would generally have to be brief to be consistent with the high transport rate through open channels. Vestibule-lining side chains could also contribute to the electrostatic potential experienced by ions. Finally, the protein lining of the vestibule effectively decreases the local dielectric constant compared to water by presenting a dielectric boundary.[27,28] Deeper residues that

line the selectivity filter presumably have the most intimate contact with permeant ions, and also perhaps with small pore blockers. Large effects on permeation or block in Na^+ channels are caused by mutations of either the DEKA selectivity ring or of the outer EEDD ring of negative charges.[1-5,13,14,18,29-32] The main exception to these generalities involves the aromatic residue Tyr401 in rat $Na_V1.4$ and aligned residues in other isoforms. A neutral, nonaromatic substitution of this residue decreases TTX affinity by as much as three orders of magnitude.[16,17,19] A substantial component of cationic TTX's binding energy is due to an electrostatic interaction with the π system of Tyr401,[33] discussed in detail in chapter 4, suggesting that the aromatic ring is oriented to face the permeation pathway. This raises the possibility that other extracellular cations, especially Na^+ and Ca^{2+}, are also attracted to the negative electrostatic potential on the aromatic face of this residue.

The electrostatic potential projecting out from the center of a benzene ring in aqueous solution, and the effects on it of fluorination, are shown in figure 3.6A. These estimates agree with experimental and theoretical analyses showing that trifluorination effectively neutralizes the quadrupole moment.[24,25] In fact the quadrupole moment is slightly reversed in sign by trifluorination (figure 3.6A), in agreement with experimental observations.[34] The results of the present study show that systematic fluorination of the aromatic ring progressively reduces Ca^{2+} block without affecting the single-channel conductance for Na^+ ions. Here it is explored whether these results are consistent with an electrostatic mechanism.

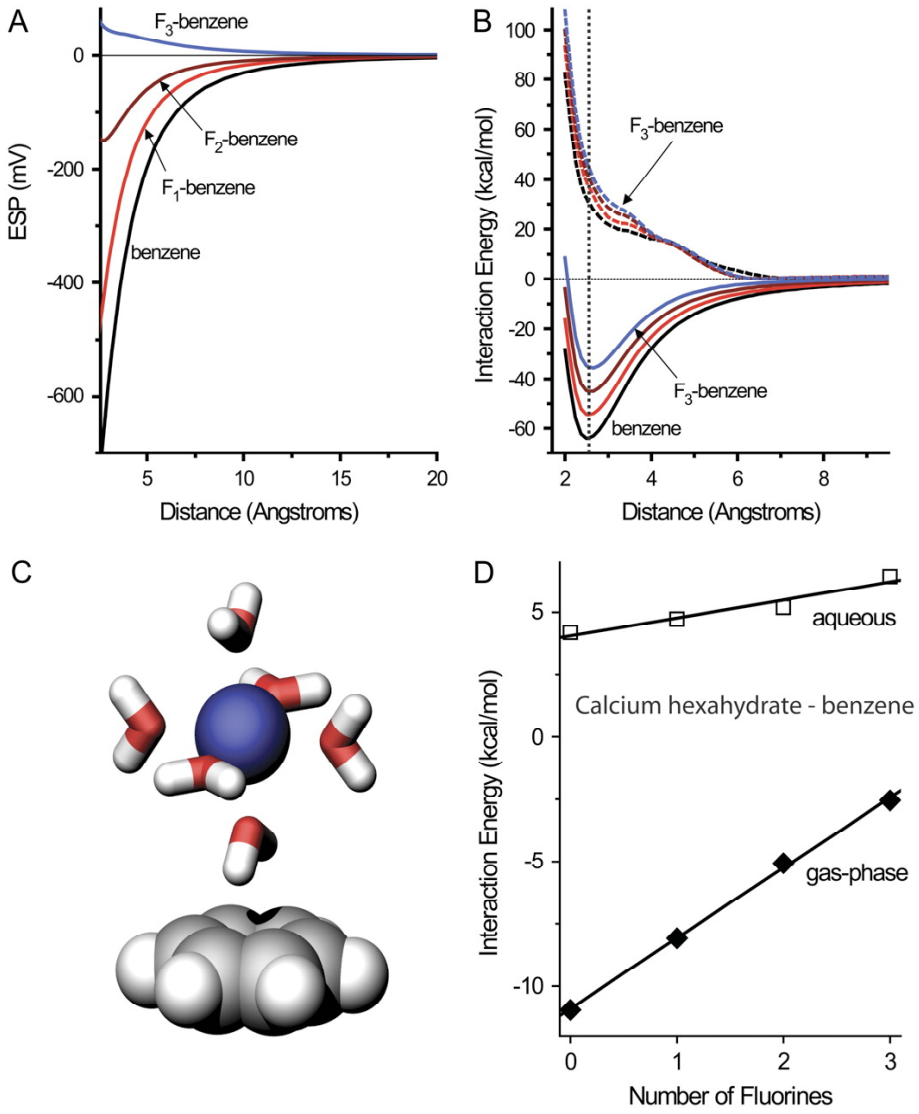

Figure 3.6. Electrostatic potentials and Ca^{2+} binding energies. A) Electrostatic potential for benzene and its fluorinated derivatives. Electrostatic potential was determined along the C_6 axis projecting from the center of the benzene ring using a polarizable continuum model of water. B) Interaction energy of a Ca^{2+} ion with benzene and fluorinated derivatives along the C_6 axis. Gas-phase energies are plotted as solid lines, and aqueous energies as dashed lines. Values were calculated in 0.5 Å increments from 2 to 4 Å and in 1 Å increments for greater distances. The vertical dotted line is set at the minimum-energy distance between the Ca^{2+} ion and benzene. This line shows that progressive fluorination monotonically destabilizes the attraction of Ca^{2+} for the aromatic ring. C) Optimized geometry of the complex between $Ca^{2+}(H_2O)_6$ and a benzene ring. D) Interaction energy between $Ca^{2+}(H_2O)_6$ and benzene, calculated in gas or in water at the optimized geometry. The energies increase linearly with the number of added fluorines.

A negative electrostatic potential on the aromatic face of residue at position 401 could enhance Ca^{2+} block in two ways. First, a Ca^{2+} ion might bind directly (essentially at van der Waals contact) to the face of the aromatic ring where it would prevent the flux of Na^{+} ions. Second, the negative potential might increase the probability that a Ca^{2+} ion would be found in the vicinity of the blocking site without direct contact between the metal ion and the aromatic ring. The second scenario is favored because direct binding of Ca^{2+} to a simple aromatic ring would require partial dehydration of the Ca^{2+} ion, an energetically costly task for the diffuse quadrupole moment of an aromatic ring.[35] To show this explicitly, the binding energy of a Ca^{2+} ion to benzene was determined using high-level (HF/6-31++G**) *ab initio* calculations. The optimized position for Ca^{2+} in the gas phase was on the C_6 symmetry axis of the benzene ring 2.54 Å from its center (figure 3.6B). Although the interaction energy is highly favorable at this position in the gas phase, −64 kcal/mol, the Gibbs free energy for Ca^{2+} binding in an aqueous environment is highly unfavorable, +31 kcal/mol, a consequence of the substantial mismatch between the hydration energies of a Ca^{2+} ion ($\Delta G_{Ca(hyd)}$ = −390 kcal/mol) and benzene ($\Delta G_{Benz(hyd)}$ = −1.5 kcal/mol). This result is presented graphically in figure 3.6B by plotting the calculated free energy of the interaction of a Ca^{2+} ion with benzene as a function of distance from the center of the benzene ring. The solid and dotted lines represent the interaction energy in the gas phase and in aqueous solution, respectively. Benzene (black) attracts a Ca^{2+} ion in the gas phase and repels it in water; this conclusion holds at any distance greater than 2 Å from the center of the aromatic ring.

Figure 3.6B also shows the effect of fluorination on these interaction energies. The vertical dotted line highlights these energies at the optimized position of Ca^{2+} in the gas

phase. Both in gas and in aqueous solution, fluorination diminishes the energy of interaction between Ca^{2+} and benzene at distances closer than 4.5 Å. Note that at larger distances water molecules would be able to penetrate the space between the cation and the aromatic ring. Therefore, although a benzene ring has a net repulsive effect on a Ca^{2+} ion in water, the repulsion is exacerbated by fluorinating the ring. From the point of view of a cation, it could be that the negative electrostatic potential ameliorates the hydrophobic (unattractive) properties of the aromatic side chain. These calculations strongly suggest that in aqueous solution Ca^{2+} ions do not make direct contact with the aromatic ring of Tyr401 (or phenylalanine at this site), but that fluorination nevertheless has an electrostatic effect on Ca^{2+} ions in the vicinity of the ring. To rationalize the unfavorable interaction energies in water, an alternative viewpoint was explored, namely that an appropriate treatment of the interaction between an aromatic ring and Ca^{2+} must include explicit water, namely the inner hydration shell of the cation.

The substantial desolvation penalty for a Ca^{2+} ion, approximately 30 kcal/mol to remove one water molecule from the inner hydration shell, indicates that when interacting with an aromatic ring, Ca^{2+} will maintain this hydration shell of 6 waters.[36,37] Nevertheless, the charge of the cation will orient and polarize the hydration waters so that the hydrated complex, $Ca^{2+}(H_2O)_6$, can interact favorably with the face of an aromatic ring.[38,39] In essence, $Ca^{2+}(H_2O)_6$ is a larger, more polarizable cation than an isolated Ca^{2+} ion. The increased size and delocalized charge are expected to decrease the interaction energy with a benzene ring.[39-41] Figure 3.6C shows the octahedral arrangement of waters in $Ca^{2+}(H_2O)_6$ and the optimized geometry of this metal-water complex with benzene. The Ca^{2+} ion lies 5.70 Å from the centroid of benzene at an angle of 8.9° from the normal of

the aromatic ring plane. The interaction energies of $Ca^{2+}(H_2O)_6$ with benzene in this optimized geometry are −10.6 and +3.7 kcal/mol in gas and water, respectively, significantly smaller in magnitude than the energies observed for an isolated Ca^{2+} ion, in part because of the greater distance between $Ca^{2+}(H_2O)_6$ and the benzene ring. The effect of fluorinating the benzene ring on the binding energy of $Ca^{2+}(H_2O)_6$ was calculated at the fixed, optimized geometry shown in figure 3.6C. These interaction energies are plotted in figure 3.6D as a function of the number of fluorine atoms appended to the benzene ring. As in the case of a nonhydrated Ca^{2+} ion (vertical dotted line in figure 3.6B), the interaction energy increases monotonically as the benzene ring is progressively fluorinated (figure 3.6D). The relationship is steeper when calculated in the gas phase.

The energetic effect of altering the benzene ring, a linear increase in interaction energy with fluorination (figure 3.6D), leads to a prediction of the consequences of fluorination on Ca^{2+} block. Figure 3.7 shows a molecular model of the outer vestibule of the pore of the Na^+ channel,[42] with $Ca^{2+}(H_2O)_6$ aligned in its optimized geometry with the aromatic ring of Tyr401. The side chains of the DEKA ring are shown below Tyr401. The transparent, solvent-accessible surface of the hydrated Ca^{2+} ion is also shown. Previous modeling and experimental evidence suggest that the aromatic ring of Tyr401 faces the central axis of the pore,[33,42] and that a stable blocking site for Ca^{2+} is likely to be at the DEKA ring where it can interact with the two acidic side chains.[3] The structural model in figure 3.7, with $Ca^{2+}(H_2O)_6$ at a more superficial location near Tyr401, is also likely to be nonconductive for Na^+ ions because of both the substantial volume occupied by the hydrated metal ion and its charge. Therefore, this conformation is also a blocked state, albeit weaker presumably than the site at the DEKA ring. We propose that the aromatic

ring does not interact with this hydrated ion when it is in its deeper blocking site at the DEKA ring. Rather, the aromatic side chain affects the local concentration of Ca^{2+} ($[Ca^{2+}]_{local}$) in the immediate vicinity of this deeper site. Within the limits of reliability of the structural model in figure 3.7, a hydrated Ca^{2+} ion must pass near the aromatic face of Tyr401 on its way to its deeper site at the DEKA ring. The probability of finding $Ca^{2+}(H_2O)_6$ at the location shown in the figure can be expressed as

$$p_j = \frac{1}{1+\exp\left(\Delta G_j \big/ RT\right)},$$

where j is the number of fluorine atoms, $\Delta G_j = \Delta G_{\mathrm{Phe}_j} + \sum_k \Delta G_k$ is the free energy of $Ca^{2+}(H_2O)_6$ at that location, R is the universal gas constant, and T is the absolute temperature. $\Delta G_{\mathrm{Phe}_j}$ is the contribution to the free energy of the aromatic ring, and $\sum_k \Delta G_k$ represents all other contributions due to the environment in the vicinity of the aromatic side chain. If it is assumed that in this aqueous environment p_j is very low, due both to the low dielectric walls of the vestibule and to the positive energy contributed by the aromatic ring (figure 3.6D), then

$$p_j \simeq \exp\left(\frac{-\sum_k \Delta G_k}{RT}\right) \cdot \exp\left(\frac{-\Delta G_{\mathrm{Phe}_j}}{RT}\right).$$

The $[Ca^{2+}]_{local}$ is proportional to p_j, leading to the prediction that the ratio of inhibition constants $K_j(0)/K_0(0) = p_0/p_j = \exp\left(\frac{\Delta G_{\mathrm{Phe}_j} - \Delta G_{\mathrm{Phe}_0}}{RT}\right) = \exp\left(\frac{\Delta\Delta G_j}{RT}\right)$. Because

$\Delta\Delta G_j$ increases linearly with fluorination (figure 3.6D), this exponential relationship conforms exactly to our experimental results (figure 3.5).

It remains to be considered why the electrostatic effect of fluorinating the aromatic has little consequence on single-channel conductance. The primary reason, we propose, is that changes in electrostatic potential will have a larger effect on divalent Ca^{2+} ions than on the monovalent Na^+ ions that carry the inward current. Using the above quantum-mechanical approach for calculating the interaction energy of a Na^+ ion with benzene in water, it was found, for example, that trifluorinating benzene has a sixfold greater effect on $[Ca^{2+}]_{local}$ than on $[Na^+]_{local}$ at a distance of 4 Å from the center of the ring. Therefore the threefold increase in $K_j(0)$ for Ca^{2+} block between phenylalanine and 3,4,5-F_3-phenylalanine (figure 3.5) would correspond roughly to a 50% decrease in $[Na^+]_{local}$. This reduction would have only a moderate effect on single-channel current amplitude, because $[Na^+]$ has a nonlinear, saturating relationship with single-channel conductance.[11,14,43]

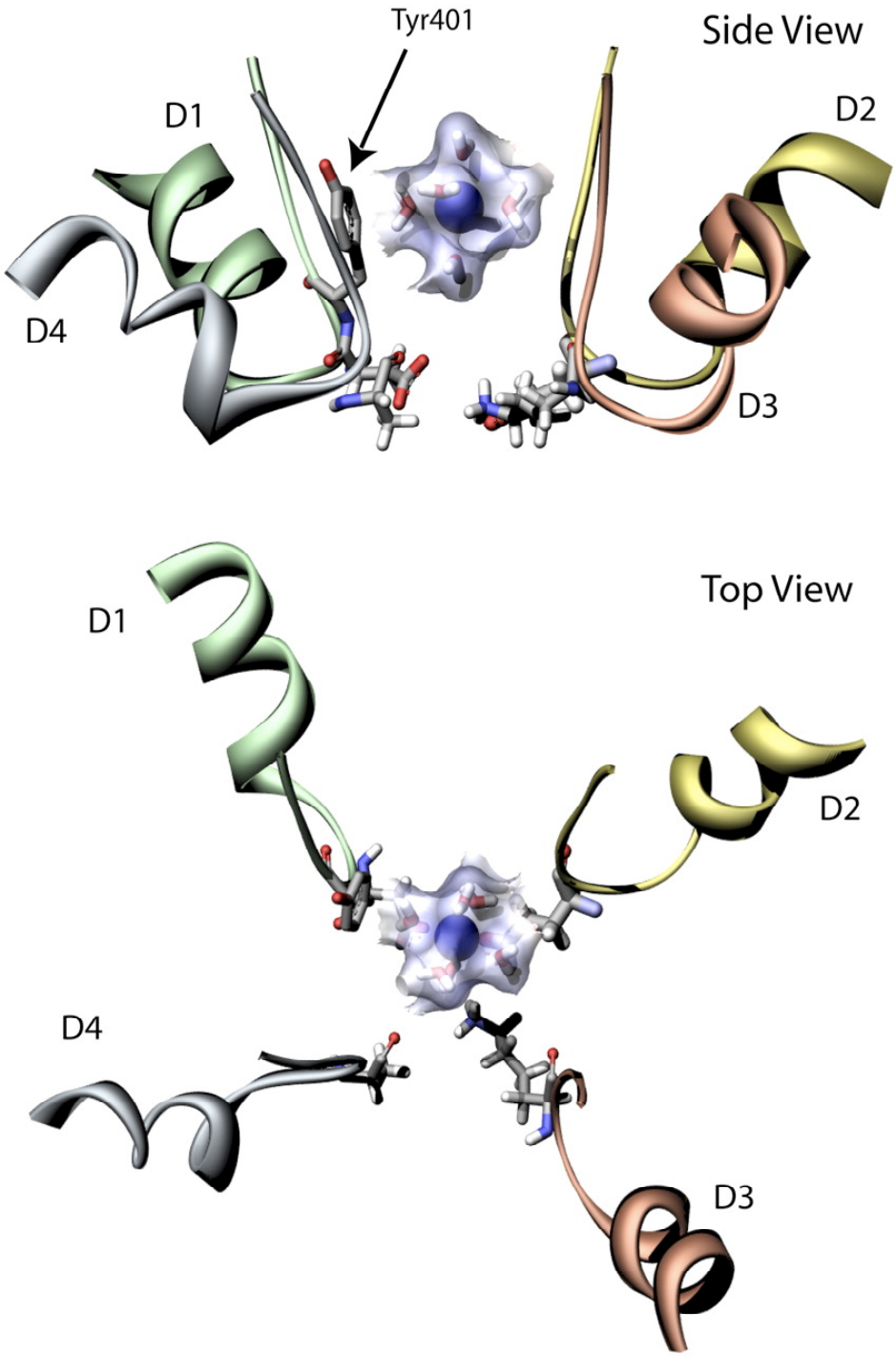

Figure 3.7. Model of the extracellular vestibule of the channel showing $Ca^{2+}(H_2O)_6$ in optimal apposition to Tyr401 (figure 3.6C). The molecular model[42] depicts part of the pore helix and pore loop from each domain of the Na^+ channel. The side chains of Tyr401 and the DEKA ring are rendered. $Ca^{2+}(H_2O)_6$ is shown enveloped by a transparent solvent-accessible surface.

The above analysis sidestepped the explicit role of the conserved negatively charged ring (EEDD, figure 3.1) that will tend to concentrate cations within the extracellular vestibule. Functional studies suggest that the negative electrostatic potential in the vestibule is in excess of −100 mV.[14,44] As was seen here, however, a more challenging task for the channel is to overcome the energetic burden for metal cations to leave the relative comfort of the extracellular solution and enter a cavity lined by low-dielectric protein. These calculations show that even in the presence of an electrostatic potential of −140 mV at a distance of 5.7 Å from a benzene ring (figure 3.6A), the aqueous environment remains unfavorable for Ca^{2+} (+15.3 kcal/mol) and only slightly favorable for Na^{+} (−0.24 kcal/mol). Nevertheless, neutralizing any of the EEDD charges has substantial effects on both cation block and single-channel conductance,[13,14,18,29,31] confirming a strong role for electrostatics.

The cation-π interaction has been examined extensively in the past two decades and is now known to play a significant energetic role in the interaction between organic cations and proteins, as well as between basic and aromatic side chains in proteins.[41,45,46] A previous study, however, found no evidence for a postulated cation-π interaction between the divalent cation Mg^{2+} and the aromatic side chain of a tryptophan residue in the NMDA receptor.[47] As was discussed here, this result may not be surprising when the cation is very small and highly charged. One feature of a strong cation-π interaction is the match of hydration energies between a large cation with its delocalized charge and an aromatic ring. In the absence of other energetic constraints the hydration mismatch between a Ca^{2+} ion and an aromatic ring precludes direct binding, in spite of a powerful electrostatic attraction. Nevertheless, a systematic reduction of blocking affinity for Ca^{2+}

was seen as the phenylalanine incorporated at position 401 is progressively fluorinated, a distinguishing characteristic of a cation-π mechanism. Although induction (polarization) energy makes an attractive energetic contribution for both monovalent and divalent cations with benzene,[48,49] the predominant consequences of fluorination arise from changes of the electrostatic interaction between the metal cation and the quadrupole moment of the aromatic ring.[24,50] In comparison to the threefold destabilization of Ca^{2+} block, incorporating 3,4,5-F_3-phenylalanine at position 401 destabilizes the organic pore-blocker TTX by 50-fold,[33] suggesting a more intimate interaction between an aromatic residue at this site and the larger toxin in its binding site (chapter 4).

Although this study reveals a modest role for a cation-π mechanism in the interaction between a Ca^{2+} ion and an aromatic residue at position 401, it does not address isoform differences between TTX-sensitive channels that have an aromatic residue at this position and TTX-resistant channels that have either a cysteine or a serine at position 401. Differences in Ca^{2+} block between these two classes of Na^+ channels is a disputed experimental observation[8,9,21,22] suggesting that other factors might contribute to functional differences between these types of channels. It is also worth bearing in mind that fluorination of phenylalanine at this site is a relatively minor perturbation of structure compared with mutating this residue into a cysteine. Notably, only two amino acids distinguish the outer vestibule residues of $Na_V1.4$, the TTX-sensitive channel studied here, and the TTX-resistant cardiac channel $Na_V1.5$. The latter isoform has a cysteine at the aligned position of Tyr401, and an arginine instead of an asparagine immediately adjacent to the outer ring of negative charge in D1. The asparagine-to-arginine substitution of this residue by itself causes a tenfold decrease in Ca^{2+} block in a TTX-

sensitive neuronal Na^+ channel,[3] suggesting another electrostatic determinant of the local concentration of Ca^{2+} ions in the outer vestibule. The relative roles of these two residues will undoubtedly lead to insights into mechanisms of permeation and block in Na^+ channels.

Conclusion

In summary, the study presented here demonstrates that an electrostatic cation-π interaction occurs between an aromatic side chain and Ca^{2+} ions within the outer mouth of a voltage-gated Na^+ channel. Using *in vivo* nonsense-suppression techniques to incorporate fluorinated-phenylalanine derivatives into $Na_V1.4$ at Tyr401, the attraction of the cation and the electronegative face of the aromatic residue was experimentally tested by recording on the single mutant channels. The cation-π interaction was found to be specific to the divalent cation Ca^{2+} and not the monovalent Na^+ since no change was observed in the single-channel conductance in the same mutant channels. High-level quantum mechanical calculations show that the interaction between Ca^{2+} and the aromatic ring is likely to occur with the hydrated cation.

Methods

The work in this chapter was a collaborative effort that included important contributions from Dr. Vincent Santarelli, Dr. Chris Ahern, and Dr. Richard Horn of the Jefferson

Medical College in Philadelphia, PA. Detailed methods for the experiments discussed in this chapter that were not performed by the author can be found in Santarelli *et al*.[51]

Unnatural Amino Acids and Molecular Biology

Phenylalanine-dCA, 3,5-F_2-phenylalanine-dCA, 3,4,5-F_3-phenylalanine-dCA were obtained as described in chapter 2. 3-F-Phenylalanine was a gift from Dr. Niki Zacharias, a former graduate student in the Dougherty laboratory. These aminoacylated dinucleotides were ligated to a modified tRNA from *Tetrahymena thermophila*, THG73, using T4 RNA ligase (New England Biolabs, Ipswich, MA).[52,53]

Acknowledgments

We thank Mary Y. Ryan for help with oocytes and molecular biology. This work was supported by grants from the NIH (GM079427 and NS34407).

References

(1) Heinemann, S. H.; Terlau, H.; Stuhmer, W.; Imoto, K.; Numa, S. *Nature* **1992**, *356*, 441-3.

(2) Favre, I.; Moczydlowski, E.; Schild, L. *Biophys. J.* **1996**, *71*, 3110-25.

(3) Schlief, T.; Schonherr, R.; Imoto, K.; Heinemann, S. H. *Eur. Biophys. J.* **1996**, *25*, 75-91.

(4) Tsushima, R. G.; Li, R. A.; Backx, P. H. *J. Gen. Physiol.* **1997**, *109*, 463-75.

(5) Sun, Y. M.; Favre, I.; Schild, L.; Moczydlowski, E. *J. Gen. Physiol.* **1997**, *110*, 693-715.

(6) Behrens, M. I.; Oberhauser, A.; Bezanilla, F.; Latorre, R. *J. Gen. Physiol.* **1989**, *93*, 23-41.

(7) Nilius, B. *J. Physiol.* **1988**, *399*, 537-58.

(8) Ravindran, A.; Schild, L.; Moczydlowski, E. *J. Gen. Physiol.* **1991**, *97*, 89-115.

(9) Sheets, M. F.; Hanck, D. A. *J. Physiol.* **1992**, *454*, 299-320.

(10) Sheets, M. F.; Scanley, B. E.; Hanck, D. A.; Makielski, J. C.; Fozzard, H. A. *Biophys. J.* **1987**, *52*, 13-22.

(11) Yamamoto, D.; Yeh, J. Z.; Narahashi, T. *Biophys. J.* **1984**, *45*, 337-44.

(12) Hille, B. *Ion Channels of Excitable Membranes*; Sunderland, MA: Sinauer Associates, 2001.

(13) Terlau, H.; Heinemann, S. H.; Stuhmer, W.; Pusch, M.; Conti, F.; Imoto, K.; Numa, S. *FEBS Lett.* **1991**, *293*, 93-6.

(14) Chiamvimonvat, N.; Perez-Garcia, M. T.; Tomaselli, G. F.; Marban, E. *J. Physiol.* **1996**, *491 (Pt. 1)*, 51-9.

(15) Khan, A.; Kyle, J. W.; Hanck, D. A.; Lipkind, G. M.; Fozzard, H. A. *J. Physiol.* **2006**, *576*, 493-501.

(16) Backx, P. H.; Yue, D. T.; Lawrence, J. H.; Marban, E.; Tomaselli, G. F. *Science* **1992**, *257*, 248-51.

(17) Chen, L. Q.; Chahine, M.; Kallen, R. G.; Barchi, R. L.; Horn, R. *FEBS Lett.* **1992**, *309*, 253-7.

(18) Penzotti, J. L.; Fozzard, H. A.; Lipkind, G. M.; Dudley, S. C., Jr. *Biophys. J.* **1998**, *75*, 2647-57.

(19) Satin, J.; Kyle, J. W.; Chen, M.; Bell, P.; Cribbs, L. L.; Fozzard, H. A.; Rogart, R. B. *Science* **1992**, *256*, 1202-5.

(20) Leffler, A.; Herzog, R. I.; Dib-Hajj, S. D.; Waxman, S. G.; Cummins, T. R. *Pflugers Arch.* **2005**, *451*, 454-63.

(21) Chahine, M.; Chen, L. Q.; Kallen, R. G.; Barchi, R. L.; Horn, R. *Biophys. J.* **1992**, *62*, 37-40.

(22) Weiss, R. E.; Horn, R. *Ann. N. Y. Acad. Sci.* **1986**, *479*, 152-61.

(23) Narahashi, T. *Adv. Neurol.* **1986**, *44*, 211-24.

(24) Mecozzi, S.; West, A. P., Jr.; Dougherty, D. A. *J. Am. Chem. Soc.* **1996**, *118*, 2307-2308.

(25) Williams, J. H. *Accounts Chem. Res.* **1993**, *26*, 593-598.

(26) Woodhull, A. M. *J. Gen. Physiol.* **1973**, *61*, 687-708.

(27) Islas, L. D.; Sigworth, F. J. *J. Gen. Physiol.* **2001**, *117*, 69-89.

(28) Sansom, M. S.; Smith, G. R.; Adcock, C.; Biggin, P. C. *Biophys. J.* **1997**, *73*, 2404-15.

(29) Noda, M.; Suzuki, H.; Numa, S.; Stuhmer, W. *FEBS Lett.* **1989**, *259*, 213-6.

(30) Chen, S.; Hartmann, H. A.; Kirsch, G. E. *J. Membr. Biol.* **1997**, *155*, 11-25.

(31) Chiamvimonvat, N.; Perez-Garcia, M. T.; Ranjan, R.; Marban, E.; Tomaselli, G. F. *Neuron* **1996**, *16*, 1037-47.

(32) Perez-Garcia, M. T.; Chiamvimonvat, N.; Marban, E.; Tomaselli, G. F. *Proc. Natl. Acad. Sci. USA* **1996**, *93*, 300-4.

(33) Santarelli, V. P.; Eastwood, A. L.; Dougherty, D. A.; Horn, R.; Ahern, C. A. *J. Biol. Chem.* **2007**, *282*, 8044-51.

(34) Vrbancich, J.; Ritchie, G. L. D. *J. Chem. Soc., Faraday Trans. 2* **1980**, *76*, 648-659.

(35) Gallivan, J. P.; Dougherty, D. A. *J. Am. Chem. Soc.* **2000**, *122*, 870-874.

(36) Asthagiri, D.; Pratt, L. R.; Paulaitis, M. E.; Rempe, S. B. *J. Am. Chem. Soc.* **2004**, *126*, 1285-9.

(37) Bakó, I.; Hutter, J.; Pálinkás, G. *J. Chem. Phys.* **2002**, *117*, 9838-9843.

(38) McFail-Isom, L.; Shui, X.; Williams, L. D. *Biochemistry* **1998**, *37*, 17105-11.

(39) Zaric, S. D.; Popovic, D. M.; Knapp, E. W. *Chemistry* **2000**, *6*, 3935-42.

(40) Kumpf, R. A.; Dougherty, D. A. *Science* **1993**, *261*, 1708-10.

(41) Chipot, C.; Maigret, B.; Pearlman, D. A.; Kollman, P. A. *J. Am. Chem. Soc.* **1996**, *118*, 2998-3005.

(42) Lipkind, G. M.; Fozzard, H. A. *Mol. Pharmacol.* **2005**, *68*, 1611-22.

(43) Begenisich, T. B.; Cahalan, M. D. *J. Physiol.* **1980**, *307*, 243-57.

(44) Hui, K.; McIntyre, D.; French, R. J. *J. Gen. Physiol.* **2003**, *122*, 63-79.

(45) Gallivan, J. P.; Dougherty, D. A. *Proc. Natl. Acad. Sci. USA* **1999**, *96*, 9459-64.

(46) Ma, J. C.; Dougherty, D. A. *Chem. Rev.* **1997**, *97*, 1303-1324.

(47) McMenimen, K. A.; Petersson, E. J.; Lester, H. A.; Dougherty, D. A. *ACS Chem. Biol.* **2006**, *1*, 227-34.

(48) Cubero, E.; Luque, F. J.; Orozco, M. *Proc. Natl. Acad. Sci. USA* **1998**, *95*, 5976-80.

(49) Tsuzuki, S.; Uchimaru, T.; Mikami, M. *J. Phys. Chem. A* **2003**, *107*, 10414-10418.

(50) Mecozzi, S.; West, A. P., Jr.; Dougherty, D. A. *Proc. Natl. Acad. Sci. USA* **1996**, *93*, 10566-71.

(51) Santarelli, V. P.; Eastwood, A. L.; Dougherty, D. A.; Ahern, C. A.; Horn, R. *Biophys. J.* **2007**, *93*, 2341-9.

(52) Nowak, M. W.; Kearney, P. C.; Sampson, J. R.; Saks, M. E.; Labarca, C. G.; Silverman, S. K.; Zhong, W.; Thorson, J.; Abelson, J. N.; Davidson, N.; *et al. Science* **1995**, *268*, 439-42.

(53) Nowak, M. W.; Gallivan, J. P.; Silverman, S. K.; Labarca, C. G.; Dougherty, D. A.; Lester, H. A. *Methods Enzymol.* **1998**, *293*, 504-29.

Chapter IV

A CATION-π INTERACTION DISCRIMINATES AMONG SODIUM CHANNELS THAT ARE EITHER SENSITIVE OR RESISTANT TO TETRODOTOXIN BLOCK

Voltage-gated Na^+ channels control the upstroke of the action potential in excitable cells of nerve and muscle tissue, making them ideal targets for exogenous toxins that aim to squelch electrical excitability. One such toxin, tetrodotoxin (TTX), blocks Na^+ channels with nanomolar affinity only when an aromatic phenylalanine or tyrosine residue is present at a specific location in the external vestibule of the ion-conducting pore. Interestingly, this specific location is the same aromatic residue studied in chapter 3, $Na_V1.4$ Tyr401. In order to test the possibility that the guanidinium group of TTX is attracted to Tyr401 through a cation-π interaction, this aromatic residue was replaced with a series of fluorinated derivatives of phenylalanine using the *in vivo* nonsense-suppression method. Consistent with a cation-π interaction, increased fluorination of a phenylalanine incorporated at 401 caused a monotonic increase in the inhibitory constant for block. Trifluorination of the aromatic ring disrupted TTX affinity by 50-fold, similar to that of outright replacement of phenylalanine at position 401 by the nonaromatic but comparably hydrophobic residue leucine. Furthermore, an energetically equivalent cation-π interaction is shown to underlie both use-dependent and tonic block by TTX. Our results are supported by high-level *ab initio* quantum mechanical calculations applied to a model of TTX binding to benzene. These results are the first of their kind to

show the incorporation of unnatural amino acids into a voltage-gated Na^+ channel and demonstrate that a cation-π interaction is responsible for the obligate nature of aromatics at this position in TTX-sensitive Na^+ channels.

Introduction

Na^+ channels control electrical excitability in muscle and nervous tissues by driving membrane depolarization during an action potential. These large (260 kDa) proteins have four homologous transmembrane domains that are arranged in a clockwise orientation around a central pore.[1] Numerous Na^+ channel isoforms exist and share the common traits of being exceptionally sensitive to voltage and highly selective for their conducting ion.[2] They can, however, differ in expression patterns, inactivation time course, sensitivity to toxins, and effects of auxiliary subunits. In terms of extracellular block by the toxin TTX, Na^+ channels have been deemed binary in their sensitivity; they are either "TTX sensitive," blocked by low nanomolar concentrations, or "TTX resistant" with blocking constants in the micromolar range.[3] Members of the former class include isoforms expressed in brain ($Na_V1.1$, $Na_V1.2$ and $Na_V1.3$), skeletal muscle ($Na_V1.4$), and peripheral nervous system (Na_V 1.6 and Na_V 1.7); the latter class includes isoforms of cardiac muscle ($Na_V1.5$) and sensory neurons ($Na_V1.8$ and $Na_V1.9$). A number of point mutations in the external vestibule of the channel can substantially disrupt TTX binding,[4-8] yet many of these residues are conserved between sensitive and resistant isoforms and therefore cannot explain isoform-specific TTX sensitivity. It has been established that a single aromatic residue conserved in the first homologous domain (DI) of TTX-sensitive

isoforms underlies isoform-specific block.[9-11] Mutagenic replacement of this aromatic residue, Tyr401 in the rat skeletal muscle Na^+ channel $Na_V1.4$, with the homologous residue from $Na_V1.5$, a cysteine, renders this isoform insensitive to TTX.[10,11] More importantly, a high-affinity TTX site with nanomolar block can be generated in $Na_V1.5$ upon a single aromatic substitution at this site,[9,11] confirming the importance for TTX block of phenylalanine or tyrosine at this position. This observation led to the proposal that a cation-π interaction would figure prominently in the binding of TTX to toxin-sensitive channels.[9,12] Here experimental evidence proves that a cation-π interaction involving Tyr401 in $Na_V1.4$ contributes to high-affinity block by TTX.

TTX block is enhanced by high-frequency stimulation of Na^+ channels. This use dependence of block was first reported in TTX-resistant cardiac Na^+ channels,[13] but is also seen in highly toxin-sensitive preparations, such as the crayfish axon,[14] and wild-type and mutated Na^+ channels heterologously expressed in oocytes.[8,15,16] It has been proposed that the lower affinity for cationic TTX in the resting or "tonic" state might be due to electrostatic interference from a Na^+ or Ca^{2+} ion trapped in the pore of the closed channel.[14] Upon repeated depolarization, channel opening allows for the escape of the trapped ion, increasing the stability of the toxin-bound state. Experiments show that extracellular Ca^{2+} and Mg^{2+} ions compete with and inhibit TTX binding, further supporting the "trapped ion" mechanism.[15,17] The relative effects of mutating pore residues on high- and low-affinity blocked states have not been examined in detail.

Many pore blockers mimic a channel's permeant ion and occlude conduction by taking its place in the permeation pathway. In the present example, the charged guanidinium moiety of TTX may replace Na^+ at the external mouth of the channel. Therefore an

understanding of block by TTX and other guanidinium toxins holds the promise of providing insight into the molecular architecture of the permeation pathway. The Na^+ channel selectivity filter has been hypothesized to be formed by the side chains of aspartate, glutamate, lysine, and alanine, one from each of the four homologous domains, DI-DIV respectively.[18,19] The "DEKA" locus is assisted by an outer ring of negative charges that electrostatically "focus" Na^+ ions toward the mouth of the selectivity filter.[20,21] Mutation of residues in either the inner or outer ring decreases both TTX affinity and single-channel conductance,[5] suggesting the TTX binding site overlaps with the extracellular entrance of the permeation pathway. The aromatic residue of interest for the current work, Tyr401 in $Na_V1.4$, is located between the two aforementioned charged rings, and its replacement with cysteine reduces single-channel conductance,[11] further suggesting a role for this site in Na^+ permeation. The homologous residue in the TTX-resistant cardiac isoform $Na_V1.5$, a cysteine, underlies sensitivity to extracellular pore block by heavy metals.[10,22]

An aromatic side chain may interact with a large organic cation like TTX through a combination of forces, including an induced dipole in the toxin and the aromatic, donor-acceptor, charge-transfer, and dispersion forces, as well as hydrophobic effects.[23] Electrostatic energy may also be provided by the attraction between the negative electrostatic potential on the face of the aromatic ring and the guanidinium moiety of TTX, an attraction termed the cation-π interaction.[23,24] Traditional site-directed mutagenesis is not helpful in discriminating among the many energetic components of binding energy, because outright amino acid substitution tends to change hydrophobicity, structure, polarizability and electrostatics concurrently. These shortcomings are readily

averted by employing *in vivo* nonsense suppression to incorporate unnatural amino acids with subtle structural changes.[25] This method has been used previously to test for cation-π interactions by incorporating a series of progressively fluorinated aromatic derivatives into the ligand-binding pockets of a variety of ion channels.[26-29] We have also used this approach to explore extracellular block of potassium channels by cationic tetraethylammonium.[30] The principle underlying this strategy is rather simple. Each fluorine atom substitution progressively reduces the negative electrostatic potential on the face of the aromatic, thereby reducing the electrostatic component of binding affinity. For studies of this kind, unnatural amino acids are clearly superior to their traditional counterparts. Serial fluorination does not substantially change the size, shape, polarizability, or hydrophobicity of the aromatic side chain,[23,31] so any loss in binding energy is due to cation-π electrostatics.

In the present study, the *in vivo* nonsense-suppression method was used to introduce a series of progressively fluorinated phenylalanine residues at position 401 in $Na_V1.4$, and the resulting channels were assayed for their sensitivity to TTX. Block was studied under both tonic and stimulated conditions, and both blocked states were found to rely heavily on a cation-π interaction at position 401. Specifically, stepwise fluorination monotonically increased the equilibrium binding constant, as observed in other known organic cation-π systems. Furthermore, complete neutralization of the negative electrostatic potential of the aromatic face by trifluorination of the aromatic side chain resulted in a TTX block that was similar to replacement of the residue at position 401 by leucine, suggesting that hydrophobicity alone cannot explain high-affinity block. Analysis of the blocking kinetics reveals that withdrawal of π electrons from the aromatic

face of phenylalanine at position 401 is manifested primarily as a decrease in the association rate constant for TTX block. These results demonstrate that phenylalanine at position 401 interacts with TTX through a substantial cation-π interaction, which, along with other energetic contributions, supports high-affinity block in TTX-sensitive isoforms.

Results

TTX affinity is nearly 3 orders of magnitude higher in TTX-sensitive Na^+ channels than in TTX-resistant isoforms, a difference that has been attributed to the lack of an aromatic residue in the external vestibule of the later class of channels. Specifically, high-affinity block requires the presence a tyrosine or phenylalanine at position 401 in the pore loop of domain DI of the rat $Na_V1.4$ channel from skeletal muscle.[9-11] Here the goal was to measure the energetic contribution of a cation-π interaction between TTX and the aromatic face of residue 401. A substantial cation-π interaction would provide insight into both the orientation of this residue in the extracellular mouth of the channel and of TTX in its blocking site. To this end electron-withdrawing fluorine atoms were substituted for hydrogen atoms on the aromatic ring of residue 401, creating a series of fluorinated analogues of phenylalanine, as described in chapter 2. The same fluorinated-phenylalanine-dCA derivatives used in the study of tetraethylammonium (TEA) binding to the voltage-gated Shaker B K^+ channel (ShB) were used in this study (see chapter 2 of this thesis).

The functional equivalence of phenylalanine and tyrosine at position 401 with respect to TTX block (table 4.1) allows us to employ analogs of phenylalanine in our analysis. This work represents the first attempt to directly test the contribution of the π electrons of the aromatic ring at position 401 in TTX binding.

Table 4.1. Affinity and kinetics of TTX block in tonic and stimulated states.*

$Na_V1.4$ (Suppressed at 401)	K_i^L Tonic (nM)	K_i^H Stim (nM)	k_{off}^L Tonic (s^{-1})	k_{off}^H Stim (s^{-1})	k_{on} (s^{-1}*μM^{-1})
WT (Tyr401)	19 ± 6 (5)	6 ± 1 (5)	0.13 ± 0.04 (5)	0.037 ± 0.002 (4)	6.84 ± 0.79 (9)
Tyr401Phe	25 ± 2 (4)	5 ± 0.9 (4)	0.161 ± 0.017 (4)	0.033 ± 0.001 (4)	6.58 ± 0.17 (4)
Phe	25 ± 3 (6)	7 ± 0.9 (6)	0.1545 ± 0.0128 (6)	0.040 ± 0.004 (5)	6.13 ± 1.04 (6)
3-F-Phe	49 ± 7 (6)	10 ± 1 (6)	0.208 ± 0.032 (5)	0.040 ± 0.002 (5)	4.08 ± 0.46 (5)
3,5-F_2-Phe	316 ± 32 (6)	93 ± 9 (6)	0.642 ± 0.064 (6)	0.181 ± 0.019 (6)	2.04 ± 0.27 (6)
3,4,5-F_3-Phe	974 ± 61 (6)	350 ± 28 (6)	0.352 ± 0.022 (6)	0.134 ± 0.032 (6)	0.361 ± 0.058 (6)
Tyr401Leu	2070 ± 223 (6)	1006 ± 104 (6)	0.363 ± 0.082 (4)	0.171 ± 0.031 (4)	0.209 ± 0.052 (4)
Tyr401Cys	108,000 ± 14,000 (4)	108,000 ± 14,000 (4)	-	-	-

An energy-minimized structure (A) and the electrostatic potential (B) of TTX are shown in figure 4.1. Although a monovalent cation at neutral pH, TTX also has a large dipole moment of approximately 10 D, with an excess of positive charge (blue) near the guanidinium group, which would be expected to affect the orientation of TTX due to electrostatic interactions with its binding site.

* Rate constants (k_{off}^H, k_{off}^L, and k_{on}) and equilibrium inhibitory constants (K_i^L and K_i^H) were determined as described in Santarelli *et al.*[32] The number of cells is enclosed in parentheses. The mutants indicated in red were generated by nonsense suppression.

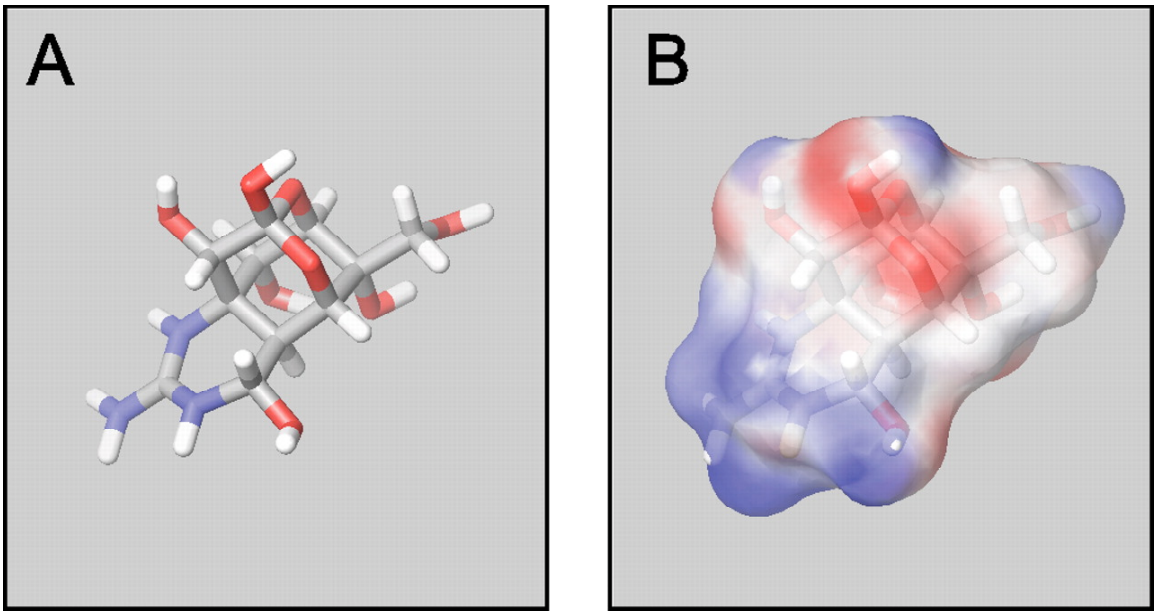

Figure 4.1. Structure of TTX. A) Energy-minimized structure and B) surface rendering of TTX with electrostatic potential ranging from +100 kcal/mol (blue) to +40 kcal/mol (red). Note that the delocalized charge of TTX presents a substantial dipole moment, with positive charge concentrated near the guanidinium moiety.

Figure 4.2 shows representative examples of inward Na^+ currents elicited by depolarizations to −10 mV from a holding potential of −100 mV. The Tyr401Phe mutant (figure 4.2A) was constructed by standard site-directed mutagenesis, while the remaining panels show currents for mutations introduced by nonsense suppression in which the cRNA encoding for $Na_V1.4$ was identical, containing a UAG codon at position 401. Figures 4.2B-E show the similarity of Na^+ currents coexpressing this cRNA construct with suppressor tRNAs ligated to the indicated derivatives of phenylalanine. In addition, the peak current-voltage relationships from the fluorinated unnatural amino acids resulted in less than 5 mV shifts in activation compared with wild-type channels. Injection of $Na_V1.4$ Tyr401UAG cRNA without a complementary suppressor tRNA failed to produce

Na^+ currents, allowing for the ruling out of enzymatic manipulation within the oocyte expression system resulting in the incorporation of unexpected and unwanted natural amino acids (figure 4.2F). As a further control, no Na^+ current was seen when a tRNA lacking an appended amino acid (dCA-tRNA) was coinjected with the $Na_V1.4$ Tyr401UAG cRNA.

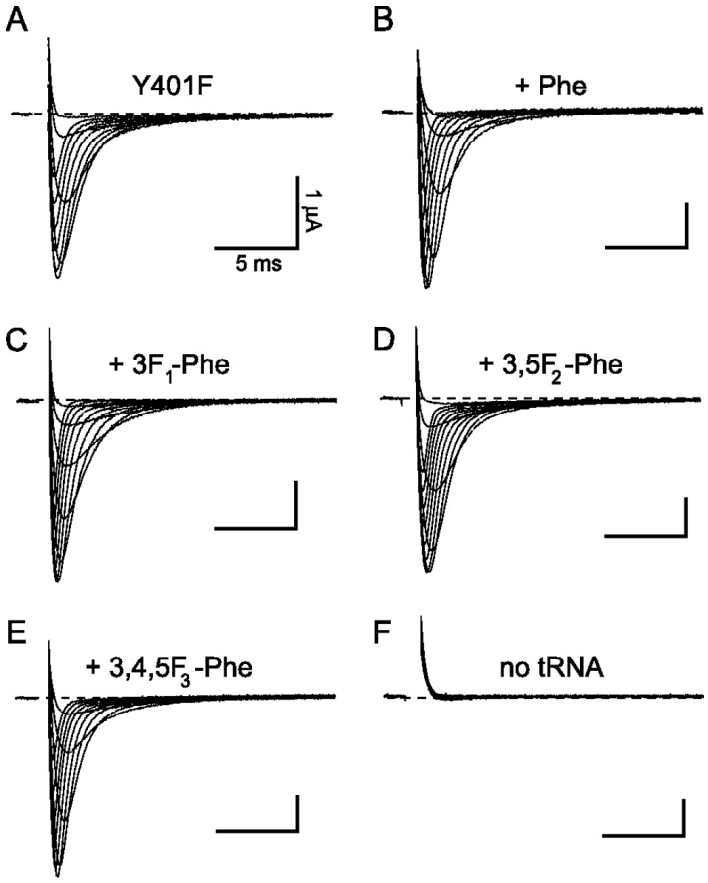

Figure 4.2. Representative current traces from either Tyr401Phe or channels constructed from coinjection of Tyr401TAG mRNA with a complementary tRNA appended with the indicated amino acid. Families of Na^+ currents are shown from depolarization from −30 to +20 mV in 5 mV increments and were elicited from a holding potential of −100 mV. The voltage dependence and kinetics of currents of A) the Tyr401Phe point mutation are indistinguishable from B-E) those of both natural and unnatural substitutions. Note the absence of currents upon injection of $Na_V1.4$ Tyr401UAG mRNA alone. Scale bars in each case are 5 ms and 1 μA.

Figure 4.3 demonstrates the effect of serial fluorination of the phenylalanine incorporated at position 401 on TTX affinity. The red traces from the same cells were recorded in the presence of the indicated concentrations of TTX. The six panels show currents for a variety of mutations at $Na_V1.4$ Tyr401. Consistent with a cation-π interaction, increasing fluorination of the phenylalanine incorporated at position 401 correlates with a decreased affinity for TTX block, as shown by the TTX concentration ([TTX]) required to reduce the current moderately in each mutant. Note the similar current kinetics for all mutants. Insets in figure 4.3 show the indicated aromatic rings of the unnatural amino acids as electrostatic potentials. Note that serial fluorination reduces the negative electrostatic potential (red) on the aromatic face with a minimal change in the overall structure.

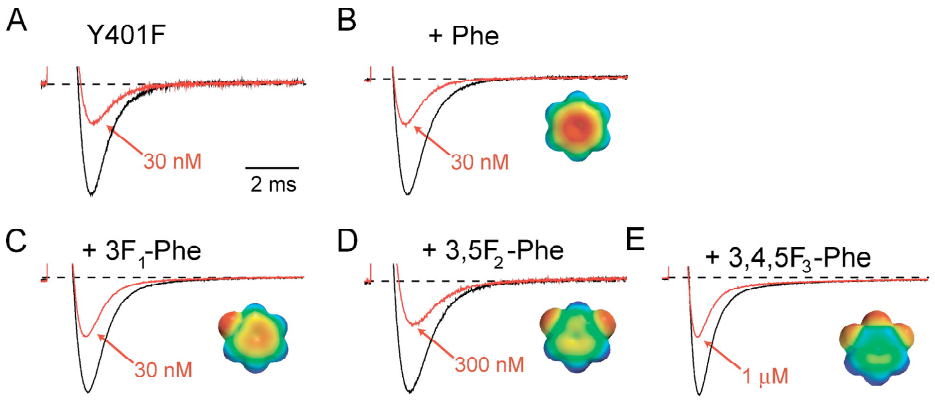

Figure 4.3. Fluorination of the phenylalanine at position 401 reduces TTX block. Normalized currents recorded during a 10 ms depolarization to −10 mV from a holding potential of −100 mV. Control (bath) traces in black, and TTX at the labeled concentration in red. As phenylalanine is fluorinated sequentially, a higher [TTX] is required for channel block. The inserts represent electrostatic potentials of benzene with red negative (−20 kcal/mol), blue positive (+20 kcal/mol), and green neutral. Before normalization the peak inward currents were (in μA): Tyr401Phe, −1.92; Phe, −3.75; 3-F-Phe, −3.72; 3,5-F_2-Phe, −2.43; 3,4,5-F_3-Phe, −5.29.

Extracellular block of Na^+ channels by TTX is use dependent, with repeated stimulation enhancing TTX affinity. This increase has been suggested to be due to electrostatic repulsion between TTX and a trapped Na^+ or Ca^{2+} ion within the pore, which is relieved upon channel opening during which the trapped ion is released.[8,14,15] Figure 4.4A shows an example of a dose-response experiment that reveals both tonic (low-affinity) and stimulated (high-affinity) inhibition for 3,4,5-F_3-phenylalanine. For each TTX concentration, the experiment consists of recording the current resulting from 100 depolarizations, each a 10 ms depolarization to −10 mV given at 2 Hz after a 3 minute application of TTX. The first pulse in the train is used for determining the tonic inhibition, whereas the current elicited by the 100th pulse provides the stimulated block. TTX is perfused at the next higher concentration for 3 minutes to allow for the stimulated, TTX-bound state to reequilibrate into the low-affinity tonic state.[15] After application of the highest [TTX], a concentration close to the inhibition constant K_i of block is applied, in this case 0.3 μM. Under continuous 2 Hz stimulation to hold blocked channels in the stimulated state, TTX is removed from the bath altogether. The time-dependent increase of current during washout is fit with a single-exponential relaxation, which provides an estimate of the first-order dissociation rate constant k_{off}^{H} for the high-affinity stimulated state. Figure 4.4B and C show inhibition plots for the indicated amino acids in the tonic and stimulated states, respectively. Each data set is fit by a single binding isotherm with a Hill coefficient of 1. The trend for each condition is that serial reduction in electrostatic potential from the face of the aromatic ring at residue 401 leads to a monotonic increase in the inhibition constant K_i (table 4.1), with the trifluorinated

derivative increasing K_i by 50-fold. Although the stimulated state consistently shows a higher affinity for TTX, both states are similarly affected by fluorination.

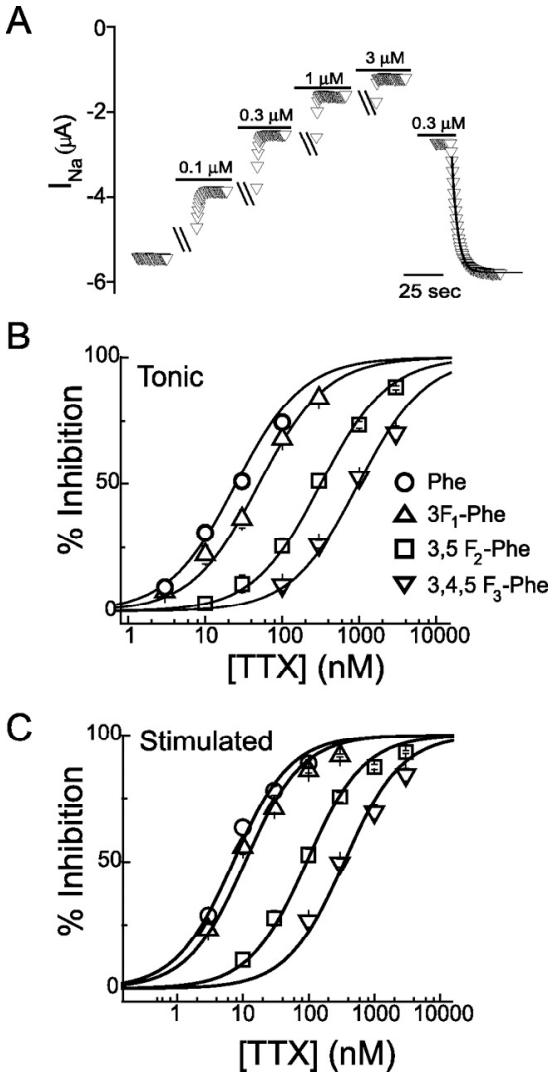

Figure 4.4. Effect of fluorination on the dose-response relationship for TTX block. A) Cumulative dose-response experiment and washout of TTX. Peak currents simulated at 2 Hz in the presence of bath alone or bath + TTX. Three minutes were given between concentration exchange and stimulation, allowing the channels to recover to the tonic state (represented as hash marks). Rate and equilibrium constants of block (table 4.1) were determined as described in Santarelli, *et al.*[32] In most cases a full dose-response relationship was obtained for each oocyte. The washout rates were fit well by a single exponential relaxation. B) TTX inhibition of $Na_v1.4$ in the tonic state. C) TTX inhibition of $Na_v1.4$ in the stimulated high-affinity state.

Estimates of rate constants for TTX block derived from these experimental data are shown in table 4.1. The association rate constant (k_{on}) undergoes a 17-fold decrease as residue 401 is converted from phenylalanine to 3,4,5-F_3-phenylalanine, whereas the dissociation rate constant (k_{off}) increases threefold. The general direction of the change in each rate constant is consistent with the progressive loss in TTX affinity with successive fluorination. Figure 4.5 shows the effect of fluorination on TTX binding energies derived from experimental K_i values, plotted against the relative TTX binding energies obtained from an *ab initio* model of TTX binding to an increasingly fluorinated benzene ring (table 4.2). Consistent with a cation-π interaction, each added fluorine results in a stepwise increase in the relative free energy of the TTX-bound state, for both the experimental results and the theoretical model. The identical effect of fluorination on both tonic and stimulated states strongly suggests that both states involve the same physical interaction between TTX and the channel. The higher affinity of the stimulated state therefore represents a separate contribution to the binding energy, independent of the cation-π interaction we have been testing. A parsimonious interpretation of the data is that the nanomolar affinity of TTX for $Na_V1.4$ depends in part on a substantial cation-π interaction with an aromatic side chain at position 401.

Table 4.2. Theoretical binding energies of TTX with fluorinated derivatives of benzene.*

		Hydration Energies					
	ΔE (gas)	TTX	F_n-Benzene	Complex	ΔG_{solv}	$\Delta G_{binding}$	$\Delta\Delta G$
Benzene	−7.91	−89.88	−1.59	−77.87	13.6	5.69	0
3-F-Benzene	−5.14	−89.88	−2.09	−79.95	12.02	6.88	1.19
3,5-F_2-Benzene	−2.14	−89.88	−2.22	−81.51	10.59	8.45	2.76
3,4,5-F_3-Benzene	0.14	−89.88	−2.79	−82.96	9.71	9.85	4.16

Discussion

Guanidinium toxins like TTX are potent blockers of voltage-gated Na^+ channels and have been invaluable both in the cloning of Na^+ channels[33,34] and in the exploration of mechanisms of cation permeation. Early studies proposed a model whereby the guanidinium moiety of TTX acts as a mimic of a Na^+ ion and blocks at the outer entrance to the selectivity filter.[35,36] In the absence of an atomic structure of a Na^+ channel, the TTX binding site with its numerous contact points has been helpful in modeling both the external vestibule and the selectivity filter of voltage-gated Na^+ channels. Many such pore models are based on existing K^+ channel structures, which are refined further by

* Calculations described in Santarelli *et al.*[32] The geometry and orientation of TTX binding was set by a gas-phase optimization, followed by aligning TTX with the structure in Figure 4.6 to know which positions to fluorinate. All values are in kcal/mol. ΔE is the binding energy of TTX to the benzene derivatives (F_n-Benzene, where n = number of fluorines) calculated in the gas phase. The energy caused by fluorination at 3-F-Benzene was calculated from the average energies of both *meta*-positions on the ring. The hydration energies for TTX, benzene derivatives, and the TTX-benzene complex were calculated using a Poisson-Boltzmann equation solver. ΔG_{solv} is the change in solvation free energy caused by TTX binding to the benzene derivative. $\Delta G_{binding} = \Delta E + \Delta G_{solv}$ is the Gibbs free energy of TTX binding, and $\Delta\Delta G$ is the effect of fluorination on TTX binding.

consideration of the Na^+ channel point mutations that affect permeation and pore block.[1,37-40] Among the extracellular residues that affect toxin block, $Na_V1.4$ Tyr401, and the homologous residue in other Na^+ channels, plays a unique role in discriminating between TTX-sensitive and TTX-resistant channels.[7,9-11] Only TTX-sensitive channels have an aromatic residue (phenylalanine or tyrosine) at this position. While other residues in the extracellular vestibule of the pore, especially charged residues, may affect TTX block dramatically when mutated, they tend to be highly conserved among all Na^+ channel isoforms. Although the importance of a phenylalanine or tyrosine residue at this discriminatory site is agreed universally, its energetic contributions to TTX binding are not well understood. Here it was asked whether a cation-π interaction involving residue 401 contributes to TTX binding energy. Because an optimal cation-π interaction requires a close approach of the cation to the face, not the edge, of the aromatic ring, evidence for such an interaction adds another layer of structural information, in that the aromatic must orient towards the permeation pathway where it may interact electrostatically with cationic pore blockers and permeant cations alike.

The well-established strategy that was employed to test for a cation-π interaction involved the successive fluorination of the aromatic ring[26-30,41] and depends on the assumption that the predominant effect of fluorine substitution is to decrease the negative electrostatic potential on the face of the aromatic residue. The involvement of a cation-π interaction is in complete accord with our results. As expected, each added fluorine atom impacts K_i with a roughly equal increase in the free energy of binding (figure 4.5). The magnitude of the effect, 2.2 kcal/mol for trifluorinating the aromatic ring, is roughly half that observed in previous studies of organic ligands binding to ion channels.[26,27,30] This

decrease may be a consequence of the delocalized charge of the relatively large TTX molecule—the diffuse positive charge would tend to have a reduced electrostatic attraction to the aromatic ring. Although essential to high-affinity block, the cation-π component of binding cannot account for all of the binding energy, a fact evident from an examination of the consequence of trifluorinating the phenylalanine incorporated at position 401. Earlier studies showed that trifluorobenzene is a good model for an aromatic that has little or no electrostatic binding ability,[42,43] but the data presented here show that trifluorination of the phenylalanine at position 401 still results in a channel with low micromolar affinity for TTX. This observation is unsurprising given the multitude of possible interactions between TTX and its binding pocket.

In order to explore a hydrophobic contribution to TTX binding, the Tyr401Leu mutation was made. Leucine is slightly more hydrophobic than phenylalanine.[44] The Tyr401Leu mutant has a comparable affinity for TTX as that of the trifluorinated derivative of phenylalanine, 2.1 versus 0.97 μM, respectively, in the tonic state (table 4.1). This result suggests that hydrophobic contributions alone cannot generate a high-affinity binding site for TTX, and therefore the 50-fold increase of K_i caused by trifluorinating the phenylalanine incorporated at position 401 is due primarily to a loss of electrostatic attractiveness of the aromatic ring, namely a cation-π interaction. Note also that the effects of these two mutations are in stark contrast to the dramatic loss of TTX affinity seen by replacement with more polar amino acids such as cysteine with a K_i of 108 μM (table 4.1) or glutamate with a K_i of 170 μM.[7] This result may seem surprising at first glance, especially given that the monopole negative charge of glutamate might be expected to attract a cation at least as well as the quadrupole potential on the aromatic

face of phenylalanine. For example, a highly conserved ring of four basic residues, two glutamates and two aspartates, produces an electrostatic potential in excess of −100 mV in the extracellular mouth of Na^+ channels.[45] This ring of negative charge is believed to attract both permeant cations and positively charged blockers like TTX. An additional glutamate at position 401 would also be expected to attract TTX. Why, then, does the Tyr401Glu mutation reduce the affinity of TTX binding?

For binding to be optimal, there has to be a balance between the electrostatic attraction between the toxin and the side chain and the energies of hydration of both TTX and its binding site.[46,47] Certainly, the dehydration cost is much less for an aromatic side chain than for the anionic glutamate. As such, the innately weaker TTX•••aromatic interaction could, after considering solvation, contribute more to binding than the instrinsically stronger TTX•••carboxlate interaction. Although this thermodynamic principle may account in part for TTX's preference for tyrosine or phenylalanine over glutamate, it is not clear whether this argument can explain the low affinity for the Tyr401Cys mutant or whether, for example, some mutations of this residue produce local conformational changes that disrupt TTX binding. Evidence for this possibility is that the Tyr401Cys mutant loses its use dependence (table 4.1). The possibility of conformational disruption of the binding site does not, however, invalidate the use of fluorinated phenylalanine side chains because of the subtle nature of the mutations, by comparison with Tyr401Cys for example, and the simple monotonic relationship between TTX binding energy and the number of fluorine atoms substituted onto the aromatic ring (figure 4.5).

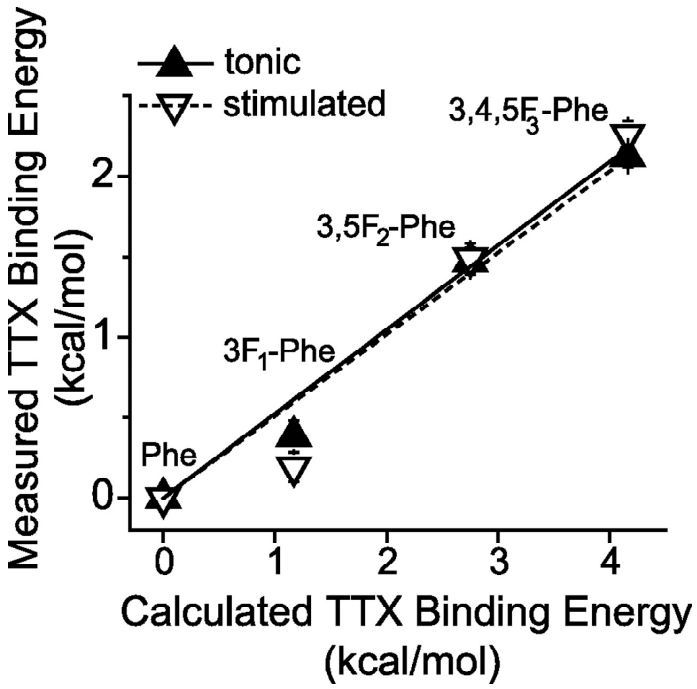

Figure 4.5. Effect of fluorination on free energy of TTX binding. TTX binding energy relative to unfluorinated phenylalanine at position 401 is plotted against the calculated TTX binding energy between TTX and a benzene ring (table 4.2). Fluorinating the aromatic ring monotonically increases the relative free energy of the bound state. The change in binding energy is nearly identical for both the low- and high-affinity states.

The effect of fluorination of the phenylalanine at position 401 was identical for the tonic and stimulated states in both the trend and magnitude of binding free energy (figure 4.5). Although few molecular details are available on the use-dependent mechanism of TTX block, this result suggests that the critical TTX:aromatic complex has the same structure in both states. The different affinities of the tonic and stimulated states are therefore due to other energetic factors, such as the electrostatic repulsion between the toxin and cations trapped within the permeation pathway.[14,15]

Kinetic analysis reveals that withdrawing electrostatic potential from the aromatic face of the aromatic at position 401 primarily affects the association rate constant k_{on} of TTX block (table 4.1). A similar conclusion was reached previously by conventional mutagenic analysis of this and most other residues in the external vestibule. That is, reduction of TTX affinity often (but not always) involves a reduction of k_{on} rather than an increase of k_{off}.[7,8] Larger effects on k_{on} than k_{off} were also reported for block of ShB by the peptide charybdotoxin in response to charge-altering mutations.[48] The principal similarity in these studies is that the mutations were designed to alter the electrostatics of block using either standard mutagenesis or, in this study, changes of electrostatic potentials on the surface of an aromatic ring. Moreover, the empirical association rate constants in all of these studies are well below the Smoluchowski limit expected for diffusional collision between a small blocker and an ion channel,[49] indicating that the observed blocking rate is not diffusion limited. The challenge in interpreting these results is that alteration of the electrostatic attraction between a ligand and its binding site might be expected to affect both association and dissociation rate constants.

The role of a cation-π interaction in the blocking equilibrium is clear (figure 4.5), whether a TTX-aromatic complex is involved in the blocked state or in a transient intermediate. The blocked state itself likely includes hydrogen bonds and other short-range interactions. Also, a recent study of toxin block of a K^+ channel raises the possibility that the conformation of the binding site and the toxin might both change with the toxin binds.[50]

In figure 4.6 a snapshot of one possible configuration of the encounter complex was visualized. The coordinates of the pore mouth for $Na_V1.4$ from the model of Lipkind and Fozzard were used.[39] In an alternative model the aromatic ring of Tyr401 was not oriented to face the permeation pathway[51] and was therefore inconsistent with the data in this chapter. To model the configuration in figure 4.6, first the structure of TTX and its minimum-energy conformation in complex with benzene were optimized using high-level *ab initio* calculations. The benzene of this complex was then aligned with the aromatic ring of Tyr401. Because of sixfold symmetry of the ring, there are six possible orientations of the TTX-benzene complex with Tyr401. The minimum energy orientation was estimated using molecular mechanics. This structure is shown from above (figure 4.6A) and from the side (figure 4.6B). Notice that the guanidinium group, besides being in close apposition to the aromatic face of Tyr401, is pointed downward towards the deeper residues of the selectivity filter. Further study will reveal whether this complex prevents Na^+ ion flux, either sterically or electrostatically, or whether the blocked state involves a subsequent movement of the toxin into a deeper position where it would plug the pore. Our model of block nevertheless supports the idea that a fundamental role of the TTX-aromatic interaction is to orient the toxin optimally to block the channel.

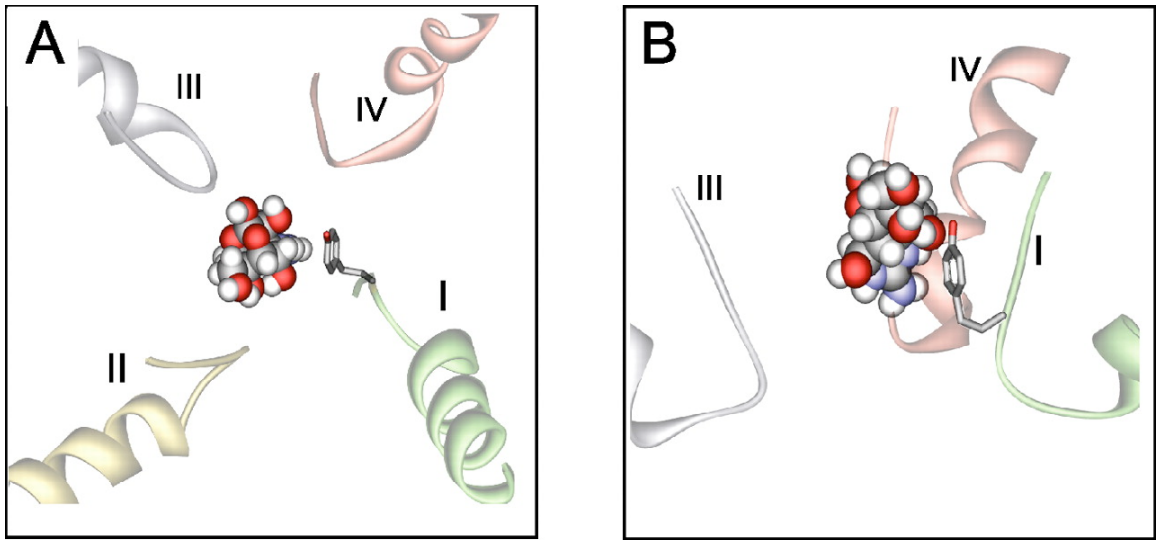

Figure 4.6. Model of TTX docking in the pore mouth of $Na_v1.4$. A) Top view of TTX interacting with the pore loops of domains DI – DIV in the Lipkind-Fozzard model.[39] This structure represents one possible configuration of the encounter complex. Note the guanidinium group of TTX in apposition with the face of the aromatic ring of Tyr401. B) Side view of TTX in the pore.

Conclusion

The conclusions of the present study are threefold. First, it was demonstrated that the high-affinity TTX block supported by a phenylalanine or a tyrosine at position 401 is energetically based on a cation-π interaction between the TTX and the aromatic face of the side chain. These results therefore serve to answer a long-standing puzzle regarding the conserved nature of a pore domain aromatic in high-affinity Na^+ channel isoforms. Secondly, it was shown that the side chain at Tyr401 presents its aromatic face toward the permeation pathway where it can interact favorably with TTX and other cations. These results place geometric constraints on this side chain both in current structural models and in future atomic level structures of the sodium channel pore. Lastly, though

presented in this thesis after chapter 3, in which Ca^{2+} was found to bind to $Na_V1.4$ through a cation-π interaction using similar techniques,[52] these results actually represent the first published application of the *in vivo* nonsense-suppression method for the incorporation of unnatural amino acids into a voltage-gated Na^+ channel. This work therefore serves as proof of principle to pave the way for future experiments utilizing this powerful technique to explore a variety of structural and mechanistic issues concerning sodium channels, including the energetics that underlie cationic blockade by antiarrhythmia, antiepilepsy, and analgesic drugs.

Methods

The work in this chapter was a collaborative effort that included important contributions from Dr. Vincent Santarelli, Dr. Chris Ahern, and Dr. Richard Horn of the Jefferson Medical College in Philadelphia, PA. Detailed methods for the experiments discussed in this chapter that were not performed by the author can be found in Santarelli *et al*.[32]

Unnatural Amino Acids and Molecular Biology

Phenylalanine-dCA, 3,5-F_2-phenylalanine-dCA, and 3,4,5-F_3-phenylalanine-dCA were obtained as described in chapter 2. 3-F-Phenylalanine was a gift from Dr. Niki Zacharias, a former graduate student in the Dougherty laboratory. These aminoacylated dinucleotides were ligated to a modified tRNA from *Tetrahymena thermophila*, THG73, using T4 RNA ligase (New England Biolabs, Ipswich, MA).[25,53]

Acknowledgements

We thank Mary Y. Ryan for help with oocytes and molecular biology. Supported by grants from the NIH (GM079427and NS34407).

References

(1) Dudley, S. C., Jr.; Chang, N.; Hall, J.; Lipkind, G.; Fozzard, H. A.; French, R. J. *J. Gen. Physiol.* **2000**, *116*, 679-90.

(2) Yu, F. H.; Catterall, W. A. *Genome Biol.* **2003**, *4*, 207.

(3) Goldin, A. L.; Barchi, R. L.; Caldwell, J. H.; Hofmann, F.; Howe, J. R.; Hunter, J. C.; Kallen, R. G.; Mandel, G.; Meisler, M. H.; Netter, Y. B.; Noda, M.; Tamkun, M. M.; Waxman, S. G.; Wood, J. N.; Catterall, W. A. *Neuron* **2000**, *28*, 365-8.

(4) Noda, M.; Suzuki, H.; Numa, S.; Stuhmer, W. *FEBS Lett.* **1989**, *259*, 213-6.

(5) Terlau, H.; Heinemann, S. H.; Stuhmer, W.; Pusch, M.; Conti, F.; Imoto, K.; Numa, S. *FEBS Lett.* **1991**, *293*, 93-6.

(6) Kontis, K. J.; Goldin, A. L. *Mol. Pharmacol.* **1993**, *43*, 635-44.

(7) Penzotti, J. L.; Fozzard, H. A.; Lipkind, G. M.; Dudley, S. C., Jr. *Biophys. J.* **1998**, *75*, 2647-57.

(8) Boccaccio, A.; Moran, O.; Imoto, K.; Conti, F. *Biophys. J.* **1999**, *77*, 229-40.

(9) Satin, J.; Kyle, J. W.; Chen, M.; Bell, P.; Cribbs, L. L.; Fozzard, H. A.; Rogart, R. B. *Science* **1992**, *256*, 1202-5.

(10) Backx, P. H.; Yue, D. T.; Lawrence, J. H.; Marban, E.; Tomaselli, G. F. *Science* **1992**, *257*, 248-51.

(11) Chen, L. Q.; Chahine, M.; Kallen, R. G.; Barchi, R. L.; Horn, R. *FEBS Lett.* **1992**, *309*, 253-7.

(12) Dougherty, D. A. *Science* **1996**, *271*, 163-8.

(13) Baer, M.; Best, P. M.; Reuter, H. *Nature* **1976**, *263*, 344-5.

(14) Salgado, V. L.; Yeh, J. Z.; Narahashi, T. *Ann. N. Y. Acad. Sci.* **1986**, *479*, 84-95.

(15) Conti, F.; Gheri, A.; Pusch, M.; Moran, O. *Biophys. J.* **1996**, *71*, 1295-312.

(16) Satin, J.; Limberis, J. T.; Kyle, J. W.; Rogart, R. B.; Fozzard, H. A. *Biophys. J.* **1994**, *67*, 1007-14.

(17) Weigele, J. B.; Barchi, R. L. *FEBS Lett.* **1978**, *95*, 49-53.

(18) Heinemann, S. H.; Terlau, H.; Stuhmer, W.; Imoto, K.; Numa, S. *Nature* **1992**, *356*, 441-3.

(19) Schlief, T.; Schonherr, R.; Imoto, K.; Heinemann, S. H. *Eur. Biophys. J.* **1996**, *25*, 75-91.

(20) Chiamvimonvat, N.; Perez-Garcia, M. T.; Tomaselli, G. F.; Marban, E. *J. Physiol.* **1996**, *491 (Pt. 1)*, 51-9.

(21) MacKinnon, R.; Latorre, R.; Miller, C. *Biochemistry* **1989**, *28*, 8092-9.

(22) Favre, I.; Moczydlowski, E.; Schild, L. *Biophys. J.* **1996**, *71*, 3110-25.

(23) Ma, J. C.; Dougherty, D. A. *Chem. Rev.* **1997**, *97*, 1303-1324.

(24) Gallivan, J. P.; Dougherty, D. A. *Proc. Natl. Acad. Sci. USA* **1999**, *96*, 9459-64.

(25) Nowak, M. W.; Gallivan, J. P.; Silverman, S. K.; Labarca, C. G.; Dougherty, D. A.; Lester, H. A. *Methods Enzymol.* **1998**, *293*, 504-29.

(26) Beene, D. L.; Brandt, G. S.; Zhong, W.; Zacharias, N. M.; Lester, H. A.; Dougherty, D. A. *Biochemistry* **2002**, *41*, 10262-9.

(27) Lummis, S. C.; D, L. B.; Harrison, N. J.; Lester, H. A.; Dougherty, D. A. *Chem. Biol.* **2005**, *12*, 993-7.

(28) McMenimen, K. A.; Petersson, E. J.; Lester, H. A.; Dougherty, D. A. *ACS Chem. Biol.* **2006**, *1*, 227-34.

(29) Zhong, W.; Gallivan, J. P.; Zhang, Y.; Li, L.; Lester, H. A.; Dougherty, D. A. *Proc. Natl. Acad. Sci. USA* **1998**, *95*, 12088-93.

(30) Ahern, C. A.; Eastwood, A. L.; Lester, H. A.; Dougherty, D. A.; Horn, R. *J. Gen. Physiol.* **2006**, *128*, 649-57.

(31) Leo, A.; Hansch, C.; Elkins, D. *Chem. Rev.* **1971**, *71*, 525-616.

(32) Santarelli, V. P.; Eastwood, A. L.; Dougherty, D. A.; Horn, R.; Ahern, C. A. *J. Biol. Chem.* **2007**, *282*, 8044-51.

(33) Noda, M.; Ikeda, T.; Kayano, T.; Suzuki, H.; Takeshima, H.; Kurasaki, M.; Takahashi, H.; Numa, S. *Nature* **1986**, *320*, 188-92.

(34) Noda, M.; Shimizu, S.; Tanabe, T.; Takai, T.; Kayano, T.; Ikeda, T.; Takahashi, H.; Nakayama, H.; Kanaoka, Y.; Minamino, N.; et al. *Nature* **1984**, *312*, 121-7.

(35) Hille, B. *J. Gen. Physiol.* **1971**, *58*, 599-619.

(36) Hille, B. *Biophys. J.* **1975**, *15*, 615-9.

(37) Bruhova, I.; Zhorov, B. S. *Biophys. J.* **2005**, *89*, 1020-9.

(38) Lipkind, G. M.; Fozzard, H. A. *Biochemistry* **2000**, *39*, 8161-70.

(39) Lipkind, G. M.; Fozzard, H. A. *Mol. Pharmacol.* **2005**, *68*, 1611-22.

(40) Penzotti, J. L.; Lipkind, G.; Fozzard, H. A.; Dudley, S. C., Jr. *Biophys. J.* **2001**, *80*, 698-706.

(41) Morikubo, N.; Fukuda, Y.; Ohtake, K.; Shinya, N.; Kiga, D.; Sakamoto, K.; Asanuma, M.; Hirota, H.; Yokoyama, S.; Hoshino, T. *J. Am. Chem. Soc.* **2006**, *128*, 13184-94.

(42) Mecozzi, S.; West, A. P., Jr.; Dougherty, D. A. *J. Am. Chem. Soc.* **1996**, *118*, 2307-2308.

(43) Williams, J. H. *Accounts Chem. Res.* **1993**, *26*, 593-598.

(44) Radzicka, A.; Pedersen, L.; Wolfenden, R. *Biochemistry* **1988**, *27*, 4538-41.

(45) Hui, K.; McIntyre, D.; French, R. J. *J. Gen. Physiol.* **2003**, *122*, 63-79.

(46) Eisenman, G. *Biophys. J.* **1962**, *2*, 259-323.

(47) Eisenman, G.; Horn, R. *J. Membr. Biol.* **1983**, *76*, 197-225.

(48) Escobar, L.; Root, M. J.; MacKinnon, R. *Biochemistry* **1993**, *32*, 6982-7.

(49) Camacho, C. J.; Weng, Z.; Vajda, S.; DeLisi, C. *Biophys. J.* **1999**, *76*, 1166-78.

(50) Lange, A.; Giller, K.; Hornig, S.; Martin-Eauclaire, M. F.; Pongs, O.; Becker, S.; Baldus, M. *Nature* **2006**, *440*, 959-62.

(51) Tikhonov, D. B.; Zhorov, B. S. *Biophys. J.* **2005**, *88*, 184-97.

(52) Santarelli, V. P.; Eastwood, A. L.; Dougherty, D. A.; Ahern, C. A.; Horn, R. *Biophys. J.* **2007**, *93*, 2341-9.

(53) Nowak, M. W.; Kearney, P. C.; Sampson, J. R.; Saks, M. E.; Labarca, C. G.; Silverman, S. K.; Zhong, W.; Thorson, J.; Abelson, J. N.; Davidson, N.; *et al. Science* **1995**, *268*, 439-42.

Chapter V

ELECTROSTATIC CONTRIBUTIONS OF AROMATIC RESIDUES IN THE LOCAL ANESTHETIC RECEPTOR OF VOLTAGE-GATED SODIUM CHANNELS

Antiarrhythmics, anticonvulsants, and local anesthetics target voltage-gated Na^+ channels, decreasing excitability of nerve and muscle cells. Channel inhibition by members of this family of cationic, hydrophobic drugs relies on the presence of highly conserved aromatic residues in the sixth pore-lining segment (S6) of the fourth homologous domain (D4) of the channel. It was proposed that these aromatic residues functioned in channel inhibition though a cation-π interaction with lidocaine. To test this hypothesis, the *in vivo* nonsense-suppression method was employed to incorporate a series of unnatural phenylalanine derivatives designed to systematically reduce the negative electrostatic potential on the face of the aromatic ring and thus decrease the favorable interaction between the aromatic and the cation. In contrast to standard point mutations at the same sites, these subtly modified amino acids preserve the wild-type voltage dependence of channel activation and inactivation. Although these phenylalanine derivatives have no effect on low-affinity tonic inhibition by lidocaine or its permanently charged derivative QX-314 at any of the substituted sites, high-affinity use-dependent inhibition displays substantial cation-π energetics for one residue only, Phe1579 in rat $Na_V1.4$. Suppression at Phe1579 with cyclohexylalanine, for example, strongly reduces use-dependent inhibition and speeds recovery of lidocaine-engaged channels. Channel

block by the neutral local anesthetic benzocaine is unaffected by the distribution of π electrons at Phe1579, indicating that our aromatic manipulations expose electrostatic contributions to channel inhibition. These results fine tune our understanding of local anesthetic inhibition of voltage-gated Na^+ channels and will help the design of safer and more salutary therapeutic agents.

Introduction

Voltage-gated Na^+ channels underlie the upstroke and propagation of the action potential in excitable cells of nerve and muscle, making them ideal targets in pharmacological interventions for cardiac arrhythmias, epilepsy, and pain. Antiarrythmics, anticonvulsants, and local anesthetics comprise a family of Na^+ channel inhibitors that share chemical and structural similarity. All Na^+ channel isoforms, including the cardiac channel $Na_V1.5$, are inhibited by these compounds,[1-3] with differences in sensitivity largely attributed to divergent biophysical aspects of gating kinetics.[3] At physiological pH these inhibitors are typically lipid-soluble cations that are highly efficacious in the treatment of hyperexcitability disorders due to their preference for inactivated channels, a conformational state that is prevalent during high-frequency firing of action potentials. This state-dependent inhibition is rationalized by models that propose that inactivation exposes a high-affinity binding site.

A general deficiency of this class of compounds is their lack of specificity. For example, the antiepileptic drug carbamezepine may adversely effect cardiac rhythms,[4,5] but it has also been used for pain management.[6] Multiple sites of action, whether expressly

intended or not, are common to many of these inhibitors and arise from the highly conserved nature of both the compounds and their binding site within the channel where the three aromatic residues of relevance for the present study are 100% conserved across eukaryotic voltage-gated Na^+ channel isoforms.

An abundance of experimental data implicates pore-lining residues of the S6 segment of D4 of the Na^+ channel α subunit in the binding of local anesthetics. Alanine scanning mutagenesis exposed the crucial role of two D4/S6 aromatics, Phe1579 and Tyr1586 (rat $Na_V1.4$ numbering), in the block by the anticonvulsant etidocaine and the quaternary amine QX-314.[2] Further study revealed a near universal importance of these two aromatic residues in the inhibition of Na^+ channels by the class 1A and 1B antiarrhythmic drugs and anticonvulsants.[7]

These two residues are ideally placed to interact with drugs that inhibit channel function. Na^+ channel pore domain models based on the crystal structures of K^+ channels predict that both residues face the inner vestibule of the permeation pathway where they could interact readily with cationic blockers and are in close proximity to the selectivity filter where they might influence Na^+ permeation.[8,9] The mechanistic details of local anesthetic action, while poorly resolved, may involve electrostatic repulsion of Na^+ ions at the selectivity filter,[10] pore occlusion,[11] stabilization of nonconducting states of the channel, a combination of all three mechanisms, or other possibilities such as gating charge immobilization.[12] The additional relevance of these aromatic residues to channel function is readily seen in experiments where outright side chain replacement, for example with either alanine or cysteine, not only disrupts inhibition by local anesthetics,

but also perturbs the biophysics of channel gating,[2,13-15] possibly obscuring the interpretation of their involvement in channel inhibition.

How do neutral aromatic residues contribute to channel inhibition by organic cations? One proposed but untested possibility is that local anesthetics have an electrostatic attraction to the negative electrostatic potential on the face of pore-lining aromatic side chains,[1] a cation-π interaction. This hypothesis can be tested directly using the *in vivo* nonsense-suppression method, which allows for the site-directed incorporation of subtly modified variants of the aromatic amino acid phenylalanine.[16] If a cation-π mechanism contributes to the attraction between a cationic blocker and the aromatic side chain, reduction of π electron density on the face of the aromatic, for example by fluorinating the aromatic ring, will reduce the binding affinity.[17] A benefit of this approach is that fluorination does not substantially alter the polarizability, size, shape, or hydrophobicity of the side chain.[17,18] Therefore, this benign manipulation of side chain structure obviates the inconvenient functional consequences of standard mutagenesis. This strategy has been applied successfully in Na^+ channels to test for cation-π interactions between an extracellular aromatic residue and either tetrodotoxin[19] or calcium ions.[20]

In this study progressively fluorinated phenylalanine derivatives and cyclohexylalanine were incorporated at three positions of the D4/S6 segment of the rat $Na_V1.4$ voltage-gated Na^+ channel, and in each case channels showed robust expression with normal voltage dependence and kinetics of both activation and fast inactivation. Only one site, Phe1579, exhibited a strong cation-π interaction with lidocaine. Furthermore, it was found that channel inhibition by the neutral local anesthetic benzocaine was oblivious to manipulations that affected the electrostatic potential on the aromatic face of Phe1579.

These experiments establish a substantial electrostatic component in the binding energy between cationic local anesthetics and a single pore-lining aromatic. This careful dissection of the energetic factors underlying the binding of these inhibitory compounds to Na^+ channels holds promise for the synthesis of more specific therapeutic agents for treatment of disorders of hyperexcitability.

Results

While a cation-π interaction has been proposed to occur between local anesthetics and D4/S6 aromatics,[1] this hypothesis remains entirely unsubstantiated and was therefore targeted directly in this study. Lidocaine, like most local anesthetics, can exist in two forms, neutral or cationic. At physiological pH roughly three-quarters of lidocaine molecules are protonated, and this charged form is a stronger pore blocker than the neutral molecule.[21-23] Figure 5.1A shows the protonated form of lidocaine and a color-coded map of the electrostatic potential on the surface of the molecule. The positive charge has an asymmetric distribution focused most strongly (blue) near the protonated nitrogen, positioned to the right in each panel of figure 5.1A.

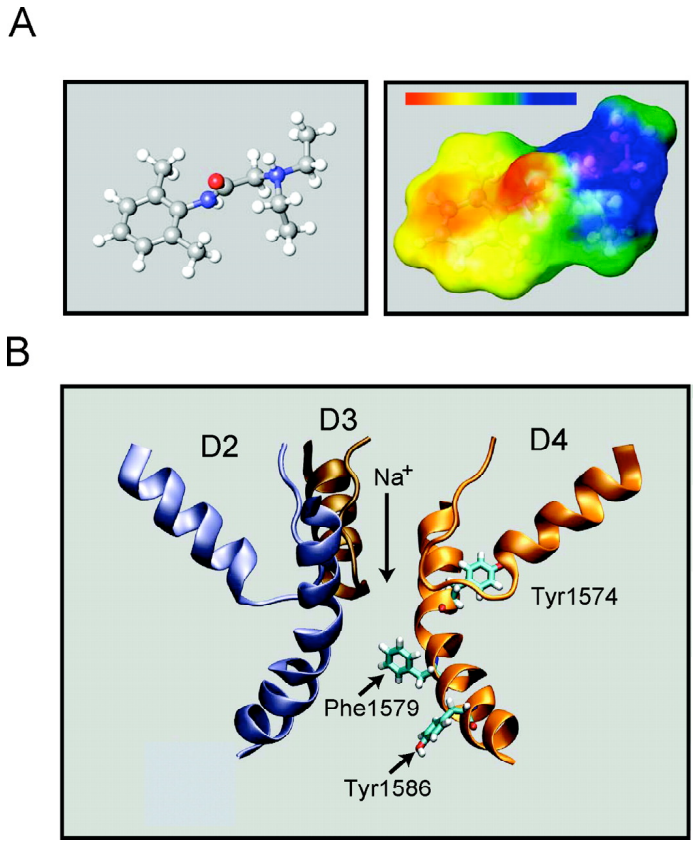

Figure 5.1. Lidocaine and the Na^+ channel pore. A) Structure and the electrostatic surface of protonated lidocaine. Left panel shows the structure of lidocaine optimized at the HF/6-31++G** level, with carbon, hydrogen, nitrogen and oxygen shown as grey, white, blue and red, respectively. Right panel shows the results of an *ab initio* determination of the electrostatic surface of protonated lidocaine in water. The red to blue spectrum shown on the scale bar corresponds to a range of 0 to +150 kcal/mol. B) Side view of a putative local anesthetic receptor in a voltage-gated Na^+ channel. The image is adapted from the Na^+ channel pore model of Lipkind and Fozzard,[8] as described in the text.

Figure 5.1B shows a side view of a portion of the putative local anesthetic binding site in a model of the voltage-gated skeletal muscle Na^+ channel rat $Na_V1.4$ adopted from Lipkind and Fozzard.[8] The pore helices and extracellular pore loops of domains D2-D4 and the opposing transmembrane S6 segments of domains D2 (silver) and D4 (orange)

are shown in an open-channel conformation. Note the proximity of the residues Phe1579 and Tyr1586 to each other and to the selectivity filter above them. Figure 5.1B is intended to represent a side view of the aqueous vestibule in which lidocaine binds, and to illustrate that lidocaine is large enough (approximately 11 x 6 Å) to interact simultaneously with Phe1579 and Tyr1586 in this structural model. By contrast Tyr1574 is on the "backside" of the S6 segment facing away from the permeation pathway.

Although standard point mutants of Phe1579 typically alter the channel's biophysical properties,[2,13,15] the unnatural mutants generated by *in vivo* nonsense suppression resulted in channels that were indistinguishable from wild-type $Na_V1.4$ with respect to kinetics of activation and inactivation. Figure 5.2A shows families of normalized Na^+ currents from oocytes expressing wild-type $Na_V1.4$ or channels with the indicated amino acid at position 1579. Inward currents shown in figure 5.2A were elicited in increments of 5 mV depolarizations from −30 to +10 mV from a holding potential of −100 mV. Figure 5.2A, lower right panel, shows that oocytes coinjected with Phe1579TAG cRNA and a tRNA lacking an appended amino acid (dCA-tRNA) did not generate measurable Na^+ currents, ruling out counterfeit channel expression due to enzymatic manipulation of the coinjected tRNA within the oocyte. Insets in figure 5.2A show the consequences of trifluorination on the electrostatic potential of benzene, where red and blue represent negative and positive, respectively, and green is neutral. Peak conductance-voltage relationships for activation are shown in figure 5.2B for wild-type $Na_V1.4$ or channels with the indicated amino acids at the 1579 position. There was no change in either voltage dependence or slope of activation for any of the mutants (table 5.1). Moreover, replacement of Phe1579 with either serially fluorinated derivatives of phenylalanine or nonaromatic

cyclohexylalanine resulted in insignificant effects on steady-state inactivation (figure 5.2C). We also incorporated the same series of side chains at Tyr1586, a site roughly two turns downstream along the S6 α helix. Like the 1579 site, the incorporation of unnatural amino acids was well tolerated, producing channels with healthy expression and normal gating (table 5.1).

A phenomenological hallmark of local anesthetic action on Na^+ channels is a hyperpolarizing shift of the steady-state inactivation relationship.[21,22,24] To test a possible role for cation-π energetics at Phe1579, oocytes expressing the indicated channel type were incubated for 5 minutes in 200 μM lidocaine at −100 mV and then steady-state inactivation was measured (figure 5.2D). Consistent with previous studies, incubation with lidocaine caused a roughly −8 mV shift for Phe1579 channels,[24,25] but this effect was serially diminished with each added fluorine to a minimum of −2.5 mV for either 3,4,5-F_3-phenylalanine or cyclohexylalanine incorporated at position 1579 (inset). These results suggest that the reduction of negative electrostatic potential on the aromatic face of the residue at position 1579 weakens the binding of lidocaine to inactivated channels.

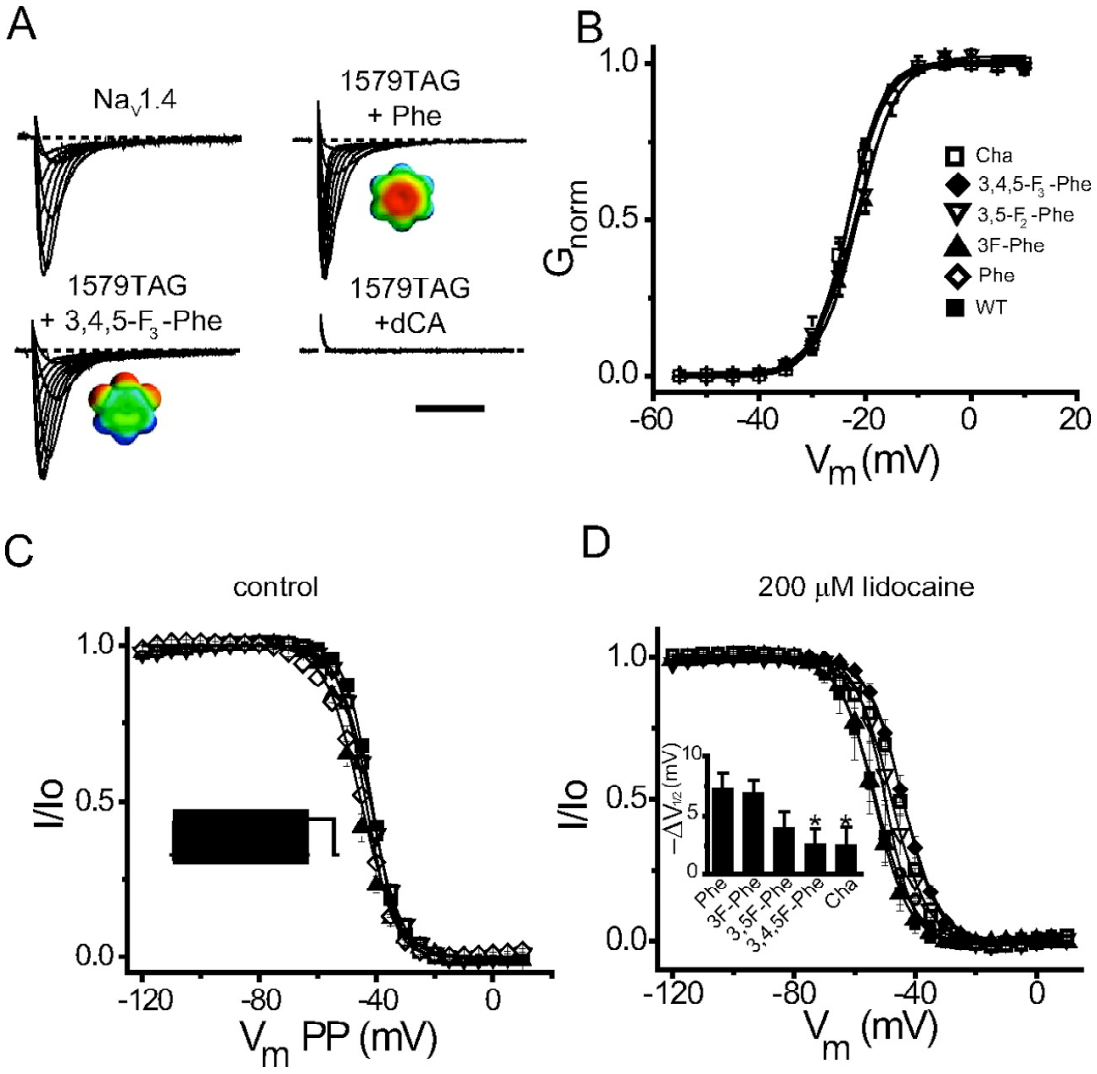

Figure 5.2. Unperturbed gating properties of $Na_V1.4$ channels containing unnatural amino acids at 1579. A) Families of Na^+ currents for the indicated channel types elicited by 5 mV steps from −30 to +25 mV from a holding potential of −100 mV, scale bar is 5 ms. Insets show the electrostatic potentials of benzene and trifluorobenzene with red negative (−20 kcal/mol) and blue positive (+20 kcal/mol). No currents were seen when cRNA from Phe1579TAG was coinjected with dCA-tRNA. B) Peak conductance-voltage relationships for indicated side chains at the 1579 site. C) Steady-state inactivation curves generated from the inset protocol. Holding potential −100 mV, 500 ms prepulse, 2 ms reset at −100 mV, −10 mV test potential. D) Same protocol as C, after a 5 minute incubation with 200 μM lidocaine. Inset summarizes the shift in steady-state voltage dependence caused by lidocaine for the indicated channel types, asterisk indicates $P < 0.05$.

Table 5.1. Boltzmann fits of normalized activation (figure 5.2B) and steady-state inactivation (figure 5.2C) for wild-type and mutant channels.*

	G-V		Steady-state Inactivation	
	$V_{0.5}$	K	$V_{0.5}$	K
$Na_V1.4$	−23.5 ± 0.8 (8)	3.1 ± 0.2	−46.4 ± 1.1 (9)	4.3 ± 0.4
Phe1579Phe	−21.8 ± 0.9 (9)	3.4 ± 0.6	−46.4 ± 0.7 (9)	5.3 ± 0.3
Phe1579F-Phe	−21.0 ± 0.9 (9)	3.8 ± 0.5	−46.6 ± 0.9 (9)	5.1 ± 0.4
Phe1579F_2-Phe	−19.8 ± 1.0 (7)	3.5 ± 0.4	−44.0 ± 0.8 (7)	5.6 ± 0.4
Phe1579F_3-Phe	−23.0 ± 0.8 (10)	3.1 ± 0.2	−43.0 ± 0.6 (9)	5.3 ± 0.2
Phe1579Cha	−23.2 ± 0.6 (9)	3.2 ± 0.2	−42.8 ± 1.0 (4)	5.5 ± 0.3
Tyr1586Phe	−22.8 ± 0.5 (11)	3.6 ± 0.2	−46.9 ± 1.9 (5)	4.4 ± 0.7
Tyr1586F-Phe	−21.0 ± 0.7 (9)	4.1 ± 0.2	−46.9 ± 0.7 (6)	4.6 ± 0.9
Phe1579F_2-Phe	−25.6 ± 0.7 (5)	3.2 ± 0.2	−49.8 ± 0.7 (4)	4.1 ± 0.2
Tyr1586F_3-Phe	−24.5 ± 0.7 (5)	4.0 ± 0.6	−47.9 ± 2.0 (4)	4.6 ± 0.6
Phe1579Cha	−26.9 ± 0.6 (5)	4.9 ± 0.2	−49.1 ± 1.7 (5)	5.4 ± 0.4

Tonic Inhibition

Local anesthetics can interact with Na^+ channels under either stimulated or resting conditions, the latter with lower affinity. Systematic replacement of the equivalents of $Na_V1.4$ Phe1579 and Tyr1586 in neuronal isoforms with nonaromatic residues reduces

* Number of cells indicated in parentheses. The normalized currents were fit by $I(V)/I_{max} = 1/(1+e^{(V-V_{0.5})/k})$, where V is membrane potential, $V_{0.5}$ is the midpoint, and k is a slope factor. Perfusion of oocytes expressing wild-type $Na_V1.4$ with 200 μM lidocaine resulted in a 8 mV hyperpolarizing shift in the $V_{0.5}$ of steady-state inactivation from −46.0 ± 0.6 to −53.5 ± 1.6 mV (P = 0.006, t-test). This lidocaine-induced shift was eliminated in the trifluorinated mutant 3,4,5-F_3-phenylalanine at position 1579, −43.0 ± 0.6 versus −45.0 ± 1.4 mV (P = 0.24), for control and lidocaine saline, respectively. No such relief was seen when 3,4,5-F_3-phenylalanine was incorporated at position 1586 as 200 μM lidocaine exposure resulted in a 7 mV hyperpolarizing shift, $V_{0.5}$ = −46.0 ± 1.2 versus −53.4 ± 1.5 mV (P = 0.02), for control and 200 μM lidocaine saline, respectively.

resting affinity for the local anesthetics etidocaine[2] and tetracaine.[1] Therefore, the possibility of a contribution of cation-π energetics to this tonic inhibition was investigated, which was defined operationally as the fractional reduction of peak current in response to a low rate of depolarization (15 ms pulses to −20 mV at 0.05 Hz). Figure 5.3A shows representative Na^+ currents before and after 5 minutes continuous perfusion of 200 μM lidocaine. Wild-type $Na_V1.4$ channels and those containing cyclohexylalanine at position 1579 showed indistinguishable tonic inhibition. The results for all the side chains introduced at the 1579 position are shown in figure 5.3B and demonstrate that a cation-π interaction with this residue is not a factor in the tonic inhibition by lidocaine.

The role of Tyr1586 was also investigated in tonic inhibition by lidocaine. Consistent with a previous study,[1] removal of the hydroxyl group by mutation to phenylalanine alleviated the tonic inhibition from 30 ± 6% to 19 ± 3%. Figure 5.3C shows that further manipulation of this side chain to withdraw electon density from the ring had no additional effect on the tonic inhibition. These data show that while the hydroxyl group of Tyr1586 plays a role in inhibition, lidocaine does not interact directly with its aromatic face under resting conditions.

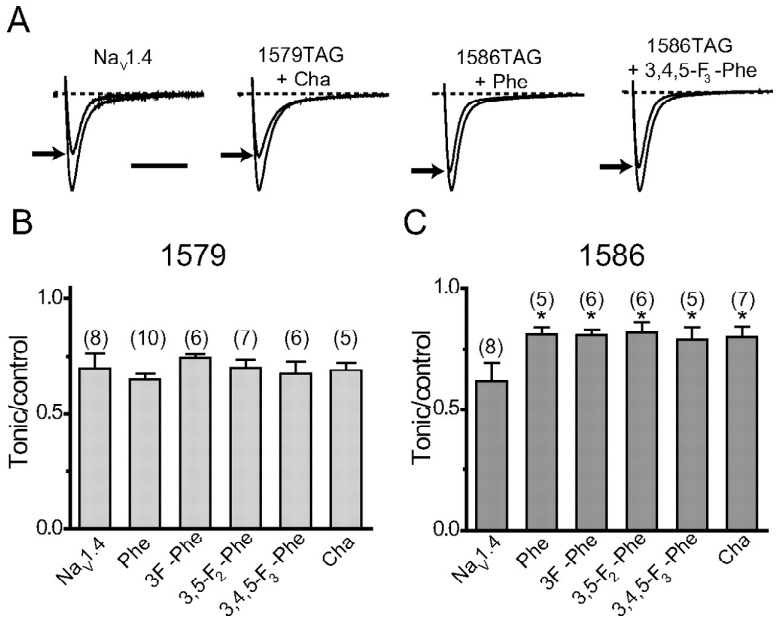

Figure 5.3. Electrostatic contributions are not involved in tonic inhibition for Phe1579 and Tyr1586. A) Normalized control and tonically inhibited currents (indicated by arrow) elicited by test pulses to −10 mV, holding potential −100 mV, scale bar is 5 ms. Tonic inhibition reached equilibrium after 5 minute of continuous perfusion of 200 μM lidocaine as measured by 15 ms pulses every 20 sec. B) Electrostatic potential of Phe1579 does not contribute to lidocaine binding (number of cells in parenthesis). C) Mutation of Tyr1586 to phenylalanine relieves tonic block but any additional manipulation of the aromaticity has no consequence, asterisk indicates $P < 0.05$ versus wild-type $Na_V1.4$.

Use Dependence

Use-dependent inhibition of Na^+ channels is manifest as progressively reduced current with increased stimulation frequency. Although experiments using site-directed mutagenesis show that use-dependent block by local anesthetics involves side chain contributions from residues in each of the four Na^+ channel domains,[2,26-28] the presence of an aromatic phenylalanine, tyrosine or tryptophan at the position aligned with 1579 is

required for use-dependent inhibition,[1] suggesting that a cation-π interaction may play a substantial role at the binding site. Figure 5.4A shows representative Na^+ currents in response to 20 Hz depolarizations to −10 mV from a holding potential of −100 mV in the presence of 200 μM lidocaine. In each example, the 1st and 50th pulses are labeled. Note that the first pulse represents a channel inhibited in its resting state. In the absence of lidocaine, Na^+ currents are stable in response to 20 Hz stimulation with no run down in amplitude. Quite dramatically, trifluorination of Phe1579 nearly abolishes the use-dependent inhibition by lidocaine (figures 5.4A and 5.4B). Similar results were obtained at a tenfold lower lidocaine concentration where tonic inhibition was negligible (figure 5.5), eliminating a substantial role of rapid open-channel block.

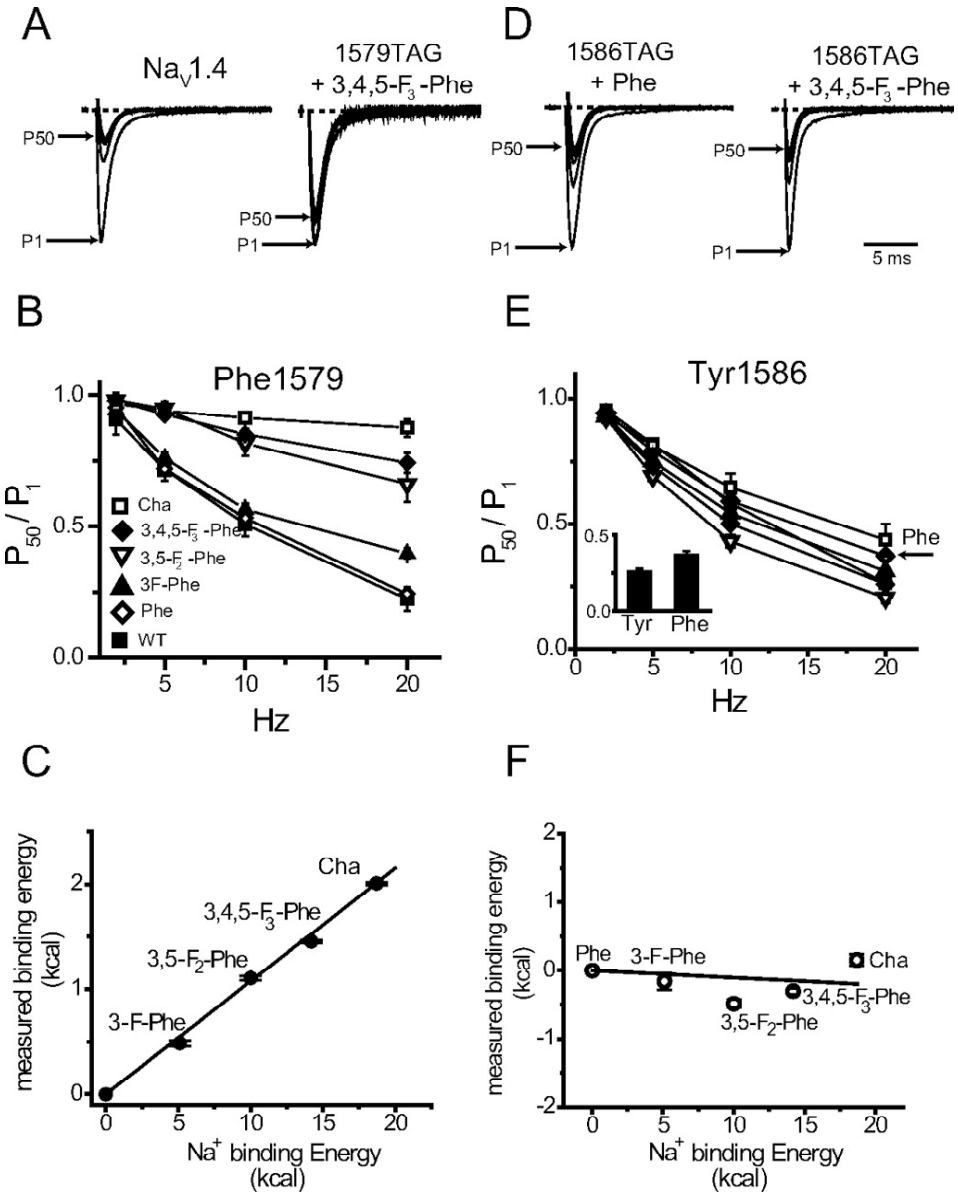

Figure 5.4. Use-dependent inhibition relies on a cation-π interaction between lidocaine and Phe1579, not Tyr1586. A) Normalized representative current traces in the presence of 200 μM lidocaine from repeated depolarizations to −10 mV from −100 mV for $Na_V1.4$ or channels with 3,4,5-F_3-phenylalanine at the 1579 site. The first ten and 50th trace of 50 total pulses are indicated. B) Frequency profile for use-dependent inhibition for cyclohexylalanine and fluorinated phenylalanine derivatives. C) Linear relationship between experimental data and theoretical predictions for a cation-π interaction. Dissociation constants estimated at 20 Hz were used to calculate the energetic effect of manipulating aromatic electrostatic potential at

Phe1579. Binding energy is defined as $0.58\ln(K_{i,\mathrm{mut}}/K_{i,\mathrm{wt}})$ kcal/mol, where $K_{i,\mathrm{mut}}/K_{i,\mathrm{wt}}$ is the fractional increase in the inhibitory constant caused by an unnatural mutant compared to benzene/phenylalanine. Theoretical data on the abscissa are based on the calculated interaction between a single Na^+ ion and the indicated benzene derivative.[29] D) Absence of a cation-π contribution at Tyr1586 to lidocaine inhibition. Normalized representative traces shown as in figure 5.4A. Complete loss of the negative electrostatic potential of the aromatic ring has no effect on use-dependent inhibition. E) Frequency profile of use-dependent inhibition for the 1586 position, as in B. Arrow represents Tyr1586Phe. Inset shows the relief of inhibition for the Tyr1586Phe mutation at 20 Hz. Neither serial fluorination nor replacement by cyclohexylalanine disrupts lidocaine block further. F) Energy plot as in panel C details the complete lack of a cation-π phenotype at 1586.

Evidence for a cation-π interaction between Phe1579 and lidocaine in the inactivated state is presented in figure 5.4B where monotonic relief of inhibition can be seen for each added fluorine, with cyclohexylalanine substitution producing almost complete relief. This effect is most apparent at high frequencies where inactivated states would be expected to dominate. Although use-dependent inhibition by lidocaine is an obvious phenotype, it is an inherently complicated process and as such, the progressive current reduction seen in figures 5.4A and 5.4B is likely a combination of interaction of lidocaine with both inactivated and open states. While acknowledging this caveat, an operationally defined inhibitory constant K_i was calculated from the fraction of current remaining at the completion of 50 pulses delivered at 20 Hz in the presence of 200 μM lidocaine. This apparent inhibitory constant was used to calculate the loss in binding energy resulting from the serial fluorination of phenylalanine or outright replacement by cyclohexylalanine. The result of this analysis is shown in figure 5.4C. The abscissa is

derived from *ab initio* estimates of the energetic effect of fluorination on the cation-π interaction between benzene and a Na^+ ion.[17] As predicted for a cation-π interaction, a stepwise reduction in electrostatic potential on the face of the aromatic results in a monotonic reduction in lidocaine inhibition.[30] Given the ambiguities presented by both the charge asymmetry of lidocaine and the interpretations of use dependence protocols, the linear relationship between our experimental results and the theoretical predictions for a canonical cation-π system is striking, confirming such an interaction between Phe1579 and lidocaine.

The results are remarkably different when the same series of phenylalanine derivatives are substituted into the nearby aromatic Tyr1586 (figure 5.4D). The complete data set in figure 5.4E lacks both the trend and the magnitude of effect that was observed at Phe1579. The inset of figure 5.4E shows the disruptive consequence of exchanging of phenylalanine for tyrosine, an effect greater than any further manipulation of the phenylalanine side chain. Figures 5.4E and 5.4F show that, contrary to the situation for Phe1579 only 11 Å away, perturbation of the electron density on the face of an aromatic residue at Tyr1586 has little consequence on use-dependent lidocaine inhibition, ruling out a cation-π interaction at this site.

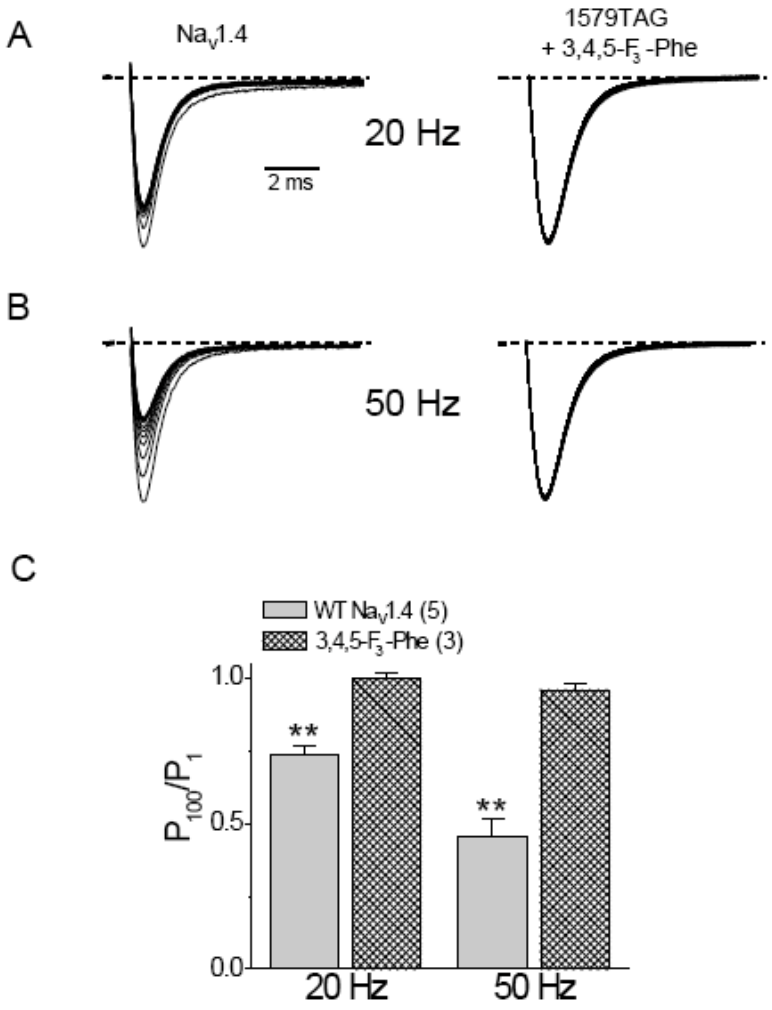

Figure 5.5. Cation-π influence on use-dependent inhibition at a low concentration (20 μM) of lidocaine. Lidocaine was applied 5 minutes before high-frequency stimulation. Tonic inhibition was negligible at this low concentration. A,B) Representative currents at −10 mV for 100 10 ms depolarizations from a holding potential of −100 mV, every 10th trace shown for clarity. Stimulation rate was either A) 20 Hz or B) 50 Hz. Currents were stable at 50 Hz in the absence of lidocaine. Left panels are for wild type, right panels are for 3,4,5-F_3-phenylalanine incorporated at position 1579. C) Fraction of control (P_{100}/P_1) after 100 depolarizations for 5 wild-type and 3 mutant oocytes. Two asterisks indicate P<0.005.

Next it was asked whether lidocaine might interact with a third D4/S6 aromatic residue, Tyr1574 (figure 5.1B) positioned roughly 10 Å upstream from Phe1579 but predicted to lie on the opposite face of the S6 helix. Alanine substitution at this site results in a modest loss of both resting and use-dependent inhibition by etidocaine in $Na_V1.2$,[2] suggesting that it may play a subtle role in stabilizing the inhibitor in its binding pocket. The unnatural amino acid 3,4,5-F_3-phenylalanine was the only residue incorporated at this site because trifluorination effectively ablates the negative electrostatic potential of the face of an aromatic ring.[19,30] As for the other two sites we examined, unnatural amino acid incorporation was well tolerated and produced channels with robust expression and voltage-dependent gating similar to that of wild-type $Na_V1.4$ channels. Trifluorination at this site had no effect on tonic (36 ± 6% versus 39 ± 8%) or use-dependent inhibition (84 ± 4% versus 74 ± 3% at 20 Hz stimulation; P=0.08) for $Na_V1.4$ and for channels with 3,4,5-F_3-phenylalanine at site 1574, respectively. Therefore, only one of the three D4/S6 aromatic residues, Phe1579, shows a robust cation-π interaction with lidocaine.

Recovery

Another experimental manifestation of lidocaine action is the emergence of a slow component in the recovery from fast inactivation.[25] In fact, use-dependent inhibition is largely a consequence of slowed recovery from inactivation. In the absence of lidocaine, all Phe1579 mutants recover rapidly from a 15 ms pulse to −10 mV (figure 5.6A), but clear differences arise in the presence of 200 μM lidocaine (figure 5.6B). For each variant of Phe1579, the recovery time course can be fit by a double exponential

relaxation. A plausible explanation for this biophysical behavior is that the fast and slow components represent unblocked and lidocaine-engaged channels, respectively. Figures 5.6C and D show that while the fast and slow time constants from the biexponential fits are the same across all channel types, the fractional weight of the fast, unblocked component is serially increased with fluorination and replacement by cyclohexylalanine. Therefore, fluorination appears to reduce the fraction of channels that trap lidocaine when they inactivate, whereas the recovery rate of the drug-modified channels is insensitive to the unnatural mutations. These results, like those describing use-dependent inhibition, demonstrate a cation-π interaction between lidocaine and Phe1579. By contrast, neither fluorination of the phenylalanine derivatives incorporated at position 1586 nor replacement with cyclohexylalanine had a measurable effect on the recovery time course, consistent with the use-dependent inhibition experiments summarized in figure 5.4F.

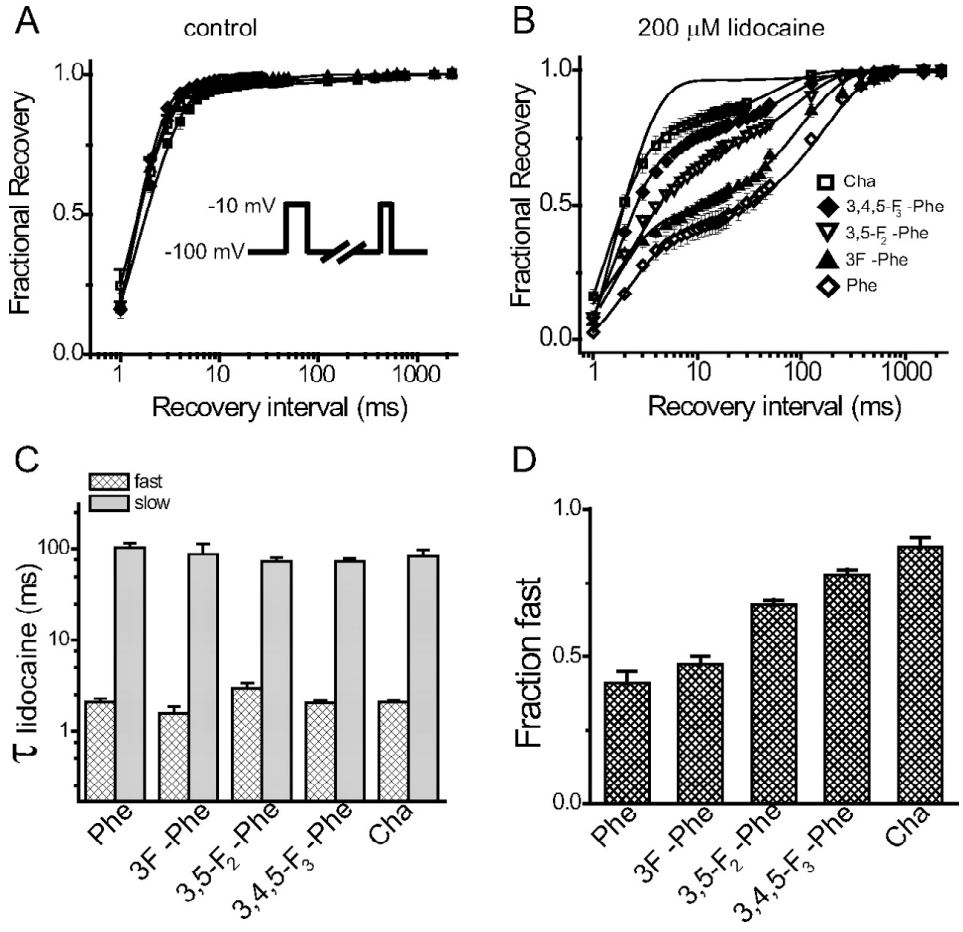

Figure 5.6. Recovery from lidocaine inhibition affected by a cation-π interaction with Phe1579. A) Recovery from inactivation in absence of lidocaine has an indistinguishable double-exponential time course among phenylalanine derivatives. B-D) Fluorination or cyclohexylalanine substitution increases the fractional amplitude of the fast component of recovery in 200 μM lidocaine without affecting the recovery time constants.

Role of Charge

To further test the role of electrostatics in the interaction between a local anesthetic and Phe1579, two nontitratable, structurally similar derivatives of lidocaine were studied, one neutral (benzocaine) and the other permanently charged (QX-314). Both compounds are

postulated to have overlapping binding sites with other local anesthetics and, more importantly, to rely on the presence of an aromatic side chain at Phe1579.[23,31] Benzocaine does not cause use-dependent inhibition in Na^+ channels.[21,22,31] Replacement of the residue at position 1579 by either 3,4,5-F_3-phenylalanine or cyclohexylalanine, both of which effectively abolish the negative electrostatic potential on the aromatic face of phenylalanine, had no effect on tonic inhibition by 1 mM benzocaine (fraction of inhibition was 0.49 ± 0.02, 0.46 ± 0.04, 0.44 ± 0.02, respectively, for wild type and the two unnatural mutants). If benzocaine's binding site overlaps that of lidocaine, the data suggest that the fundamental effect of these manipulations of the aromatic ring of Phe1579 involves electrostatics, leaving benzocaine inhibition unaffected.

The lack of an effect of 3,4,5-F_3-phenylalanine at position 1579 on tonic inhibition by lidocaine (figure 5.3) raises the possibility that lidocaine is deprotonated (uncharged) in its tonically inhibited state. This possibility can be tested directly with permanently charged QX-314 that causes both tonic block and use-dependent inhibition.[2,24,32] If the tonically blocked state involves an intimate interaction between QX-314 and Phe1579, then it should be substantially affected by trifluorination of the aromatic side chain. QX-314 was injected directly into voltage-clamped oocytes to yield an approximate cytoplasmic concentration of 0.5 mM. This concentration produces dramatic resting-state and use-dependent (1 Hz) inhibition in wild-type channels, and only the use-dependent component is ameliorated when 3,4,5-F_3-phenylalanine is incorporated at position 1579 (figure 5.7A), similar to our results with lidocaine. The time course of use dependence and extent of block for the two oocytes shown in figure 5.7A are plotted in figure 5.7C. The summarized data in figures 5.7E and F show that trifluorinating Phe1579 has a

similar effect on binding energy for lidocaine and QX-314, suggesting comparable modes of inhibition. The faster rate of use-dependent inhibition in the unnatural mutant suggests an increased dissociation rate for QX-314 in the drug-bound inactivated state. The results further show that the tonically blocked state does not involve a close interaction between the blocker and Phe1579, yet a substantial cation-π interaction underlies use-dependent inhibition by QX-314.

By contrast with Phe1579, trifluorophenylalanine incorporated at position 1586 causes a mild (<0.5 kcal/mol) stabilization of QX-314 block in both the tonic and stimulated states (figures 5.7D-F). The effect on stimulated-state inhibition is energetically indistinguishable for lidocaine and QX-314 (figure 5.7F).

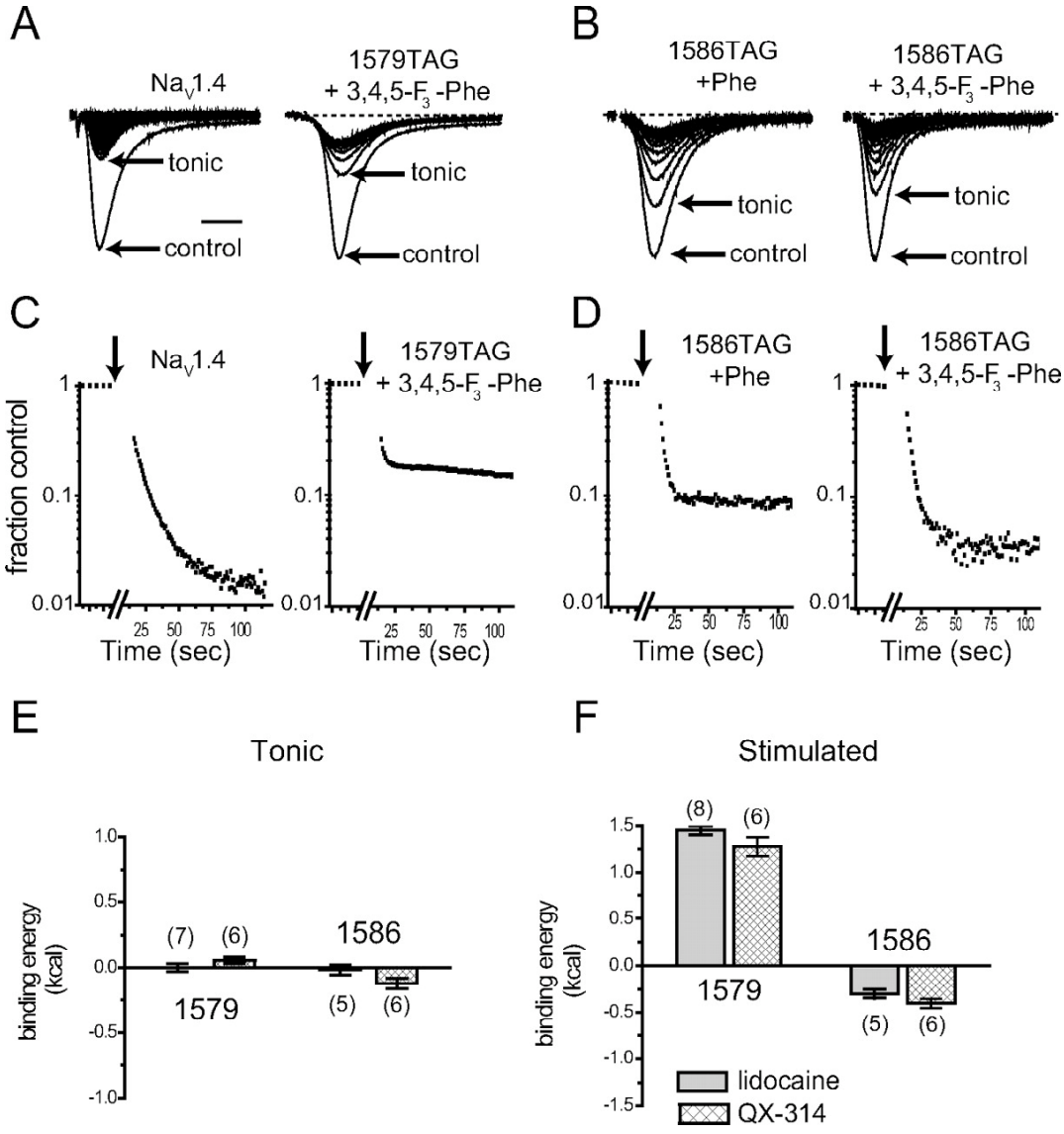

Figure 5.7. Use-dependent and tonic block by QX-314. A) Control is a representative trace at −10 mV (0.1 Hz) after which 25 nL of 20 mM QX-314 was injected to give an estimated final concentration of 0.5 mM QX-314, assuming a 1 μL volume for the oocyte. The oocyte was held at −100 mV for 5 min without depolarization to allow for diffusion, followed by 100 1 Hz, 15 ms depolarizations, the first of which represents the tonic block. Right panel is from an oocyte expressing trifluorinated Phe1579. B) Comparable experiments for residue Phe1586. C,D) Normalized peak currents from records in panels A & B. Arrow indicates time of QX-314 injection. Time break is 5 minutes. E,F) Effect of trifluorination on both lidocaine and QX-314 binding energy (number of cells in parentheses). Lidocaine data from figures 5.3 and 5.4.

Discussion

Three D4/S6 aromatic residues were mutated to determine if any contributed to local anesthetic block through the electrostatic allure of their aromatic π electrons. In contrast with previous studies using traditional site-directed mutagenesis, incorporation of unnatural amino acids at each site resulted in channels with normal gating, substantially simplifying the interpretation of their role in pore block. A cation-π interaction with lidocaine during use-dependent inhibition was observed for only one site, Phe1579, while ablation of the negative electrostatic potential on the face of either Tyr1574 or Tyr1586 had relatively little consequence. The roles of these tyrosine residues in block cited by previous reports may therefore be due to the fact that replacement with a nonaromatic amino acid is a more drastic alteration of side chain chemistry, and often changes the channel's biophysical properties.[2,13-15] Fluorination of phenylalanine, by contrast, has no effect on channel gating at any of the three D4/S6 positions. Although these results suggest that cationic blockers have an electrostatic attraction for the electron density on the face of residue 1579, it may be surprising that replacement of this aromatic residue with negatively charged glutamate or aspartate obliterates use-dependent inhibition by lidocaine.[10] A possible explanation for these apparently contradictory observations is that in an aqueous milieu an organic cation typically has a higher affinity for an aromatic ring than an acidic residue,[33] due to the substantial energetic penalty for dehydrating the acidic residue.

This study provides several structural insights into the local anesthetic binding site in the high-affinity state created by high-frequency stimulation. The cation-π interaction at Phe1579 suggests that lidocaine's positive charge, concentrated in the vicinity of its

titratable amine group, is situated near the aromatic face of Phe1579 in the inactivated state. By contrast, Tyr1574 and Tyr1586 have neither cation-π interactions nor π-π stacking[34] interactions with lidocaine, as either would be disrupted by fluorination of the aromatic ring. Furthermore, cyclohexylalanine lacks the quadrupole moment of an aromatic, and therefore its substitution should reduce any attraction with lidocaine's aromatic moiety through π-π stacking, ruling out this type of attraction between the blocker and the tyrosine residues.

Electrostatic manipulations of Phe1579 affect use-dependent, but not tonic, inhibition. This exception contrasts with the interaction between the cationic Na^+ channel blocker tetrodotoxin and an extracellular pore aromatic, Tyr401, in $Na_V1.4$.[19] In the case of tetrodotoxin, both the tonic and use-dependent block are weakened identically with serial fluorination, implying that a similar physical interaction is present in both states. The results in the present study suggest that tonic and use-dependent block either represent differences in the lidocaine binding site or arise from differences in the charged state of lidocaine (protonated versus deprotonated). The latter possibility is ruled out by our experiments with the permanently charged QX-314 (figure 5.7). Both tonic and use-dependent block are observable with QX-314, but trifluorination of Phe1579 only alleviates use-dependent block. The composite results show not only that tonic and stimulated states represent distinct conformations, but also that in the tonic state lidocaine is not close to any of the three aromatic residues examined. While lack of a cation-π interaction does not rule out other energetic attractions (e.g., hydrophobic, charge transfer, or induced dipoles in the aromatic), an intimate contact between an aromatic side chain and a charged blocker would be expected to be affected by the dramatic

manipulations of electrostatic potential introduced (changes of >600 mV within 2 Å of the aromatic ring.[19]

What, then, accounts for the differences between tonic and use-dependent inhibition? Because the two inhibited states have the same voltage dependence, equivalent to a blocker residing 70% of the way into the electric field from the cytoplasmic side,[35] it was assumed that lidocaine occupies a comparably deep site within the pore in both states. A cation-π interaction only appears between Phe1579 and a charged blocker during repeated depolarizations, indicating that stimulation moves this side chain closer to the blocker. The electrostatic invisibility of Phe1579 in the tonic state suggests that its side chain does not point into the aqueous cavity of the pore, and that it is unveiled, for example, by a rotation of the D4/S6 helix during a conformational transition that accompanies inactivation.[26,36-38] Note that this mechanism contrasts with a previous proposal in which the pore lining remains stationary while the blocker moves.[35] Future experiments should resolve the gating motions that underlie the exposure of a high-affinity receptor.

Conclusion

In this chapter three aromatic residues found in the pore domain of $Na_V1.4$ were probed to determine if they were involved in a cation-π interaction with anesthetics such as lidocaine. Fluorinated-phenylalanine derivatives and the nonaromatic cyclohexylalanine were incorporated into $Na_V1.4$ at the three sites of interest using the *in vivo* nonsense-suppression methodology. Only one residue, Phe1579 in S6 of D4, was found to make a

cation-π interaction with lidocaine and the permanently cationic QX-314, but only during high-affinity use-dependent channel block by the anesthetic. Low-affinity channel block and block by the neutral anesthetic benzocaine were not affected by any of the mutations. These results suggest that when the channel goes from the tonic blocked state to the use-dependent blocked state, the channel moves in a manner that brings Phe1579 closer to the blocker. When the blocker is cationic, the appearance of the electronegative face of the aromatic ring allows it to bind tightly to the channel, but the same is not necessary when the blocker is neutral.

Methods

The work in this chapter was a collaborative effort that included important contributions from Dr. Chris Ahern and Dr. Richard Horn of the Jefferson Medical College in Philadelphia, PA. Detailed methods for the experiments discussed in this chapter that were not performed by the author can be found in Ahern *et al*.[39]

Unnatural Amino Acids and Molecular Biology

Phenylalanine-dCA, 4-F-phenylalanine, 3,5-F_2-phenylalanine-dCA, 3,4,5-F_3-phenylalanine-dCA, and cyclohexylalanine were obtained as described in chapter 2. These aminoacylated dinucleotides were ligated to a modified tRNA from *Tetrahymena thermophila*, THG73, using T4 RNA ligase (New England Biolabs, Ipswich, MA).[16,40]

Acknowledgements

We thank Drs Michael O'Leary and Dottie Hanck for advice, Gregory Lipkind for help with modeling and Mary Y. Ryan for help with oocytes and molecular biology. Supported by grants from the NIH (GM079427 and NS34407).

References

(1) Li, H. L.; Galue, A.; Meadows, L.; Ragsdale, D. S. *Mol. Pharmacol.* **1999**, *55*, 134-41.

(2) Ragsdale, D. S.; McPhee, J. C.; Scheuer, T.; Catterall, W. A. *Science* **1994**, *265*, 1724-8.

(3) Nuss, H. B.; Kambouris, N. G.; Marban, E.; Tomaselli, G. F.; Balser, J. R. *Biophys. J.* **2000**, *78*, 200-10.

(4) Hamilton, D. V. *Lancet* **1978**, *1*, 1365.

(5) Herzberg, L. *Lancet* **1978**, *1*, 1097-8.

(6) Eisenberg, E.; River, Y.; Shifrin, A.; Krivoy, N. *Drugs* **2007**, *67*, 1265-89.

(7) Nau, C.; Wang, G. K. *J. Membr. Biol.* **2004**, *201*, 1-8.

(8) Lipkind, G. M.; Fozzard, H. A. *Mol. Pharmacol.* **2005**, *68*, 1611-22.

(9) Tikhonov, D. B.; Bruhova, I.; Zhorov, B. S. *FEBS Lett.* **2006**, *580*, 6027-32.

(10) McNulty, M. M.; Edgerton, G. B.; Shah, R. D.; Hanck, D. A.; Fozzard, H. A.; Lipkind, G. M. *J. Physiol.* **2007**, *581*, 741-55.

(11) Ramos, E.; O'Leary M, E. *J. Physiol.* **2004**, *560*, 37-49.

(12) Hanck, D. A.; Makielski, J. C.; Sheets, M. F. *Pflugers Arch.* **2000**, *439*, 814-21.

(13) Wright, S. N.; Wang, S. Y.; Wang, G. K. *Mol. Pharmacol.* **1998**, *54*, 733-9.

(14) Xiao, Y. F.; Ke, Q.; Wang, S. Y.; Yang, Y.; Wang, G. K.; Morgan, J. P.; Leaf, A. *Biochem. Biophys. Res. Commun.* **2001**, *281*, 45-52.

(15) Carboni, M.; Zhang, Z. S.; Nepliouéva, V.; Starmer, C. F.; Grant, A. O. *J. Membr. Biol.* **2005**, *207*, 107-17.

(16) Nowak, M. W.; Kearney, P. C.; Sampson, J. R.; Saks, M. E.; Labarca, C. G.; Silverman, S. K.; Zhong, W.; Thorson, J.; Abelson, J. N.; Davidson, N.; et al. *Science* **1995**, *268*, 439-42.

(17) Ma, J. C.; Dougherty, D. A. *Chem. Rev.* **1997**, *97*, 1303-1324.

(18) Leo, A.; Hansch, C.; Elkins, D. *Chem. Rev.* **1971**, *71*, 525-616.

(19) Santarelli, V. P.; Eastwood, A. L.; Dougherty, D. A.; Horn, R.; Ahern, C. A. *J. Biol. Chem.* **2007**, *282*, 8044-51.

(20) Santarelli, V. P.; Eastwood, A. L.; Dougherty, D. A.; Ahern, C. A.; Horn, R. *Biophys. J.* **2007**, *93*, 2341-9.

(21) Hille, B. *J. Gen. Physiol.* **1977**, *69*, 497-515.

(22) Hille, B. *J. Gen. Physiol.* **1977**, *69*, 475-96.

(23) Liu, H.; Atkins, J.; Kass, R. S. *J. Gen. Physiol.* **2003**, *121*, 199-214.

(24) Strichartz, G. R. *J. Gen. Physiol.* **1973**, *62*, 37-57.

(25) Bean, B. P.; Cohen, C. J.; Tsien, R. W. *J. Gen. Physiol.* **1983**, *81*, 613-42.

(26) Kondratiev, A.; Tomaselli, G. F. *Mol. Pharmacol.* **2003**, *64*, 741-52.

(27) Yarov-Yarovoy, V.; McPhee, J. C.; Idsvoog, D.; Pate, C.; Scheuer, T.; Catterall, W. A. *J. Biol. Chem.* **2002**, *277*, 35393-401.

(28) Yarov-Yarovoy, V.; Brown, J.; Sharp, E. M.; Clare, J. J.; Scheuer, T.; Catterall, W. A. *J. Biol. Chem.* **2001**, *276*, 20-7.

(29) Ahern, C. A.; Eastwood, A. L.; Lester, H. A.; Dougherty, D. A.; Horn, R. *J. Gen. Physiol.* **2006**, *128*, 649-57.

(30) Mecozzi, S.; West, A. P., Jr.; Dougherty, D. A. *J. Am. Chem. Soc.* **1996**, *118*, 2307-2308.

(31) Wang, G. K.; Quan, C.; Wang, S. *Pflugers Arch.* **1998**, *435*, 293-302.

(32) Cahalan, M. D. *Biophys. J.* **1978**, *23*, 285-311.

(33) Gallivan, J. P.; Dougherty, D. A. *Proc. Natl. Acad. Sci. USA* **1999**, *96*, 9459-64.

(34) Burley, S. K.; Petsko, G. A. *Science* **1985**, *229*, 23-8.

(35) Gingrich, K. J.; Beardsley, D.; Yue, D. T. *J. Physiol.* **1993**, *471*, 319-41.

(36) Chen, J.; Seebohm, G.; Sanguinetti, M. C. *Proc. Natl. Acad. Sci. USA* **2002**, *99*, 12461-6.

(37) Panyi, G.; Deutsch, C. *J. Gen. Physiol.* **2007**, *129*, 403-18.

(38) Sunami, A.; Tracey, A.; Glaaser, I. W.; Lipkind, G. M.; Hanck, D. A.; Fozzard, H. A. *J. Physiol.* **2004**, *561*, 403-13.

(39) Ahern, C. A.; Eastwood, A. L.; Dougherty, D. A.; Horn, R. *Circ. Res.* **2008**, *102*, 86-94.

(40) Nowak, M. W.; Gallivan, J. P.; Silverman, S. K.; Labarca, C. G.; Dougherty, D. A.; Lester, H. A. *Methods Enzymol.* **1998**, *293*, 504-29.

Chapter VI

ATTEMPTS TO INCORPORATE D-AMINO ACIDS INTO ION CHANNELS USING NONSENSE SUPPRESSION

All ribosomally encoded chiral amino acids are L-amino acids. D-Amino acids have to be incorporated into proteins in nature through nonribosomal peptide synthesis or from the conversion of an L-amino acid by various posttranslational mechanisms. Glycine, the only achiral encoded amino acid, can mimic the backbone propensities of a D-amino acid because of its flexibility, and therefore act as an encoded D-amino acid surrogate. One example where a glycine has the backbone structure favorable for a D-amino acid is the first glycine in the well-known **G**-Y-G selectivity filter of K^+ channels. We hypothesized that this glycine could be substituted with D-alanine and still result in functional channels, and we intended to test this hypothesis using *in vivo* nonsense suppression. The challenge with using this method is that it relies on the natural translational machinery for successful incorporation. All of the previously published attempts to incorporate D-amino acids using nonsense suppression failed, but, to our knowledge, the combination of the tRNA THG73 and the *Xenopus laevis* protein translational machinery had never been tested. A positive result in one of the negative controls prevented the initial *in vivo* nonsennse-suppression experiments in the Shaker B K^+ channel (ShB) from providing any data, but a shift to the nAChR gave promising D-alanine suppression results for both *in vitro* and *in vivo* nonsense suppression with predictable results from the controls.

Unfortunately, the successful suppression experiments in the nAChR were ultimately attributed to the contamination of the D-Ala-tRNA with a small amount of L-Ala-tRNA. The slight racemization of the D-alanine was determined to have occurred during the coupling of the amino acid to dCA, the analog of the aminoacylated end of the tRNA. Preliminary tests attributed the cause of the racemization to the counter ion used to make the dCA soluble in the reaction, but no definitive patterns or solutions were identified. Since the purity of the D-Ala-tRNA was questionable, since neither the THG73 tRNA nor the *Xenopus laevis* translational machinery showed exceptional potential for D-amino acid incorporation into proteins, and since the goal hypothesis was proven true by MacKinnon and Muir through the incorporation of D-alanine into KcsA using expressed protein ligation semisynthesis,[1] these studies were not continued into more depth.

Introduction

Nature plays favorites when it comes to the building blocks of proteins. Nineteen of the twenty coded amino acids have the same general backbone structure: centering around the α-carbon, with the amine group on the left and the carboxylic acid on the right, the bulky sidechain always presents itself forward and the subtle hydrogen hides in the back. The achiral glycine is the only exception. Amino acids with the described structure are denoted L-amino acids after their similarity to L-glyceraldehyde, which was given the "L" notation due to its levorotatory optical activity (figure 6.1A). The "L" notation for amino acids is a misnomer since all L-amino acids do not rotate light counterclockwise as L-glyceraldehyde does. But, the terminology does allow for consistency. If the "R" or

"S" configuration rules were used instead, cysteine, with the SH of its sidechain outweighing the carboxylic acid of its backbone, would represent the lone "R" amino acid.

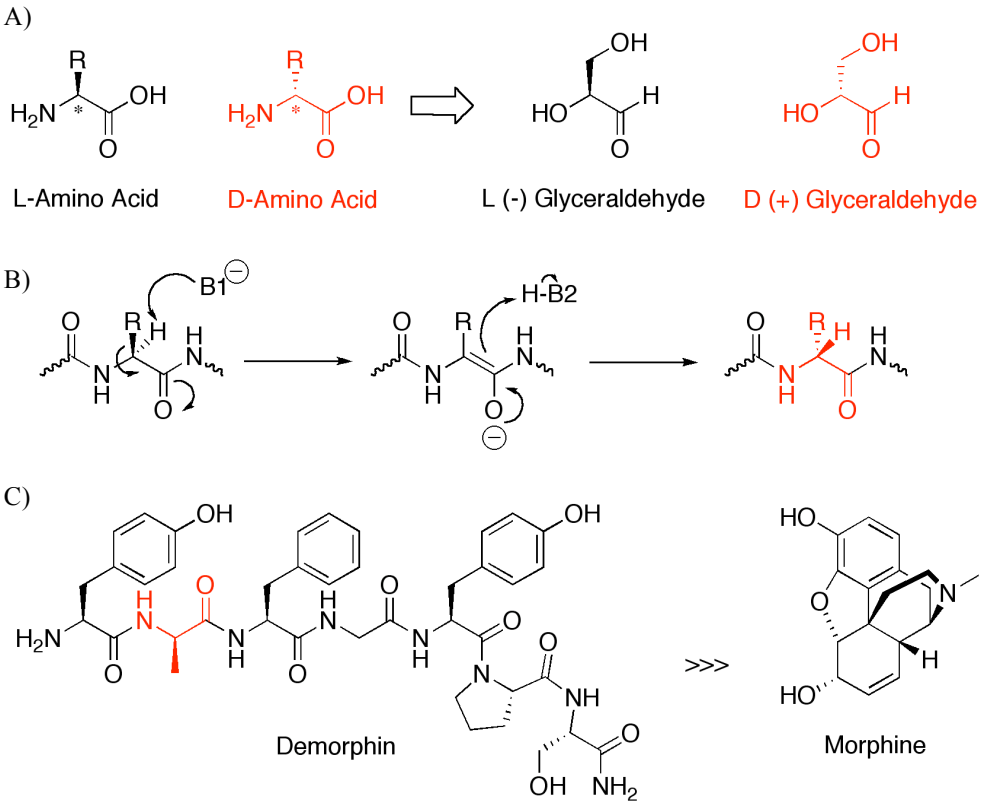

Figure 6.1. The structure of D-amino acids. A) The physical differences of L-amino acids and D-amino acids and their relationship with L (−) glyceraldehyde and D (+) glyceraldehyde. B) The proposed mechanism for amino acid isomerases. C) The structure of demorphin as compared with the less potent morphine. All "D" structures are shown in red.

Amino acids with the opposite orientation, D-amino acids (figure 6.1A), are never used in ribosomal protein synthesis. Instead, these amino acids are only found in nature through conversion of an L-amino acid with an amino acid isomerase (figure 6.1B),[2,3] through

nonribosomal peptide synthesis, and through posttranslational modifications.[4] Common places where nature uses D-amino acids include bacterial cell walls, spider venom, and neurologically active peptides. The neurologically active peptides are an interesting example on which to pause since the overarching theme of this thesis is the chemical-scale exploration of neurobiological targets. One such example, demorphin, is a hepta-peptide excreted from the skin of the South African tree frog *Phyllomedusa sauvagei* (figure 6.1C). Demorphin targets the same G-protein coupled receptor in the brain as morphine, the μ-opioid receptor, but demorphin is a vastly more potent analgesic than morphine and shows reduced tolerance and use dependence than morphine does.[5] Interestingly, the second residue of demorphin is D-alanine (red, figure 6.1C), which is likely converted from the L-amino acid posttranslationally. The presence of this D-alanine is critical to the activity of the peptide: when the second amino acid is L-alanine, the typical analgesic properties of the peptide are not seen in mice. This example shows the power of disrupting nature's bias. The conversion from L-alanine to D-alanine, the simple shift of a single methyl group from one orientation to another, enables this peptide to bind to a neuroreceptor and results in potent pain-relieving downstream events.

The Use of Glycine as a D-Amino Acid Surrogate

The achiral glycine is the natural amino acid that is best suited to be genetically encoded at sites where the backbone structural constraints of a D-amino acid would be appropriate. Glycine's α-carbon has two hydrogen atoms instead of a hydrogen atom and an alkyl side chain. This feature allows it to encompass many possible combinations of ϕ

and ψ angles, including angles that are heavily favored for D-amino acids (figure 6.2). These glycines are often found in loops and turns. McDonnell and Imperiali studied the role of D-amino acids in the hinge region of the synthetic ββα peptide BBAT1, a peptide that forms a trimer when a glycine is located at the hinge between the α-helix and the β-hairpin.[6] The authors made unnatural amino acid substitutions to this important hinge site using solid phase peptide synthesis. Both β-alanine and L-alanine disrupted trimer formation, but substitution to D-alanine retained the trimeric oligomerization. Substituting the glycine for other D-amino acids, such as D-serine and D-asparagine, also retained the trimeric oligomerization, while the large, hydrophobic amino acids D-leucine and D-phenylalanine resulted in tetrameric protein association. Certain other D-amino acids, such as charged residues, still disrupted oligomerization. The authors predict that glycine allows for dihedral angles favorable for oligomerization of the peptide monomer, while D-amino acids, such as D-alanine, actually lock the protein in the geometry necessary for oligomerization. A similar study by Anil *et al.* focused on several glycine residues with positive ϕ angles in two different globular proteins: Gly24 and Gly34 of NTL9, both located in loops, and Gly331 of UBA domain, located at the turn at the end of an α-helix.[7] This study found that replacing these specific glycines with D-alanine using solid-phase peptide synthesis increased the stability of the protein. They reasoned that D-alanine stabilized the folded state by decreasing the entropy of the unfolded state. Thus, in each of these sites in these proteins, glycine was essentially acting as a surrogate D-amino acid, conforming to dihedral angles not possible for L-amino acids.

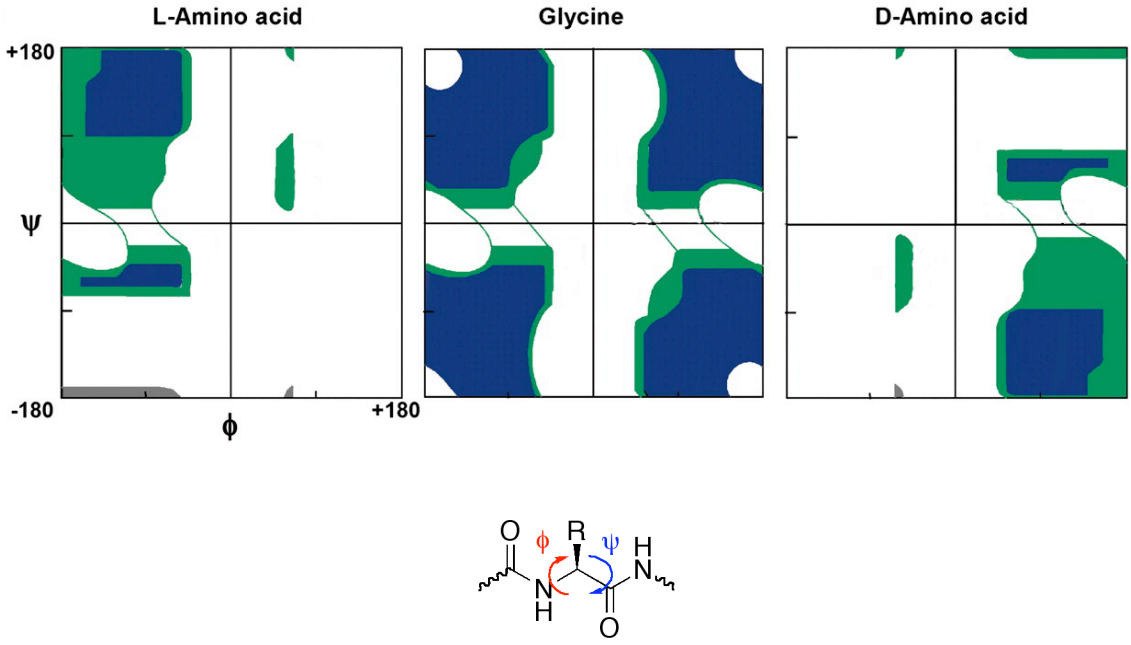

Figure 6.2. Ramachandran plots for L-amino acids, glycine, and D-amino acids. Favorable angle combinations are shown in blue, and allowed angle combinations are shown in green. The rotatable bonds that equate to ϕ and ψ are shown below the plots. Adapted from Valiyaveetil *et al*.[1]

More relevant to this thesis, the high-resolution crystal structure of the bacterical K^+ channel KcsA showed that the first of the famous glycines in the **G**-Y-G motif is in a left-handed helical conformation,[8] which is favorable for D-amino acids but not L-amino acids. The **G**-Y-G motif is an important feature of the selectivity filter, which consists of the highly conserved T-X-X-T/S-X-**G**-Y-G sequence.[8] Incorporating L-amino acids at this site fails to give functional channels.[9] We hypothesized that substituting D-alanine at this site would give functional channels because the dihedral angles are correct and because the side chain would produce the smallest steric perturbation of the familiar chiral amino acids. The method we pursued to test this hypothesis was *in vivo* nonsense suppression.

The Exclusion of D-Amino Acids from Ribosomal Translation

Nature's bias shows up in quality control mechanisms used by the protein translational machinery (figure 6.3). These checkpoints are invoked to maximize proper and efficient protein synthesis,[10] and each checkpoint will be described in more detail below. The use of nonsense suppression bypasses the first of these checkpoints, the aminoacylation of the tRNA by the synthetase, but every other checkpoint must still be passed.

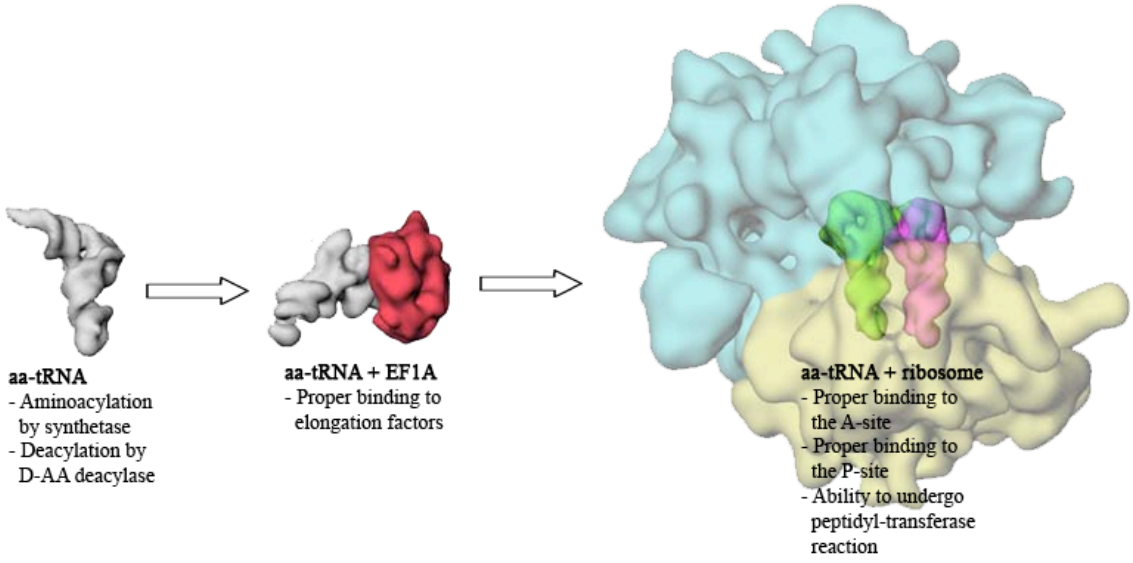

Figure 6.3. The quality control mechanisms that occur during translation. Images adapted from http://www.rpi.edu/dept/bcbp/molbiochem/MBWeb/mb2/part1/translate.htm.

To ensure translational fidelity, each tRNA must be properly aminoacylated with its specific amino acid. Therefore, editing mechanisms have evolved to hydrolyze off incorrect amino acids. It was determined from *in vitro* studies that D-amino acids can be misacylated onto tRNAs by certain synthetases.[11] These tRNAs can be recycled by an enzyme called the D-amino acid deacylase, which recognizes D-amino acids that have

been improperly added to tRNA and removes them from the tRNA. This enzyme was discovered by Calendar and Berg when they determined that extracts from *E. coli*, yeast, rabbit reticulocyte lysate, and rat liver could rapidly and selectively hydrolyze the ester linkage of *E. coli* D-Tyr-tRNA.[12] The deacylase gene has been found in many organisms through both experiment and sequence alignment,[13-15] making this enzyme's prevalence important to the study of D-amino acid incorporation using nonsense suppression. In this chapter the potential D-amino acid deacylase is never addressed in our experiments, but one could imagine that if the *Xenopus laevis* produced D-amino acid deacylase, then as soon as the D-aminoacyl-tRNA was injected into the oocyte, the D-amino acid would be stripped from the tRNA by the enzyme. Our experiments are reliant on the lack of the deacylase in *Xenopus* or on overwhelming of the deacylase in the cytosol with the amount of injected tRNA.

The answer to incorporating D-amino acids into proteins is not as simple as removing the D-amino acid deacylase. Work done by Cornish and co-workers testing the functionality of D-amino acids appended to a designed *E. coli* tRNA in an *in vitro* system that lacked D-amino acid deacylase did not detect any incorporation of D-amino acids into their model tripeptides.[16] Thus, at least in *E. coli*, removal of the D-amino acid deacylase does not allow for ribosomal D-amino acid incorporation.

Next, the aminoacylated tRNA (aa-tRNA) must bind to an elongation factor, EF1A in bacteria and eEF1A in eukaryotes, in a ternary complex with GTP for proper delivery of the tRNA to the ribosome. Together each cognate aa-tRNA has approximately the same affinity for EF1A,[17] but Uhlenbeck and co-workers found that the relative affinities for certain tRNAs and certain amino acids for EF1A vary over a large range.[18-21] Thus, a

model of thermodynamic compensation was proposed.[18] This model states that an amino acid with a strong affinity must pair with a tRNA with a weak affinity, and vice versa, so that each combined aa-tRNA has the same relative affinity for EF1A. If two strong partners are paired, the aa-tRNA binds too tightly to the EF1A, and if two weak partners are paired, then the aa-tRNA does not bind tightly enough to the EF1A. Protein synthesis is limited in both of the nonideal cases.

The affinity of D-amino acids for eEF1A is not known, but the difference in conformation likely puts them into the weak-binding amino acids category. Therefore, according to the model, a tight tRNA-EF1A binding interaction would be crucial for the delivery of the D-aa-tRNA to the ribosome. In practice the model of thermodynamic compensation does not limit the effectiveness of the nonsennse-suppression method. A large variety of both natural and unnatural amino acids can be incorporated into proteins using a single tRNA.[22] The work discussed in this chapter relies on this trend to continue and include D-alanine.

Finally, the aminoacylated tRNA must be able to enter the ribosome at the acceptor site, the A site, undergo the peptidyl transferase reaction by accepting the growing peptidyl chain, and then move to the donor site, the P site, to continue the synthesis of the protein. The ribosome is compatible with a variety of different amino acids and hydroxy acids as seen through the many residues incorporated with nonsense suppression. But, D-amino acids have exhibited low compatibility to date.[23-25] D-Amino acids have been shown to bind in both the A and P sites of the ribosome.[26,27] Using the model of puromycin, an analog of the aminoacyl end of tRNA that enters the A site of the ribosome, participates in the peptidyltransferase reaction, and therefore halts further protein synthesis, Starck *et*

al. showed that D-puromycin can also inhibit protein translation through its participation in the peptidyltransferase reaction, though it is 150 times less potent than its natural L-analog.[28] This result, along with the fact that D-amino acid dipeptides have been made *in vitro,*[29,30] argues that D-amino acids should be able to function in at least the first step of ribosomal synthesis.

Unfortunately, to date D-amino acids have not been shown to be competent for ribosomal incorporation into larger peptides or proteins with wild-type ribosomes. Work by Hecht and coworkers showed that certain mutant *E. coli* ribosomes incorporate D-amino acids into full proteins.[24,31] The critical mutations occurred in the 23S rRNA in the peptidyltransferase center (PTC) and in helix 89. These mutations were thought to alter the ribosome conformation around the PTC in a manner conducive for D-amino acids to be accepted into protein synthesis. Since mutations in the PTC cause the ribosomes to form peptide bonds at a reduced rate and since these mutated ribosomes are only viable in *in vitro* protein synthesizing systems,[32-34] this approach is not compatible with *in vivo* nonsense suppression.

Qualitatively viewing each checkpoint in protein synthesis individually, the bias against D-amino acids looks small and indirect. Quantitatively, the L-enantiomer is favored over the D-enantiomer by a factor of 25 for aminoacylation,[35,36] 25 for ternary complex formation, 10 for EF1A-promoted binding to the A site of the ribosome, and 5 for peptidyl transfer.[29] Therefore, when viewed together, translation favors L-amino acids by a factor of $3x10^4$, which means if the L-enantiomer is present, the D-amino acid is virtually excluded from ribosomal protein synthesis.

Testing D-Amino Acids in the Xenopus laevis *System*

Our first goal was to ascertain whether D-amino acids could be incorporated into proteins in *Xenopus laevis* oocytes using *in vivo* nonsense suppression. Many early *in vitro* nonsennse-suppression studies attempted to incorporate D-amino acids into proteins.[25,37-39] Since the nonsennse-suppression method involves tRNA chemically aminoacylated to the unnatural amino acid, aminoacylation by the synthetase is not a competing factor. Also, by coupling pure D-amino acid to tRNA, the favoritism for the L-enantiomer is removed. These studies were repeatedly unsuccessful, but *E. coli* and rabbit reticulocyte lysate translational machineries were the only systems studied. To our knowledge, the ability of the *Xenopus laevis* translational system to incorporate D-amino acids through the *in vivo* nonsennse-suppression method had never been probed. Herein the results of our study are discussed. Preliminary data looked promising until it was discovered that the amino acid chirality was compromised in one of the last steps of the synthesis of the aminoacylated tRNA.

During the course of this thesis, the glycine-to-D-alanine substitution in the **G**-Y-G of the selectivity filter of KcsA was shown to give function channels by MacKinnon and Muir using expressed protein ligation semisynthesis.[1] They proved the hypothesis intended to be tested in this work by determining that a D-amino acid is functionally accepted at this site in a K^+ channel.

The combination of the literature precedent for the failure of the incorporation of D-amino acids into large proteins by nonsense suppression, the racemization that was seen in coupling reactions, and the success of the expressed protein ligation semisynthesis

method deterred the continuation of this project much beyond the preliminary examination of the coupling reaction for the cause of the small amount of observed racemization.

Results and Discussion

Synthesis of L- and D-Alanine-tRNA

The D-amino acid of interest was D-alanine since its minimal size makes it most appropriate for study in the **G**-Y-G of the K^+ channel. It is the least sterically hindered of all the chiral amino acids, which should minimize any steric clash that might result from the inverted stereochemistry during translation and protein folding. The synthesis of L- and D-alanine is shown in scheme 6.1.[40-42] The amine was first protected with the nitroveratryloxycarbonyl (NVOC) photolabile protecting group.[43] Next, the acid was activated as a cyanomethyl ester. This compound was then coupled to the tetrabutylammonium salt of dCA. At this point, the amino acid can be attached to either the 2' or the 3' hydroxyl of dCA since it is thought to rapidly sample both sites. Finally, the aminoacylated dCA was ligated to THG-73 using T4 RNA ligase.

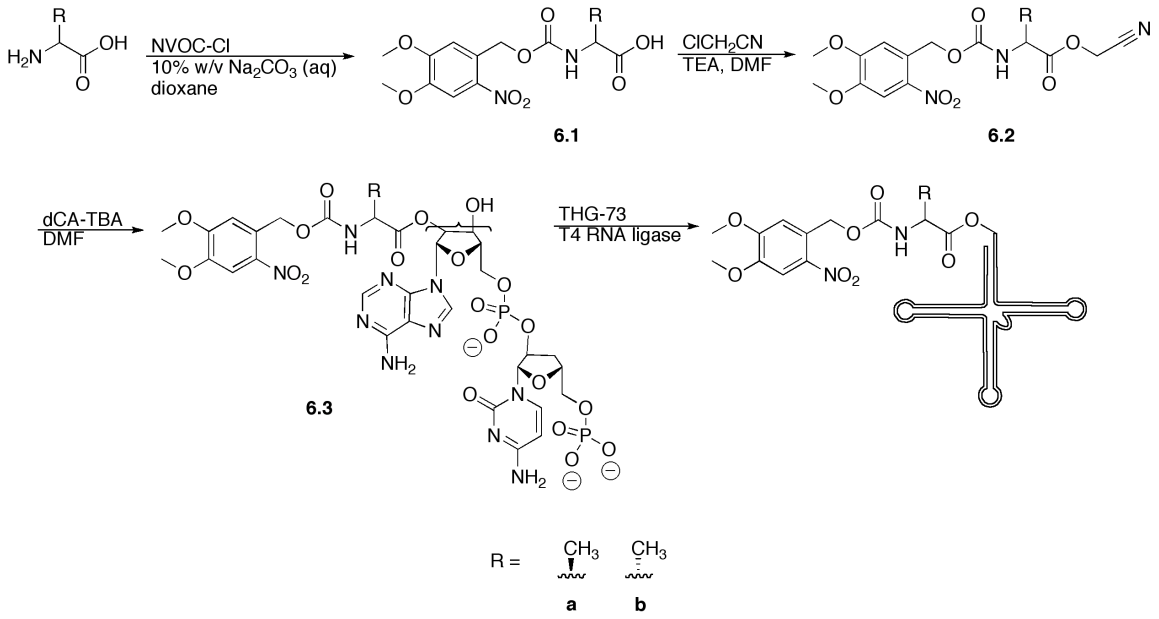

Scheme 6.1. General method for the synthesis of aa-tRNAs.

The First Test System for D-Amino Acid Incorporation: The Shaker B K^+ Channel

The first target protein to test for D-amino acid incorporation was ShB. This protein was chosen not for the study of its **G**-Y-G motif but because a relatively straightforward test for incorporation was envisioned. As introduced in chapter 1, ShB is a voltage-gated K^+ channel that is made up of four identical subunits. The first twenty amino acids of each subunit make up a channel-blocking "ball" that is connected through a "chain" of the next twenty amino acids (residues 23 through 40) to the channel. N-type channel inactivation occurs when one of the four balls of the homotetrameric channel swings up and plugs the channel.[44-47]

Previously published unnatural amino acid studies using *in vivo* nonsense suppression have targeted two sites in the chain of this receptor, Leu47 and Pro64, both denoted with

the * in figure 6.4.[48] These sites were selected for study in this work for several reasons. First, since these two sites are part of the chain, a region thought to be loosely organized due to its ability to rapidly move to block the channel, it was predicted that incorporation of a D-amino acid here would not cause any negative folding effects to the main transmembrane region the channel. Second, since these sites occur at the beginning of the protein sequence, if the D-amino acid is not incorporated, synthesis of the channel subunit will be ceased before the bulk of the channel has been made, eliminating the possibility of a functional truncated channel. Finally, the DNA with the necessary TAG codon at these two sites was already available. If any currents from ShB were seen, then it would be likely that D-amino acids were accepted by the *Xenopus* oocyte protein translational machinery.

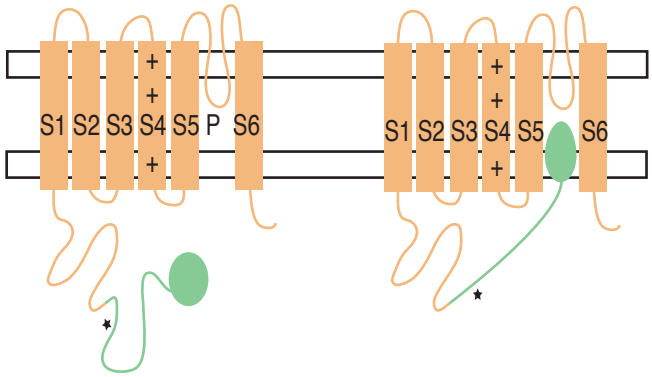

Figure 6.4. Schematic of a ShB subunit with the ball and chain highlighted in green. The * marks the approximate site of unnatural amino acid incorporation.

Experiments were done on *Xenopus* oocytes in a two-electrode voltage-clamp configuration using a voltage-jump protocol that began at −80 mV and increased in 25

mV increments to +70 mV (figure 6.5, "Representative Voltage Jumps"). General published procedures for whole cell recording on the ShB were followed.[48] Upon membrane depolarization, a wild-type ShB opens, allowing potassium ions to pass out of the cell until the N-terminal inactivating "ball" blocks the channel from conducting. This response is seen as a steep rise in current followed by a slightly less steep decrease in current to a steady state during the entire period of depolarization (figure 6.5, wild type). Larger channel currents are seen with larger depolarizations. Thus, typically at +70 mV, the I_{max}, or maximal current, is obtained. The typical experiments included recording from oocytes injected 24 hours previously with (a) ShB wild-type mRNA; (b) ShB lacking the N-terminal "ball" (ShB Inactivation Removed or ShIR); ShB Leu47TAG mRNA (c) with L-Ala-tRNA, (d) with D-Ala-tRNA, (e) with unaminoacylated-tRNA (tRNA that had been ligated to unaminoacylated-dCA), and (f) by itself; and ShB Pro64TAG mRNA (g) with L-Ala-tRNA, (h) with D-Ala-tRNA, (i) with unaminoacylated tRNA, and (j) by itself. The wild-type mRNA (a) and ShIR mRNA (b) were used as positive controls to determine how well the oocytes were expressing the injected mRNA. Large currents seen here correlated with successful nonsennse-suppression experiments. The L-Ala-tRNA experiments (c, g) are positive controls for the success of the nonsennse-suppression experiment. The unaminoacylated-tRNA experiments (e, i) were negative controls for reaminoacylation of the tRNA. The injected unaminoacylated-tRNA mimics the state of the aa-tRNA once it has been used in protein synthesis or once the amino acid is removed (through a chemical event or from a cellular editing mechanism). Any current seen in these negative controls is from the tRNA being recognized by cellular synthetases, reaminoacylated with a natural amino acid, and then

being used in protein synthesis. Since it is necessary for the experiment that reaminoacylation be kept to a minimum so that the protein being expressed has the desired amino acid, the current seen in this negative control must be negligible compared to the amount of current seen in the nonsennse-suppression experiment. The mRNA only experiments (f, j) were negative controls for the amount of read through seen with the TAG codon at the specific site in the ShB. If current is seen here, then the translational machinery has essentially read through the designed stop codon as it is synthesizing the protein and produced a functional protein without the desired amino acid incorporated into it.

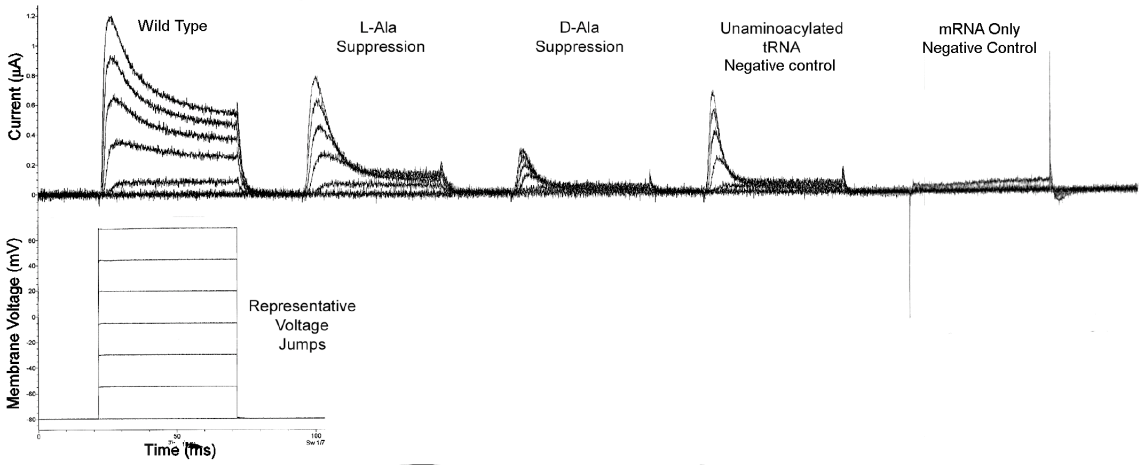

Figure 6.5. Representative traces for the suppression at both Leu47TAG and Pro64TAG. The specific suppression experiments were recorded from Pro64TAG mRNA.

Unfortunately, the incorporation of D-alanine could not be confirmed since there was substantial current seen in the unaminoacylated-tRNA negative control (figure 6.5). The current was not due to read through since injecting only the TAG-containing mRNA

leads to negligible current. This susceptibility to reaminoacylation by THG73 has been shown to be problematic in other studies.[49] Since current was seen here, it is presumed that these two sites can contain a variety of natural amino acids, the leucine or proline originally encoded, the alanine used in this study, and glutamine, the likely residue added through reaminoacylation,[50] and still gate in response to voltage changes and still N-type inactivate. Incidentally, this promiscuity is one of the reasons these sites were chosen as good sites for incorporation of D-amino acids. An explanation for why the reaminoacylation current was larger than the current seen in the D-alanine studies is because the reaminoacylation of injected unaminoacylated-tRNA is more facile than the eventual reaminoacylation of aa-tRNA.[49,51]

Sequencing the DNA showed that the genetic sequence was as expected at the N-terminus, and remaking the mRNA and tRNA did not improve the results. Controlling the amount of tRNA, mRNA, or incubation time was not attempted, though studies have shown that these factors can reduce THG73 reaminoacylation.[52] Studies have also shown that using a four-base codon suppression approach can limit reaminoacylation,[49,53] but the incorporation of D-alanine was never tested with the available ShB masked gene containing the Pro64GGGU mutation and the tRNA YFaFS.[49] Instead, this region of this protein was abandoned as a test system for D-amino acid incorporation.

D-Amino Acid Incorporation In Vitro *Using Rabbit Reticulocyte Lysate*

Rabbit reticulocyte lysate is an *in vitro* translation system used to quickly test whether an unnatural amino acid is translationally competent. Since the incorporation of D-alanine

into ShB could not be confirmed, rabbit reticulocyte lysate was used as a rapid test of D-alanine suppression *in vitro*. Rabbit reticulocyte lysate has been unsuccessful at incorporating D-amino acids in previously published studies,[54] but no studies have ever attempted the *in vitro* synthesis with the suppressor tRNA THG73. Protein synthesis was visualized using Western blotting techniques, using previously published methods.[55] The muscle nicotinic acetylcholine receptor (nAChR) was chosen as the protein construct in this *in vitro* study because of its extensive use in the Dougherty laboratory in rabbit reticulocyte lysate experiments. This receptor will be discussed in more detail below. Specifically, nAChR α1Leu250UAG mRNA containing a hemagglutinin (HA) epitope between residues 347 and 348 was used. Western blotting was preformed using a mouse antibody against the HA sequence and a chemiluminescent goat-anti-mouse antibody and showed full length protein in the *in vitro* experiment containing mRNA and L-alanine charged tRNA and, most importantly, in the *in vitro* experiment containing mRNA and D-alanine charged tRNA (figure 6.6).

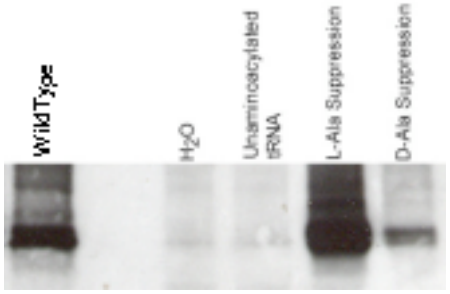

Figure 6.6. Western blot showing D-alanine suppression.

The amount of protein in the D-Ala experiment was estimated to be 10% of that in the L-alanine experiment. Though the amount of protein suppression was greatly reduced

between L- and D-alanine, this result was exciting as it was the first evidence of D-amino acid incorporation into a protein.

The Second Test System for D-Amino Acid Incorporation: The Muscle nAChR

Because of the positive results in the rabbit reticulocyte lysate *in vitro* system with the muscle nAChR, this same receptor was chosen as the second test system for D-amino acid incorporation. Sites in the α subunit were targeted with the goal of finding one where both D-alanine and L-alanine would not only express but also show distinctive differences in channel function. An assortment of sites was selected based on easily available DNA: α1Ala122, α1Ile123, α1Pro236, and α1Leu250 (the same site used in the *in vitro* experiments above). These sites are highlighted in figure 6.7. The first two are found in a β-sheet in the extracellular domain, and the latter two are found in α-helices in the transmembrane domain. These sites are not ideal for D-amino acids due to their rigid structures, but it was hoped that they would show obvious changes in channel function if D-amino acids were incorporated.

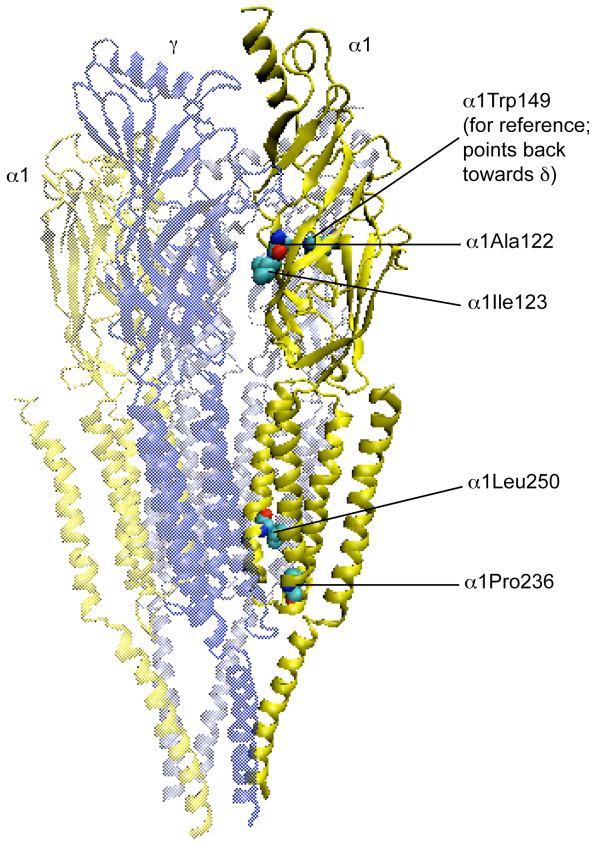

Figure 6.7. A representation of the muscle nAChR with the sites studied in this chapter highlighted and shown as space-filling (light blue = carbon, red = oxygen, blue = nitrogen), adapted from the cryoelectron microscopy homology model of the nAChR 2BG9.[56]

Whole-cell recordings were made on the OpusXpress workstation. This instrument allows multiple oocytes to be studied in parallel through automatic impalement, fluidics, voltage clamp, and data acquisition. The data collected were the nAChR's responses to agonist concentrations from 1 to 1000 μM ACh. The binding of agonist to the nAChR causes a conformational change that opens a central pore in the transmembrane domains of the channel, which allows an influx of cations into the cell. This gating response is seen as a downward current. An increase in agonist concentration correlates with an

increase in current response. The range of agonist concentrations specified above was chosen because the lowest ACh concentrations stimulated no response, and the highest ACh concentrations stimulated maximal response from the receptor.

Suppression of both L-alanine and D-alanine at α1Ala122TAG gave whole-cell currents (figure 6.8), and no current was seen in the negative controls (same as above, mRNA injected with unaminoacylated-tRNA or by itself). The L-alanine experiment was essentially a wild-type recovery experiment, since the naturally encoded amino acid is alanine. Here, current began with the addition of 5 μM ACh, and the maximum current (approximately 10 to 15 μA) was seen around 500 μM ACh. In the case of D-Ala suppression, expression seemed to confirm the results seen in the *in vitro* Western blot experiments. Current began with the addition of 25 μM ACh, and the maximum current (approximately 1 to 5 μA) was seen around 500 μM ACh. There was a small upward current seen at low agonist concentrations in the D-alanine suppression experiments (figure 6.8, D-alanine suppression with 5 μM ACh) that was an artifact attributed to the change in fluidics from bath solution to agonist solution that is only seen in recordings on oocytes with low nAChR expression.

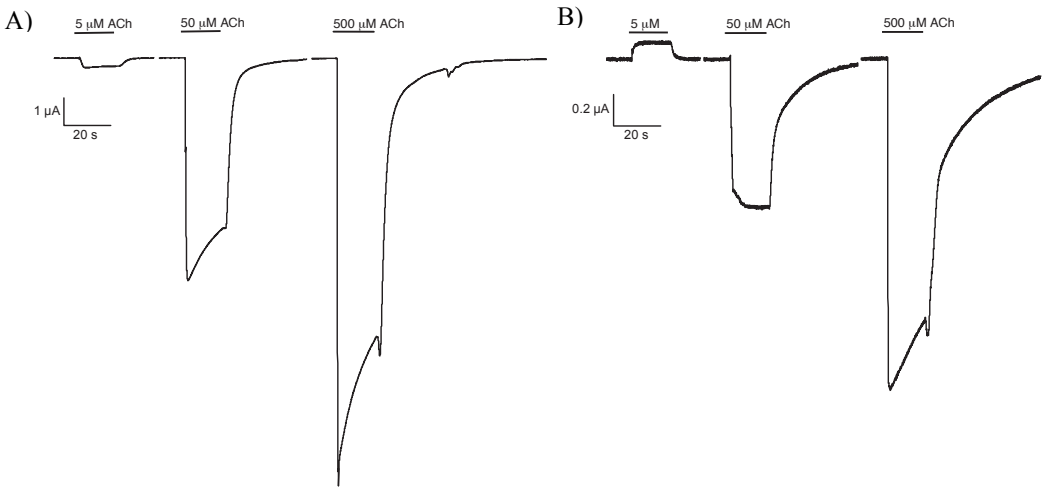

Figure 6.8. Representative current traces for suppression at nAChR α1Ala122. A) L-Alanine suppression. B) D-Alanine suppression.

The current responses of both L-alanine and D-alanine at α1Ala122UAG were then normalized and plotted against the concentration of agonist used on a log scale, producing the dose-response curve seen in figure 6.9.

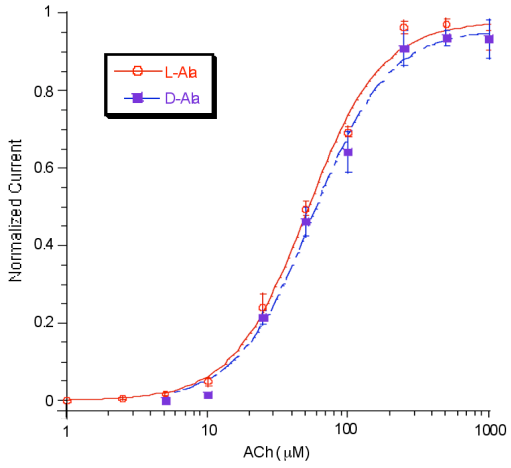

Figure 6.9. Dose-response curve from L-alanine and D-alanine suppression at α1Ala122TAG.

These data were further analyzed by obtaining an EC_{50} value and a Hill coefficient (h) from fitting the current response (I) versus agonist concentration (A) to the Hill equation.

$$I = \frac{I_{\max} A^h}{EC_{50}{}^h + A^h}$$

The EC_{50} value is the agonist concentration that stimulates half-maximal current response, and it reflects the receptor's sensitivity for a given agonist. This value is not a true binding constant; rather it is a composite value incorporating the equilibrium for both agonist binding and channel gating.[57] The Hill coefficient is a measure of the cooperativity a receptor displays in binding multiple ligands. Data analysis was completed for the suppression of L- and D-alanine at α1Ala122TAG and also for the various other α1 nAChR sites probed during this study (table 6.1). The only other successful suppression experiment was L-alanine at α1Ile123. Current was seen upon suppression of D-alanine at α1Ile123, but no interpretable trend was established between the amount of current and the concentration of agonist. No current was seen for either L- or D-alanine at α1Pro236 or α1Leu250.

The EC_{50} value obtained from the wild-type recovery experiment with L-alanine suppression was 51.1 ± 3.5 μM with a Hill coefficient of 1.65 ± 0.16 (n = 9) (table 6.1). This EC_{50} value is within error of 49 μM, the EC_{50} previously published by Dougherty and coworkers for wild-type muscle nAChR.[40] Surprisingly, the EC_{50} value and Hill coefficient obtained from the D-alanine suppression experiment were within error of L-alanine: 56.3 ± 4.5 μM and 1.63 ± 0.19 (n = 5). According to our hypothesis, the incorporation of D-alanine into a β-sheet at α1Ala122 in the muscle nAChR should

impact channel function, but our data show that D-alanine is essentially the same as L-alanine. The similarity between the EC_{50} and Hill data obtained for the incorporation of L- and D-alanine led us to speculate that our pure D-alanine tRNA was not actually pure—that sometime during the synthesis of the aminoacylated-dCA, the enantiopurity of D-alanine had been compromised. These studies were halted, and the focus of the work became the analysis of the enantiopurity of the D-alanine analog.

Table 6.1. Data obtained for incorporation of L- and D-alanine at various sites in the α1 subunit of the muscle nAChR.*

Site	Amino Acid	EC_{50} (μM)	Hill
α1Ala122TAG	L-Ala	51.1 ± 3.5	1.65 ± 0.16
	D-Ala	56.3 ± 4.5	1.63 ± 0.19
α1Ile123TAG	L-Ala	24.6 ± 2.7	1.64 ± 0.24
	D-Ala	ND	ND
α1Pro236TAG	L-Ala	NR	NR
	D-Ala	NR	NR
α1Leu250TAG	L-Ala	NR	NR
	D-Ala	NR	NR

Analysis of Unnatural Amino Acid Chirality

One method of quantitatively measuring the stereochemical purity of a compound is chiral column chromatography using high-performance liquid chromatography (HPLC).[58] Chiral HPLC columns contain single enantiomers immobilized on their stationary phase. Resolution of enantiomeric organic compounds is due to the formation of transient

* ND = No interpretable data. NR = No response.

diastereomers on the surface of the column; the enantiomer that forms the most stable diastereomer will be retained longer than the opposite enantiomer.

The goal was to analyze *N*-nitroveratryloxycarbonyl (NVOC) alanine cyanomethyl ester **6.2a** and **6.2b** both prior to the dCA coupling reaction and after the unreacted portion was recovered from the dCA coupling reaction, since these two points would reflect the stereochemical purity of the general NVOC-protection and cyanomethyl ester activation reactions and of the coupling reaction. A racemic mixture of **6.2a** and **6.2b** was found to separate using a Chiralcel OD-H column with 12% ethanol in hexanes. The OD-H column is cellulose tris(3,5-dimethylphenyl) carbamate on a 5 μm silica-gel substrate.

Both **6.2a** and **6.2b** were individually run on the chiral HPLC and were found to be pure enantiomers (figure 6.10). Thus, neither the NVOC protection nor the cyanomethyl ester activation compromised the α-stereocenter. To determine whether the coupling of these derivatives to dCA destroyed the enantiomeric purity, the unreacted amino acid starting material from each coupling was recovered and run on the chiral HPLC. The D-alanine reaction was allowed to run for 2 hours, whereas the L-alanine reaction was allowed to run for 20 hours. In both the D-alanine and the L-alanine reactions, roughly 5 to 10% of the recovered starting material was the opposite enantiomer, which proved that the conditions used in the dCA coupling reaction led to compromised enantiopurity, but not total racemization.

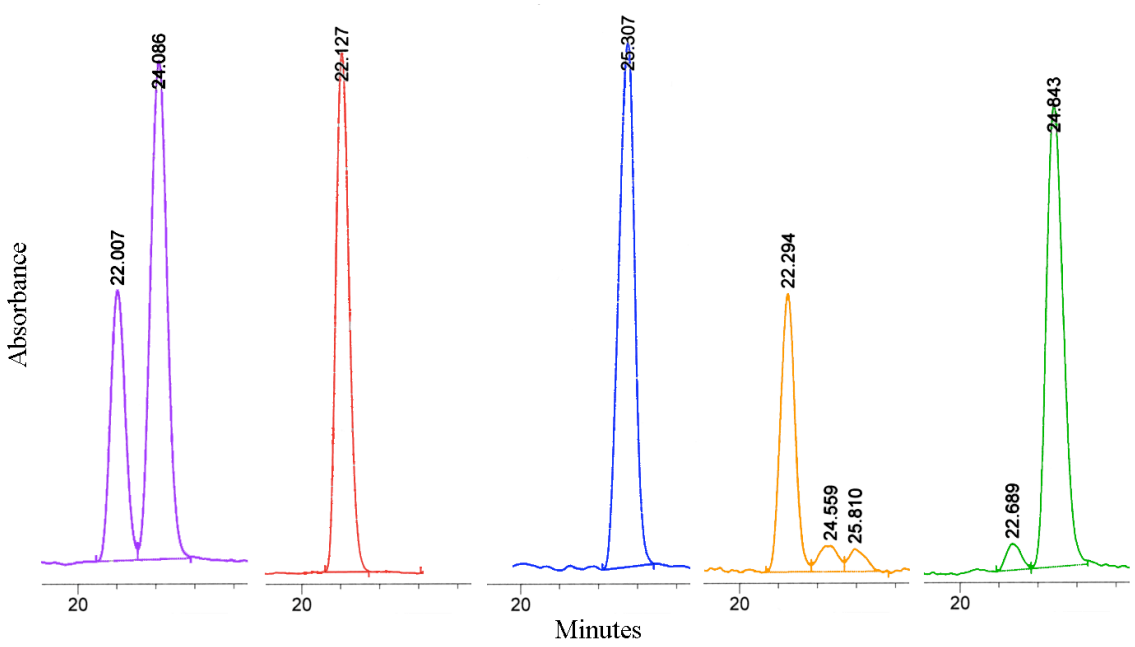

Figure 6.10. Representative chrial HPLC traces showing the difference between the enantiopurity of the NVOC-alanine cyanomethyl ester before (**6.2b** red, **6.2a** blue, both pure) and after (**6.2b** orange, **6.2a** green, both contain small amounts of the opposite enantiomer) entering the coupling reaction. The racemic mixture of **6.2a** and **6.2b** is shown in purple. The identity of the third peak in the orange trace (25.810 minutes) was never determined, but it is likely NVOC-D-alanine.

Our typical dCA coupling uses 3.0 equivalents of the NVOC-protected cyanomethyl ester, 2.4 equivalents of the tetrabutylammonium counter ion, and 1.0 equivalent of dCA in DMF at room temperature. Prior to this work, these conditions had never been tested for racemization in our laboratory. To determine what was compromising the stereochemical purity of the amino acid, each component of the coupling reaction was analyzed. Taking the variables in the coupling reaction as time, solvent, dCA, and identity of counter ion salt, we isolated each one to determine if any could be linked to the racemization of **6.2a** and **6.2b**. The reactions that were set up are listed in table 6.2.

Table 6.2. The various reaction conditions tested for racemization.*

NVOC-Ala-CME (eq)	Time (h)	Solvent	dCA (eq)	Salt (eq)		Racemization
1	0	0	0	0	0	0.0%
3	1	DMF	1	TBA	2.4	3.8%
3	24	DMF	1	TBA	2.4	6.3%
3	48	DMF	1	TBA	2.4	4.9%
1	48	DMF	0	0	0	0.0%
1	48	H_2O	0	0	0	0.0%
7	48	DMF	1	0	0	0.0%
1.25	48	DMF	0	TBA-OAc	1	6.0%
1.25	720	DMF	0	TBA-OAc	1	3.9%
1.25	48	DMF	0	TBA-Cl	1	0.0%
1.25	48	DMF	0	TBA-I	1	0.1%
1.25	48	DMF	0	Na-OAc	1	0.1%
1.25	48	DMF	0	TEA-OAc	1	6.2%

The first variable, time, was tested by altering the length of the coupling reaction from 1 hour to 24 hours to 48 hours. No significant trend was seen between the amount of racemization and the length of time the reaction was allowed to run. Next, the variable of solvent was added. Either **6.2a** or **6.2b** was dissolved in either DMF or H_2O, stirred for 48 hours, and then purified on the preparatory HPLC. In both cases, no racemization was observed. These two experiments also eliminated the method of purification, preparatory HPLC, as being the cause of the racemization. Next, dCA was added to the mixture to determine its effects on racemization. When NVOC-D-alanine-cyanomethyl ester **6.2b** and unsalted dCA were stirred in DMF for 48 hours, no racemization was observed. Unfortunately, no aminoacylated-dCA coupling product was formed either. Since dCA is not very soluble in DMF without a counter ion, it may be that the dCA never went into solution and thus never encountered NVOC-D-alanine-cyanomethyl ester **6.2b**.

* Reactions are grouped based on similarity with the major differences highlighted in red.

Finally, the role that the counter ion plays in the coupling reaction was addressed. In each of these tests, either **6.2a** or **6.2b** and the noted salt were dissolved in DMF and stirred for at least 48 hours. Approximately the same amount of racemization was seen from a solution of either **6.2a** or **6.2b** and tetrabutylammonium acetate in DMF that was stirred at room temperature for both 48 hours and one month. The racemization was eliminated if the acetate was exchanged with either chloride or iodide or if the tetrabutylammonium was exchanged with sodium. Equivalent racemization was observed when tetraethylammonium acetate was tested.

The data are not clearly suggestive of one mechanism for racemization, but the presence of the counter ion salt is sufficient. The data trend towards racemization when either the negatively charged phosphates on dCA or the negatively charge acetate are countered by either tetrabutylammonium or tetraethylammonium. Unfortunately, the tetrabutylammonium counter ion is necessary for the dCA to be soluble in DMF at room temperature.[59] Having greater than two equivalents of this counter ion also enhances the coupling reaction.[59]

This chapter is not the first account of racemization occurring during the coupling reaction. In 1991 Robertson, Schultz, *et al.* reported on the degree of racemization caused by similar conditions.[59] They determined that 5.0 equivalents of the NVOC-protected cyanomethyl ester and 2.2 equivalents of the tetrabutylammonium counter ion for 1.0 equivalent of dCA when reacted for 2.5 hours at room temperature led to no racemization. An aside in the work suggests that no racemization means less than 5% was seen. They further state that lowering the equivalents of the NVOC-protected cyanomethyl ester from 5.0 to 1.5 leads to 2% to 5% racemization. They hypothesize

that this value is due to the longer reaction time necessary to get an efficient yield with these conditions, but our data suggest that time is not a crucial component to the amount of racemization seen in the coupling reaction. Our preliminary studies did not address the equivalents of NVOC-protected cyanomethyl ester. The only case where we increased the equivalents of NVOC-protected cyanomethyl ester was when we did not include a counter ion in the reaction mixture. It may be that the increase in equivalents of NVOC-D-alanine-cyanomethyl ester **6.2b** to dCA favored a decrease in racemization—an interpretation that follows the data presented by Robertson, Schultz, *et al.*[59] Further work would be needed to expound this hypothesis.

Conclusion

This study explored the *Xenopus laevis* ooctye's translational machinery using the tRNA THG73 that was chemically aminoacylated with D-alanine. A positive result in one of the negative controls prevented the initial *in vivo* nonsennse-suppression experiments in ShB from providing any data, but preliminary results from suppression in the α1 subunit of the nAChR looked promising through both *in vitro* and *in vivo* nonsense suppression. Initially, the difference in the amount of protein seen in the Western blot from *in vitro* suppression of D-alanine and the low current size from channel activity from the *in vivo* suppression of D-alanine were attributed to lower suppression efficiency of the D-amino acid. Later, the lower efficiency was attributed to a small amount of L-alanine contamination in the D-alanine tRNA, as it was discovered that the amino acid chirality was compromised in one of the last steps of the synthesis of the aminoacylated tRNA.

Any positive D-alanine suppression results from the Western blots and the *in vivo* nonsennse-suppression method are attributed to the L-amino acid contamination that resulted from the coupling of the NVOC-protected D-alanine cyanomethyl ester to dCA. Therefore, the D-alanine-tRNA present was either effectively removed or outcompeted by the L-alanine-tRNA. Through the lack of any other suppression results, this study supports previous studies that found that D-amino acids were difficult to incorporate into proteins using nonsense suppression. The most important result found from this study was that the conditions normally used in our lab for the coupling of unnatural amino acids to dCA compromise the enantiopurity of the amino acid.

Ideally, we will eventually be able to modify the methods of nonsense suppression to be able to incorporate D-amino acids at will. This ability will allow us to test the importance of conformation and ϕ and ψ angles in structure-function relationships in ion channels. The first goal will be to determine coupling conditions that retain the enantiopurity of the NVOC-protected cyanomethyl ester. In this study we did not address the equivalents of the various coupling reaction components thoroughly. If the observations of Robertson, Schultz, *et al.* hold true,[59] increasing the amount of NVOC-protected cyanomethyl ester to that of dCA may eliminate the racemization. Otherwise, modifying the methods of Starck *et al.* in their use of L-amino acid oxidase to remove impurities[28] may also be a viable solution that avoids altering conditions in the already optimized coupling reaction.

Methods

Synthesis

All reactions were performed at ambient temperature and pressure unless otherwise noted. All reactions involving potentially air-sensitive compounds were conducted under an inert atmosphere using Schlenk techniques. Solvents were purified by passage through alumina.[60] Unless otherwise noted, all chemicals and reagents were used as received without further purification. Flash chromatography was performed using EMD (Gibbstown, NJ) silica gel 60 (particle size 0.040-0.063 mm). Thin-layer chromatography (TLC) was performed using EMD (Gibbstown, NJ) silica gel 60 F_{254} precoated plates (0.25 mm) and visualized by UV and potassium permanganate. Nuclear magnetic resonance spectroscopy (NMR) was preformed on either a Varian (Palo Alto, CA) Mercury 300 instrument, and NMR resonances are reported relative to Me_4Si (δ 0.0) or CD_3OD (δ 3.31). Data for ^1H NMR spectra are reported as follows: chemical shift (δ ppm), integration, multiplicity, and coupling constant (Hz). Mass spectroscopy (MS) spectra were obtained from the Caltech Mass Spectrometry Lab. Electrospray ionization mass spectrometry (ESI-MS) was preformed on an LCQ Classic ion trap (ThermoFinnigan, Waltham, MA) in direct infusion mode. HPLC was preformed using Waters (Milford, MA) equipment and software (510 HPLC pumps and 996 Photodiode Array Detector) and reverse-phase Nova-Pak ^{18}C columns (3.9 × 150 mm analytical column, 7.8 × 300 mm preparatory column).

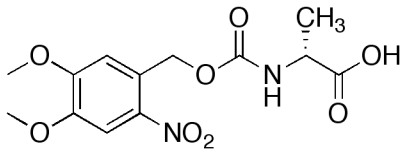

6.1b

NVOC-D-alanine **6.1b**: D-Alanine (0.32 g, 3.6 mmol, 1 eq) was added to a round-bottom flask and dissolved in 10% (w/v) sodium carbonate in water (14 mL). To this solution was added dioxane (14 mL) at 0 °C, followed by the slow addition of nitroveratryloxycarbonyl chloride (1.0 g, 3.8 mmol, 1.1 eq). The mixture was allowed to warm to room temperature while stirring for 4 hours. The mixture was then poured into distilled water (200 mL) and washed with ether (3×). Under vigorous stirring, the aqueous solution was adjusted to pH 2 by slowly adding 5 M HCl. Once an orange-yellow precipitate began to form, the solution was refrigerated overnight to encourage the formation of more solid. The subsequent day the precipitate was filtered to afford NVOC-D-alanine **6.1b** as a yellow solid (0.99 g, 3.0 mmol, 83% yield). R_f = 0.24 (1% AcOH in EtOAc); ^{1}H NMR (300 MHz, CD_3OD, 298 K) δ 7.72 (1H, s), 7.17 (1H, s), 5.52 (1H, d, *J* = 15.3 Hz), 5.36 (1H, d, *J* = 15.3 Hz), 4.19 (1H, q, *J* = 7.2 Hz), 3.96 (3H, s), 3.86 (3H, s), 1.40 (3H, d, *J* = 7.2 Hz).

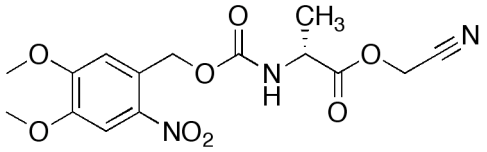

6.2b

NVOC-D-alanine cyanomethyl ester **6.2b**: NVOC-D-alanine **6.1b** (0.21 g, 0.63 mmol) was added to a round-bottom flask under Ar (g) and dissolved in DMF (2 mL). Chloroacetonitrile (2 mL) and then triethylamine (0.25 mL) were added to the solution.

The mixture was stirred at room temperature for 75 minutes and then the solvent was removed under vacuum. The residue was purified by flash column chromatography (CH_2Cl_2, then 5% EtOAc in CH_2Cl_2 once the yellow product started eluting) to afford NVOC-D-alanine cyanomethyl ester **6.2b** as pale yellow crystals (0.17 g, 0.46 mmol, 73% yield). R_f = 0.44 (17% EtOAc in CH_2Cl_2); ^{1}H NMR (300 MHz, $CDCl_3$, 298 K) δ 7.68 (1H, s), 6.98 (1H, s), 5.56 (1H, d, *J* = 15.6 Hz), 5.43 (1H, d, *J* = 14.7 Hz), 4.78 (2H, q, *J* = 15.6 Hz), 4.45 (1H, m), 3.99 (3H, s), 3.93 (3H, s), 1.48 (3H, d, *J* = 7.2 Hz).

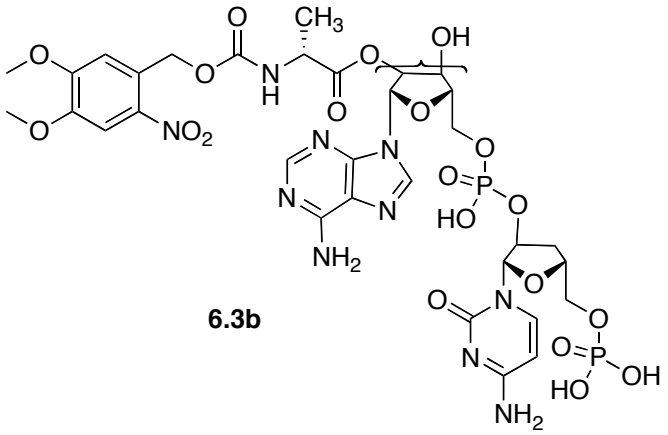

6.3b

NVOC-D-alanine-dCA **6.3b**: NVOC-D-alanine cyanomethyl ester **6.2b** (0.020 g, 0.054 mmol, 3 eq) was added to a round-bottom flask under Ar (g) and dissolved in DMF (1 mL). This solution was transferred to another round-bottom flask under Ar (g), which contained dCA (0.020 g, 0.017 mmol, 1 eq) as a tetrabutylammonium salt (2.4 eq). The reaction was stirred at room temperature for 18 hours while being monitored by reverse-phase analytical HPLC with a linear solvent gradient from 5% acetonitrile in 25 mM NH_4OAc buffer pH 4.5 to 100% acetonitrile. The crude product was purified using reverse-phase semipreparative HPLC with the same linear solvent gradient. The fractions containing the NVOC-D-alanine-dCA **6.3b** were combined, and the solvent was removed

by lyophilization. The solid was redissolved in 10 mM acetic acid and reconcentrated via lyophilization (3×) to afford NVOC-D-alanine-dCA **6.3b** as a white powder (0.0053 g, 0.0056 mmol, 33% yield). FAB-MS *m/z* calc'd for $C_{32}H_{41}N_{10}O_{20}P_2$ [M−H]: 947.2; found: 947.1.

Nonsense Suppression In Vivo

The site-directed mutagenesis of TAG mutants, gene construction, synthesis of suppressor tRNA, and ligation of aminoacyl-tRNA to tRNA have been described previously.[40,48,61,62] Plasmid DNAs were linearized with Not1, and mRNA was transcribed using the T7 mMESSAGE mMACHINE kit (Ambion, Austin, TX).

Oocytes from *Xenopus laevis* were isolated and maintained at 18 °C in ND96 solution (96 mM sodium chloride, 2 mM potassium chloride, 1.8 mM calcium chloride, 1 mM magnesium chloride, 5 mM HEPES, 2.5 mM sodium pyruvate, 0.5 mM theophyline, 10 μg/mL gentamycin at pH 7.5) according to published procedures.[63] Each oocyte was microinjected with 50 nL of a 1:1 mixture of mRNA (0.04 ng/nL for ShB and 0.5 ng/nL of a 20:1:1:1 α:β:γ:δ for nAChR) and tRNA (1 μg/μL) or unaminoacylated dCA-tRNA (1 μg/μL). NVOC-protected aminoacylated tRNA was deprotected prior to injection by irradiating the sample for 5 minutes with a 1000 W Hg/Xe arc lamp (Oriel, Irvine, CA) operating at 400 W equipped with WG-335 and UG-11 filters (Schott, Duryea, PA).[42]

Electrophysiology

Electrophysiological recordings were carried out 24 to 48 hours after injection. Whole-cell currents from oocytes were measured using a Geneclamp 500 amplifier (ShB) or an OpusXpress (nAChR) and pCLAMP software (Axon Instruments, Foster City, CA) in the two-electrode voltage-clamp configuration. Microelectrodes were filled with 3 M potassium chloride and had resistances ranging from 0.5 to 1.5 MΩ. Oocytes were continuously perfused with a nominally calcium-free bath solution consisting of 96 mM sodium chloride, 2 mM potassium chloride, 1 mM magnesium chloride, and 5 mM HEPES at pH 7.5. In the ShB experiments, the currents from ShB expressing oocytes were measured during depolarizing jumps from the holding potential to +70 mV in 25 mV increments. In the nAChR experiments, microscopic ACh-induced currents were recorded in response to bath application of ACh at a holding potential of −80 mV.

Nonsense Suppression In Vitro

Translation was carried out using rabbit reticulocyte lysate translation system (Promega, Madison, WI) according to manufacturer's protocol. Lysate mix (8.75 μL), amino acid mix (0.35 μL), RNAse inhibitor (0.25 μL), H_2O (1.75 μL), mRNA (0.5 μL, 1 μg/μL for suppression experiments and 0.3 μg/μL for wild-type experiments), and either tRNA (1 μL, 1 μg/μL) or water (1 μL, for mRNA-only negative control) were combined and incubated at 30 °C for 106 minutes. The *in vitro* translation mix was then kept at −80 °C until further use.

To prepare for gel loading, the *in vitro* translation mix (2.5 μL) was added to 4% sodium dodecyl sulfate (SDS) (2.5 μL) and then that mixture was added to 10% SDS (2 μL), H_2O (7 μL), and 2× SDS loading buffer (100 mM tris chloride at pH 6.8, 4% SDS, 0.2% bromophenol blue, 20% glycerol) (14 μL). Samples were loaded in 5 μL aliquots into prepoured 12% tris chloride gels (Bio-Rad, Hercules, CA) for SDS-polyacrylamide gel electrophoresis (PAGE). Western blotting was preformed using nitrocellulose transfer, a mouse anti-HA primary antibody, and a goat anti-mouse secondary antibody conjugated to horseradish-peroxidase. Protein was detected by chemiluminescence.

Analysis of Enantiopurity of NVOC-Alanine Cyanomethyl Ester

A mixture of NVOC-alanine cyanomethyl ester **6.2a** and **6.2b** (1 mg/mL in ethanol) was found to separate via chiral HPLC using a Chiralcel OD-H column with an elution of 12% ethanol in hexanes. The OD-H column is cellulose tris(3,5-dimethylphenyl) carbamate on a 5 μm silica-gel substrate. The peak for **6.2b** appeared approximately 2 minutes prior to the appearance of **6.2a**, approximately 22 minutes and 24 minutes, respectively, for a 60 minute run. Each chiral HPLC run included a 20 minute prewash and 20 minute postwash of 100% isopropanol.

Generally, each reaction for testing by chiral HPLC was set up as follows: NVOC-alanine cyanomethyl ester **6.2a** or **6.2b** (0.19g, 0.050 mmol, equivalents as listed in table 6.2) was added to a round-bottom flask under Ar (g) and dissolved in *N,N*-dimethyl formamide or water (0.4 mL). To this solution was added either dCA (equivalents as listed in table 6.2) or counter ion salt (identity and equivalents as listed in table 6.2) or

both. The reaction was then allowed to stir at room temperature for the amount of time listed in table 6.2. The components of the mixture were then separated using reverse-phase semipreparative HPLC with a linear solvent gradient from 5% acetonitrile in 25 mM ammonium acetate (pH 4.5) to 100% acetonitrile. The desired fractions containing the unreacted NVOC-alanine cyanomethyl ester **6.2a** or **6.2b** were combined, and the solvent was removed by lyophilization. The resulting white solid was dissolved in ethanol (1 mg/mL) and analyzed for enantiopurity by the chiral HPLC method described above.

References

(1) Valiyaveetil, F. I.; Sekedat, M.; Mackinnon, R.; Muir, T. W. *Proc. Natl. Acad. Sci. USA* **2004**, *101*, 17045-9.

(2) Yoshimura, T.; Esaki, N. *J. Biosci. Bioeng.* **2003**, *96*, 103-109.

(3) Heck, S. D.; Faraci, W. S.; Kelbaugh, P. R.; Saccomano, N. A.; Thadeio, P. F.; Volkmann, R. A. *Proc. Natl. Acad. Sci. USA* **1996**, *93*, 4036-9.

(4) Kreil, G. *Annu. Rev. Biochem.* **1997**, *66*, 337-345.

(5) Broccardo, M.; Erspamer, V.; Falconieri Erspamer, G.; Improta, G.; Linari, G.; Melchiorri, P.; Montecucchi, P. C. *Br. J. Pharmacol.* **1981**, *73*, 625-31.

(6) McDonnell, K. A.; Imperiali, B. *J. Am. Chem. Soc.* **2002**, *124*, 428-33.

(7) Anil, B.; Song, B.; Tang, Y.; Raleigh, D. P. *J. Am. Chem. Soc.* **2004**, *126*, 13194-5.

(8) Doyle, D. A.; Morais Cabral, J.; Pfuetzner, R. A.; Kuo, A.; Gulbis, J. M.; Cohen, S. L.; Chait, B. T.; MacKinnon, R. *Science* **1998**, *280*, 69-77.

(9) Heginbotham, L.; Lu, Z.; Abramson, T.; MacKinnon, R. *Biophys. J.* **1994**, *66*, 1061-7.

(10) Ibba, M.; Soll, D. *Science* **1999**, *286*, 1893-1897.

(11) Soutourina, J.; Plateau, P.; Delort, F.; Peirotes, A.; Blanquet, S. *J. Biol. Chem.* **1999**, *274*, 19109-14.

(12) Calendar, R.; Berg, P. *J. Mol. Biol.* **1967**, *26*, 39-54.

(13) Ferri-Fioni, M. L.; Schmitt, E.; Soutourina, J.; Plateau, P.; Mechulam, Y.; Blanquet, S. *J. Biol. Chem.* **2001**, *276*, 47285-47290.

(14) Yang, H. B.; Zheng, G.; Peng, X. Z.; Qiang, B. Q.; Yuan, J. G. *FEBS Lett.* **2003**, *552*, 95-98.

(15) Zheng, G.; Liu, W.; Gong, Y.; Yang, H.; Yin, B.; Zhu, J.; Xie, Y.; Peng, X.; Qiang, B.; Yuan, J. *Biochem. J.* **2008**.

(16) Tan, Z.; Forster, A. C.; Blacklow, S. C.; Cornish, V. W. *J. Am. Chem. Soc.* **2004**, *126*, 12752-3.

(17) Louie, A.; Ribeiro, N. S.; Reid, B. R.; Jurnak, F. *J. Biol. Chem.* **1984**, *259*, 5010-6.

(18) LaRiviere, F. J.; Wolfson, A. D.; Uhlenbeck, O. C. *Science* **2001**, *294*, 165-168.

(19) Asahara, H.; Uhlenbeck, O. C. *Proc. Natl. Acad. Sci. USA* **2002**, *99*, 3499-3504.

(20) Dale, T.; Sanderson, L. E.; Uhlenbeck, O. C. *Biochemistry* **2004**, *43*, 6159-66.

(21) Sanderson, L. E.; Uhlenbeck, O. C. *Biochemistry* **2007**, *46*, 6194-200.

(22) England, P. M. *Biochemistry* **2004**, *43*, 11623-9.

(23) Ellman, J.; Mendel, D.; Anthony-Cahill, S.; Noren, C. J.; Schultz, P. G. *Methods Enzymol.* **1991**, *202*, 301-36.

(24) Dedkova, L. M.; Fahmi, N. E.; Golovine, S. Y.; Hecht, S. M. *J. Am. Chem. Soc.* **2003**, *125*, 6616-6617.

(25) Bain, J. D.; Wacker, D. A.; Kuo, E. E.; Chamberlin, A. R. *Tetrahedron* **1991**, *47*, 2389-2400.

(26) Quiggle, K.; Kumar, G.; Ott, T. W.; Ryu, E. K.; Chladek, S. *Biochemistry* **1981**, *20*, 3480-5.

(27) Bhuta, A.; Quiggle, K.; Ott, T.; Ringer, D.; Chladek, S. *Biochemistry* **1981**, *20*, 8-15.

(28) Starck, S. R.; Qi, X.; Olsen, B. N.; Roberts, R. W. *J. Am. Chem. Soc.* **2003**, *125*, 8090-8091.

(29) Yamane, T.; Miller, D. L.; Hopfield, J. J. *Biochemistry* **1981**, *20*, 7059-7064.

(30) Heckler, T. G.; Roesser, J. R.; Xu, C.; Chang, P. I.; Hecht, S. M. *Biochemistry* **1988**, *27*, 7254-62.

(31) Dedkova, L. M.; Fahmi, N. E.; Golovine, S. Y.; Hecht, S. M. *Biochemistry* **2006**, *45*, 15541-51.

(32) Thompson, J.; Kim, D. F.; O'Connor, M.; Lieberman, K. R.; Bayfield, M. A.; Gregory, S. T.; Green, R.; Noller, H. F.; Dahlberg, A. E. *Proc. Natl. Acad. Sci. USA* **2001**, *98*, 9002-7.

(33) O'Connor, M.; Lee, W. M.; Mankad, A.; Squires, C. L.; Dahlberg, A. E. *Nucleic Acids Res.* **2001**, *29*, 710-5.

(34) Polacek, N.; Gaynor, M.; Yassin, A.; Mankin, A. S. *Nature* **2001**, *411*, 498-501.

(35) Calendar, R.; Berg, P. *Biochemistry* **1966**, *5*, 1681-90.

(36) Calendar, R.; Berg, P. *Biochemistry* **1966**, *5*, 1690-5.

(37) Noren, C. J.; Anthonycahill, S. J.; Griffith, M. C.; Schultz, P. G. *Science* **1989**, *244*, 182-188.

(38) Ellman, J. A.; Mendel, D.; Schultz, P. G. *Science* **1992**, *255*, 197-200.

(39) Mendel, D.; Ellman, J.; Schultz, P. G. *J. Am. Chem. Soc.* **1993**, *115*, 4359-4360.

(40) Nowak, M. W.; Kearney, P. C.; Sampson, J. R.; Saks, M. E.; Labarca, C. G.; Silverman, S. K.; Zhong, W.; Thorson, J.; Abelson, J. N.; Davidson, N.; Schultz, P. G.; Dougherty, D. A.; Lester, H. A. *Science* **1995**, *268*, 439-442.

(41) Nowak, M. W.; Gallivan, J. P.; Silverman, S. K.; Labarca, C. G.; Dougherty, D. A.; Lester, H. A. In *Ion Channels, Pt. B* 1998; Vol. 293, p 504-529.

(42) Li, L. T.; Zhong, W. G.; Zacharias, N.; Gibbs, C.; Lester, H. A.; Dougherty, D. A. *Chemistry & Biology* **2001**, *8*, 47-58.

(43) Vossmeyer, T.; Jia, S.; Delonno, E.; Diehl, M. R.; Kim, S. H.; Peng, X.; Alivisatos, A. P.; Heath, J. R. *J. Appl. Phys.* **1998**, *84*, 3664-3670.

(44) Hoshi, T.; Zagotta, W. N.; Aldrich, R. W. *Science* **1990**, *250*, 533-538.

(45) Zagotta, W. N.; Hoshi, T.; Aldrich, R. W. *Science* **1990**, *250*, 568-571.

(46) Demo, S. D.; Yellen, G. *Neuron* **1991**, *7*, 743-753.

(47) Mackinnon, R.; Aldrich, R. W.; Lee, A. W. *Science* **1993**, *262*, 757-759.

(48) England, P. M.; Lester, H. A.; Davidson, N.; Dougherty, D. A. *Proc. Natl. Acad. Sci. USA* **1997**, *94*, 11025-11030.

(49) Rodriguez, E. A.; Lester, H. A.; Dougherty, D. A. *Proc. Natl. Acad. Sci. USA* **2006**, *103*, 8650-5.

(50) Rodriguez, E. A.; Lester, H. A.; Dougherty, D. A. *RNA* **2007**, *13*, 1703-14.

(51) Saks, M. E.; Sampson, J. R.; Nowak, M. W.; Kearney, P. C.; Du, F.; Abelson, J. N.; Lester, H. A.; Dougherty, D. A. *J. Biol. Chem.* **1996**, *271*, 23169-75.

(52) Kearney, P. C.; Zhang, H.; Zhong, W.; Dougherty, D. A.; Lester, H. A. *Neuron* **1996**, *17*, 1221-9.

(53) Cashin, A. L.; Torrice, M. M.; McMenimen, K. A.; Lester, H. A.; Dougherty, D. A. *Biochemistry* **2007**, *46*, 630-9.

(54) Bain, J. D.; Diala, E. S.; Glabe, C. G.; Wacker, D. A.; Lyttle, M. H.; Dix, T. A.; Chamberlin, A. R. *Biochemistry* **1991**, *30*, 5411-21.

(55) England, P. M.; Lester, H. A.; Dougherty, D. A. *Biochemistry* **1999**, *38*, 14409-14415.

(56) Unwin, N. *J. Mol. Biol.* **2005**, *346*, 967-89.

(57) Kenakin, T. *Trends Pharmacol. Sci.* **1999**, *20*, 400-405.

(58) Earll, M. *Online Guide to Chiral HPLC*, 1999.

(59) Robertson, S. A.; Ellman, J. A.; Schultz, P. G. *J. Am. Chem. Soc.* **1991**, *113*, 2722-2729.

(60) Pangborn, A. B.; Giardell, M. A.; Grubbs, R. H.; Rosen, R. K.; Timmers, F. J. *Organometallics* **1996**, *15*, 1518-1520.

(61) Nowak, M. W.; Gallivan, J. P.; Silverman, S. K.; Labarca, C. G.; Dougherty, D. A.; Lester, H. A. *Methods Enzymol.* **1998**, *293*, 504-529.

(62) Kearney, P. C.; Nowak, M. W.; Zhong, W.; Silverman, S. K.; Lester, H. A.; Dougherty, D. A. *Molecular Pharmacology* **1996**, *50*, 1401-1412.

(63) Quick, M.; Lester, H. A. In *Ion Channels of Excitable Cells*; Narahashi, T., Ed.; San Diego, CA: Academic Press, 1994, p 261-279.

Chapter VII

EXPANDING THE REPERTOIRE OF AROMATIC UNNATURAL AMINO ACIDS USEFUL FOR STRUCTURE-FUNCTION STUDIES OF ION CHANNELS

In this chapter three separate studies, all tied together due to their focus on unnatural aromatic amino acids, are discussed. The first section describes the synthesis of four novel fluorescent methanethiosulfonate compounds for use in fluorescence resonance energy transfer (FRET) studies on ion channels. Each of these compounds can create a fluorescent amino acid *in situ* by covalent attachment to a cysteine residue. The second section focuses on the unnatural amino acid 3,5-dimethylphenylalanine in the voltage-gated Shaker B K^+ channel (ShB). This residue was designed to explore whether the cationic tetraethylamine (TEA) interacted with the 3-position of the aromatic ring at position 449 instead of the face of the aromatic as expected for a cation-π interaction. Unfortunately, this residue did not provide any clarity on the importance of the substituent at this position, but in studying the effects of methyl-substituents, 4-methyl-phenylalanine was found to further support a cation-π interaction at this site. The third section describes attempts to enhance the cation-π interaction through the use of 4-amino-phenylalanine. ShB was the initial target, but the $GABA_C$ receptor and the nicotinic acetylcholine receptor (nAChR) were also studied. No cation-π enhancement was seen for 4-amino-phenylalanine at any channel. Several attempts were made to investigate whether 4-amino-phenylalanine was being modified, which proved that the

nitroveratryloxycarbonyl (NVOC) deprotection step was not altering the aniline but did not conclusively determine if any modifications were occurring to the aniline while the amino acid was in the *Xenopus laevis* oocyte.

Development of Novel Fluorescent Conjugates for Use in Fluorescence Resonance Energy Transfer (FRET) Studies of Ion Channels

Fluorescent amino acids can be extremely useful probes of structural changes during the gating of ion channels. Their fluorescence can relay information about their environment. For example, the hydrophobicity of the environment surrounding rhodamine determines the intensity of its fluorescence emission. Because of this intrinsic feature, incorporating a fluorophore into an ion channel and monitoring its fluorescence during gating allows for real time analysis of the changes in the environment that encompass the fluorophore.

Work is currently ongoing in the Dougherty and Lester laboratories to incorporate fluorescent amino acids into proteins *in vivo*, but our laboratories and others have already sidestepped the ribosome by creating fluorescent amino acids *in situ* through site-specific labeling of cysteine residues with thiol-reactive fluorescent probes such as sulforhodamine methanethiosulfonate (MTSR), tetramethylrhodamine (TMRM), and Alexa Fluor 546 maleimide (AF546) (figure 7.1).[1-7] These fluorescent cysteines have allowed for changes in the local environment around the voltage sensor of a K^+ channel,[1,2] the extracellular region of the $GABA_C$ ρ1 receptor,[4] the pore-lining helix of the muscle nAChR,[5] the ligand-binding domain of the $GABA_A$ receptor,[6] and the pore-

lining helix of the glycine α1 receptor[7] during gating to be explored. These studies were able to identify regions of the channels that underwent molecular rearrangements during gating, and they were also able to identify differences between the effects of various agonists and antagonists on the structural dynamics of the channels. Although these results are informative, this method is limited since it cannot be used to quantitate how far the fluorophore moves during the gating process.

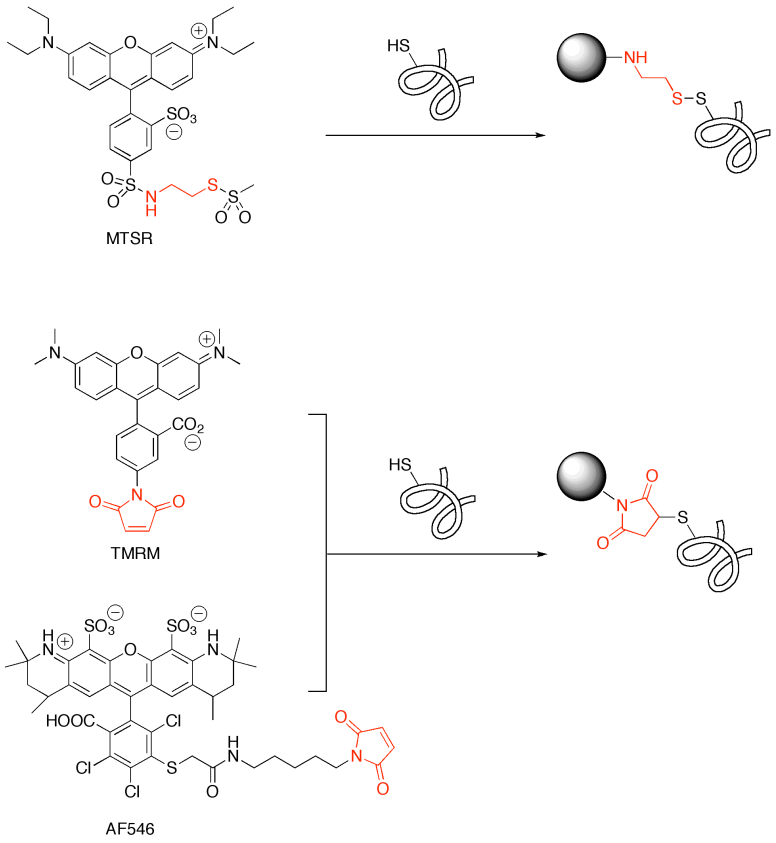

Figure 7.1. Structures of three thiol-reactive fluorescent probes.

The distance a specific site moves during channel gating can be determined from two fluorescent moieties through a process called FRET, which occurs when two

chromophore-containing compounds with overlapping spectral properties come into close proximity. Because of the properties of the FRET system, the distance between the two compounds can be calculated based on fluorescence measurements. FRET begins with the absorption of light by one fluorophore, called the donor. If there is a second chromophore nearby, typically within 1 to 10 nm, whose absorption properties overlap with the emission properties of the donor, a radiationless transfer of energy from the excited donor molecule to the acceptor chromophore will occur. Interestingly, the energy passes from the donor to the acceptor through long-range dipole-dipole interactions. If the acceptor is a fluorescent compound, then FRET is seen as the quenching of the donor fluorescence and the appearance of the acceptor fluorescence. The extent of the energy transfer between the donor and the acceptor is relayed in the intensity of the acceptor fluorescence and is dependent on the distance between the two compounds. Thus, the occurrence of FRET and even changes in FRET intensity can be quantified into distances between the two chromophores.

The Lester laboratory has appended yellow fluorescent protein (YFP) and cyan fluorescent protein (CFP) to nAChR subunits to determine through FRET if two subunits colocalize in a receptor *in vivo*,[8,9] but these large proteins would not be able to answer questions about how far a specific site moves during channel gating. The small fluorophores that were used to study the local environment, as described above, are more appropriate. The Lester laboratory has used the thiol-reactive fluorophores MTSR and TMRM (figure 7.1).[5,7] In order to take advantage of these two compounds in FRET studies, chromophores with spectra overlapping the absorption or emission spectra of these compounds are needed. Fortunately, there were already well-established FRET

partners for both MTSR and TMRM: 7-nitro-2,1,3-benzoxadiazol-4-yl (NBD)[10] and fluorescein, respectively (figure 7.2).

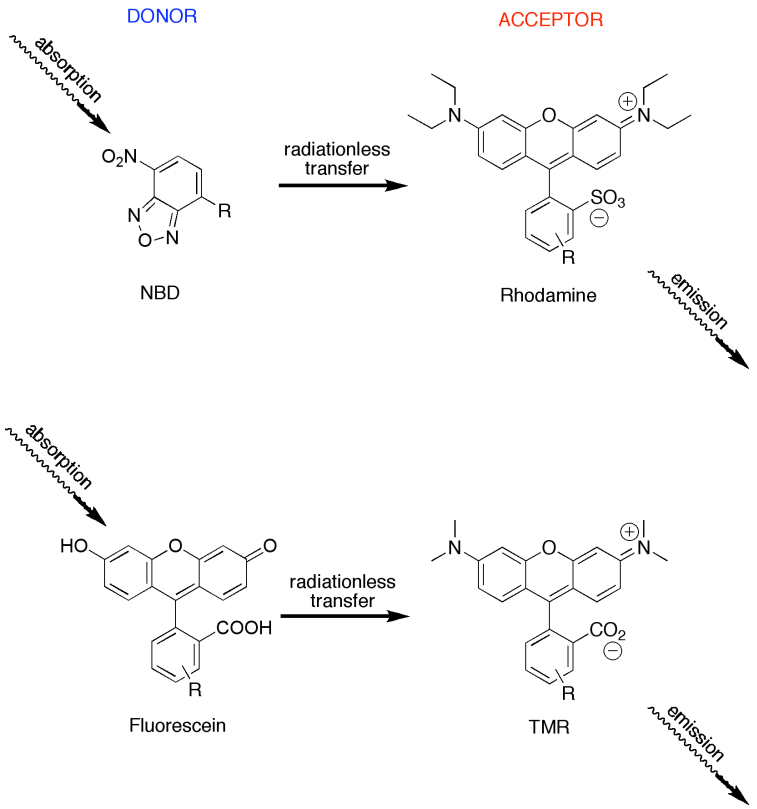

Figure 7.2. A depiction of FRET between the fluorophores discussed in the text.

Three FRET pairs were designed to allow for versatility in experimentation. If one FRET pair did not work well, potentially because one partner was incapable of reacting with the desired thiol or because the sterics of their local environment did not allow the pair to orient correctly for FRET, then another pair could be tried.

To illustrate the spectral overlap between the donor and the acceptor, the absorption and emission spectra of a rhodamine similar to MTSR (red) and the absorption and emission

spectra of a NBD derivative (blue) are shown in figure 7.3A. The region on the plot that is important for FRET is the overlap of the emission of NBD (solid blue line) and the absorption of the rhodamine (dashed red line). The fluorescein derivative Oregon Green 488 (green) is shown along with its FRET partner TMR (black) in figure 7.3B. Oregon Green 488 was chosen over fluorescein because it is more photostable and less pH sensitive at physiological pH (pKa approximately 4.7) than its parent compound (fluorescein has a pKa of approximately 6.4).[11] Again, the important region is the overlap between the emission of the Oregon Green 488 and the absorption of the TMR. The third donor-acceptor spectra pair shown in figure 7.3C is for a coumarin (purple) and Oregon Green 488 (green). These two compounds have less spectral overlap than the others, but there is still enough overlap for FRET to occur.

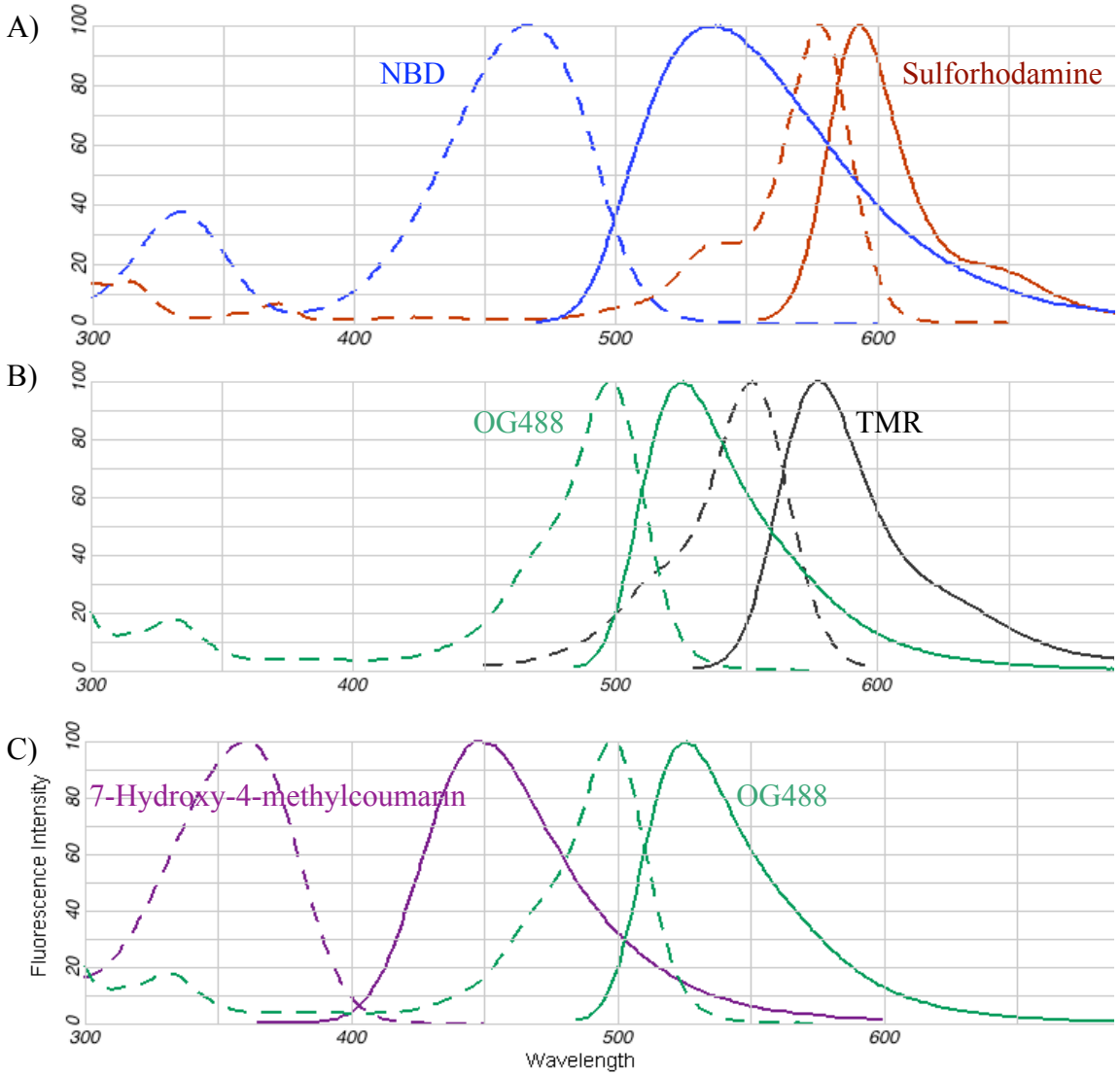

Figure 7.3. Absorption (dashed lines) and emission (solid lines) spectra for the various FRET pairs. Figures made at www.invitrogen.com using compounds similar to those in the text. A) NBD aminohexanoic acid in methanol (blue) and sulforhodamine 101 in ethanol (red). B) Oregon Green 488 goat anti-mouse IgG antibody I pH 8.0 buffer (green) and TMR goat anti-mouse IgG antibody in pH 8.0 buffer (black). C) 7-Hydroxy-4-methylcoumarin in pH 9.0 buffer (purple) and Oregon Green 488 goat anti-mouse IgG antibody I pH 8.0 buffer (green).

Synthesis of Fluorescent Methanethiosulfonate Compounds

Before the *in vivo* FRET studies could begin, the methanethiosulfonate-derivatized FRET partners had to be synthesized. 7-Dimethylaminocoumarin-4-acetic acid (DMAC), 6-(N-(NBD)amino)hexanoate (extended NBD), and Oregon Green 488 were commercially available as succinimidyl esters, allowing for the conversion to the methanethiosulfonate using the method by Gruber *et al.* (scheme 7.1).[12] To our knowledge, this work represents the first such synthesis of these compounds. Since the extended NBD could potentially occupy a wide breadth of space, its accuracy at quantifying distance was questioned. Thus, an NBD with a shorter tether (compact NBD) was synthesized. The same conditions used for the conversion of the succinimidyl ester promoted nucleophilic aromatic substitution on NBD-chloride.

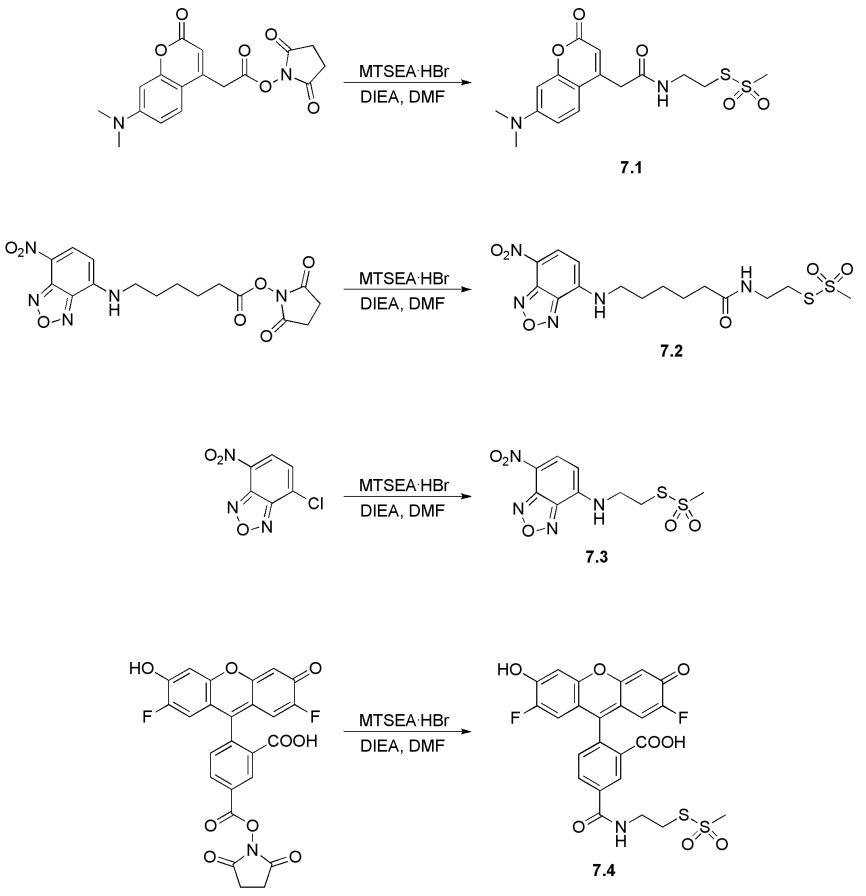

Scheme 7.1. The syntheses of four novel fluorescent methanethiosulfonates: DMAC **7.1**, extended NBD **7.2**, compact NBD **7.3**, and Oregon Green 488 **7.4**.

Thiol-Labeling of nAChRs

These fluorescent methanethiosulfonates were to be used by Dr. Mohammed Dibas in the Lester laboratory for FRET studies on the muscle nAChR. The specific receptor was only going to have two cysteine residues, one on the extracellular domain and one at β1Ala272, the 19' residue used previously by Dahan *et al.*[5] The labeling procedure was going to be similar to that described by Dahan *et al*. except instead of washing first with

10 mM sodium (2-sulfonatoethyl)methanethiosulfonate to block all endogenous surface thiol groups,[5] one of the FRET partners would instead be washed over the oocyte. This wash would likely add the fluorescent moiety to many proteins, but since the fluorescence from FRET would be the only fluorescence analyzed, the nonspecific binding of the fluorophore to other proteins would be eliminated from the study. The second wash would then be 10 mM sodium (2-sulfonatoethyl)methanethiosulfonate to block any remaining surface thiols. The final wash would be a mixture of the other FRET partner with 100 μM acetylcholine (ACh). The application of ACh would open the channel and expose the 19' cysteine to the fluorescent tag. Once the protein was labeled with both fluorophores, the changes in fluorescence from FRET at various points during channel activation would be observed, and the resulting data could then be quantified into changes in distances between the two fluorophores. Unfortunately, the *in vivo* studies were never performed. Since FRET studies could provide valuable information about the specific movements that occur during the gating of the muscle nAChR and other ion channels, hopefully this project will gain momentum and be continued by future graduate students in either the Dougherty or the Lester laboratories.

Probing the Sterics Around Phenylalanine Residues Using the Unnatural Amino Acid 3,5-Dimethylphenylalanine

TEA is a well-known blocker of K^+ channels that was introduced in this thesis in chapter 2. In that chapter the cationic TEA was experimentally shown to bind to and block ShB through a cation-π interaction when an aromatic residue was present at position 449 at the

top of the channel pore, through the incorporation of fluorinated-phenylalanine derivatives using *in vivo* nonsense-suppression techniques.[13]. Though there was precedent for this type of interaction based on previous experimental work,[14] this result was controversial since a cation-π binding motif was not present in the crystal structure of the related K^+ channel KcsA when complexed with the TEA analogue TEAs (2BOC).[15] Instead of TEAs interacting with the electronegative face of Tyr82, the residue in KcsA homologous to ShB Thr449, the static picture showed TEAs in van der Waals contact with the side of the aromatic ring—"edge on" not "*en face*" (figure 7.4). Specifically, the 3-position of the ring was closest to the blocker, which argued that hydrophobics, shape, and size of the ring were what was important to TEA block of K^+ channels.

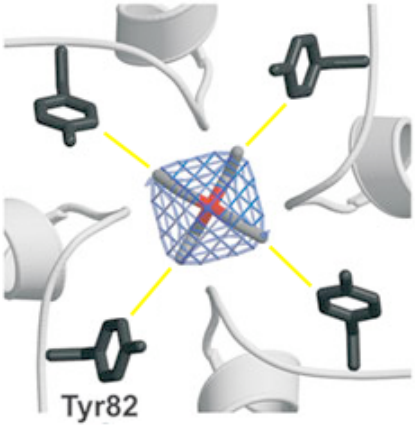

Figure 7.4. A portion of the 2BOC crystal structure focusing on KcsA Tyr82 and TEAs. The yellow lines highlight the points of closest proximity between the two, which clearly involves the 3-position of the ring. Adapted from Lenaeus *et al.*[15]

This controversy was addressed in chapter 2 through the computational modeling of the energetic differences between TEA and the various incorporated fluorinated phenylalanine derivatives that were used in the study. The calculations made from the reduced system that included only TEAs and the four phenylalanine derivatives, with their coordinates taken from 2BOC,[15] clearly demonstrated that if the edge-on interaction represented what occurred between TEA and the channel *in vivo*, the addition of fluorine atoms at the 3- and 5-positions of the phenylalanine should enhance TEA block (figure 2.5). The added negative electrostatic potential at these sites would attract the cationic blocker instead of repelling it as predicted by the cation-π interaction. Experimental work showed that the incorporation of 3,5-F_2-phenylalanine at ShB position 449 decreased the blocking efficiency of TEA, better coinciding with an *en face*, cation-π interaction than the edge-on hydrophobic interaction. Together the computational data and the experimental data suggest that the still image seen in the 2BOC crystal structure is not relevant for TEA binding to and blocking ShB.

The addition of the fluorine atoms at the 3- and 5-positions of the aromatic ring were designed to test the significance of the cation-π interaction, not the importance of the substituents at these positions. Designing a phenylalanine derivative with larger substituents at the 3- and 5-positions was anticipated to further investigate the relevance of the crystal structure 2BOC for its depiction of TEA block of ShB. 3,5-Dimethylphenylalanine was chosen since the methyl groups were anticipated to be sterically disruptive to the binding of the TEA blocker, due to the increase in size from that of a hydrogen atom or fluorine atom, in an edge-on, but not an *en face*, orientation (figure 7.5).

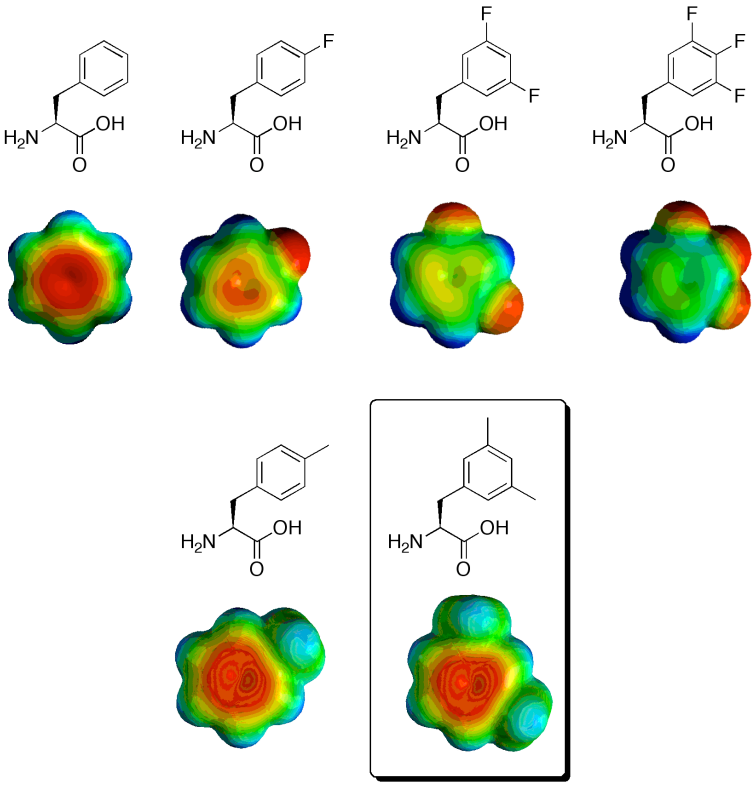

Figure 7.5. The structures and representative electrostatic potential surfaces of phenylalanine, the fluorinated phenylalanine derivatives used in the cation-π study in chapter 2, and 3,5-dimethylphenylalanine. The electrostatic potential surfaces were calculated using HF 6-31G*, where red and blue correspond to −20 and 20 kcal/mol, respectively.

Synthesis of 3,5-Dimethylphenylalanine

The synthesis of 3,5-dimethylphenylalanine began with the bromination of mesitylene using *N*-bromosuccinimide.[16] This compound was then condensed with *N*-(diphenylmethylene)glycine *tert*-butyl ester to yield the protected, racemic 3,5-dimethylphenylalanine **7.6**. The protecting groups were removed, and then the amine was reprotected with the NVOC photolabile protecting group.[17] Next, the acid was

activated as a cyanomethyl ester and coupled to the tetrabutylammonium salt of dCA to afford **7.10**. At this point the amino acid can be attached to either the 2' or the 3' hydroxyl of dCA since it is thought to rapidly sample both sites. Finally, the aminoacylated dCA was ligated to THG-73 using T4 RNA ligase.

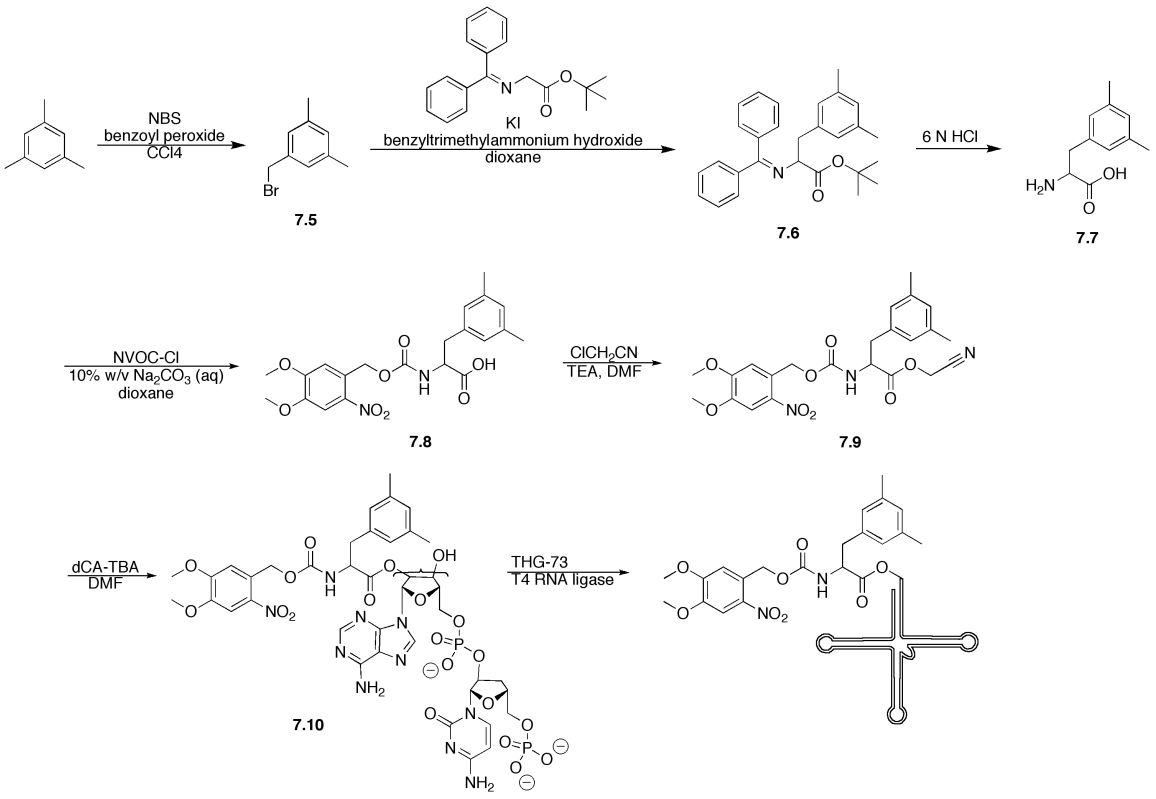

Scheme 7.2. Synthesis of 3,5-dimethylphenylalanine-tRNA.

Evaluating the Effects of 3,5-Dimethylphenylalanine on TEA Block

3,5-Dimethylphenylalanine was incorporated into ShB using the same Thr449UAG cRNA as in chapter 2.[13] As stated above studying the ability of TEA to block this mutant channel was expected to give more evidence as to how TEA interacts with the channel *in*

vivo. Therefore, the IC_{50} for TEA and the dimethyl-containing channel was expected to be similar to that for ShB Thr449Phe if the TEA interacted with the aromatic in an *en face*, cation-π favorable manner. Conversely, TEA was expected to be much less effective at blocking the mutant channel, and thus have a higher IC_{50}, if the edge-on interaction with the ring was as important as predicted by the crystal structure.[15]

Surprisingly, the IC_{50} for TEA block of the dimethyl-containing mutant channel did not follow either expected trend. As can be seen in figure 7.6, the IC_{50} for ShB with 3,5-dimethylphenylalanine incorporated at position 449 is just slightly less than the IC_{50} when 3,5-F_2-phenylalanine is incorporated. Thus, the addition of the methyl substituents at the 3- and 5-positions of the aromatic ring is less disruptive than when the fluorine atoms are there, although the methyl groups were predicted to be more disruptive in the edge-on orientation because of their larger size or not disruptive at all in the *en face* orientation. Since the addition of the methyl substituents does have an adverse effect on the binding of the TEA that was not predicted by a pure cation-π interaction between the blocker and the aromatic side chain, an intermediary interaction with the substituents at these positions on the aromatic ring, either with TEA or with the channel, could be important for block.

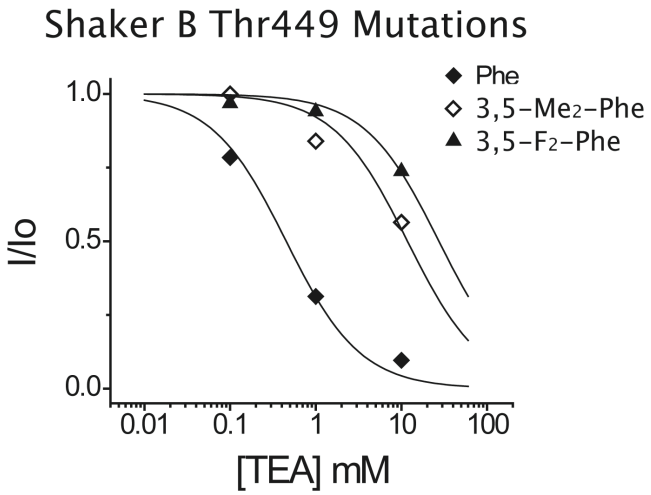

Figure 7.6. Dose-response curves for channels with three different amino acids incorporated at position 449 in ShB by nonsense suppression.

To test whether all of the position on the aromatic ring were as sensitive to the addition of a methyl group as the 3- and 5-positions were, 4-methyl-phenylalanine-tRNA (made from a dCA analog that was previously synthesized by a past member of the Dougherty laboratory) was incorporated into position 449 of ShB. The IC_{50} for the 4-methyl-phenylalanine-containing channel was 0.26 ± 0.1 mM TEA, similar to that expected if the cation-π interaction controlled the binding of TEA to the channel (figure 7.7). The methyl group is slightly electron donating, therefore it is expected to have a slightly enhanced cation-π interaction with TEA, as is seen. The incorporation of 4-methyl-phenylalanine was exciting in that it further substantiated that the cation-π, *en face* orientation dominanted *in vivo* for ShB. But, this result also confirmed that the location of the methyl substituents at the 3- and 5-positions were specific for the slight disruption of receptor function in the earlier work.

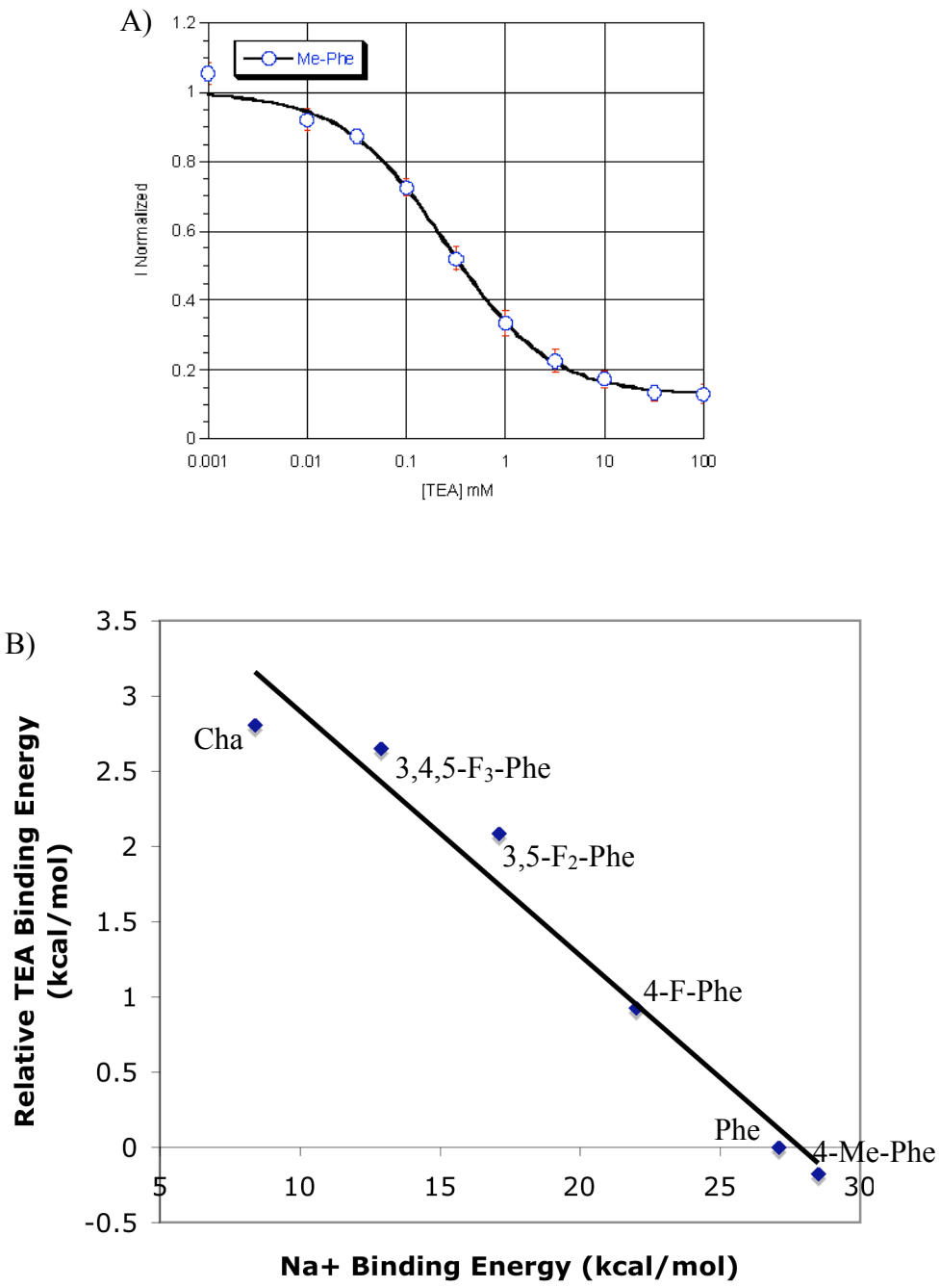

Figure 7.7. Data collected for 4-methyl-phenylalanine in ShB. A) IC_{50} curve for 4-methyl-phenylalanine at ShB position 449. B) Cation-π plot for ShB Thr449 mutations. The line represents the best fit for all of the points, $y = -0.16x + 4.5$ and $R^2 = 0.96$.

To ensure that the addition of the two methyl groups at the 3- and 5-positions was not disruptive for all cation-π interactions in the same degree as was seen in ShB, 3,5-dimethylphenylalanine was incorporated into the voltage-gated Na^+ channel $Na_V1.4$ in place of Phe1579. Note that this channel and residue are involved in a cation-π interaction with lidocaine, as discussed in chapter 5.[18] As seen in figure 7.8, the additional methyl groups do not negatively impact the cation-π interaction between the aromatic residue and lidocaine. Thus, the shift in IC_{50} for TEA and ShB with 3,5-dimethylphenylalanine incorporated at position 449 is specific for this blocker and this mutant channel. Somehow the addition of the methyl groups decreases the affinity of TEA for the channel, thus lowering its ability to block, but not in a manner that firmly discredits either model.

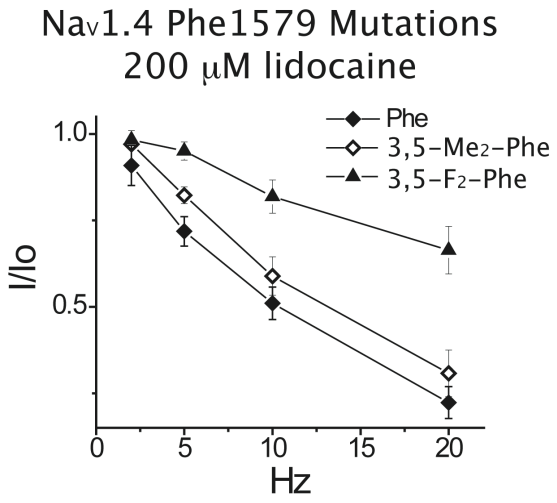

Figure 7.8. Frequency profile for use-dependent block for three different amino acids incorporated at position 1579 of $Na_V1.4$.

Even though 3,5-dimethylphenylalanine did not provide conclusive results in this study, it has been useful in studies interested in understanding the sterics around phenylalanine residues in two other ion channels. Walrati (Kay) Limapichat, a current graduate student in the Dougherty laboratory, has used this residue to understand the steric environment around the conserved FPF sequence in the α1 subunit of the muscle nAChR. She found that its incorporation at Phe166 lowered the EC_{50} of ACh tenfold from that of the wild-type channel. Comparison with the EC_{50} values for mutant channels with 4-methyl-phenylalanine, 4-F-phenylalanine, and 3,5-F_2-phenylalanine incorporated at this site suggested that the decrease in EC_{50} correlated with the size and location of the substituents on the aromatic ring. Kiowa Bower, another graduate student in the Dougherty laboratory, has used 3,5-dimethylphenylalanine to probe the importance of sterics around the aromatic residues located in the ligand-binding region of the dopamine D_2 G-protein coupled receptor (GPCR). Again, at certain sites he found trends that ran linearly with the size and location of the substituents on the aromatic ring. These two examples are only a small sampling of the possible sites for incorporation of 3,5-dimethylphenylalanine. In the future, this unnatural amino acid should continue to provide valuable information about the sterics around important phenylalanines in ion channels.

Attempts to Enhance the Binding Affinity of Cationic Ligands for their Receptors Using the Unnatural Amino Acid 4-Amino-Phenylalanine

As seen throughout the literature,[19] this thesis (chapters 2, 3, 4, 5),[13,18,20,21] and earlier this chapter, the cation-π interaction is a motif commonly employed by proteins to bind cationic ligands. Currently, the method used to confirm the presence of a cation-π interaction between a ligand and a receptor is through the incorporation of fluorinated phenylalanine or tryptophan residues in place of the aromatic residue proposed to donate the "π" portion of the interaction. The addition of the electronegative fluorine atoms withdraws electron density from the face of the aromatic, reducing the ability of the residue to bind cations. Other electron withdrawing substituents, such as a bromine atom or a cyano group, have also been shown to decrease the binding ability of the mutant receptor for a cationic ligand.[22] To date the unnatural amino acid 4-*O*-methyl-phenylalanine is the only published example of a slightly strengthened cation-π interaction in a receptor.[23] When Lummis *et al.* incorporated 4-*O*-methyl-phenylalanine at position 198 of the $GABA_C$ receptor, the EC_{50} was lower than that of the phenylalanine-containing receptor.[23] Earlier in this chapter another example of a slight enhancement of the cation-π interaction was seen in the ShB channel with 4-methyl-phenylalanine incorporated at position 449.

Both the *O*-methyl and the methyl strengthen the ability of the aromatic to bind a cation through the donation of electron density to the aromatic ring. An even stronger electron donating group is the amino group. For example, 5-amino-trypotphan has a cation-π binding ability of 36.4 kcal/mol, up from the 32.6 kcal/mol of tryptophan.[22] These

energy values represent the binding of a Na^+ to the noted aromatic as calculated from their optimized geometry using HF 6-31G**.[24] Unfortunately, when Zhong *et al.* incorporated 5-amino-tryptophan into the muscle nAChR at its cation-π interaction site, α1Trp149, the predicted decrease in EC_{50} was not seen.[22] Instead the EC_{50} increased over fivefold, from 50 to 280 μM ACh. The authors note that the increase could be from adverse interactions of the 5-amine with the receptor or because the amine may be protonated when in the receptor. As for the former explanation, 5-methyl-tryptophan has a wild-type EC_{50},[22] which argues against a purely steric clash with the receptor when a bulky group is added at this position. The 5-methyl group cannot account for the possibility that the 5-amino group could electrostatically clash with the receptor due to the added amine dipole, as seen in a study by Cashin, Torrice, *et al.* of the same receptor with the α1Asp89Asn mutant.[25] Incorporation of 5-amino-tryptophan could also have a destabilizing effect on the receptor, as seen when it was incorporated into barstar, an inhibitor of ribonuclease barnase from *Bacillus amyloliquefaciens*.[26] Potentially the difference in hydrophobicity of the amine-containing residue from the natural tryptophan could disrupt the formation of the aromatic binding box in the nAChR, resulting in a more poorly functioning receptor. As for the latter explanation, no conclusions were ever published that addressed whether the amine was protonated.

4-Amino-phenylalanine also has a cation-π binding ability greater than its natural analog phenylalanine. The addition of the amino group raises the binding energy from 27.1 kcal/mol (phenylalanine) to 31.8 kcal/mol (4-amino-phenylalanine). This residue has been incorporated into the muscle nAChR in place of several tyrosines in the binding box to study how the shift from a hydroxyl group to an amino group alters the function of the

channel,[27] and it has been incorporated into myoglobin by a completely autonomous bacterium,[28] but it has not yet been incorporated at any cation-π binding sites. The cation-π binding site in ShB provided a perfect location for the incorporation of 4-amino-phenylalanine. The initial goal of this study was twofold. First, if incorporation of 4-amino-phenylalanine at postion 449 of ShB enhanced the ability of TEA to block the channel, this result would add another point to the trend line shown in chapter 2 (figure 2.5A) and earlier in this chapter (figure 7.7), which would further support the hypothesis that a cation-π interaction occurs between TEA and the aromatic residue at position 449 and that the *en face* geometry is representative of the channel *in vivo*. Second, this work would stand as the first example of the strong enhancement of the cation-π interaction in an ion channel *in vivo*. Unfortunately, the results were not as predicted, and the project was expanded to other receptors in an attempt to understand the properties of 4-amino-phenylalanine *in vivo*.

Synthesis of 4-Amino-Phenylalanine-tRNA

Initially, 4-amino-phenyalalnine-tRNA was synthesized with two NVOC protecting groups (scheme 7.3). The synthesis did not differ much from the one described above for 3,5-dimethylphenylalanine.

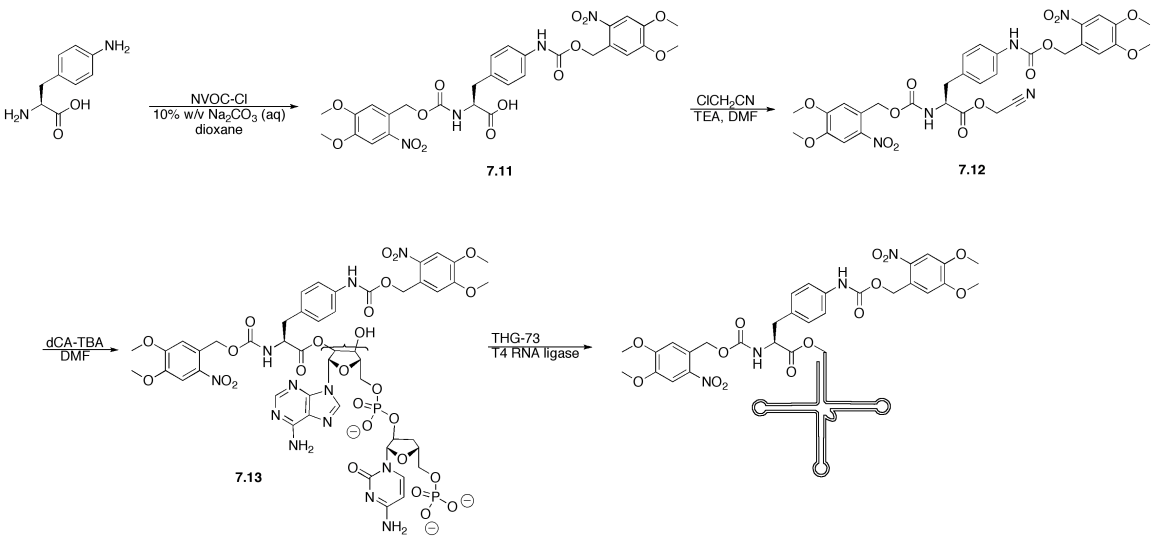

Scheme 7.3. Synthesis of di-NVOC-4-amino-phenylalanine-tRNA.

The NVOC group is generally removed by irradiating a sample of NVOC-protected amino acyl tRNA with approximately 320 nm light from a 1000 W Hg/Xe arc lamp for five minutes just prior to injecting the solution into *Xenopus laevis* oocytes, which are used as the protein expression system. Typically, an NVOC group is only present on the α-amine. To ensure that both NVOC groups on 4-amino-phenylalanine-tRNA were removed during photolysis, a sample of di-NVOC-4-amino-phenylalanine-dCA was irradiated and then analyzed by reverse-phase analytical high-pressure liquid chromatography (HPLC). The dCA derivative was used since its size and polarity were well suited for the reverse-phase column, and it would give distinct UV absorption signals for both the protected (absorbances at 260 and 350 nm) and deprotected compounds (absorbance only at 260 nm). After five minutes of irradiation, a small amount of starting material was still seen, but after ten minutes of irradiation, no starting material remained. Thus, for all of the experiments described below in which this doubly

NVOC protected 4-amino-phenylalanine was incorporated into a channel, the tRNA was irradiated for ten minutes prior to its injection into *Xenopus* oocytes.

No Cation-π Enhancement in ShB

Unfortunately, incorporation of 4-amino-phenylalanine at position 449 in ShB did not enhance the cation-π interaction. Instead of lowering the IC_{50} as compared to that of a receptor with phenylalanine incorporated at the same site, the IC_{50} was raised over fivefold from 0.39 mM TEA (phenylalanine) to 2.1 ± 0.3 mM TEA (4-amino-phenylalanine) (figure 7.9). This fivefold difference is familiar from the functional change seen in the muscle nAChR in going from tryptophan to 5-amino-tryptophan.

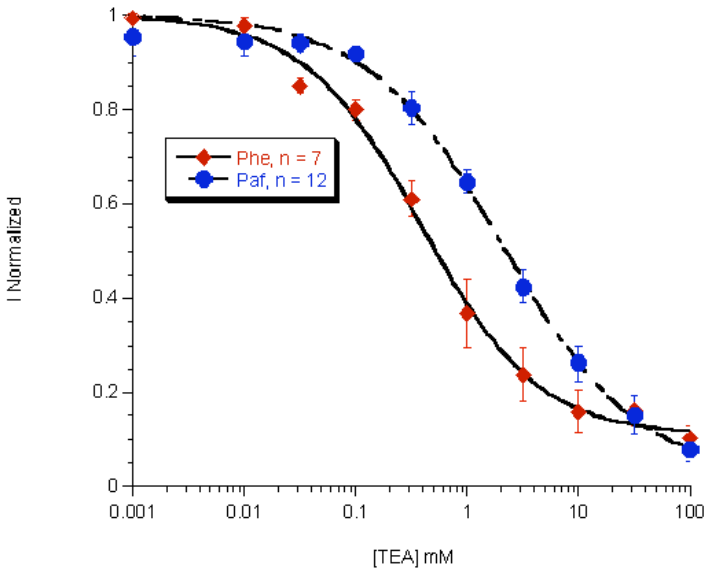

Figure 7.9. Dose-response curves for phenylalanine (red) and 4-amino-phenylalanine (blue) incorporated at ShB Thr449.

This result was very surprising since published crystal structures of related K^+ channels[15,29-33] predict that this site is located at the top of the channel pore with its side chain pointing out into solution. Thus, no steric or dipole clash should occur between this residue and the rest of the channel. To try to understand more about why 4-amino-phenylalanine did not enhance the cation-π in ShB, another system was sought in order to repeat the experiment.

No Cation-π Enhancement in the $GABA_C$ Receptor

In 2005 the first cation-π interaction between a ligand and a tyrosine was reported. ρ1Tyr198 in the $GABA_C$ receptor was found to bind GABA through a cation-π interaction. Thus, this receptor offered another opportunity to probe whether 4-amino-phenylalanine could enhance the cation-π interaction. 4-Amino-phenylalanine was incorporated into $GABA_C$ ρ1Tyr198, and an EC_{50} of 145 ± 24 μM GABA was obtained from the average of seven oocytes with a Hill coefficient of 1.2 ± 0.2 (calculated as described in chapter 6) (figure 7.9). Expression of the mutant receptor on the surface of the *Xenopus* oocyte was low, with the maximum amount of current reaching 100 nA, but the low expression was typical of a surpressed $GABA_C$ receptor. Because it is a homopentamer, the unnatural amino acid is present in each subunit in the receptor. This requirement tends to lower the number of functional receptors that get expressed on the surface of a *Xenopus* oocyte.

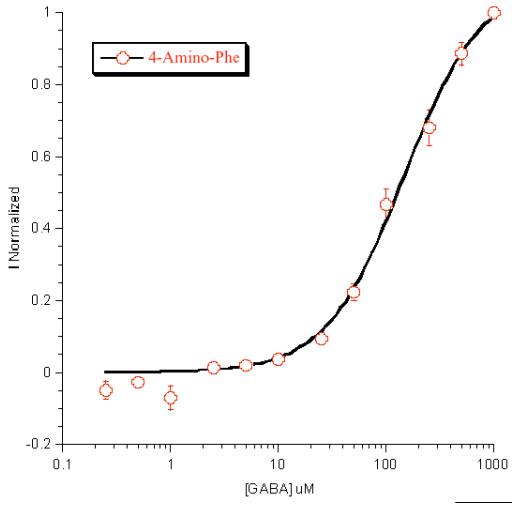

Figure 7.10. Dose-response curve for 4-amino-phenylalanine incorporated at ρ1Tyr198.

Surprisingly, this EC_{50} value was higher than Lummis *et al.* found for mutant receptors with phenylalanine, tyrosine, and even 4-F-phenylalanine incorporated at this site (table 7.1).[23] They do note the one example that falls off the trend: the EC_{50} for a receptor with tyrosine is roughly fourfold lower than what would be predicted from the phenylalanine residues and their cation-π binding energies. Thus, the hydroxyl group at the 4 position of the ring enhances the ability of GABA to activate the receptor. Potentially, the features that favor a hydroxyl group at the 4-position of the aromatic are not compatible with an amino group there. Lummis *et al.* propose that the hydroxyl group donates a hydrogen bond to another component of the system,[23] which would effectively enhance its cation-π binding energy.[34] But, the amino group of 4-amino-phenylalanine should be roughly equally as effective of a hydrogen bond donor as tyrosine. Lummis *et al.* also propose that GABA could make a favorable electrostatic interaction with the hydroxyl group on tyrosine, but they state that this possibility is less likely since the same

functional enhancement is not observed with 4-methoxy-phenylalanine, which also has an oxygen-containing substituent at the 4-position.[23] Neither proposal adequately explains why 4-amino-phenylalanine does not enhance the cation-π interaction as predicted in the $GABA_C$ receptor.

Table 7.1. The data collected for the $GABA_C$ ρ1Tyr198 cation-π site.*

Tyr198X, where X =	Cation-π Binding Energy (kcal/mol)	EC_{50} (μM) [Hill Coeff.]
4-Amino-phenylalanine	31.8	145 ± 24 [1.2 ± 0.2]
4-Methoxy-phenylalanine*	28.6	6.6 [1.6]
Phenylalanine*	27.1	9.5 [1.6]
Tyrosine*	26.9	2.1 [1.6]
4-F-Phenylalanine*	22.0	34 [1.9]
3,5-F_2-Phenylalanine*	17.1	1700 [1.4]
3,4,5-F_3-Phenylalanine*	12.9	8400 [1.5]

Another explanation for the functional disruption of the receptor caused by 4-amino-phenylalanine is that the aniline is getting modified either during the NVOC deprotection step or after injection by the *Xenopus* oocyte. The additional steric bulk could create a poorly functioning receptor. A third system was sought to further explore the effects of 4-amino-phenylalanine.

No Cation-π Enhancement in the Muscle nAChR

Despite the differences in size and shape between tryptophan and phenylalanine, the muscle nAChR was chosen as another target for 4-amino-phenylalanine due to the

* Reported by Lummis *et al.*[23]

prevalence of this receptor in the Dougherty laboratory. The expectation was not that 4-amino-phenylalanine incorporated in place of α1Trp149 would produce a wild-type receptor, but instead it was simply that 4-amino-phenylalanine would create a better nAChR than the mutant receptor that contained phenylalanine at this site. It has previously been published that the muscle nAChR with α1Trp149Phe has an EC_{50} 100 times higher than wild type.[22] Because 4-amino-phenylalanine should be able to more strongly bind ACh, it was predicted that this residue would be able to partially rescue receptor function.

Unfortunately, the desired result was not seen. When 4-amino-phenylalanine was incorporated into α1Trp149 in a channel that also consisted of the subunits β1, δ, and γ, the EC_{50} was too high to accurately measure, reminiscent of a receptor that contains α1Trp149Phe.[22] In order to quantitiate the effect of incorporating 4-amino-phenylalanine, its EC_{50} was lowered by making a mutation in the pore lining helix of the β1 subunit. When β1Leu262, the famous 9' residue that is part of a hydrophobic band of residues that forms the narrowest point in the pore of the channel, is mutated to the more polar residue serine, the channel is more easily opened. With a receptor that includes β1Leu9'Ser, the EC_{50} for 4-amino-phenylalanine incorporated at position 149 in the α1 subunit was found to be 160 ± 12 μM for ACh with a Hill coefficient was 1.8 ± 0.2. Surprisingly, this value was identical to that found for phenylalanine; its EC_{50} was 154 ± 24 μM, and its Hill coefficient was 1.7 ± 0.3 (figure 7.11). Therefore, 4-amino-phenylalanine does not rescue any of the receptor function lost upon phenylalanine incorporation. For reference, the wild-type EC_{50} for this nAChR is around 0.8 μM.[35]

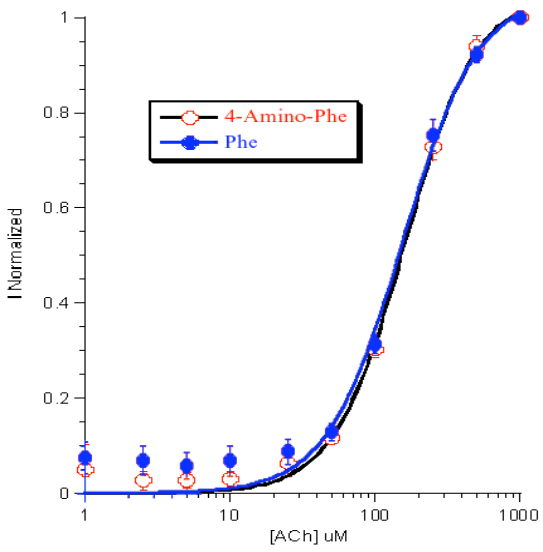

Figure 7.11. Dose-response curves for 4-amino-phenylalanine and phenylalanine incorporated at α1Trp149 in the muscle nAChR containing the β1Leu9'Ser, δ, and γ subunits.

Two explanations were proposed to account for the similarity in EC_{50} values between phenylalanine and 4-amino-phenylalanine in the nAChR. First, the amine could be modified after being deprotected in such a way as to reduce its cation-π binding ability or add inappropriate steric bulk. Second, the change in size and shape of the side chain in the receptor's binding site from the wild-type indole to a six-member ring could be the dominant factor in the reduction of receptor function. In this case the cation-π binding ability of the aromatic six-member ring was inconsequential due to its lack of necessary volume. In either case, the question as to whether 4-amino-phenylalanine could enhance the cation-π interaction was still unanswered.

The NVOC-Deprotection Conditions Do Not Modify the Aniline

If 4-amino-phenylalanine-tRNA were being altered, the modification could either occur during NVOC deprotection or by a cellular pathway once in the *Xenopus* oocyte. Because 4-amino-phenylalanine was successfully incorporated into a protein in a bacterial system without being further modified, as proved by protein sequencing,[28] the cellular environment seemed the less likely of the two possibilities. Therefore, the deprotection step was investigated first. Three different strategies were undertaken to determine whether the aniline was stable to photolysis. The first involved trapping the photolysis byproducts, the second involved identifying the mass of the major photolysis product, and the third avoided photolysis altogether.

Irradiation of di-NVOC-4-amino-phenylalanine-tRNA produces not only deprotected tRNA, but also an aldehyde (figure 7.12). This aldehyde could react with the aniline to form an imine, creating a large and sterically bulky amino acid that could affect the receptor in unpredictable ways.

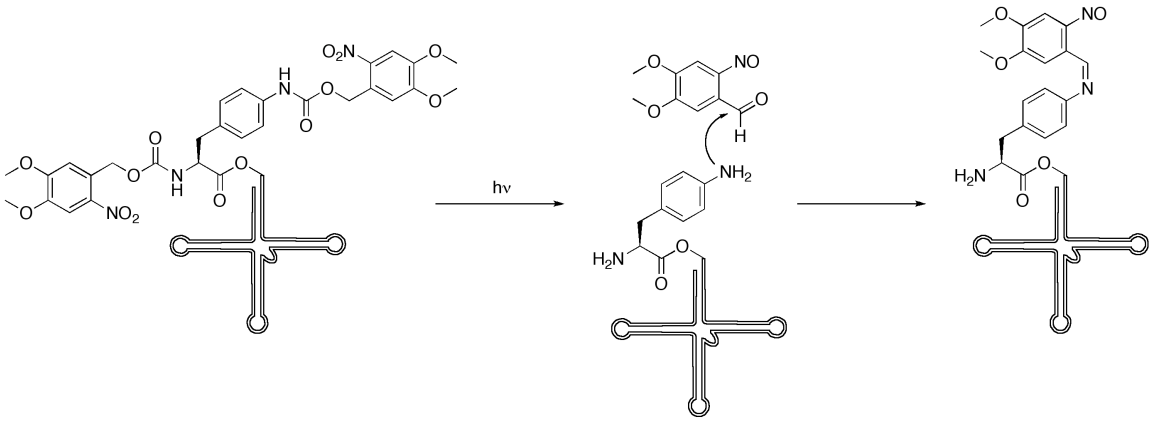

Figure 7.12. Deprotection of di-NVOC-4-amino-phenylalanine-tRNA produces an aldehyde that could react with the aniline.

To prevent the possibility of imine formation, di-NVOC-4-amino-phenylalanine tRNA was photolyzed in the presence of an excess of hydroxylamine prior to injection of the mixture into a *Xenopus* oocyte. The hydroxylamine should react with the aldehyde to produce a stable oxime. The resulting mutant nAChR channels made with this directed to the cation-π binding site had the same high EC_{50} values as reported above for the muscle nAChR with 4-amino-phenylalanine without the β1Leu9'Ser mutation. As a control, NVOC-tryptophan-tRNA was photolyzed in the presence of hydroxylamine and then injected into an oocyte with the intention of incorporating the residue at the same site as above. The wild-type recovery experiment was not affected by the hydroxylamine. The control proves that the photolysis with hydroxylamine did not negatively affect the experiment. These results suggest that imine formation was not a contributing factor to the functional response of the channel to 4-amino-phenylalanine incorporation.

In parallel, matrix-assisted laser desorption/ionization (MALDI)-mass spectrometry (MS) was used to analyze the photolysis products after irradiation of di-NVOC-4-amino-phenylalanine-dCA. The mass of the major photolysis product, given as its mass-to-charge ratio (*m/z*), was 799.3, which is the expected ratio of the aniline-dCA associated with a hydrogen atom ([M+H] *m/z* = 799.2). Although MS cannot confirm the structure of a product or relay quantitative information about how prevalent a compound is in solution, the fact that the *m/z* ratio with the largest abundance agreed with that predicted for the expected product is very encouraging.

The third strategy took a different pathway: it sidestepped the deprotection step altogether through the synthesis of 4-amino-phenylalanine-tRNA without any NVOC

protecting groups. The synthesis of deprotected 4-amino-phenylalanine-tRNA began by protecting the aniline amine of N_α-*t*Boc-4-amino-phenylalanine with another *t*Boc group[36] and activating the acid as a cyanomethyl ester. The acid-labile protecting groups were removed following the coupling of the amino acid to dCA according to the protocol that was developed by a former postdoctoral researcher in the Dougherty laboratory, Dr. Pamela England, for the deprotection of *tert*-butyl silyl protected α-hydroxy acid-dCA compounds.[37] Ligation to THG73 produced deprotected 4-amino-phenylalanine-tRNA.

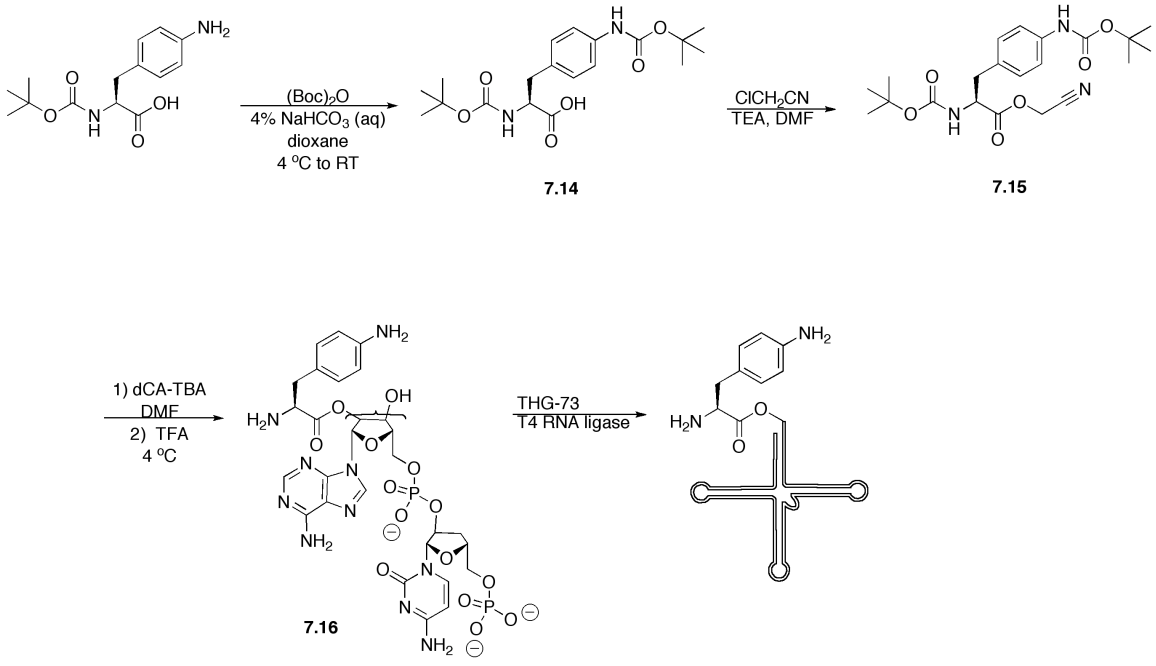

Scheme 7.4. Synthesis of deprotected 4-amino-phenylalanine-tRNA

Synthesized amino acyl tRNAs are generally proctected on their α-amine to decrease the negative inductive effect of the free amino on the stability of the complex. To minimize the degradation of the deprotected tRNA, it was divided up into small aliquots prior to

storage at −80 °C. Each aliquot was thawed immediately proceeding injection into *Xenopus* oocytes, and no added disadvantage from the lack of storage with the NVOC group was ever observed. As above with the hydroxylamine studies, the EC_{50} values for the $GABA_C$ receptor with this 4-amino-phenylalanine incorporated into its cation-π binding site gave the same values as reported for the di-NVOC version, 153 ± 32 μM GABA with a Hill coefficient of 1.1 ± 0.2.

Together these three separate experiments confirmed that the deprotection of di-NVOC-4-amino-phenylalanine-tRNA by irradiation was not disruptive to the aniline structure. Thus, what was considered the most likely explanation for the unpredicted results was eliminated. The possibility still remained though that the aniline was getting modified once inside the cell.

Attempts to Form 4-Amino-Phenylalanine In Situ

To eliminate the possibility that a cellular component in the *Xenopus* oocyte was modifyng the aniline, two unnatural amino acids were designed to either reveal or chemically convert to 4-amino-phenylalanine *in situ* upon the addition of an outside stimulus. The stimulus would be applied immediately prior to recording whole-cell currents from the mutant channels, minimizing the amount of time the aniline would be exposed to the cellular environment. The first unnatural amino acid was a caged aniline that was responsive to UV light, and the second was 4-nitro-phenylalanine, which upon exposure to a reducing agent, should become the 4-amino compound.

The synthesis of the caged 4-amino-phenylalanine-tRNA began by protecting the aniline amine of N_α-*t*Boc-4-amino-phenylalanine with NVOC (scheme 7.5). Next, the *t*Boc group was removed, and then the α-amine was reprotected with the orthogonal 4-pentenoate (4PO) group. The rest of the synthesis progressed as described above.

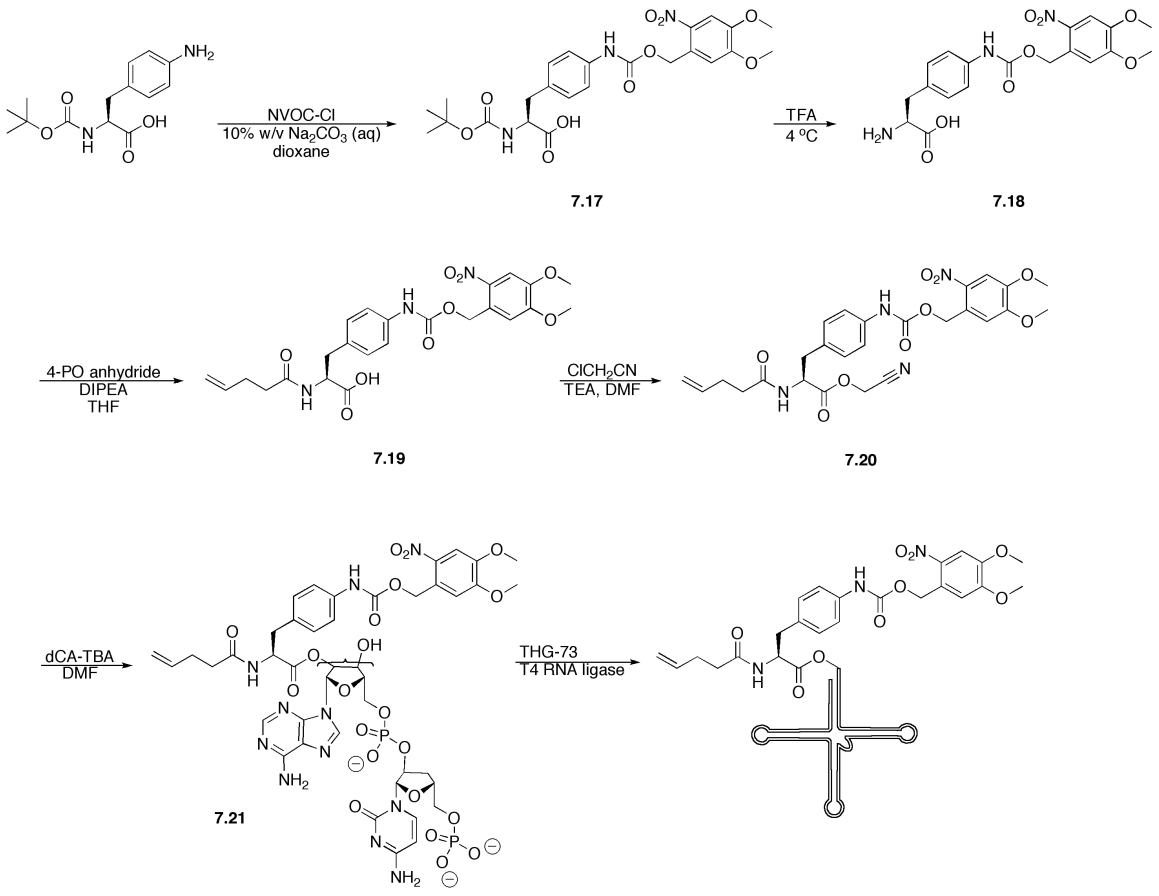

Scheme 7.5. Synthesis of N_α-4PO-4-amino(NVOC)-phenylalanine-tRNA.

The 4PO protecting group was removed prior to injecting the tRNA into a *Xenopus* oocyte by exposing the protected tRNA to a saturated, aqueous iodine solution. Since the NVOC group is resistant to these conditions, it allowed for the aniline to remain

protected during protein translation. Immediately prior to recording the oocytes were exposed to UV light from a 288 W Hg lamp (see chapter 8), which was anticipated to decage the aniline. There was precedent for this type of decaging experiment from unnatural amino acids such as tyrosine-*O*-nitrobenzyl, cysteine-*S*-nitrobenzyl, and nitrophenylglycine.[38-41] Since earlier results proved that the aldehyde photolysis by-product that is produced from the NVOC deprotection does not appear to affect the aniline, no precautionary measures were taken here.

Unfortunately, no whole-cell currents were ever seen from this caged aniline. To explore whether this amino acid was compatible with ribosomal translation, attempts were made to incorporate the residue into a protein *in vitro* using rabbit reticulocyte lysate and α1Leu250UAG mRNA with an hemagglutinin (HA) epitope tag between residues 347 and 348. No protein was ever seen by Western blot, despite the success of the positive controls. One possible explanation for the lack of protein expression could be the inadequate deprotection of the 4PO group from the α-amine. If the 4PO group were not effectively removed, then the unnatural amino acid-tRNA would not be able to participate in translation. This explanation did not seem likely though as the same deprotection methods were used to prepare 4PO-tyrosine-*O*-nitrobenzyl for *in vivo* nonsense suppression in chapter 8, and whole-cell currents were produced there. It should be noted though that no side-by-side controls were run in this study. Another explanation for the lack of protein could be that the size of the unnatural amino acid was too large for the ribosome. A study by Sisido and co-workers on the incorporation of large, aromatic unnatural amino acids was successful incorporating amino acids similar in size to the caged aniline using an *in vitro E. coli* translation system.[36] These results gave

precedent to our design and suggested that the caged aniline should be ribosomally competent. Since the Sisido study used *E. coli* ribosomes, it could still be that the *Xenopus laevis* ribosome is more discriminatory with amino acid size and was selecting against the caged aniline.

The second attempt to form 4-amino-phenylalanine *in situ* was through the reduction of 4-nitro-phenylalanine by dithionite. The reaction was modeled after the quenching of the fluorescent NBD by dithionite (see figure 7.2 for the structure of NBD).[42] Angeletti and Nichols showed that when dithionite was applied to NBD-labeled lipid vesicles, the reduction of the nitro group to the amine eliminated the fluorescence of the compound.[42] To ensure that dithionie could reduce the nitro group of 4-nitro-phenylalanine to an amino group, the UV spectra of *t*Boc-4-nitro-phenylalanine and N_{α}-*t*Boc-4-amino-phenylalanine were analyzed via reverse-phase analytical HPLC before and after at least 20 minute exposure to 100 mM sodium dithionite in 100 mM phosphate buffer pH 7.4. Prior to dithionite treatment the nitro and amino compounds had very different UV spectra, but after treatment, the UV spectra of the nitro compound had changed to resemble the amine compound (figure 7.13). The resulting UV spectra were taken as evidence that dithionite could reduce 4-nitro-phenylalanine to 4-amino-phenylalanine *in situ*. Therefore, 4-nitro-phenylalanine-tRNA was synthesized following steps similar to those described above (scheme 7.6).

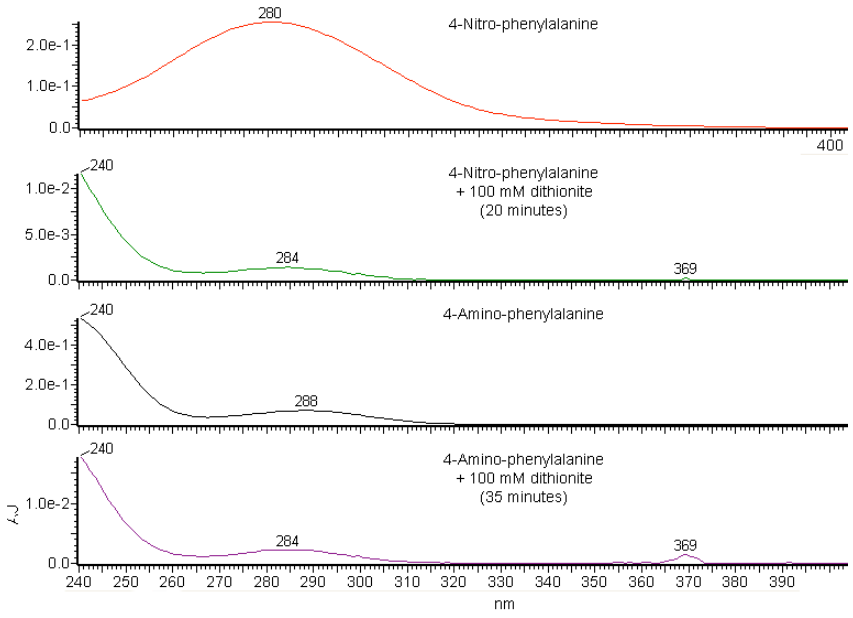

Figure 7.13. UV spectra of 4-nitro-phenylalanine and 4-amino-phenylalanine before and after exposure to 100 mM dithionite in 100 mM phosphate buffer pH 7.4 for the time indicated in the parentheses.

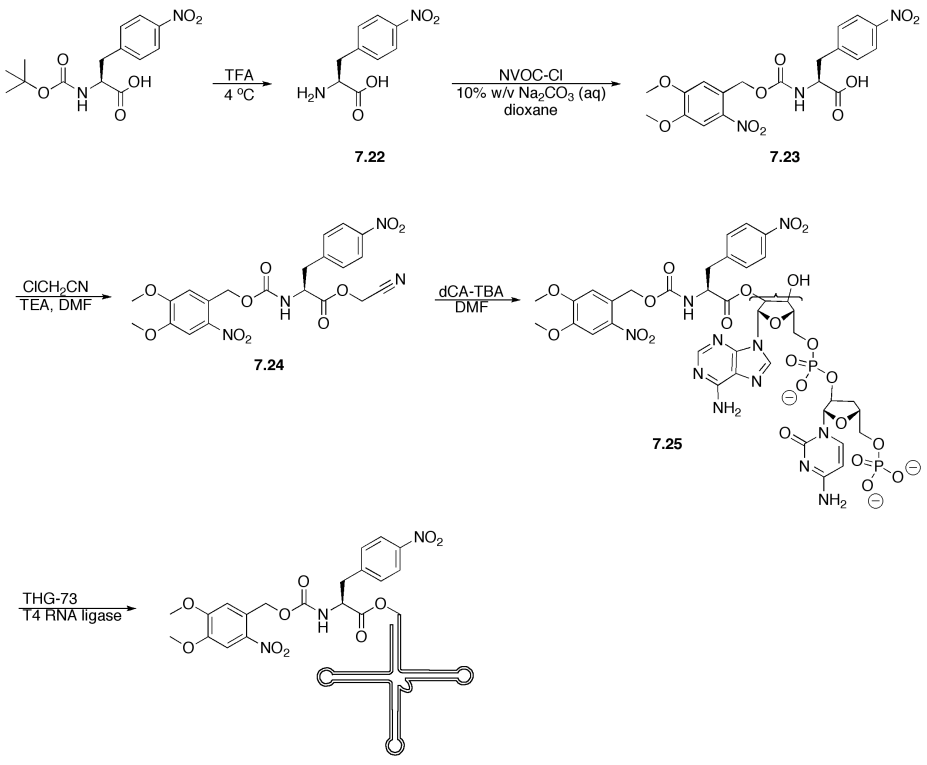

Scheme 7.6. Synthesis of NVOC-4-nitro-phenylalanine-tRNA.

4-Nitro-phenylalanine was incorporated into ShB at position 449 and produced an IC_{50} for TEA of 0.95 ± 0.1 mM TEA (figure 7.14A). Because dithionite would also reduce important elements of the electrophysiology rig, like the AgCl pellet in the bath solution, the *Xenopus* oocytes used in this study were placed in a solution of either 100 mM dithionite in 100 mM phosphate buffer pH 7.4 or 24 mM dithionite in 50 mM phosphate buffer pH 7.4 for varying amounts of time prior to recording. This second solution of dithionite was much lower in concentration than that used in the model studies, but it was chosen because its osmolarity was equivalent to that of the typical bath solution used for oocytes (ND96, 209.4 mM ions). Whole-cell recordings were attempted after exposure to dithionite, but no reliable data were obtained, presumably due to a decrease in health from the time in the dithionite solution. The addition of calcium to the dithionite solution (to aid the health of the oocytes) was not possible because calcium phosphate just precipitated out of the solution.

Incorporation of 4-Acetamido-Phenylalanine

One possible way in which the cell could be modifying 4-amino-phenylalanine could be the addition of an acetyl group, producing 4-acetamido-phenylalanine. To explore this possibility, 4-acetamido-phenylalanine was synthesized (scheme 7.7) and incorporated into ShB at position 449.

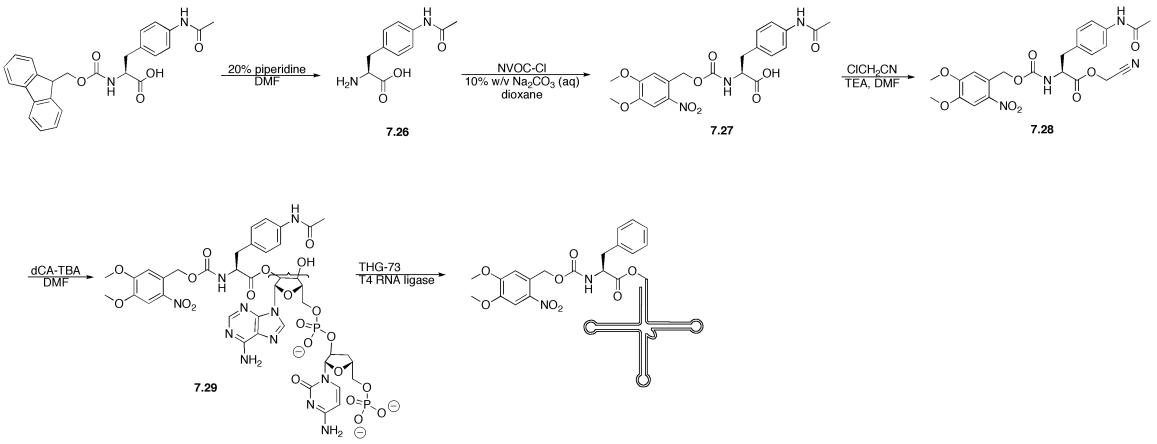

Scheme 7.7. Synthesis of NVOC-4-acetamido-phenylalanine-tRNA.

Surprisingly, the IC_{50} for the mutant channel with 4-acetamido-phenylalanine at the cation-π site was 2.1 ± 0.4 mM TEA—identical to the value obtained for 4-amino-phenylalanine (2.1 ± 0.3 mM TEA) (Fgure 7.14A). The cation-π binding energy for acetamino-benzene was calculated to be 21.4 kcal/mol with optimized geometry using HF 6-31G*. When this EC_{50} value was plotted against the cation-π binding (chapter 2),[13] it reasonably fit the cation-π trend-line (figure 7.14B). This result provided the first glimpse of understanding into the questions that had arisen around 4-amino-phenylalanine.

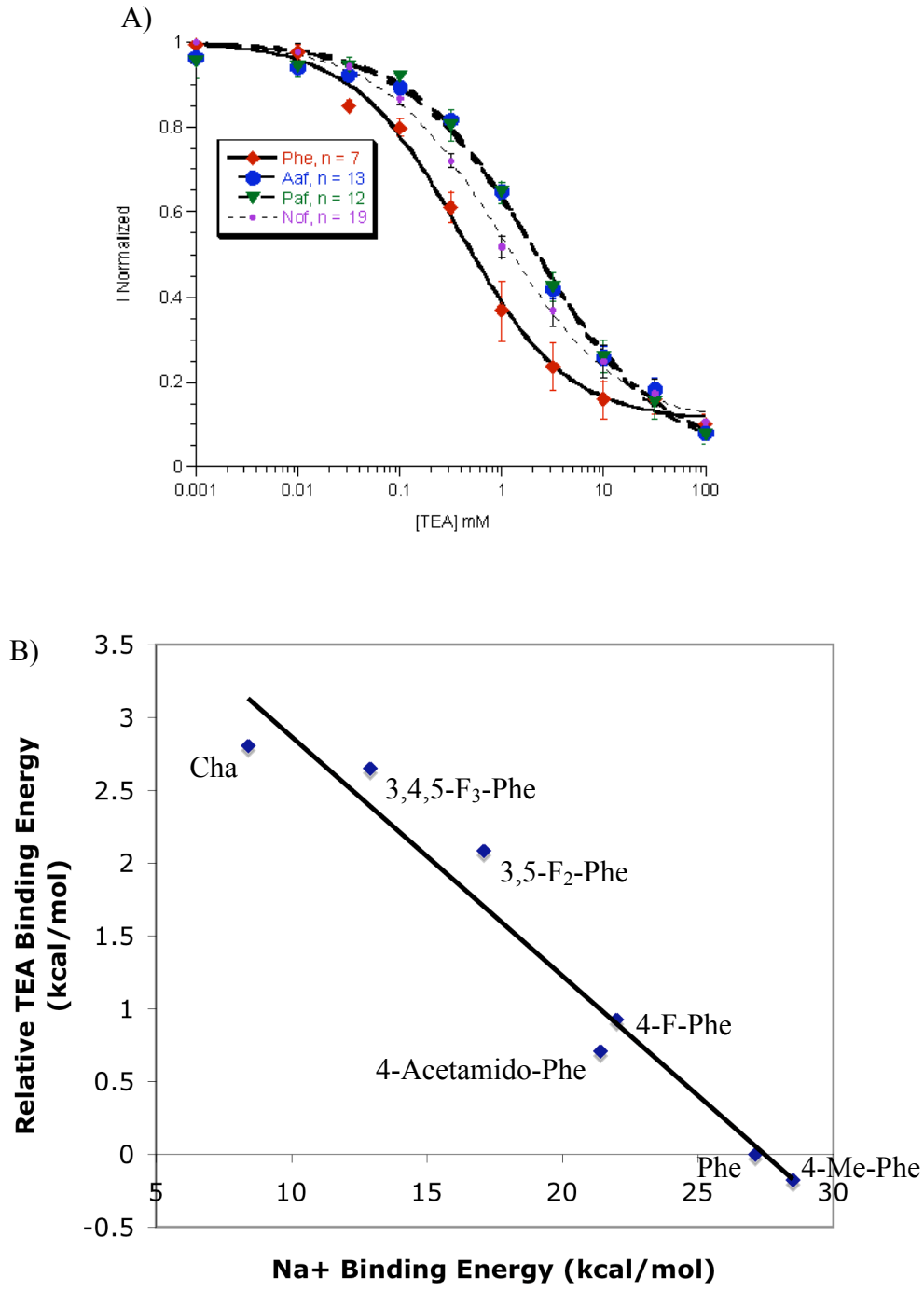

Figure 7.14. Data collected for 4-acetamido-phenylalanine in ShB. A) Dose-response curves for 4-acedamido-phenylalanine and 4-nitro-phenylalanine incorporated at ShB position 449 (phenylalanine and 4-amino-phenylalanine repeated from above). B) Cation-π plot for ShB Thr449 mutations. The line represents the best fit for all of the points, $y = -0.16x + 4.5$ and $R^2 = 0.96$.

Unfortunately, the result could not be repeated in either the nAChR or the $GABA_C$ receptor. Only three oocytes were found to express 4-acetamido-phenylalanine at the cation-π site of the muscle nAChR (with the β1Leu9'Ser muation), but their EC_{50} values varied from 2.5 μM to 8.3 μM to 31.1 μM ACh, and their EC_{50} curves even gave the slight impression that they were biphasic. None resembled the 160 μM ACh EC_{50} of 4-amino-phenylalanine. No whole-cell currents were ever seen for 4-acetamido-phenylalanine incorporated at $GABA_C$ ρ1Tyr198, while reliable expression had been observed for 4-amino-phenylalanine. Therefore, the data obtained from these two receptors did not support that 4-amino-phenylalanine was being acylated by the *Xenopus* oocyte prior to channel recording.

Future Directions

Future work towards the understanding of 4-amino-phenylalanine should consider incorporating the residue at the cation-π sites that have been recently published in the $Na_V1.4$ channel (see chapters 3, 4, and 5)[18,20,21] and the $GABA_A$ receptor.[43] These two receptors use tyrosines and phenylalanines in cation-π interactions and would hopefully supply an explanation as to why 4-amino-phenylalanine did not enhance the cation-π interaction in ShB, $GABA_C$, or nAChR.

Another possible direction for this project would be to conclusively determine whether 4-amino-phenylalanine was in fact being incorporated into the desired receptor using an aniline-specific tag. The exposed cation-π site of ShB is anticipated to be an ideal

location for such an experiment. Francis and co-workers developed an aniline-specific tag that takes advantage of the oxidative coupling of anilines,[44] but since this specific tagging of anilines requires an oxidant such as sodium *meta*-periodate, conditions would need to be optimized for use of this tag with the *Xenopus* oocyte.

Methods

Synthesis

All reactions were performed at ambient temperature and pressure unless otherwise noted. All reactions involving potentially air-sensitive compounds were conducted under an inert atmosphere using Schlenk techniques. Solvents were purified by passage through alumina.[45] Unless otherwise noted, all chemicals and reagents were used as received without further purification. Flash chromatography was performed using EMD (Gibbstown, NJ) silica gel 60 (particle size 0.040-0.063 mm). Thin-layer chromatography (TLC) was performed using EMD (Gibbstown, NJ) silica gel 60 F_{254} precoated plates (0.25 mm) and visualized by UV, ceric ammonium molybdate, ninhydrin, and potassium permanganate. Nuclear magnetic resonance spectroscopy (NMR) was preformed on a Varian (Palo Alto, CA) Mercury 300 instrument, and NMR resonances are reported relative to Me_4Si (δ 0.0), CD_3OD (δ 3.31), CD_3CN (δ 1.94), D_2O (δ 4.79), or d_6-DMSO (δ 2.50). Data for ^1H NMR spectra are reported as follows: chemical shift (δ ppm), integration, multiplicity, and coupling constant (Hz). MS spectra were obtained from the Caltech Mass Spectrometry Lab. Electrospray ionization (ESI)-MS was preformed on an LCQ Classic ion trap (ThermoFinnigan, Waltham, MA) in

direct infusion mode. MALDI-MS was performed on a Voyager-DE PRO BioSpectrometry Workstation (PerSeptive Biosystems, Foster City, CA). HPLC was preformed using Waters (Milford, MA) equipment and software (510 HPLC pumps and 996 Photodiode Array Detector) and reverse-phase Nova-Pak ^{18}C columns (3.9 × 150 mm analytical column, 7.8 × 300 mm preparatory column).

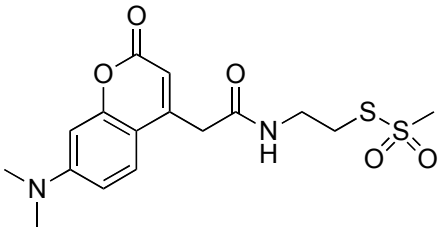

7.1

DMAC-MTSEA **7.1**: 7-Dimethylaminocoumarin-4-acetic acid succinimidyl ester (0.0019 g, 0.0057 mmol, 1 eq) was placed in a round-bottom flask under Ar (g) in the dark and dissolved in DMF (1 mL). To this solution was added 2-aminoethyl methanethiosulfonate hydrobromide (0.075 g, 0.45 mmol, 79 eq) and diisopropylethylamine (0.060 mL, 0.33 mmol, 58 eq). After stirring for 5 minutes, the reaction was halted by freezing in N_2 (liq), and the solvent was removed under vacuum. The crude product was purified using reverse-phase semipreparative HPLC with a linear solvent gradient from 5% acetonitrile in H_2O with 1% AcOH to 100% acetonitrile. The fractions containing the DMAC-MTSEA **7.1** were combined, and the solvent was removed by lyophilization. ^{1}H NMR (300 MHz, $CDCl_3$, 298 K) δ 7.45 (1H, d, J = 8.7 Hz), 6.62 (1H, dd, J = 9.0, 2.7 Hz), 6.52 (1H, m), 6.06 (1H, s), 3.65 (2H, s), 3.60 (2H, q, J = 6.3 Hz), 3.32 (3H, s), 3.27 (2H, t, J = 6.0 Hz), 3.06 (6H, s), 2.85 (4H, s); ESI-MS *m/z* calc'd for $C_{16}H_{20}N_2O_5S_2$ [M+Na]: 407.1, found: 406.9.

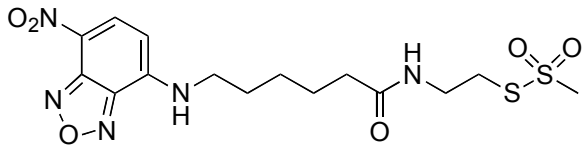

7.2

Extended NBD-MTSEA **7.2**: The procedure described above for **7.1** was repeated using succinimidyl-6-(N-(7-nitrobenz-2-oxa-1,3-diazol-4-yl)amino)hexanoate (0.022 g, 0.0057 mmol, 1 eq) as the starting material to afford extended NBD-MTSEA **7.2**. ^{1}H NMR (300 MHz, $CDCl_3$, 298 K) δ 8.51 (1H, d, J = 8.4 Hz), 6.19 (1H, d, J = 8.7 Hz), 4.17 (1H, q, J = 6.9 Hz), 3.65 (2H, m), 3.54 (2H, q, J = 6.0 Hz), 3.39 (3H, s), 3.35 (2H, m), 2.28 (2H, m), 1.80 (6H, m); ESI-MS *m/z* calc'd for $C_{15}H_{21}N_5O_6S_2$ [M−H]: 430.1, found: 430.0.

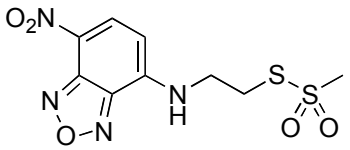

7.3

Compact NBD-MTSEA **7.3**: The procedure described above for **7.1** was repeated using 4-chloro-7-nitrobenzofurazan (0.011 g, 0.0057 mmol, 1 eq) as the starting material to afford compact NBD-MTSEA **7.3**. ^{1}H NMR (300 MHz, $CDCl_3$, 298 K) δ 8.53 (1H, d, J = 8.4 Hz), 6.36 (1H, d, J = 8.7 Hz), 3.97 (2H, q, J = 6.3 Hz), 3.51 (2H, t, J = 6.6 Hz), 3.43 (3H, s); ESI-MS *m/z* calc'd for $C_9H_{10}N_4O_5S_2$ [M−H]: 317.0, found: 316.8.

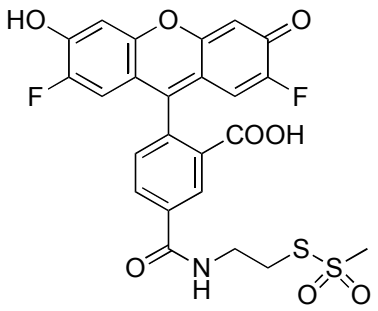

7.4

Oregon Green-MTSEA **7.4**: The procedure described above for **7.1** was repeated using Oregon Green 488 carboxylic acid 5-isomer succinimidyl ester (0.0030 g, 0.0057 mmol, 1 eq) as the starting material to afford Oregon Green-MTSEA **7.4**. ^{1}H NMR (300 MHz, $CDCl_3$, 298 K) δ 8.43 (1H, s), 8.01 (1H, m), 7.31 (1H, d, J = 8.1 Hz), 6.69 (2H, d, J = 7.2 Hz), 6.60 (2H, d, J = 11.1 Hz), 3.74 (2H, t, J = 6.9 Hz), 3.43 (2H, t, J = 7.2 Hz), 3.40 (3H, s); ESI-MS *m/z* calc'd for $C_{24}H_{17}F_2NO_8S_2$ [M−H]: 548.0, found: 548.0.

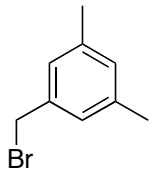

7.5

Bromomesitylene **7.5**: Mesitylene (7.30 mL, 52.4 mmol, 1.1 eq), *N*-bromosuccinimide (8.90 g, 50.0 mmol, 1 eq), and benzoyl peroxide (0.050 g, 0.20 mmol, 0.004 eq) were placed in a round-bottom flask under Ar (g) and dissolved in carbon tetrachloride (20 mL). The reaction was allowed to reflux for 1 hour. The solution was then filtered (5×) to remove the solid precipitate and concentrated to afford bromomesitylene **7.5** (4.0902 g, 20.5 mmol, 739% yield). R_f = 0.56 (11% EtOAC in hexanes); ^{1}H NMR (300 MHz, $CDCl_3$, 298 K) δ 7.02 (2H, s), 6.95 (1H, s), 4.45 (2H, s), 2.32 (6H, s).

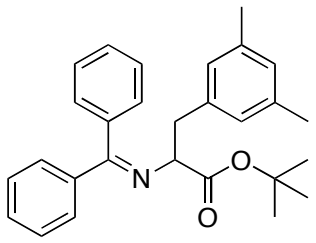

7.6

N-(Diphenylmethylene)dimethylphenylalanine *tert*-butyl ester **7.6**: Bromomesitylene **7.5** (0.597 g, 3.00 mmol, 1 eq), *N*-(diphenylmethylene)glycine *tert*-butyl ester (0.975 g, 3.30 mmol, 1.1 eq), and KI (0.054 g, 0.33 mmol, 0.11 eq) were placed in a round-bottom flask under Ar (g) and dissolved in dioxane (27 mL). The solution was cooled to 10 °C and then charged with the dropwise addition of benzyltrimethylammonium hydroxide (40% solution in H_2O, 0.4 mL). The reaction changed color from yellow to white as it was stirred for 3 hours. It was then quenched with H_2O, extracted with toluene (6×), washed with H_2O, and dried over $CaCl_2$ (s). The now yellow solution was concentrated under vacuum, and the crude product was purified by flash column chromatography (5% EtOAc in hexanes) to yield *N*-(diphenylmethylene)dimethylphenylalanine *tert*-butyl ester **7.6** (0.880 g, 2.13 mmol, 70% yield). R_f = 0.48 (11% EtOAC in hexanes); ^{1}H NMR (300 MHz, $CDCl_3$, 298 K) δ 7.82 (1H, d, J = 6.9 Hz), 7.61 (2H, m), 7.50 (2H, m), 7.31 (4H, m), 6.79 (1H, s), 6.67 (2H, s), 4.11 (1H, m), 3.17 (2H, m), 2.19 (6H, s), 1.48 (9H, s); ESI-MS *m/z* calc'd for $C_{28}H_{31}NO_2$ [M+H]: 414.2, found 414.0.

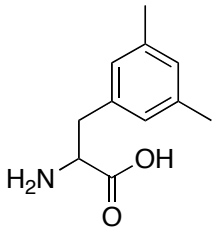

7.7

Dimethylphenylalanine **7.7**: *N*-(Diphenylmethylene)glycine *tert*-butyl ester **7.6** (0.440 g, 1.06 mmol) was added to a round-bottom flask and dissolved in 6 N HCl (20 mL). The reaction was refluxed for 6 hours. The solution was then washed with ether, and the aqueous layer was concentrated by lyophilization to yield dimethylphenylalanine **7.7** (0.052 g, 0.27 mmol, 25% yield). ^{1}H NMR (300 MHz, D_2O, 298 K) δ 7.04 (1H, s), 6.92 (1H, s), 4.17 (1H, dd, J = 7.5, 5.7 Hz), 3.01 (2H, m), 2.11 (6H, s).

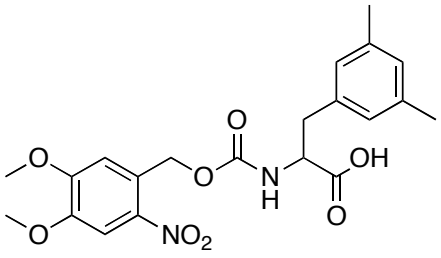

7.8

NVOC-dimethylphenylalanine **7.8**: Dimethylphenylalanine **7.7** (0.0515 g, 0.270 mmol, 1 eq) was added to a round-bottom flask and dissolved in 10% (w/v) sodium carbonate in H_2O (1.03 mL, 0.972 mmol, 3.6 eq). To this solution was added dioxane (1 mL). The mixture was stirred in an ice bath and nitroveratryloxycarbonyl chloride (0.078 g, 0.283 mmol, 1.1 eq) was added slowly. The mixture was allowed to warm to room temperature while stirring for 4 hours. The mixture was then poured into distilled H_2O (200 mL) and washed with ether (3×). Under vigorous stirring, the aqueous solution was adjusted to

pH 2 by slowly adding 5 M HCl and then the solution was extracted with ether, dried over $MgSO_4$ (s), and concentrated to afford NVOC-dimethylphenylalanine **7.8** as a yellow oil (0.0728 g, 0.170 mmol, 63% yield). ^{1}H NMR (300 MHz, CD_3OD, 298 K) δ 7.73 (1H, s), 7.17 (1H, s), 7.08 (1H, s), 6.85 (2H, s), 5.42 (2H, m), 4.39 (1H, m), 3.89 (3H, s), 3.84 (3H, s), 3.14 (1H, m), 2.84 (1H, m), 2.24 (6H, s); ESI-MS *m/z* calc'd for $C_{21}H_{24}N_2O_8$ [M+Na]: 455.2, found 455.0.

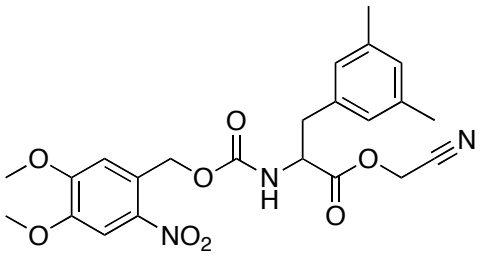

7.9

NVOC-dimethylphenylalanine cyanomethyl ester **7.9**: NVOC-dimethylphenylalanine **7.8** (0.72 g, 0.17 mmol) was added to a round-bottom flask under Ar (g) and dissolved in DMF (0.5 mL). Chloroacetonitrile (0.5 mL) and then triethylamine (0.07 mL) were added to the solution. The mixture was stirred at room temperature for 90 minutes and then the solvent was removed under vacuum. The residue was purified by flash column chromatography (5% EtOAc in hexanes) to afford NVOC-dimethylphenylalanine cyanomethyl ester **7.9** as white crystals (0.0166 g, 0.0352 mmol, 21% yield). ^{1}H NMR (300 MHz, d_6-DMSO, 298 K) δ 7.69 (1H, s), 7.11 (1H, s), 6.84 (3H, s), 5.33 (2H, m), 5.00 (2H, s), 4.33 (1H, m), 3.86 (3H, s), 3.85 (3H, s), 2.92 (2H, m), 2.20 (6H, s).

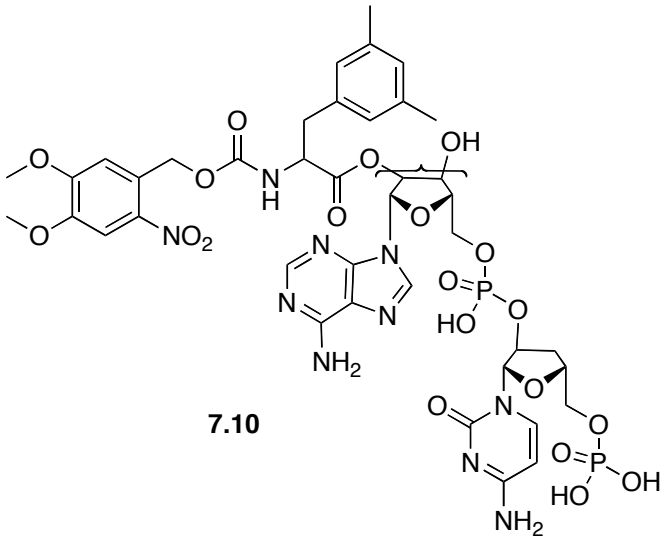

7.10

NVOC-dimethylphenylalanine-dCA **7.10**: NVOC-dimethylphenylalanine cyanomethyl ester **7.9** (0.011 g, 0.025 mmol, 3 eq) was added to a round-bottom flask under Ar (g) and dissolved in DMF (0.5 mL). This solution was transferred to another round-bottom flask under Ar (g), which contained dCA (0.010 g, 0.0085 mmol, 1 eq) as a tetrabutylammonium salt (2.4 eq). The reaction was stirred at room temperature for 18 hours while being monitored by reverse-phase analytical HPLC with a linear solvent gradient from 5% acetonitrile in 25 mM NH_4OAc buffer pH 4.5 to 100% acetonitrile. The crude product was purified using reverse-phase semipreparative HPLC with the same linear solvent gradient. The fractions containing the NVOC-dimethylphenylalanine-dCA **7.10** were combined, and the solvent was removed by lyophilization. The solid was redissolved in 10 mM acetic acid and reconcentrated via lyophilization (3×) to afford NVOC-dimethylphenylalanine-dCA **7.10** as a white powder (0.0019 g, 0.0020 mmol, 25% yield). ESI-MS *m/z* calc'd for $C_{40}H_{48}N_{10}O_{20}P_2$ [M−H]: 1049.3; found: 1049.4.

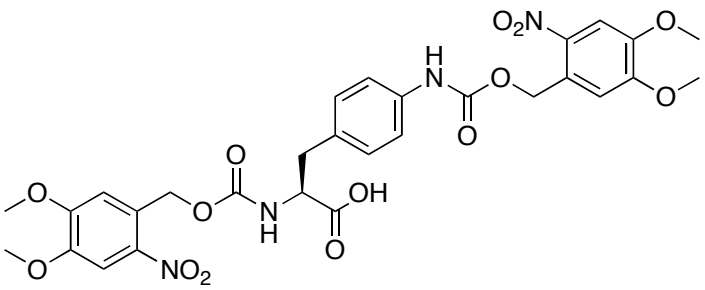

7.11

Di-NVOC-4-amino-phenylalanine **7.11**: L-4-Amino-phenylalanine (0.65 g, 3.6 mmol, 1 eq) was added to a round-bottom flask and dissolved in 10% (w/v) sodium carbonate in H_2O (28 mL). To this solution was added dioxane (28 mL) at 4 °C, followed by the slow addition of nitroveratryloxycarbonyl chloride (2.0 g, 7.6 mmol, 2.1 eq). The mixture was allowed to warm to room temperature while stirring for 18 hours. The mixture was then poured into distilled H_2O (200 mL) and ether (50 mL), and the solid precipitate was filtered to afford di-NVOC-4-amino-phenylalanine **7.11** as a solid (1.80 g, 2.7 mmol, 76% yield). R_f = 0.56 (1% AcOH in EtOAc); ^{1}H NMR (300 MHz, d_6DMSO, 298 K) δ 9.9 (1H, b), 7.7 (1H, s), 7.6 (1H, s), 7.3-7.0 (6H, m), 6.8 (1H, d), 5.4 (4H, s), 5.2 (1H, d), 3.9 (12H, m), 3.1-2.7 (2H, m); ESI-MS *m/z* calc'd for $C_{29}H_{30}N_4O_{14}$ [M−H]: 657.2; found: 656.8.

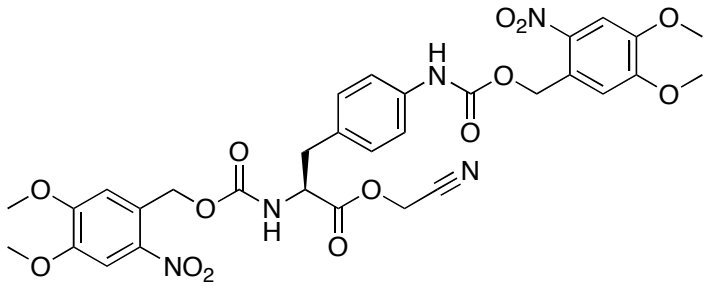

7.12

Di-NVOC-4-amino-phenylalanine cyanomethyl ester **7.12**: The procedure described above for **7.9** was repeated using di-NVOC-4-amino-phenylalanine **7.11** (0.41 g, 0.63 mmol) as the starting material. The reaction was stirred at room temperature for 75 minutes, and then a small amount of H_2O was added to the flask. The resulting precipitate was filtered to afford di-NVOC-4-amino-phenylalanine cyanomethyl ester **7.12** (0.19 g, 0.20 mmol, 44% yield). R_f = 0.91 (17% EtOAc in CH_2Cl_2); ^{1}H NMR (300 MHz, d_6DMSO, 298 K) δ 9.9 (1H, b), 8.2 (1H, d), 7.72 (1H, s), 7.69 (1H, s), 7.4-7.1 (6H, m), 5.44 (2H, s), 5.3 (2H, d), 5.01 (2H, s), 4.4 (1H, m), 3.90 (3H, s), 3.87 (3H, s), 3.85 (3H, s), 3.84 (3H, s), 3.1-2.8 (2H, m); ESI-MS *m/z* calc'd for $C_{31}H_{31}N_5O_{14}$ [M+K]: 736.3; found: 736.0.

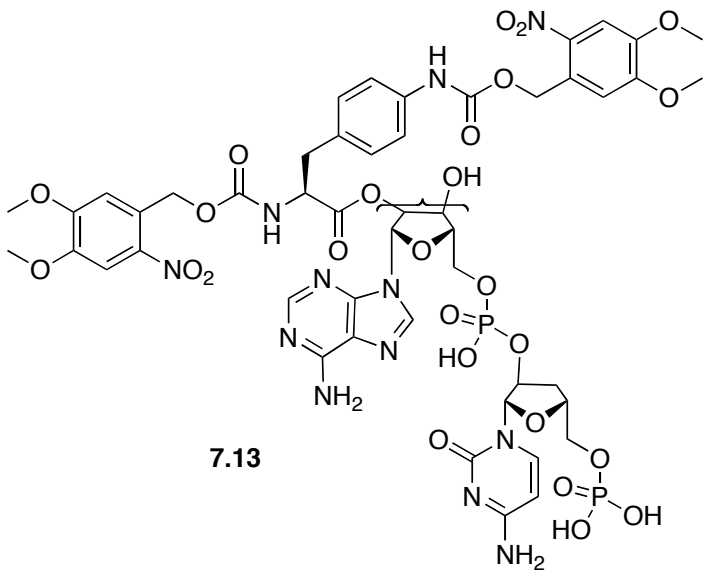

7.13

Di-NVOC-4-amino-phenylalanine-dCA **7.13**: The procedure described above for **7.10** was repeated using di-NVOC-4-amino-phenylalanine cyanomethyl ester **7.12** (0.017 g, 0.025 mmol, 3 eq) as the starting material, except that the reaction was only stirred at room temperature for 1 hour, to afford di-NVOC-4-amino-phenylalanine-dCA **7.13** as a white powder (0.00052 g, 0.00041 mmol, 5% yield). ESI-MS *m/z* calc'd for $C_{48}H_{54}N_{12}O_{26}P_2$ [M−H]: 1275.3; found: 1275.4.

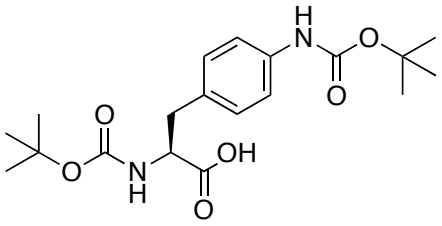

7.14

Di-*t*Boc-4-amino-phenylalanine **7.14**: N_α-(*tert*-Butoxycarbonyl)-4-amino-phenylalanine (1.0 g, 3.5 mmol, 1 eq) was placed in a round-bottom flask and dissolved in dioxane (15 mL) and 4% $NaHCO_3$ (aq) (15 mL) at 4 °C. To this solution was added di-*tert*-

butyldicarbonate (1.2 mL, 7.0 mmol, 1.5 eq). The opaque white reaction was stirred at 4 °C for 2 hours, and then it was allowed to come to room temperature, at which point the reaction turned opaque orange, and stirred for another 20 hours. At the end of the reaction, the orange solution had become clear. The solvent was removed under vacuum, and then the crude product was resuspended in 5% $KHSO_4$ (aq), extracted with EtOAc, washed with brine, dried over $MgSO_4$ (s), and concentrated to afford di-*t*Boc-4-amino-phenylalanine **7.14** as a pale yellow solid (1.3 g, 3.5 mmol, 97%). R_f = 0.25 (100% EtOAc); ^{1}H NMR (300 MHz, CD_3OD, 298 K) δ 8.71 (1H, b), 7.19 (2H, d, *J* = 8.4 Hz), 7.01 (2H, d, *J* = 8.7 Hz), 4.19 (1H, m), 2.98 (1H, dd, *J* = 14.1, 5.1 Hz), 2.74 (1H, dd, *J* = 14.0, 9.0 Hz), 1.40 (9H, s), 1.28 (9H, s); ESI-MS *m/z* calc'd for $C_{19}H_{28}N_2O_6$ [M−H]: 379.2; found: 379.1.

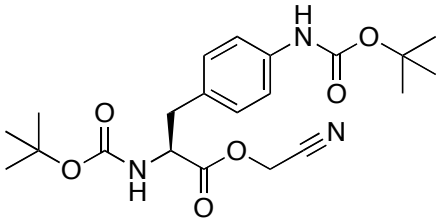

7.15

Di-*t*Boc-4-amino-phenylalanine cyanomethyl ester **7.15**: The procedure described above for **7.9** was repeated using di-*t*Boc-4-amino-phenylalanine **7.14** (0.25 g, 0.66 mmol) as the starting material. The crude product was purified by flash column chromatography (CH_2Cl_2, then 5% EtOAc in CH_2Cl_2 once the yellow product started eluting) to afford di-*t*Boc-4-amino-phenylalanine cyanomethyl ester **7.15** (0.20 g, 0.47 mmol, 78% yield). R_f = 0.82 (17% EtOAc in CH_2Cl_2); ^{1}H NMR (300 MHz, $CDCl_3$, 298 K) δ 7.3-6.8 (4H, m),

6.47 (1H, b), 4.70 (2H, m), 4.6 (1H, m), 3.05 (2H, d, J = 7.2 Hz), 1.51 (9H, s), 1.42 (9H, s); ESI-MS *m/z* calc'd for $C_{21}H_{29}N_3O_6$ [M+Cl]: 454.7; found: 454.1.

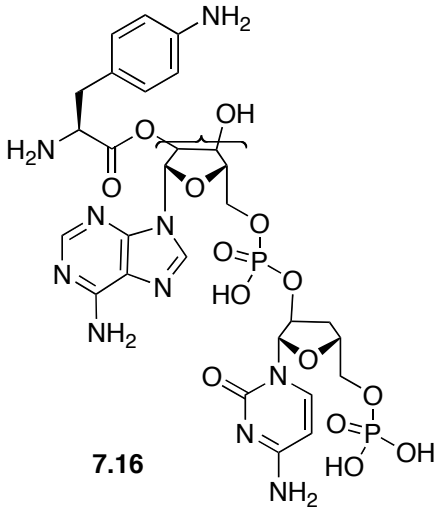

7.16

4-Amino-phenylalanine-dCA **7.16**: The procedure described above for **7.10** was repeated using di-*t*Boc-4-amino-phenylalanine cyanomethyl ester **7.15** (0.011 g, 0.025 mmol, 3 eq) as the starting material, except that the reaction was allowed to stir for 48 hours before purification by HPLC. The HPLC fractions containing the di-*t*Boc-4-amino-phenylalanine-dCA were combined, the solvent was removed by lyophilization, and the solid was redissolved in trifluoroacetic acid (0.10 mL) at 4 °C. After 20 minutes the solvent was removed by bubbling Ar through the solution to afford 4-amino-phenylalanine-dCA **7.16** as a white powder (0.00018 g, 0.00027 mmol, 3% yield). ESI-MS *m/z* calc'd for $C_{28}H_{36}N_{10}O_{14}P_2$ [M+H]: 799.2; found: 800.5.

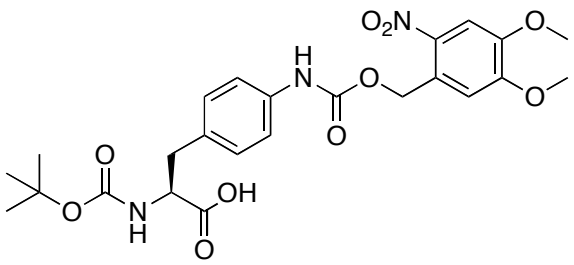

7.17

N_α-*t*Boc-4-amino(NVOC)-phenylalanine **7.17**: The procedure described above for **7.8** was repeated using N_α-(*tert*-Butoxycarbonyl)-4-amino-phenylalanine (1.0 g, 3.6 mmol, 1 eq) to afford N_a-*t*Boc-4-amino(NVOC)-phenylalanine **7.17** (0.48 g, 0.9 mmol, 26% yield). ^{1}H NMR (300 MHz, CD_3OD, 298 K) δ 7.77 (1H, s), 7.38 (2H, m), 7.25 (1H, s), 7.16 (2H, d, J = 8.4 Hz), 5.54 (2H, s), 4.30 (1H, m), 3.91 (3H, s), 3.88 (3H, s), 3.11 (1H, dd, J = 14.0, 5.1 Hz), 2.86 (1H, dd, J = 13.8, 9 Hz). 1.38 (9H, s).

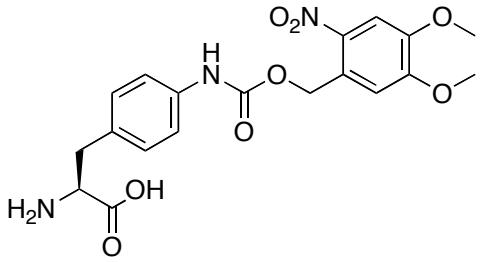

7.18

4-Amino(NVOC)-phenylalanine **7.18**: N_α-*t*Boc-4-amino(NVOC)-phenylalanine **7.17** (0.48 g, 0.9 mmol) was placed in a round-bottom flask under Ar (g) and dissolved in trifluoroacetic acid (16 mL) at 0 °C. After 30 minutes the solvent was removed under vacuum to afford 4-amino(NVOC)-phenylalanine **7.18**. ^{1}H NMR (300 MHz, CD_3OD, 298 K) δ 7.76 (1H, s), 7.47 (2H, d, J = 8.7 Hz), 7.24 (2H, d, J = 2.7 Hz), 7.21 (1H, s),

5.54 (2H, s), 4.21 (1H,dd, *J* = 7.5, 5.1 Hz), 3.95 (3H, s), 3.91 (3H, s), 3.25 (1H, m), 3.11 (1H, m).

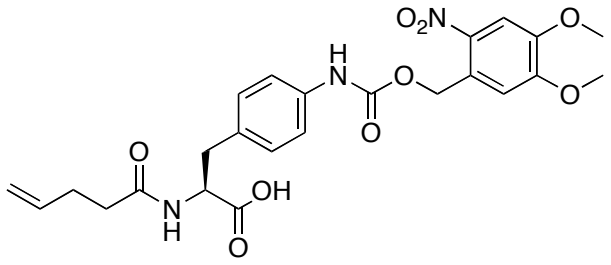

7.19

N_α-4PO-4-amino(NVOC)-phenylalanine **7.19**: 4-Amino(NVOC)-phenylalanine **7.18** (0.38 g, 0.90 mmol, 1 eq) and *N*,*N*-diisopropylethylamine (0.18 mL, 1.1 mmol, 1.2 eq) were placed in a round-bottom flask and dissolved in THF (8.7 mL) and H_2O (8.7 mL). To this solution was added 4-pentenoic anhydride (0.20 mL, 1.1 mmol, 1.2 eq). The reaction was allowed to stir for 18 hours. The THF was then removed under vacuum, and the aqueous solution was washed with EtOAc (3×). The pH of the resulting aqueous solution was lowered to 2 with 6 N HCl and extracted with EtOAc (3×) to afford N_α-4PO-4-amino(NVOC)-phenylalanine **7.19** (0.41 g, 0.81 mmol, 90% yield). ^{1}H NMR (300 MHz, CD_3OD, 298 K) δ 7.77 (1H, s), 7.37 (2H, d, *J* = 8.7 Hz), 7.25 (1H, s), 7.16 (2H, d, *J* = 8.4 Hz), 5.70 (1H, m), 4.97 (2H, d, *J* = 12.6 Hz), 4.93 (2H, s), 4.63 (1H, dd, *J* = 9.2, 5.4 Hz), 3.94 (3H, s), 3.91 (3H, s), 3.16 (1H, dd, *J* = 14.0, 4.8 Hz), 2.89 (1H, dd, *J* = 14.1, 9.3 Hz), 2.24 (4H, m); ESI-MS *m/z* calc'd for $C_{24}H_{27}N_3O_9$ [M+Na]: 524.2; found: 523.9.

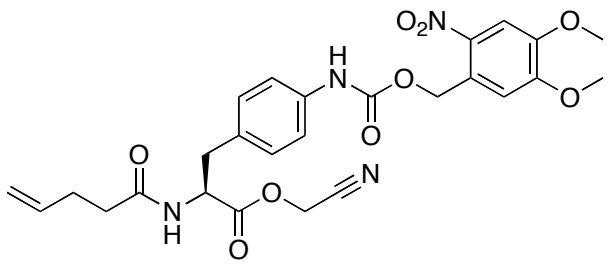

7.20

N_α-4PO-4-amino(NVOC)-phenylalanine cyanomethyl ester **7.20**: The procedure described above for **7.9** was repeated using N_α-4PO-4-amino(NVOC)-phenylalanine **7.19** (0.16 g, 0.32 mmol) as the starting material. The crude product was purified by flash column chromatography (CH_2Cl_2, then 50% EtOAc in CH_2Cl_2 once the yellow product started eluting) to afford N_α-4PO-4-amino(NVOC)-phenylalanine cyanomethyl ester **7.20** (0.091 g, 0.17 mmol, 54% yield). R_f = 0.20 (17% EtOAc in CH_2Cl_2); ^{1}H NMR (300 MHz, CD_3CN, 298 K) δ 8.01 (1H, s), 7.74 (1H, s), 7.41 (2H, d, J = 8.7 Hz), 7.20 (3H, m), 6.75 (1H, d, J = 7.8 Hz), 5.78 (1H, m), 5.52 (2H, s), 5.00 (2H, m), 4.79 (2H, s), 4.67 (1H, m), 3.96 (3H, s), 3.91 (3H, s), 3.03 (2H, m), 2.25 (2H, m), 1.97 (2H, m); ESI-MS *m/z* calc'd for $C_{26}H_{28}N_4O_9$ [M+Na]: 563.2; found: 563.1.

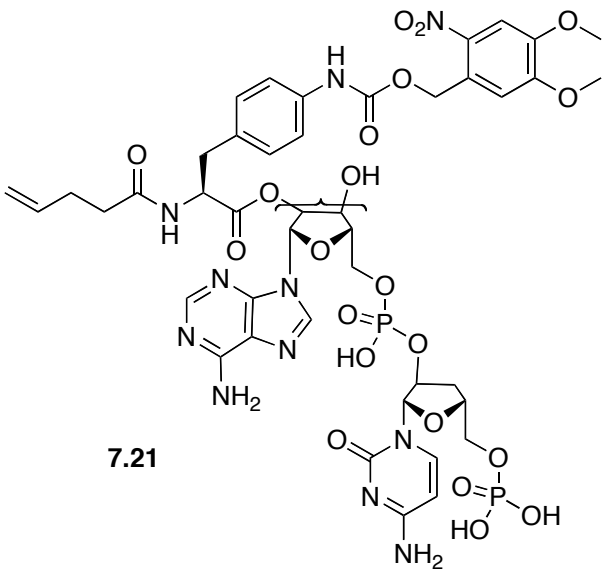

7.21

N_α-4PO-4-amino(NVOC)-phenylalanine-dCA **7.21**: The procedure described above for **7.10** was repeated using N_α-4PO-4-amino(NVOC)-phenylalanine **7.19** (0.017 g, 0.025 mmol, 3 eq) as the starting material, except that the reaction was allowed to stir for 6 hours, to afford N_α-4PO-4-amino(NVOC)-phenylalanine-dCA **7.21** (0.00071 g, 0.00064 mmol, 8% yield). MALDI-MS *m/z* calc'd for $C_{43}H_{51}N_{11}O_{21}P_2$ [M+H]: 1120.3; found: 1120.5

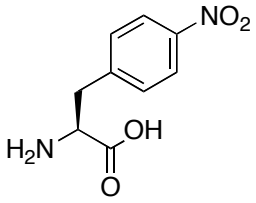

7.22

4-Nitro-phenylalanine **7.22**: The procedure described above for **7.18** was repeated using *t*Boc-4-nitro-phenylalanine (0.31 g, 1.0 mmol) as the starting material to afford 4-nitro-phenylalanine **7.22** (0.21 g, 1.0 mmol, 100% yield). ^{1}H NMR (300 MHz, D_2O, 298 K) δ

8.10 (2H, d, *J* = 2.1 Hz), 7.41 (2H, d, *J* = 8.7 Hz), 4.27 (1H, dd, *J* = 7.7, 6.3 Hz), 3.33 (1H, dd, *J* = 14.6, 6.0 Hz), 3.22 (1H, dd, *J* = 14.6, 7.8 Hz).

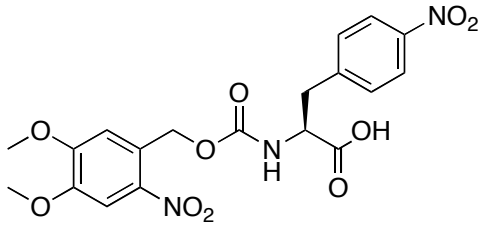

7.23

NVOC-4-nitro-phenylalanine **7.23**: The procedure described above for **7.8** was repeated using 4-nitro-phenylalanine **7.22** (0.21 g, 1.0 mmol, 1 eq) as the starting material. After stirring for 4 hours, the mixture was poured into distilled H_2O (200 mL) and washed with ether (3×). Under vigorous stirring, the aqueous solution was adjusted to pH 2 by slowly adding 6 N HCl. Once a white precipitate began to form in the yellow solution, the mixture was refrigerated overnight to encourage the formation of more solid. The subsequent day the precipitate was filtered to afford NVOC-4-nitro-phenylalanine **7.23** as a solid (0.34 g, 0.75 mmol, 75% yield). ^{1}H NMR (300 MHz, d_6DMSO, 298 K) δ 8.13 (2H, d, *J* = 8.7 Hz), 7.93 (1H, d, *J* = 8.4 Hz), 7.68 (1H, s), 7.54 (2H, d, *J* = 8.7 Hz), 7.09 (1H, s), 5.30 (2H, q, *J* = 15 Hz), 4.27 (1H, m), 3.86 (6H, s), 3.25 (1H, m), 3.01 (1H, dd, *J* = 14.1, 10.5 Hz).

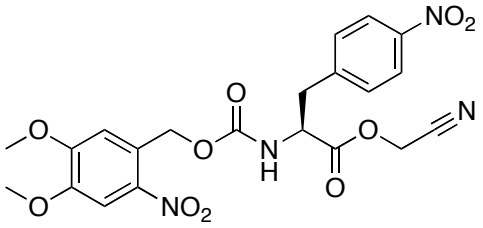

7.24

NVOC-4-nitro-phenylalanine cyanomethyl ester **7.24**: The procedure described above for **7.9** was repeated using NVOC-4-nitro-phenylalanine **7.23** (0.28 g, 0.63 mmol) as the starting material. The crude product was purified by flash column chromatography (CH_2Cl_2, then 5% EtOAc in CH_2Cl_2 once the yellow product started eluting) to afford NVOC-4-nitro-phenylalanine cyanomethyl ester **7.24**. ^{1}H NMR (300 MHz, d_6DMSO, 298 K) δ 8.20 (2H, d, *J* = 8.1 Hz), 8.12 (2H, d, *J* = 8.4 Hz), 7.67 (1H, s), 7.54 (2H, d, *J* = 8.7 Hz), 7.08 (1H, s), 5.29 (2H, d, *J* = 6.0 Hz), 5.02 (2H, s), 4.51 (1H, m), 3.85 (3H, s), 3.84 (3H, s), 3.24 (1H, dd, *J* = 13.8, 5.4 Hz), 3.07 (1H, dd, *J* = 13.8, 10.5 Hz).

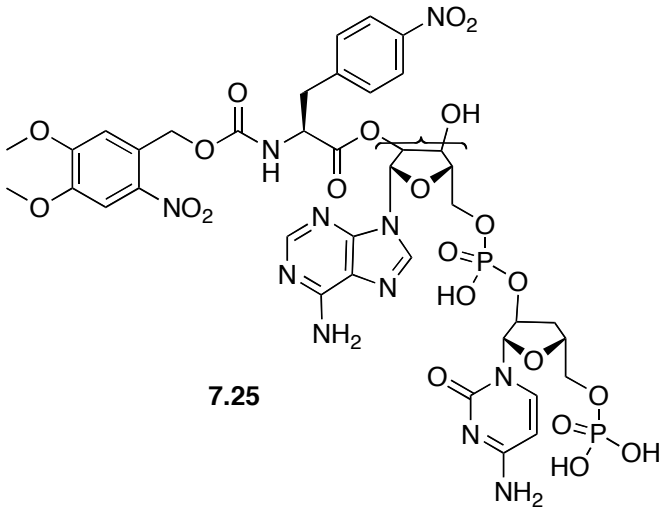

7.25

NVOC-4-nitro-phenylalanine-dCA **7.25**: The procedure described above for **7.10** was repeated using NVOC-4-nitro-phenylalanine cyanomethyl ester **7.24** (0.020 g, 0.040

mmol, 5 eq) as the starting material, except that the reaction was stirred for 24 hours, to afford NVOC-4-nitro-phenylalanine **7.25**. MALDI-MS *m/z* calc'd for $C_{38}H_{43}N_{11}O_{22}P_2$ [M+H]: 1068.2; found: 1068.3.

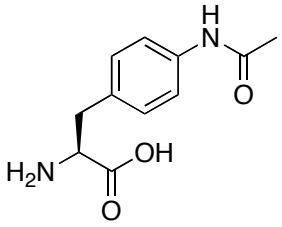

7.26

4-Acetamido-phenylalanine **7.26**: *N*-FMOC-4-acetamido-phenylalanine (0.25 g, 0.56 mmol) was placed in a round-bottom flask under Ar (g) and dissolved in 20% piperidine in DMF (10 mL). The reaction was stirred for 30 minutes, and then the solvent was removed under vacuum to afford 4-acetamido-phenylalanine **7.26**. ^{1}H NMR (300 MHz, d_6DMSO, 298 K) δ 9.87 (1H, s), 7.45 (2H, d, *J* = 8.4 Hz), 7.14 (2H, d, *J* = 8.4 Hz), 4.09 (1H, t, *J* = 8.4 Hz), 3.06 (1H, dd, *J* = 14.6, 3.9 Hz), 2.75 (1H, dd, *J* = 14.4, 8.1 Hz); ESI-MS *m/z* calc'd for $C_{11}H_{14}N_2O_3$ [M+H]: 223.1; found: 223.2.

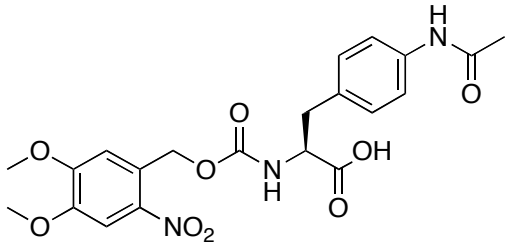

7.27

NVOC-4-acetamido-phenylalanine **7.27**: The procedure described above for **7.8** was repeated using 4-acetamido-phenylalanine **7.26** (0.080 g, 0.36 mmol, 1 eq) as the starting material to afford NVOC-4-acetamido-phenylalanine **7.27** (0.073 g, 0.16 mmol, 44%

yield). ^{1}H NMR (300 MHz, CD_3OD, 298 K) δ 7.74 (1H, s), 7.44 (2H, d, J = 8.7 Hz), 7.20 (2H, d, J = 9.0 Hz), 5.42 (2H, m), 4.6 (2H, m), 4.4 (1H, m), 3.90 (3H, s), 3.86 (3H, s), 3.2-2.8 (2H, m), 2.01 (3H, s); ESI-MS *m/z* calc'd for $C_{21}H_{23}N_3O_9$ [M+Na]: 484.1; found: 484.1.

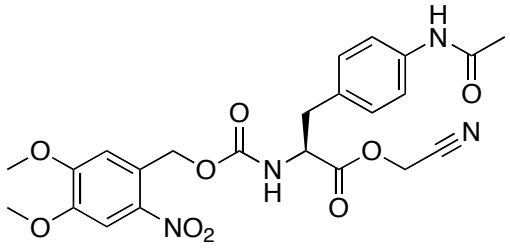

7.28

NVOC-4-acetamido-phenylalanine cyanomethyl ester **7.28**: The procedure described above for **7.9** was repeated using NVOC-4-acetamido-phenylalanine **7.27** (0.073 g, 0.16 mmol) as the starting material. The crude product was purified by flash column chromatography (CH_2Cl_2, then 40% EtOAc in CH_2Cl_2 once the yellow product started eluting) to afford NVOC-4-acetamido-phenylalanine cyanomethyl ester **7.28** (0.050 g, 0.10 mmol, 63% yield). ESI-MS *m/z* calc'd for $C_{23}H_{24}N_4O_9$ [M+Cl]: 535.6; found: 535.1.

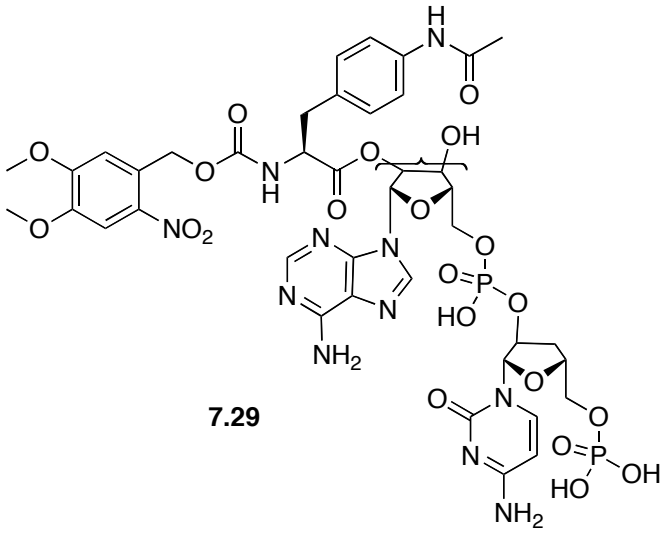

7.29

NVOC-4-acetamido-phenylalanine-dCA **7.29**: The procedure described above for **7.10** was repeated using NVOC-4-acetamido-phenylalanine cyanomethyl ester **7.28** (0.020 g, 0.040 mmol, 5 eq) as the starting material, except that the reaction was allowed to stir for 24 hours, to afford NVOC-4-acetamido-phenylalanine-dCA **7.29** (0.00016 g, 0.0015 mmol, 2% yield). MALDI-MS *m/z* calc'd for $C_{40}H_{47}N_{11}O_{21}P_2$ [M+H]: 1080.2; found: 1080.3.

Nonsense Suppression In Vivo

The site-directed mutagenesis of TAG mutants, gene construction, synthesis of suppressor tRNA, and ligation of aminoacyl-tRNA to tRNA have been described previously.[46-49] Plasmid DNAs were linearized with Not1, and mRNA was transcribed using the T7 mMESSAGE mMACHINE kit (Ambion, Austin, TX).

Oocytes from *Xenopus laevis* were isolated and maintained at 18 °C in ND96 solution (96 mM sodium chloride, 2 mM potassium chloride, 1.8 mM calcium chloride, 1 mM

magnesium chloride, 5 mM HEPES, 2.5 mM sodium pyruvate, 0.5 mM theophyline, 10 μg/mL gentamycin at pH 7.5) according to published procedures.[50] Each oocyte was microinjected with 50 nL of a 1:1 mixture of mRNA (0.04 ng/nL for ShB and $GABA_C$, 0.5 ng/nL of a 20:1:1:1 α:β:γ:δ for nAChR) and tRNA (1 μg/μL).

NVOC-protected aminoacylated tRNA was deprotected prior to injection by irradiating the sample for either 5 or 10 minutes with a 1000 W Hg/Xe arc lamp (Oriel, Irvine, CA) operating at 400 W equipped with WG-335 and UG-11 filters (Schott, Duryea, PA).[51] In certain cases noted in the text, hydroxylamine hydrochloride (0.029 M solution in H_2O, 0.2× volume of tRNA solution) was added to the tRNA solution prior to photolysis.

4PO-protected aminoacylated tRNA was deprotected prior to injection by incubating the sample for 15 minutes in saturated I_2 (aq). This saturated I_2 solution was made by adding an excess of I_2 to H_2O, then sonicating the mixture for 5 minutes, and then heating the mixture to 60 °C for 5 minutes.

Electrophysiology

The work in the 3,5-dimethylphenylalanine section was a collaborative effort that included important contributions from Dr. Christopher Ahern. Representative methods for the electrophysiological studies discussed in this section that were not performed by the author can be found in Ahern *et al.*[13] and Ahern *et al.*[18]

Electrophysiological recordings on ShB were carried out 24 hours after injection. Whole-cell currents from oocytes were measured using an OpusXpress and pCLAMP

software (Axon Instruments, Foster City, CA) in the two-electrode voltage-clamp configuration. Microelectrodes were filled with 3 M potassium chloride and had resistances ranging from 0.5 to 1.5 MΩ. Oocytes were continuously perfused with a nominally calcium-free bath solution consisting of 96 mM sodium chloride, 2 mM potassium chloride, 1 mM magnesium chloride, and 5 mM HEPES at pH 7.5. The current from ShB expressing oocytes was measured during a depolarizing jump from the holding potential to +70 mV. Varying concentrations of TEA were applied, and then the depolarizing jump was repeated. The amount of current blocked by TEA was taken as the difference between the first and the second depolarizing jump. As noted in the text, some of the recordings were interrupted to bathe the oocytes in a solution of either 100 mM sodium dithionite in 100 mM phosphate buffer pH 7.4 or 24 mM sodium dithionite in 50 mM phosphate buffer pH 7.4 for varying amounts of time.

Electrophysiological recordings on $GABA_C$ were carried out 48 to 72 hours after injection. Whole-cell currents from oocytes were measured as above. Microelectrodes were also as above. Oocytes were continuously perfused with a bath solution consisting of 96 mM sodium chloride, 2 mM potassium chloride, 1 mM magnesium chloride, 1.8 mM calcium chloride, and 5 mM HEPES at pH 7.5. Microscopic GABA-induced currents were recorded in response to bath application of GABA at a holding potential of −80 mV.

Electrophysiological recordings on nAChR were carried out 48 hours after injection. Whole-cell currents from oocytes were measured as above. Microelectrodes were also as above. Oocytes were continuously perfused with a nominally calcium-free bath solution consisting of 96 mM sodium chloride, 2 mM potassium chloride, 1 mM magnesium

chloride, and 5 mM HEPES at pH 7.5. Microscopic ACh-induced currents were recorded in response to bath application of ACh at a holding potential of −80 mV.

Analyzing the Extent of NVOC Deprotection and 4-Nitro-Phenylalanine Conversion

Di-NVOC-4-amino-phenylalanine-dCA (3 mM solution in DMSO, 3 μL) was placed in front of the 1000 W Hg/Xe arc lamp described above and irradiated for varying amounts of time. The sample was then analyzed by reverse-phase analytical HPLC with a linear solvent gradient from 5% acetonitrile in 25 mM NH_4OAc buffer pH 4.5 to 100% acetonitrile. An unphotolyzed sample was used as the control.

*t*Boc-4-nitro-phenylalanine (0.0059 g, 0.021 mmol) was dissolved in DMSO (50 μL) and analyzed by reverse-phase analytical HPLC with a linear solvent gradient from 5% acetonitrile in 25 mM NH_4OAc buffer pH 4.5 to 100% acetonitrile. To this solution was added sodium dithionite (100 mM in 100 mM phosphate buffer pH 7.4, 50 μL), and the reaction was allowed to sit for varying amounts of time before it was analyzed again by reverse-phase analytical HPLC with the same linear solvent gradient as above. This procedure was repeated for *t*Boc-4-amino-phenylalanine (0.0049 g, 0.017 mmol).

Nonsense Suppression In Vitro

Translation was carried out using rabbit reticulocyte lysate translation system (Promega, Madison, WI) according to manufacturer's protocol. Lysate mix (8.75 μL), amino acid

mix (0.35 μL), RNAse inhibitor (0.25 μL), H_2O (1.75 μL), mRNA (0.5 μL, 1 μg/μL for suppression experiments and 0.3 μg/μL for wild-type experiments), and either tRNA (1 μL, 1 μg/μL) or H_2O (1 μL, for mRNA-only negative control) were combined and incubated at 30 °C for 106 minutes. The *in vitro* translation mix was then kept at −80 °C until further use.

To prepare for gel loading, the *in vitro* translation mix (2.5 μL) was added to 4% sodium dodecyl sulfate (SDS) (2.5 μL) and then that mixture was added to 10% SDS (2 μL), H_2O (7 μL), and 2× SDS loading buffer (100 mM tris chloride at pH 6.8, 4% SDS, 0.2% bromophenol blue, 20% glycerol) (14 μL). Samples were loaded in 5 μL aliquots into prepoured 12% tris chloride gels (Bio-Rad, Hercules, CA) for SDS-polyacrylamide gel electrophoresis (PAGE). Western blotting was preformed using nitrocellulose transfer, a mouse anti-HA primary antibody, and a goat anti-mouse secondary antibody conjugated to horseradish-peroxidase. Protein was detected by chemiluminescence.

References

(1) Mannuzzu, L. M.; Moronne, M. M.; Isacoff, E. Y. *Science* **1996**, *271*, 213-6.

(2) Cha, A.; Bezanilla, F. *Neuron* **1997**, *19*, 1127-40.

(3) Li, M.; Farley, R. A.; Lester, H. A. *J. Gen. Physiol.* **2000**, *115*, 491-508.

(4) Chang, Y.; Weiss, D. S. *Nat. Neurosci.* **2002**, *5*, 1163-8.

(5) Dahan, D. S.; Dibas, M. I.; Petersson, E. J.; Auyeung, V. C.; Chanda, B.; Bezanilla, F.; Dougherty, D. A.; Lester, H. A. *Proc. Natl. Acad. Sci. USA* **2004**, *101*, 10195-200.

(6) Muroi, Y.; Czajkowski, C.; Jackson, M. B. *Biochemistry* **2006**, *45*, 7013-22.

(7) Pless, S. A.; Dibas, M. I.; Lester, H. A.; Lynch, J. W. *J. Biol. Chem.* **2007**, *282*, 36057-67.

(8) Nashmi, R.; Dickinson, M. E.; McKinney, S.; Jareb, M.; Labarca, C.; Fraser, S. E.; Lester, H. A. *J. Neurosci.* **2003**, *23*, 11554-67.

(9) Drenan, R. M.; Nashmi, R.; Imoukhuede, P.; Just, H.; McKinney, S.; Lester, H. A. *Mol. Pharmacol.* **2008**, *73*, 27-41.

(10) Struck, D. K.; Hoekstra, D.; Pagano, R. E. *Biochemistry* **1981**, *20*, 4093-9.

(11) http://probes.invitrogen.com/handbook/sections/0105.html.

(12) Gruber, H. J.; Kada, G.; Pragl, B.; Riener, C.; Hahn, C. D.; Harms, G. S.; Ahrer, W.; Dax, T. G.; Hohenthanner, K.; Knaus, H. G. *Bioconjug. Chem.* **2000**, *11*, 161-6.

(13) Ahern, C. A.; Eastwood, A. L.; Lester, H. A.; Dougherty, D. A.; Horn, R. *J. Gen. Physiol.* **2006**, *128*, 649-57.

(14) Heginbotham, L.; MacKinnon, R. *Neuron* **1992**, *8*, 483-91.

(15) Lenaeus, M. J.; Vamvouka, M.; Focia, P. J.; Gross, A. *Nat. Struct. Mol. Biol.* **2005**, *12*, 454-9.

(16) Herr, R. R.; Enkoji, T.; Dailey, J. P. *J. Am. Chem. Soc.* **1957**, *79*, 4229-4232.

(17) Vossmeyer, T.; Jia, S.; Delonno, E.; Diehl, M. R.; Kim, S. H.; Peng, X.; Alivisatos, A. P.; Heath, J. R. *J. Appl. Phys.* **1998**, *84*, 3664-3670.

(18) Ahern, C. A.; Eastwood, A. L.; Dougherty, D. A.; Horn, R. *Circ. Res.* **2008**, *102*, 86-94.

(19) Ma, J. C.; Dougherty, D. A. *Chem. Rev.* **1997**, *97*, 1303-1324.

(20) Santarelli, V. P.; Eastwood, A. L.; Dougherty, D. A.; Horn, R.; Ahern, C. A. *J. Biol. Chem.* **2007**, *282*, 8044-51.

(21) Santarelli, V. P.; Eastwood, A. L.; Dougherty, D. A.; Ahern, C. A.; Horn, R. *Biophys. J.* **2007**, *93*, 2341-9.

(22) Zhong, W.; Gallivan, J. P.; Zhang, Y.; Li, L.; Lester, H. A.; Dougherty, D. A. *Proc. Natl. Acad. Sci. USA* **1998**, *95*, 12088-93.

(23) Lummis, S. C.; D, L. B.; Harrison, N. J.; Lester, H. A.; Dougherty, D. A. *Chem. Biol.* **2005**, *12*, 993-7.

(24) Mecozzi, S.; West, A. P., Jr.; Dougherty, D. A. *J. Am. Chem. Soc.* **1996**, *118*, 2307-2308.

(25) Cashin, A. L.; Torrice, M. M.; McMenimen, K. A.; Lester, H. A.; Dougherty, D. A. *Biochemistry* **2007**, *46*, 630-9.

(26) Rubini, M.; Lepthien, S.; Golbik, R.; Budisa, N. *Biochim. Biophys. Acta* **2006**, *1764*, 1147-58.

(27) Nowak, M. W.; Kearney, P. C.; Sampson, J. R.; Saks, M. E.; Labarca, C. G.; Silverman, S. K.; Zhong, W.; Thorson, J.; Abelson, J. N.; Davidson, N.; et al. *Science* **1995**, *268*, 439-42.

(28) Mehl, R. A.; Anderson, J. C.; Santoro, S. W.; Wang, L.; Martin, A. B.; King, D. S.; Horn, D. M.; Schultz, P. G. *J. Am. Chem. Soc.* **2003**, *125*, 935-9.

(29) Doyle, D. A.; Morais Cabral, J.; Pfuetzner, R. A.; Kuo, A.; Gulbis, J. M.; Cohen, S. L.; Chait, B. T.; MacKinnon, R. *Science* **1998**, *280*, 69-77.

(30) Cordero-Morales, J. F.; Cuello, L. G.; Zhao, Y.; Jogini, V.; Cortes, D. M.; Roux, B.; Perozo, E. *Nat. Struct. Mol. Biol.* **2006**, *13*, 311-8.

(31) Yu, L.; Sun, C.; Song, D.; Shen, J.; Xu, N.; Gunasekera, A.; Hajduk, P. J.; Olejniczak, E. T. *Biochemistry* **2005**, *44*, 15834-41.

(32) Zhou, Y.; MacKinnon, R. *J. Mol. Biol.* **2003**, *333*, 965-75.

(33) Zhou, Y.; Morais-Cabral, J. H.; Kaufman, A.; MacKinnon, R. *Nature* **2001**, *414*, 43-8.

(34) Mecozzi, S.; West, A. P., Jr.; Dougherty, D. A. *Proc. Natl. Acad. Sci. USA* **1996**, *93*, 10566-71.

(35) Cashin, A. L.; Petersson, E. J.; Lester, H. A.; Dougherty, D. A. *J. Am. Chem. Soc.* **2005**, *127*, 350-6.

(36) Hohsaka, T.; Kajihara, D.; Ashizuka, Y.; Murakami, H.; Sisido, M. *J. Am. Chem. Soc.* **1999**, *121*, 34-40.

(37) England, P. M.; Lester, H. A.; Dougherty, D. A. *Tet. Lett.* **1999**, *40*, 6189-6192.

(38) Miller, J. C.; Silverman, S. K.; England, P. M.; Dougherty, D. A.; Lester, H. A. *Neuron* **1998**, *20*, 619-24.

(39) Tong, Y.; Brandt, G. S.; Li, M.; Shapovalov, G.; Slimko, E.; Karschin, A.; Dougherty, D. A.; Lester, H. A. *J. Gen. Physiol.* **2001**, *117*, 103-18.

(40) Philipson, K. D.; Gallivan, J. P.; Brandt, G. S.; Dougherty, D. A.; Lester, H. A. *Am. J. Physiol. Cell. Physiol*. **2001**, *281*, C195-206.

(41) England, P. M.; Lester, H. A.; Davidson, N.; Dougherty, D. A. *Proc. Natl. Acad. Sci. USA* **1997**, *94*, 11025-30.

(42) Angeletti, C.; Nichols, J. W. *Biochemistry* **1998**, *37*, 15114-9.

(43) Padgett, C. L.; Hanek, A. P.; Lester, H. A.; Dougherty, D. A.; Lummis, S. C. *J. Neurosci.* **2007**, *27*, 886-92.

(44) Hooker, J. M.; Esser-Kahn, A. P.; Francis, M. B. *J. Am. Chem. Soc.* **2006**, *128*, 15558-9.

(45) Pangborn, A. B.; Giardell, M. A.; Grubbs, R. H.; Rosen, R. K.; Timmers, F. J. *Organometallics* **1996**, *15*, 1518-1520.

(46) England, P. M.; Lester, H. A.; Davidson, N.; Dougherty, D. A. *Proc. Natl. Acad. Sci. USA* **1997**, *94*, 11025-11030.

(47) Nowak, M. W.; Kearney, P. C.; Sampson, J. R.; Saks, M. E.; Labarca, C. G.; Silverman, S. K.; Zhong, W.; Thorson, J.; Abelson, J. N.; Davidson, N.; Schultz, P. G.; Dougherty, D. A.; Lester, H. A. *Science* **1995**, *268*, 439-442.

(48) Nowak, M. W.; Gallivan, J. P.; Silverman, S. K.; Labarca, C. G.; Dougherty, D. A.; Lester, H. A. *Methods Enzymol.* **1998**, *293*, 504-529.

(49) Kearney, P. C.; Nowak, M. W.; Zhong, W.; Silverman, S. K.; Lester, H. A.; Dougherty, D. A. *Mol. Pharm.* **1996**, *50*, 1401-1412.

(50) Quick, M.; Lester, H. A. In *Ion Channels of Excitable Cells*; Narahashi, T., Ed.; San Diego, CA: Academic Press, 1994, p. 261-279.

(51) Li, L. T.; Zhong, W. G.; Zacharias, N.; Gibbs, C.; Lester, H. A.; Dougherty, D. A. *Chemistry & Biology* **2001**, *8*, 47-58.

Chapter VIII

A NEW APPROACH TO PHOTOCHEMICAL CLEAVAGE OF PROTEIN AND PEPTIDE BACKBONES

Nature has an array of important processes that rely on distinct protein cleavage events for their initiation. Site-specific proteolysis upon the addition of an outside experimental stimulus would allow for the scientific exploration of these events and, more generally, of protein function and modular design. *o*-Nitrophenylglycine (Npg) was the first example of an unnatural amino acid that could site-specifically cleave the protein backbone upon irradiation with UV light, but this amino acid was inefficient at ribosomal incorporation and required prolonged photolysis times for productive proteolysis. Subsequently, other examples of similar compounds followed in the literature, but none of them were designed for use with *in vivo* nonsense-suppression techniques. Herein are presented two α-hydroxy acids that were specifically designed to overcome the limitations of Npg. Through the use of model reactions, these two selenium-containing compounds were found to be capable of cleaving the peptide through an S_N2 attack at the carbinol carbon that was integrated into the backbone upon the incorporation of the α-hydroxy acid. Unfortunately, the same success was not seen when ribosomally expressed in proteins. Though both were compatible with nonsense-suppression techniques, neither has yet been observed to cleave a full protein in *in vitro* or *in vivo* experiments.

Introduction

Many proteins have a modular design, with different structural domains that work in unison to achieve a function or perform separate functions in complex systems. In addition, many proteins are processed by cleavage into smaller fragments, revealing a previously protected reactive center or producing smaller signaling molecules. The processing of the amyloid-β protein into a neurodegenerative element,[1] the partitioning of the hepatitis C polyprotein into its viral components,[2] and the activation of caspase-3 into a cysteine protease that triggers apoptosis,[3] are a few examples of the powerful consequences of nature's ability to cleave the protein backbone at specific sites. Mimicking this process by inserting a photolabile group into a protein allows for synthetic control over proteolysis. The function of a specific protein can be either turned on or turned off simply by exposing the system to UV light.

In 1997 Dr. Pamela England, a postdoctoral researcher in the Dougherty laboratory, spearheaded such a strategy for photochemically initiating backbone cleavage of a protein, allowing dissection of a protein into its separate domains or processing a preprotein with temporal and spatial control.[4] She synthesized and tested the unnatural amino acid *o*-nitrophenylglycine (Npg, figure 8.1), which creates an *o*-nitrobenzylamide on incorporation into a protein. Photolysis then launches the well known *o*-nitrobenzyl "deprotection" of the amide, cutting the protein backbone.

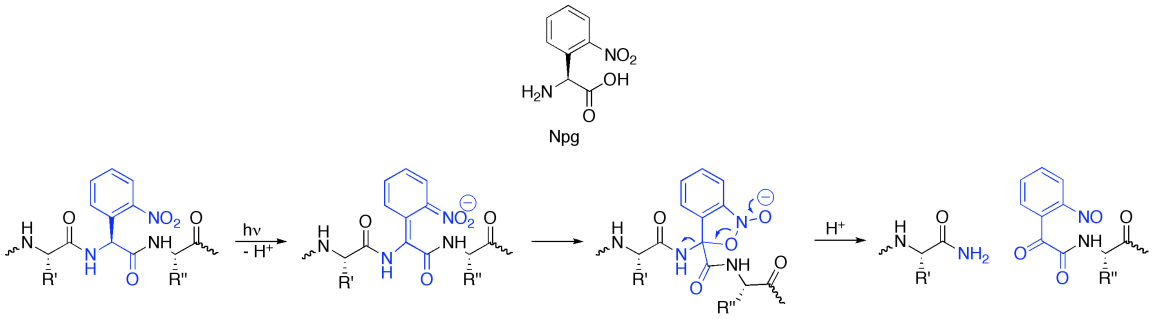

Figure 8.1. Npg and its mechanism for cleaving the peptide backbone.

Npg was incorporated into both the Shaker B voltage-gated K^+ channel (ShB) and the muscle nicotinic acetylcholine receptor (nAChR), two channels introduced earlier in this thesis, by *in vivo* nonsense suppression in *Xenopus* oocytes.[4] Photolysis produced site-specific, nitrobenzyl-induced photochemical proteolysis (SNIPP). In ShB England incorporated Npg into two sites, Leu47 and Pro64, both of which are located in the "chain" that connects the channel blocking "ball" to the six transmembrane helices (figure 8.2). These two sites have been previously discussed in chapter 6 of this thesis. Irradiation and proteolysis destroys a link in the chain connecting the "ball" and the channel. Without the covalent attachment of the "ball," the potential for N-terminal inactivation is eliminated.

Npg was also incorporated into two sites in the nAChR: α1Val132 and β1Leu262 (figure 8.3).[4] α1Val132 is located in the extracellular domain of the channel in the Cys-loop. This site was chosen since proteolysis was expected to result in a loss of the integrity of this structurally and functionally important loop, thus inhibiting channel function. β1Leu262 is the famous 9' residue in the β1 subunit, and it is found in the

transmembrane region of the channel. This residue is part of a hydrophobic band of residues that forms the narrowest point in the pore of the channel. A conformational change in the protein induced by the binding of ACh widens this band of leucines enough to allow ions to diffuse through the channel pore. Disruption of the protein at this site was expected to hinder this gating process. As expected, incorporation of Npg at both sites showed a reduction in channel activity after irradiation.

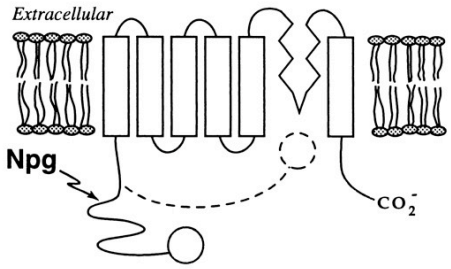

Figure 8.2. Incorporation of Npg into ShB. Figure adapted from England *et al.*[4]

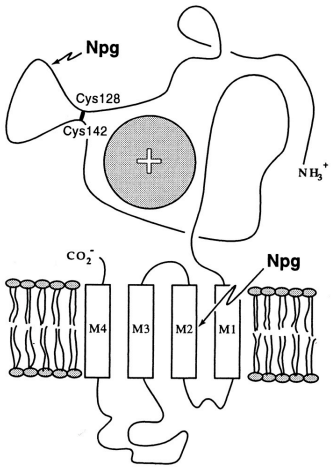

Figure 8.3. Incorporation of Npg into the α1 subunit of the nAChR. Figure adapted from England *et al.*[4]

Together these data demonstrate that Npg can produce SNIPP regardless of whether it is in an intracellular site, an extracellular site, or the transmembrane region. Although successful in demonstrating the essential SNIPP concept, Npg was not an ideal reagent. Its incorporation into proteins by nonsense suppression was often inefficient, perhaps because of the steric crowding associated with an *ortho*-substituted phenylglycine derivative. At α1Val132 three separate injections of Npg-tRNA into each oocyte were necessary for efficient *in vivo* nonsense suppression. In addition, while *o*-nitrobenzyl "caged" side chains of Tyr and Cys have been efficiently photocleaved in *Xenopus* oocytes,[5-8] photochemical decaging of proteins containing Npg can require prolonged photolysis times. England found 4 to 7.5 hours of irradiation necessary for the functional effects of proteolysis via Npg to be evident. More recently, however, Endo *et al.* did achieve efficient photolysis of Npg when incorporated into the soluble protein caspase-3.[9] In their *in vitro* experiment, proteolysis released a functional enzyme after only one minute of irradiation.

Other strategies for photochemical cleavage of protein and peptide backbones have recently appeared. Bosques and Imperiali[10] and Kron and co-workers[11] have employed *o*-nitro-β-phenylalanine as a linker between two protein or peptide fragments (figure 8.4A), while Pellois and Muir[12] have employed a highly expanded nitrobenzyl linker that can both ligate to the C-terminus of a recombinant protein and photorelease upon irradiation (figure 8.4B). Otaka and co-workers introduced a novel system based on a nitrobenzyl-caged phenol and the "trimethyl lock" motif, in which intramolecular cleavage of the backbone amide occurs through attack by the phenol once it has been decaged (figure 8.4C).[13] While these newer approaches are attractive, they would not

likely be compatible with *in vivo* protein expression, as β-amino acids and highly crowded systems such as the trimethyl lock are not compatible with nonsense-suppression and other approaches to incorporating unnatural amino acids into proteins expressed in cells.

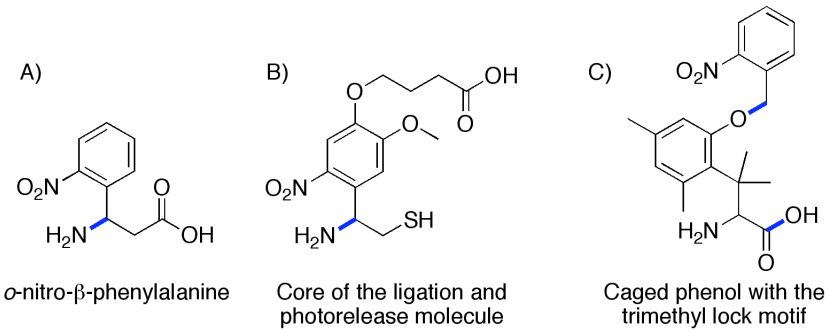

Figure 8.4. Other strategies for the photochemical cleavage of peptides and proteins. The bonds that break are highlighted in blue. A) *o*-Nitro-β-phenylalanine.[10,11] B) The core of the ligation and photorelease molecule.[12] C) The *o*-nitrobenzyl-caged phenol with its trimethyl lock motif.[13] Note here that two bonds break, the first is the nitrobenzyl-phenol bond, and the second is in the backbone through the attack of the carbonyl by the decaged phenol.

A Novel Direction for SNIPP

In this chapter the design and synthesis of two new residues that can induce backbone cleavage by an unprecedented reaction mechanism are described (figure 8.5). This novel approach to SNIPP has the potential to be superior to Npg while still being compatible with *in vivo* protein expression by nonsense suppression. First, selenide anions are among the strongest of known nucleophiles. Since selenols have pKa values on the order of 5-6,[14] the selenide anion should be the dominant moiety at physiological pH. Selenium should be well tolerated in nonsense suppression, as both selenocysteine and

selenomethionine are known to be incorporated into proteins. In fact selenocysteine is frequently referred to as the 21st amino acid because it has its own tRNA that contranslationally inserts it at certain UGA opal stop codons.[15]

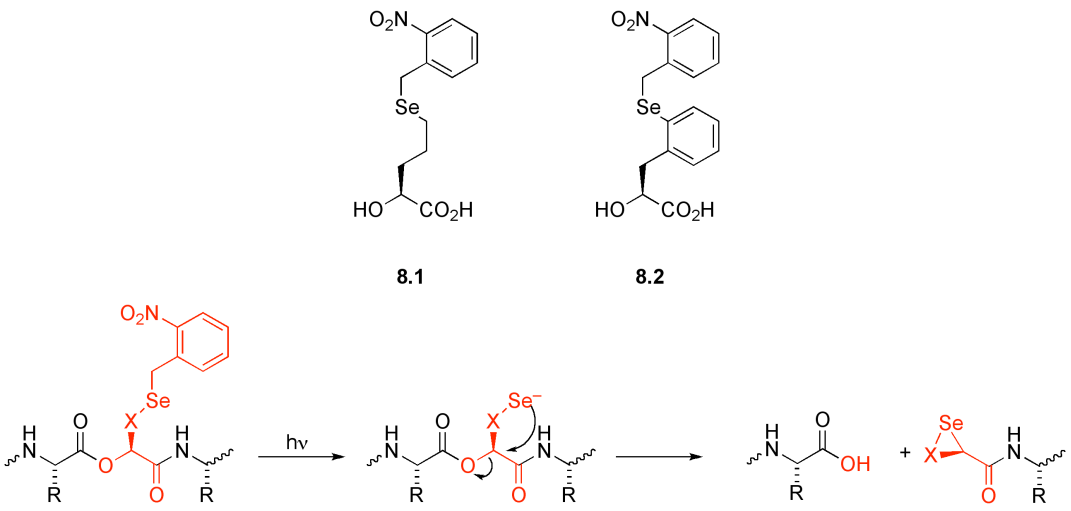

Figure 8.5. The two novel SNIPP-capable compounds described in this chapter and their predicted mechanism of proteolysis.

Second, α-hydroxy acids (instead of α-amino acids) are quite compatible with ribosomal protein synthesis,[16-20] as well as standard solid-phase protocols for peptide synthesis.[21,22] Incorporation of an α-hydroxy acid produces a backbone ester bond, and selenides can "hydrolyze" esters (but not amides) by an S_N2-type mechanism—the softness of the selenide favors attack of the soft carbinol carbon over the hard carbonyl carbon.[23] While this is typically efficient only with methyl esters, the anticipation is that the intramolecularity of the reaction proposed here will compensate for the fact that the reaction is occurring at a tertiary center. In addition, the inductive effect of the adjacent carbonyl could accelerate the S_N2 reaction.

We also anticipate that the new system could overcome the limitations of Npg. First, the steric congestion associated with Npg, which appears to limit its efficiency in ribosomal protein incorporation, has been decreased. Second, decaging of an unencumbered selenide should be more efficient than "deprotection" of a backbone amide, based on both steric factors and the much lower pKa of a selenol versus an amide.

The final design issue is the nature of X in figure 8.5. Formation of a five-membered ring is generally most favorable in such systems, and our initial design employed a simple aliphatic chain, X = $–CH_2CH_2CH_2–$, making the target α-hydroxy acid compound **8.1**. We subsequently considered a second design, **8.2**, in which an aromatic ring was incorporated into X. Both strategies have advantages. Compound **8.1** contains an aliphatic selenide, which is anticipated to be a stronger nucleophile than the aromatic selenide of **8.2.**[24] On the other hand, compound **8.2** more closely resembles the phenyl selenide anion typically used in the S_N2 cleavage of esters, and fewer rotatable bonds have to be restricted to form the S_N2 transition state for **8.2**. In addition, the arylalkyl selenide of **8.2** is likely more stable to oxidative degradation since its lack of δ-hydrogen atoms prevents the possibility of syn elimination of any selenoxide that forms. However, the increased steric size of **8.2** could be a problem for ribosomal incorporation into proteins.

The design and predicted mechanism of these two compounds represents novel chemistry, and therefore, before applying it to a biological system, we felt it was essential to establish that the chemistry does indeed proceed as predicted, including isolation and full characterization of the novel selenacyclopentane fragmentation product. The simplest relevant synthetic targets were depsipeptides containing **8.1** and **8.2**. With these

in hand, photolysis conditions were optimized, and the novel selenacyclopentane fragmentation products were successfully isolated, proving that indeed, proteolysis was possible through the proposed mechanism for each novel compound. Unfortunately, though the chemistry was shown to work, photolysis-induced proteolysis was never seen in a full protein in either *in vitro* or *in vivo* experiments.

Results and Discussion

*Synthesis of Alkyl Selenide α-Hydroxy Acid **8.1***

A former graduate student in the Dougherty laboratory, Dr. Niki Zacharias, completed the first synthesis of alkyl selenide α-hydroxy acid **8.1**. The molecule was made racemically via the procedure shown in scheme 8.1. First, δ-valerlactone was hydroxylated following the procedure of Best *et al.*[25] Opening of the lactone[26,27] with 30% hydrogen bromide in acetic acid followed by treatment with ethanol resulted in the basic frame of the α-hydroxy acid protected as the ethyl ester. The bromine was exchanged for selenium from reaction with disodium diselenide.[28] Reduction of the diselenide, addition of *o*-nitrobenzylbromide,[29,30] and treatment with base produced the final product, racemic **8.1**. A large amount of work went into the development of the synthesis; a full description of which is in Zachrias's thesis.[31]

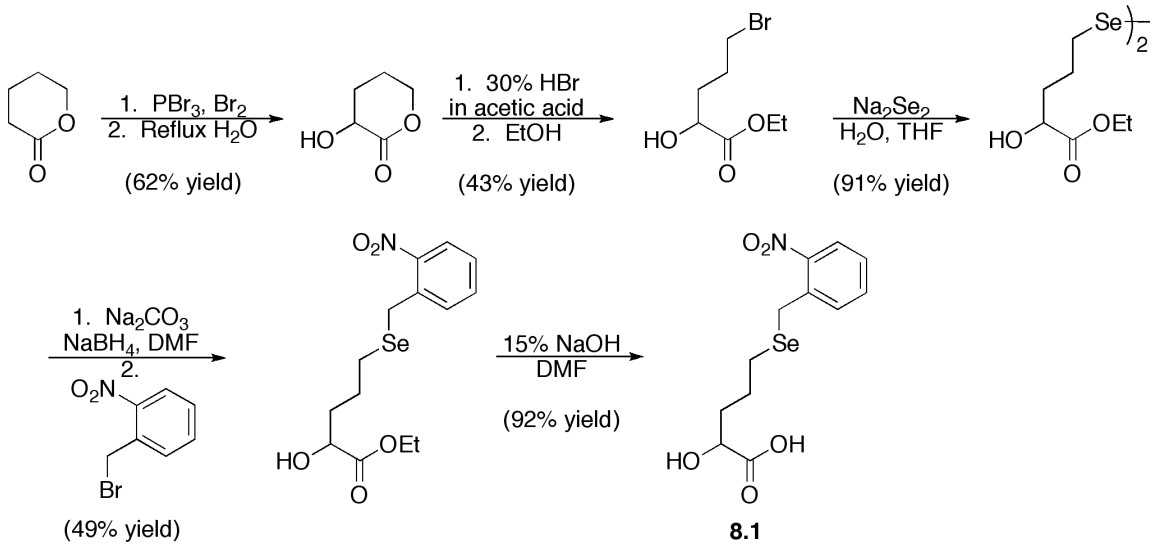

Scheme 8.1. The first synthesis of racemic alkyl selenide α-hydroxy acid **8.1**.

The major limitation of this scheme was that it resulted in racemic **8.1**. Since the initial goal was to synthesize a depsipeptide containing **8.1** that could be used to test the proteolytic capabilities of the α-hydroxy acid, having enantiopure **8.1** would allow for a single diastereomeric depsipeptide instead of the mixture of diastereomers that would be produced from racemic **8.1**. After the completion of the racemic synthesis, Zacharias discovered a publication by Guindon *et al.* that described the opening of a furan ring with dimethylboron bromide.[32] This reaction framed the retrosynthetic design of the pathway to enantiopure **8.1** (figure 8.6).

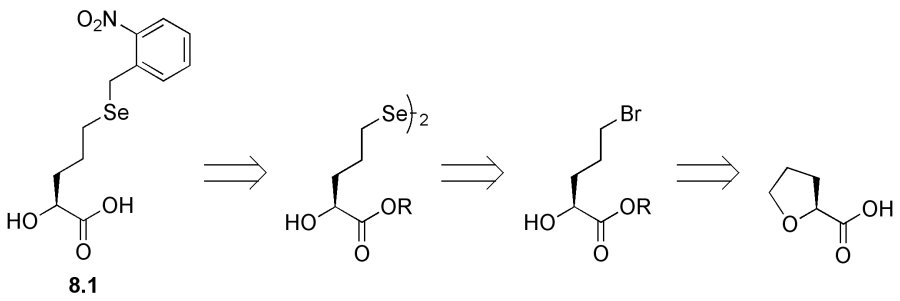

Figure 8.6. Retrosynthesis for enantiopure alkyl selenide α-hydroxy acid **8.1**.

A small but important feature of this new synthetic plan was the nature of the group that masked the acid during the central steps of the synthesis. *tert*-Butyl esters are commonly used during both solution- and solid-phase peptide synthesis to mask acids. Thus, this moiety was chosen since it would allow the esterified **8.1** to be taken directly into the first peptide coupling reaction. While the *tert*-butyl esterification of S-(−)-tetrahydro-2-furoic acid was successful, the subsequent reaction with dimethylboron bromide[32] converted the *tert*-butyl ester **8.3** back to the original acid.

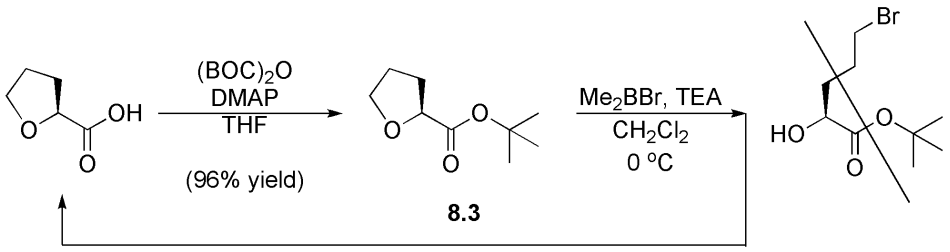

Scheme 8.2. The acid-labile *tert*-butyl ester was not compatible with the conditions for furan ring opening.

There was literature precedent for successful ring opening of the racemic ethyl ester version of **8.3** by dimethylboron bromide.[32] Therefore, S-(−)-tetrahydro-2-furoic acid was converted to the ethyl ester (scheme 8.3).[33] As per the precedent in the literature, ring opening with dimethylboron bromide was now successful.[32] Conversion to the diselenide from the *in situ* formation of the reactive disodium diselenide[31] and ester hydrolysis then produced **8.7**.[34] This acid diselenide was directly reduced with sodium borohydride and the product alkylated with *o*-nitrobenzyl bromide to give the target compound **8.1**.[29]

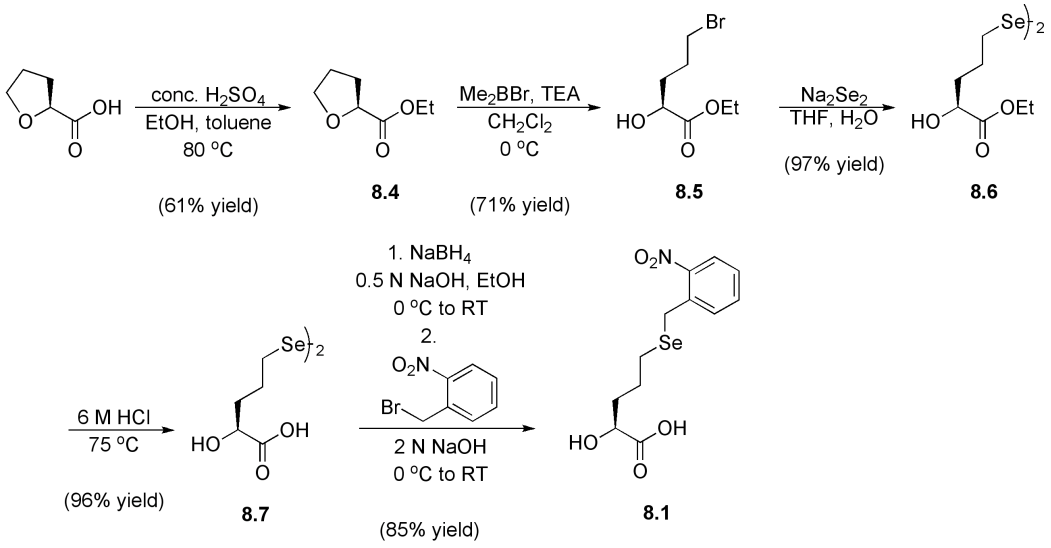

Scheme 8.3. Successful synthesis of enantiopure alkyl selenide α-hydroxy acid **8.1**.

Though this synthesis greatly benefited from Zacharias's previous synthesis, each step shown in scheme 8.3 was evaluated and optimized. Most notably, it was found that if the ethyl ester was acidified prior to being reduced and alkylated by *o*-nitrobenzylbromide, then the combined yield for the two steps could be improved from 45% (scheme 8.1) to

82% (scheme 8.3). The yield probably also benefited from the care that was taken of the compounds after the addition of the selenium. Compounds **8.6**, **8.7**, and **8.1** readily decomposed under mildly oxidative conditions. The instability of the compounds was believed to be due to the presence of the δ-hydrogen atoms that enabled syn elimination of any selenides that had been oxidized to the selenoxide.

Design of the Depsipeptide Model System

A depsipeptide was envisioned as the simplest model system to test the proteolytic capability of **8.1** (figure 8.7). By using a small peptide instead of a larger protein, the isolation and charaterization of the major photolysis product could be carried out by traditional organic synthetic methods. The design of the depsipeptide was first discussed in Zacharias's thesis.[31] Phenylalanine was chosen to be the N-terminal amino acid in order to add hydrophobicity to the depsipeptide. The novel **8.1** was the central piece so that any cleavage that occurs through the proposed mechanism will essentially split the backbone in half. Glutamate was chosen to be the C-terminal amino acid since it could add even more hydrophobicity to the depsipeptide if each of its acids are masked as esters or it could make a hydrophilic depsipeptide if each of its acids were left as acids. This feature of the design created the ability for the model studies to be carried out in both organic and aqueous solvents.

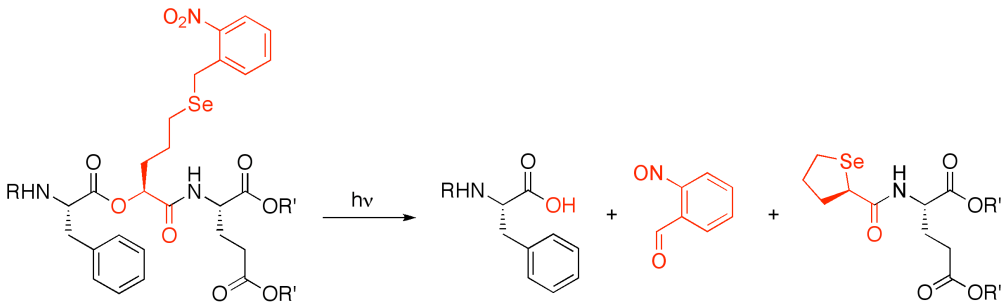

Figure 8.7. Design of the depsipeptide model system.

Synthesis of Depsipeptides Containing Alkyl Selenide α-Hydroxy Acid ***8.1***

In a typical peptide coupling reaction, the desired N-terminal amino acid is protected as an amide, and the desired C-terminal amino acid is protected as an ester. This strategy insures that the carboxylic acid of the former will react with the free amine of the latter to form the desired amide bond. Since **8.1** was envisioned as the central of three amino acids in the depsipeptide, either end could be protected in the initial peptide coupling reaction. Previously, Zacharias had protected the acid of racemic **8.1** as a *tert*-butyl ester using *N,N*-dimethylformamide di-*tert*-butyl acetal in refluxing toluene,[35] but she found the selenium elimination product, 2-hydroxy-pent-4-enoic acid *tert*-butyl ester, to be a major product of the reaction.[31]

To reduce the production of the unwanted elimination product, a new protection strategy was sought. After planning various methods for protecting either the acid or the alcohol of **8.1**, we realized that we could simply take advantage of the difference in reactivity of an alcohol and a primary amine for a carboxylic acid, capitalizing on **8.1** being an α-*hydroxy* acid, not an α-*amino* acid. Since a primary amine reacts much more readily with

a carboxylic acid and forms a stable amide bond, the alcohol is already "protected" in the reaction.

With this strategy in hand, the first peptide coupling reaction was set up between **8.1** and di-*tert*-butyl glutamate (scheme 8.4). Several different reaction conditions were tried in order to maximize the yield of dipeptide **8.8**.[36,37] In all cases the yields were low, but the combination of benzotriazol-1-yl-oxytripyrrolidinophosphonium hexafluorophosphate (PyBop) and N-methylmorpholine was found to be the best available.

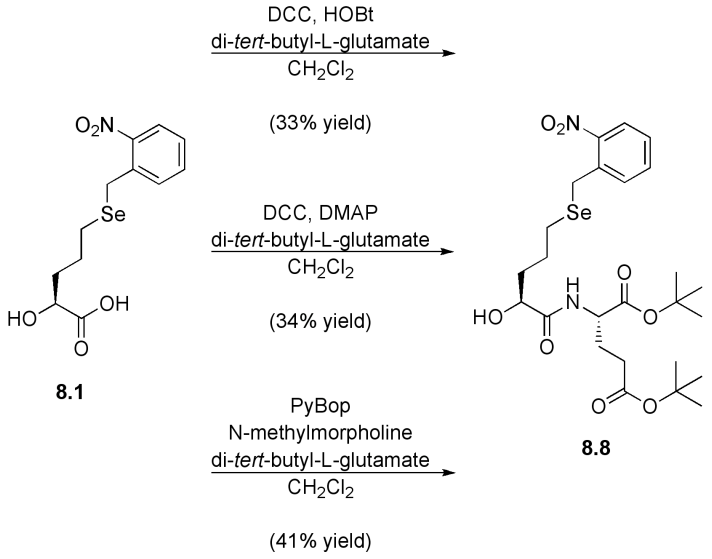

Scheme 8.4. Three sets of reagents were used to make dipeptide **8.8**.

Three different model depsipeptides were made by varying the aromatic N-terminal amino acid (scheme 8.5). Depsipeptides **8.9** and **8.11** differed only in the nature of the N-terminal amide. Depsipeptide **8.10** varied from the original design by the addition of tryptophan to the N-terminus. Tryptophan was chosen for its hydrophobicity and for its

variety. Because the central and C-terminal residues are the same, these three different depsipeptides will produce the same selenacyclopentane product upon photolysis and proteolysis. While it was anticipated that the α-hydroxy acid might be difficult to couple, the only change required from a traditional coupling reaction was the lengthening of the reaction time—each reaction was allowed to stir at room temperature for one to two days before the reaction was quenched.

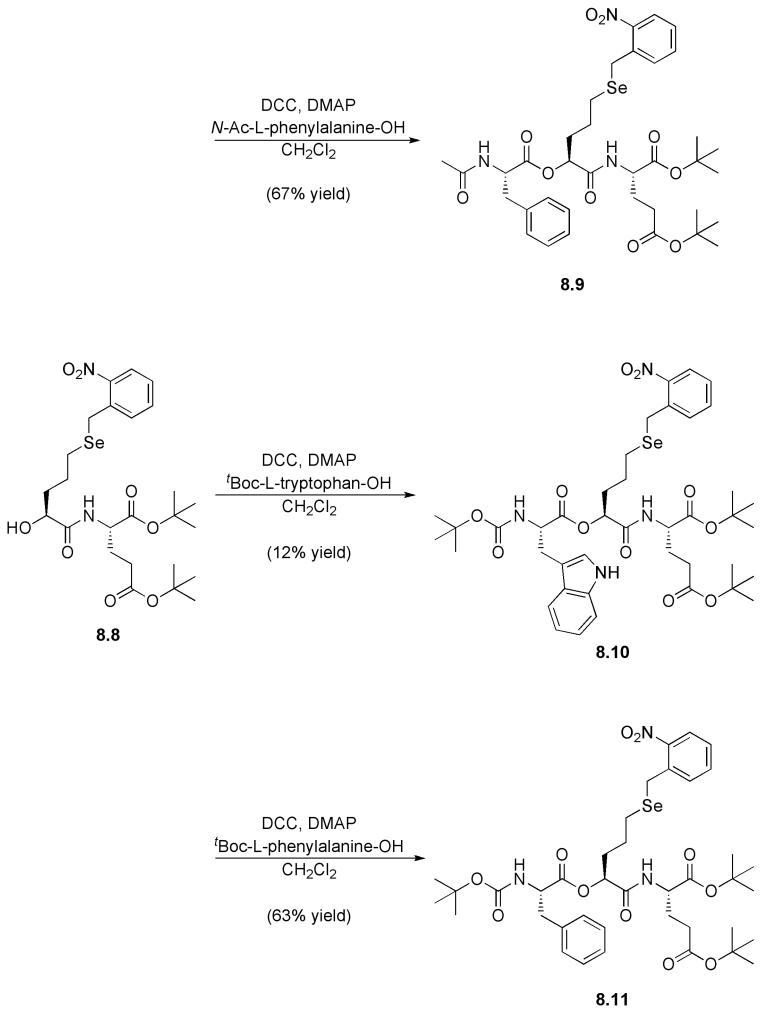

Scheme 8.5. The second peptide coupling reaction in the synthesis of three different depsipeptide model systems.

*Initial Photolysis Studies on Depsipeptides **8.9** and **8.10***

Prior to these studies Zacharias had run a single photolysis reaction on **8.1** in a dipeptide.[31] Because of the low yield she obtained in the formation of racemic **8.1** *tert*-butyl ester, she only had enough material to make the dipeptide, *N*-acetyl-phenylalanine-**8.1**-*tert*-butyl ester. She irradiated this dipeptide in deuterated acetonitrile that had been purged with argon and followed the progress of the reaction by nuclear magnetic resonance (NMR) spectrometry.[38] The photolysis products were purified by preparatory thin-layer chromatography (TLC), and gas chromatography mass spectrometry (GC-MS) suggested that the product with an R_f of 0.77 (50% ethyl acetate in hexanes) contained the selenide cleavage product. To get firmer evidence that **8.1** could cleave the peptide backbone through the predicted mechanism, the photolysis products of the newly synthesized depsipeptides, **8.9**, **8.10**, and **8.11**, were pursued.

The initial photolysis studies consisted of a 0.1 μM solution of depsipeptide in dry acetonitrile, and typically, 50 μL samples were exposed to 320 nm light from a 1000 W Hg/Xe arc lamp for five minutes. Tetrahydrofuran, another common solvent compatible with photolysis studies, could not be used since the depsipeptides quickly decomposed while in this solvent. Reactions were followed by electrospray ionization (ESI)-MS. NMR spectroscopy, TLC, and high-pressure liquid chromatography (HPLC) were difficult to use with such small-scale reactions and were therefore not performed in parallel to follow the reactions. In ESI-MS the analyte (M) being measured exists as an ion in solution, typically as [M+H], [M+Na], [M+K], or [M−H]. Therefore, ESI-MS can both interpret the small quantities of material and also identify the selenium-containing mass-to-charge (*m/z*) ratios because of the characteristic selenium isotope pattern.

Unfortunately, ESI-MS is not quantitative, and the structures of products have to be inferred from likely candidate structures.

Disappointingly, the desired selenacyclopentane was not seen by ESI-MS after photolysis of depsipeptide **8.9**. Instead, the major product *m/z* ratio was 1292.7, which by its ratio and isotope pattern agreed with the compound that would be formed upon *o*-nitrobenzyl deprotection and diselenide formation ([M+K] *m/z* = 1293.5) (figure 8.8A). Although the formation of the diselenide prevents the possibility for cleavage to occur, its appearance suggested that the *o*-nitrobenzyl group was rapidly and efficiently decaging, one of the predicted advantages of **8.1** over Npg. Formation of a diselenide is an oxidative process, which suggests that the photolysis reaction is taking place in an oxidative environment. Several other *m/z* ratios present in the ESI-MS also reinforced this assumption. First, the *m/z* ratio with a selenium-isotope pattern nearest to the predicted mass for the decaged selenol ([M+K] *m/z* = 667.2) was 698.7, a ratio that could be explained by the oxidation of the selenol to selenic acid ([M+K] *m/z* = 699.3). Second, another set of *m/z* ratios was seen at 568.8, 584.8, and 600.8. These ratios, which did not contain the selenium isotope pattern, were suggestive of a depsipeptide that contained dehydronorvaline ([M+Na] *m/z* = 569.3, [M+K] *m/z* = 585.4) and the equivalent epoxide ([M+Na] *m/z* = 585.3, [M+K] *m/z* = 601.4) as its central component. These unwanted side products could be produced from the syn elimination of the selenoxide formed under oxidative conditions (figure 8.8B).[39] All products seen for depsipeptide **8.9** were similarly reproduced with depsipeptide **8.10**, giving more credit to the assigned identities.

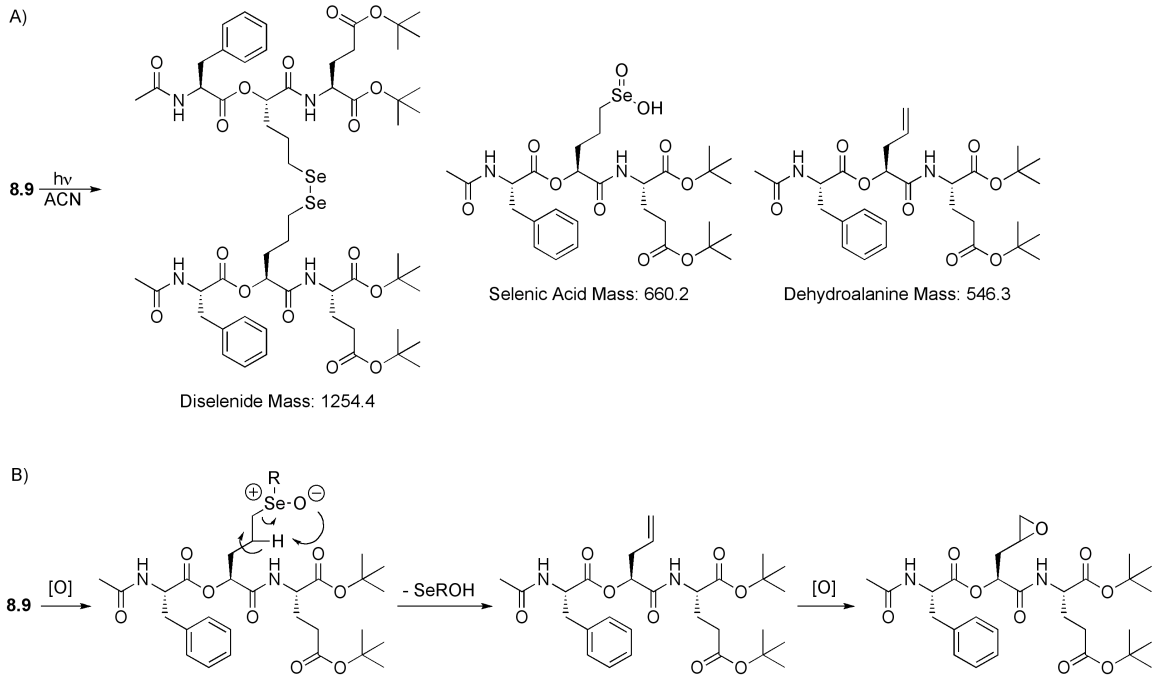

Figure 8.8. ESI-MS suggests oxidative products are formed upon irradiation of the depsipeptides in acetonitrile. A) Predicted products from the initial photolysis reaction of **8.9**. Similar products were predicted for **8.10**. B) Predicted oxidation and syn elimination of the selenoxide-containing depsipeptide **8.9**. **8.10** is expected to produce the same oxidation products.

*Oxidation Studies on Depsipeptides **8.9** and **8.10***

To confirm that the oxidative products predicted from the ESI-MS above would in fact be formed if depsipeptides **8.9** and **8.10** were exposed to an oxidative environment, these depsipeptides were subjected to a solution of the oxidant hydrogen peroxide. Solutions of 0.1 μM **8.9** or **8.10** in acetonitrile were combined with twice the volume of 30% hydrogen peroxide. After an hour of exposure to the oxidative hydrogen peroxide solution, ESI-MS of depsipeptide **8.9** showed *m/z* ratios of 546.9, 568.8, 698.8, 779.8, and 817.7, which corresponded to the dehydronorvaline containing depsipeptide ([M+H]

m/z = 547.3, [M+Na] *m/z* = 569.3), the selenic acid ([M+K] *m/z* = 699.3), and the selenoxide ([M+H] *m/z* = 780.3, [M+K] *m/z* = 818.4) (figure 8.9). The presence of the same *m/z* ratios in this experiment as in the photolysis reactions above reaffirms that the products in the photolysis reaction were being created by oxidation. The lack of *m/z* ratios for the diselenide and the presence of the selenoxide were expected since no means was provided for *o*-nitrobenzyl decaging. The same reaction conditions were repeated with water replacing the oxidant for a negative control. The addition of water did not have an effect on the depsipeptide as studied by ESI-MS. Depsipeptide **8.10** showed similar predicted products via ESI-MS after one hour of exposure to the hydrogen peroxide solution, but each had an increase of +16 over the predicted *m/z* ratio. This increase was accredited to the concurrent oxidation of the tryptophan to oxindolylalanine.[40]

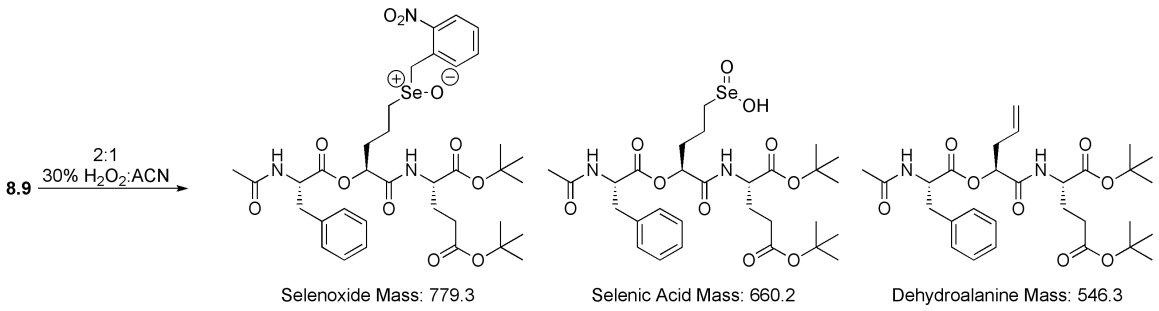

Figure 8.9. Predicted oxidative products from the reaction of **8.9** with hydrogen peroxide. The oxidation of depsipeptide **8.10** showed similar predicted products, but with the tryptophan oxidized to oxindolylalanine.

*Photolysis of Depsipeptides **8.9** and **8.10** in a Reducing Environment*

Creating a reducing environment in the photolysis reaction was expected to minimize the unwanted oxidative side products. Dithiothreitol (DTT) is a commonly used reducing agent, and a study by Besse *et al.* found that 44 equivalents of DTT could reduce 50% of the diselenide bonds in their model depsipeptide system.[41] Following this example, 50 equivalents of DTT were added to the depsipeptide/acetonitrile mixture prior to photolysis. After photolysis in this reducing environment, the dehydronorvaline-containing depsipeptide was not seen or was seen in low abundance via ESI-MS. The diselenide was seen in much lower abundance as well. Therefore, irradiation in a reducing environment was successful at decreasing the oxidative side products. Unfortunately, the expected *m/z* ratio for the selenacyclopentane product was still not seen in the ESI-MS. Instead, the new major product in the ESI-MS after irradiating **8.9** was at an *m/z* ratio of 650.8, which corresponds to the decaged selenol product ([M+Na] *m/z* = 651.2). Therefore, in this reducing, organic environment, the favored state of the alkyl selenium was the selenol, not the selenide anion expected to attack the carbinol carbon of the backbone. The same was true for the photolysis of **8.10**.

Since the selenide anion was the nucleophile expected to induce cleavage of the depsipeptide backbone, conditions were desired that would encourage anion formation over selenol formation. The pKa of decaged **8.1** was not determined in this study, but it is expected to be similar to that of selenocysteine, which has a pKa of 5.73,[14] since they are both aliphatic selenols. Thus, **8.1** should be anionic at physiological pH. To test the effects of pH on the photolysis reaction, depsipeptides **8.9** and **8.10** were photolyzed in a solution of equal volumes of acetonitrile and pH 7 water in the presence of 50 equivalents

of DTT, but ESI-MS of the postphotolysis solution suggested only selenol was formed. Raising the pH to 8, 9, or 10 was also unsuccessful at eliciting the cleavage reaction. Increasing the relative amount of pH 10 water was also unsuccessful at inducing proteolysis. Finally, addition of the organic base triethylamine also did not encourage any selenacyclopentane product formation as visualized by ESI-MS.

Contrary to the results seen if water with high pH was added to the reaction prior to photolysis, if water with a pH of 8 or 9 was added after irradiation, a low-abundance *m/z* ratio with the selenium isotope pattern was seen at 443.9 in the ESI-MS, agreeing with the expected mass of the selencyclopentane ([M+Na] *m/z* = 444.1) (figure 8.10). Encouragingly, both MS/MS and MS/MS/MS on 443.9 caused the loss of the mass of a *tert*-butyl group (*m/z* Δ = 56.1), and the 443.9 *m/z* ratio was seen in the ESI-MS when the same conditions were repeated on **8.10**. These results were viewed as the first successful peptide cleavage induced by **8.1** in a depsipeptide. It was surprising that successful cleavage required a much higher pH than expected and only when the pH was rasied after irradiation. It was also disappointing that the low abundance of the *m/z* ratio in the ESI-MS implied that the cleavage reaction was inefficient under these conditions.

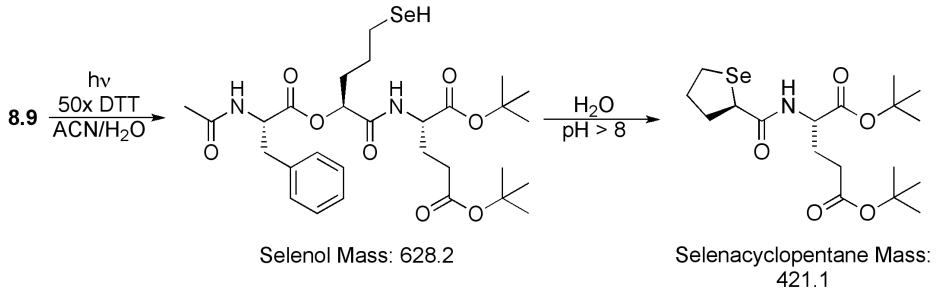

Figure 8.10. Representation of the first successful peptide cleavage reaction with **8.9**. Only relevant products are shown. Depsipeptide **8.10** showed the same pattern.

Photolysis Studies in a Reducing, Aqueous Environment

The small-scale photolysis reactions thus far suggested that the deprotonation of the selenol encouraged proteolysis in the manner predicted by the design, but there were many facets to the formation of the selenide anion and subsequent proteolysis reaction. Importantly, the addition of base only encouraged cleavage of the peptide backbone once the selenol had already been decaged. To probe whether the partially organic environment was hindering the cleavage reaction, a hydrophilic depsipeptide was desired so that the photolysis could be run in an entirely aqueous environment. Thus, a mixture of trifluoroacetic acid in methylene chloride was used to remove the acid-sensitive protecting groups from the depsipeptides **8.9** and **8.10** (scheme 8.6).

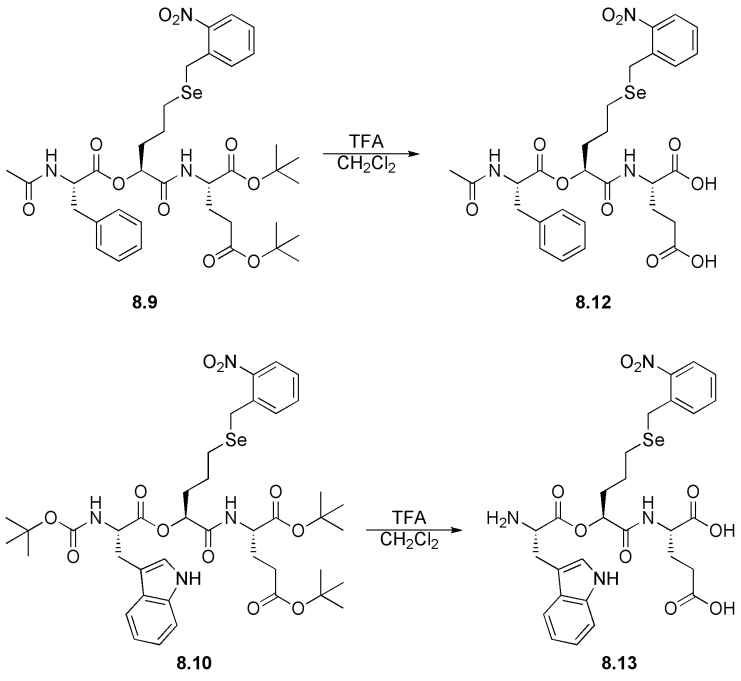

Scheme 8.6. Removal of the acid-sensitive protecting groups reveals hydrophilic depsipeptides.

When **8.12** was photolyzed in the presence of 50 equivalents of DTT in double-distilled water, the ESI-MS postphotolysis contained an *m/z* ratio at 308.0, which corresponded to the desired selenacyclopentane ([M−H] *m/z* = 308.0) (figure 8.11). The *m/z* ratio for the selenol, 514.9 ([M−H] *m/z* = 515.1), was also present. Since the pH of the double-distilled water is near the pKa of the selenol, it was hoped that raising the pH to a more physiologically relevant value would shift the equilibrium towards the selenide anion and, therefore, a higher abundance of the selenacyclopentane *m/z* ratio would be seen via ESI-MS. But, the same products were seen if water pH 7, water pH 7.6, or phosphate buffer pH 7 was used. Thus, there was a higher propensity for cleavage in this aqueous environment, but there was still something allowing selenol formation.

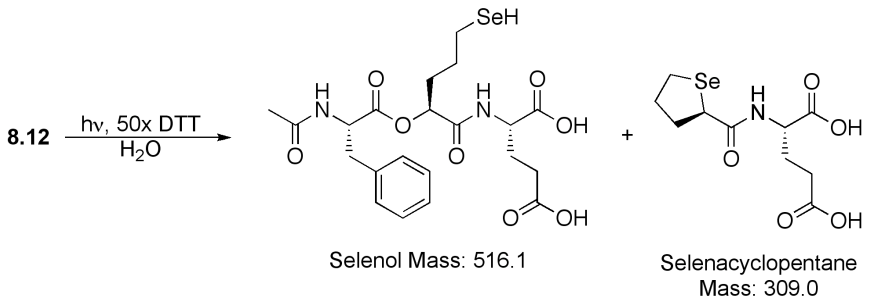

Figure 8.11. An aqueous environment was capable of producing some amount of the desired cleavage product. Only relevant products shown.

Exploring the Effects of DTT on the Cleavage Reaction

DTT reduces diselenides by first forming a sulfur-selenium bond. To probe the possibility that DTT was enhancing selenol formation through this mechanism of reduction, triscarboxyethylphosphine (TCEP) was substituted into the photolysis reaction

as the reducing agent. TCEP is a highly potent reducer of diselenides. By reducing diselenides through a mechanism involving its phosphine with the aid of water, TCEP allows for a nonthiol-based reduction mechanism to be tested in the photolysis and cleavage reaction. TCEP could also be purchased immobilized on agarose, which allowed for easy removal after irradiation. After depsipeptides **8.12** and **8.13** were irradiated in an aqueous environment with excess TCEP, ESI-MS still showed that the same two major products in this reaction were produced with TCEP as with DTT: selenacyclopentane and selenol. Therefore, specific attributes of DTT were not increasing the probability of selenol formation.

Using N-*Methyl Maleimide to Test for Selenol Formation*

After irradiation of **8.12** in water with either DTT or TCEP, an *m/z* ratio of 514.9 in the product ESI-MS had always been assigned as the selenol (figure 8.11). The same conclusions were made in the ESI-MS after the photolysis of **8.9**, **8.10**, and **8.13** as well. But, if the decaged selenide anion attacked the ester carbonyl instead of the carbinol carbon, a selenoester would be produced (figure 8.12). The simple rearrangement of atoms means the selenoester has the same mass as the selenol, 516.1 g/mol. The attack of the ester carbonyl requires a seven-member ring transition state, a much less likely occurrence than the five-member ring formed if the desired carbinol carbon were attacked to form the selenacyclopentane, but since both the selenol and the selenoester would give identical *m/z* ratios, neither can be excluded by the original ESI-MS data.

The addition of *N*-methyl maleimide to the reaction mixture after photolysis would discriminate between the two products since the maleimide can react with the selenol but not the selenoester. Thus, after depsipeptides **8.9** and **8.10** were photolyzed in acetonitrile and after depsipeptide **8.12** was photolyzed in water, all with 50 equivalents of DTT, *N*-methyl maleimide was added to each reaction. In the ESI-MS of the resulting solution of all three depsipeptides, an *m/z* ratio corresponding to the covalent addition of the *N*-methyl maleimide to the selenol was seen. This result confirmed that the selenol was appropriately assigned in all of the previous ESI-MS data and gave further evidence that the selenium was not as efficient as desired at the intramolecular cleavage reaction.

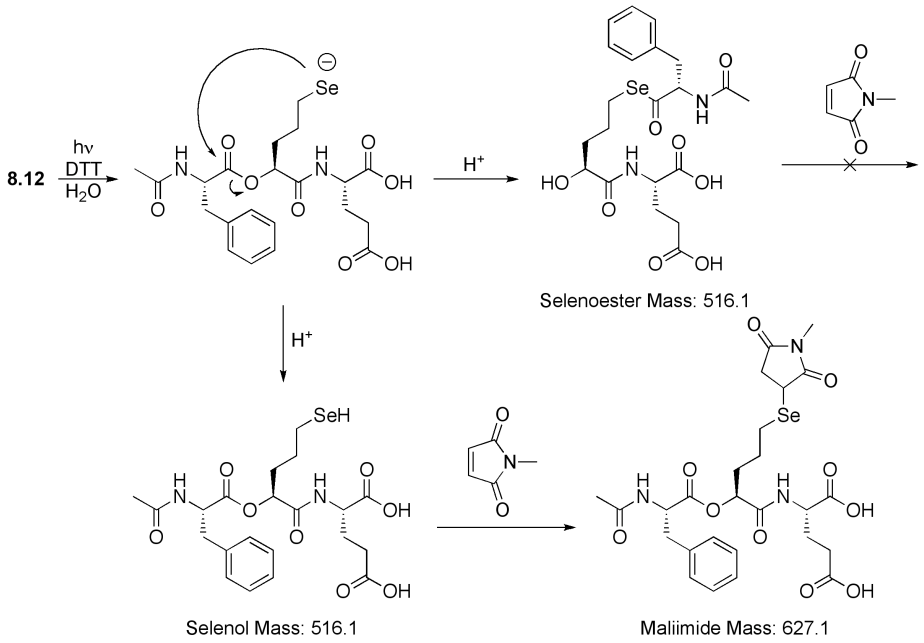

Figure 8.12. The possible products formed by the decaged selenide that have a mass of 516.1. To prove that the selenol was formed, it was trapped with N-methyl maleimide. Similar products were seen with depsipeptides **8.9** and **8.10**. Only the relevant products in each reaction are shown.

Redesign of the Photoreactive α-Hydroxy Acid

After irradiation of the depsipeptides, the repeated appearances of the *m/z* ratio that corresponded to the selenacyclopentane product in the ESI-MS were highly suggestive that **8.1** was indeed capable of cleaving the peptide backbone through the proposed mechanism. Unfortunately, a clean ESI-MS of only the cleavage product was never obtained, despite the many attempts to alter the nature and pH of the photolysis environment. We concluded that **8.1** was inefficient at SNIPP. Efficient SNIPP is necessary in an *in vivo* experiment to trust that a phenotypic response seen after irradiation is an effect of the experimentally controlled proteolysis. Ideally, all of the desired protein would be cleaved upon photolysis since results from a heterogeneous protein population could be skewed by the unknown percentage of protein that remained full and intact. Thus, a more efficient analog of **8.1** was desired.

We combined literature precedent with the knowledge gained through the previous photolysis experiments in the design of arylalkyl selenide α-hydroxy acid **8.2** (figure 8.3). Much of the inspiration for **8.2** came from the phenyl selenide anion used to cleave esters and lactones through the S_N2 attack of the carbinol carbon.[23,42,43] The decaged aryl selenide anion may be a less potent nucleophile than the decaged alkyl selenide anion in **8.1** due to its delocalization of the negative charge, but literature precedent suggests that an aryl selenide anion should be potent enough to initiate attack of the carbinol carbon. Also, fewer rotatable bonds in **8.2** have to be restricted to form the transition state during the cleavage reaction, which should lower the reaction barrier necessary to form the ring-closed product. The final important element in the design of **8.2** was the removal of the δ-hydrogen atoms that caused the syn elimination of the selenoxide. This change should

make **8.2** more stable than **8.1** to oxidative damage. The combination of these design elements are anticipated to make **8.2** a superior photoreactive α-hydroxy acid capable of site-specifically cleaving the protein backbone.

*Attempts to Synthesize Arylalkyl Selenide α-Hydroxy Acid **8.2***

The initial strategy for the synthesis of **8.2** involved either a Grignard reaction or a lithium-halogen exchange reaction for the addition of selenium to the aromatic ring (scheme 8.7). First, *o*-bromophenylalanine was converted to an α-hydroxy acid,[44] which was then protected on the acid as an oxazoline[45] and on the alcohol as a large, bulky silyl ether[46] to make **8.16**. Oxazoline and *tert*-butyldiphenyl silyl ether are protecting groups that are typically stable under Grignard and lithium-halogen exchange reactions.[47] Also, *tert*-butyldiphenylsilyl ether is supposed to be stable to acid and have a low propensity to migrate. Unfortunately, neither the Grignard reaction nor the lithium-halogen exchange reaction was capable for forming the aryl selenide.

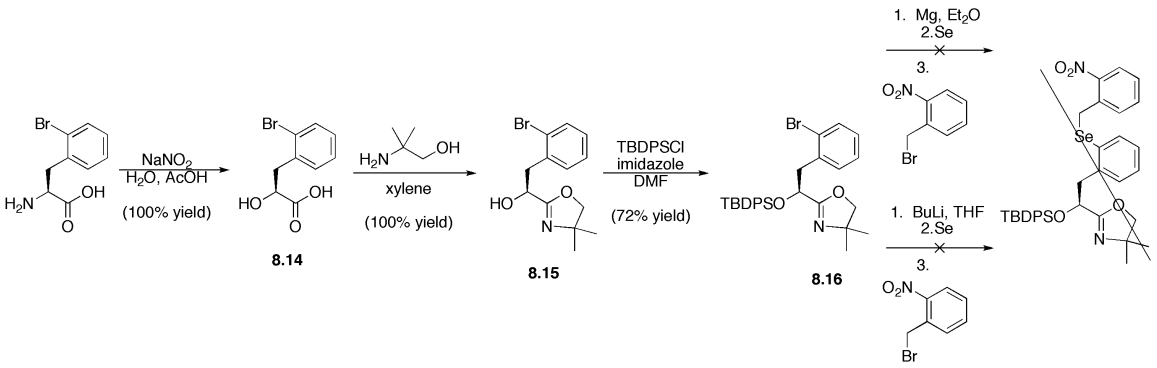

Scheme 8.7. An unsuccessful route for the synthesis of **8.2**.

*Successful Synthesis of Arylalkyl Selenide α-Hydroxy Acid **8.2***

Another graduate student in the Dougherty laboratory, Angela Blum, succeeded in synthesizing arylalkyl selenide α-hydroxy acid **8.2**. The successful synthesis of **8.2** (scheme 8.8) began with a reduction of 2-nitrophenylpyruvic acid by (+)-B-chlorodiisopinocampheylborane ("Ipc_2BCl") as reported by Wang *et al.* to yield the α-hydroxy acid in high-enantiomeric excess (94%).[48] The selenocyanate was prepared by a modification of the standard sequence, and the nitrobenzyl group was introduced by reductive alkylation. The bulky *tert*-butyl protecting groups were installed to discourage intramolecular cyclization seen during direct reduction of the nitro group of the *o*-nitro-phenylalanine α-hydroxy acid and to improve the solubility and ease of purification of subsequent compounds in the sequence.

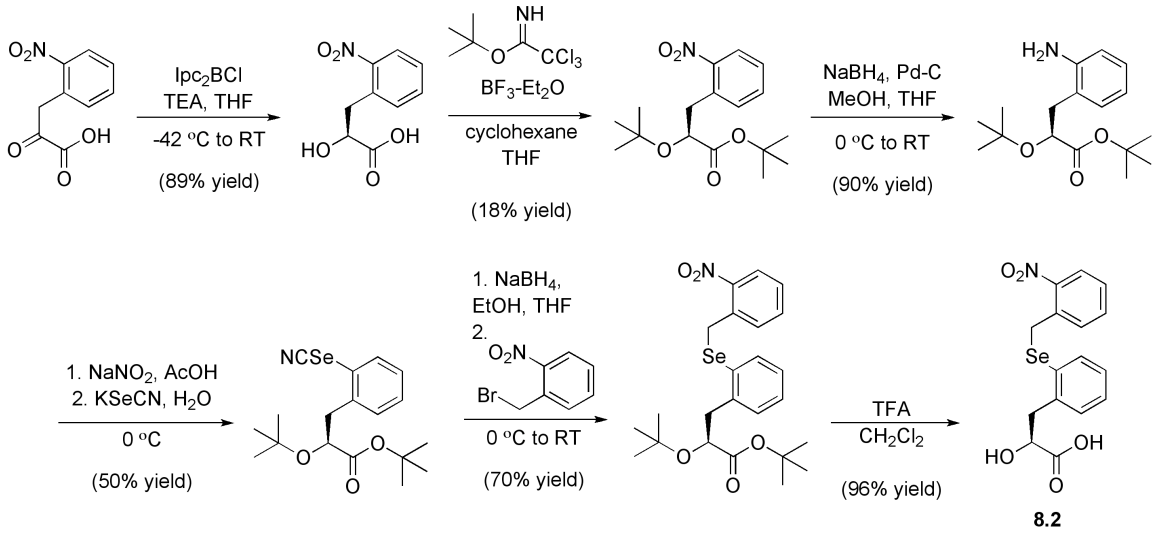

Scheme 8.8. Successful synthesis of arylalkyl selenide α-hydroxy acid **8.2**.

Using the reagents precedented in the depsipeptide syntheses described above, Blum incorporated **8.2** into a depsipeptide that was similar to depsipeptide **8.10** (scheme 8.9).

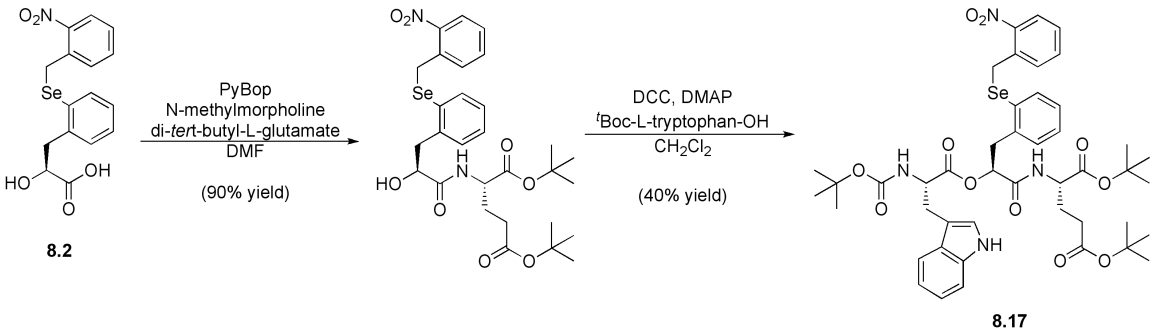

Scheme 8.9. Synthesis of depsipeptide **8.17**.

*Initial Photolysis Studies on Depsipeptide **8.17***

The conditions optimized for depsipeptides **8.9** and **8.10** were initially used in the photolysis of depsipeptide **8.17**. It was subsequently determined that a reduction to 10 equivalents of DTT was enough to minimize the oxidative side products in the photolysis of **8.17**. The requirement for severalfold less DTT confirmed one of the key design elements that was supposed to make **8.2** and improvement over **8.1**—that of increased stability to oxidative damage.

While running small-scale photolysis studies on depsipeptide **8.17**, Blum discovered that heating the reaction mixture after irradiation greatly improved the efficiency of the cleavage reaction. Heat was found to also improve the ability of **8.1** to cleave depsipeptides **8.9** and **8.11** (depsipeptides **8.10**, **8.12**, and **8.13** were not tested). Heating to 70 ºC for one hour maximized the abundance of the *m/z* ratio corresponding to the

selenacyclopentane in the ESI-MS. While heat, especially at this high of temperature, is not ideal for *in vivo* studies in *Xenopus laevis* oocytes, it allowed for the scaling up of the photolysis reaction to a preparatory scale, which was necessary to isolate and characterize the selenacyclopentane products.

Isolation and Characterization of the Selenacyclopentane Cleavage Products

Preparative-scale photolysis reactions were performed using a Hg-vapor UV immersion lamp with a pyrex filter (>300 nm). The reactions were again followed by ESI-MS. Depsipeptide **8.11** was irradiated in an equal volume mixture of acetonitrile and pH 7.6 20 mM phosphate buffer with 100 equivalents of DTT (scheme 8.10). After irradiation but before heating, the major *m/z* ratio seen in the ESI-MS was 709.1, the selenol ([M+Na] *m/z* = 709.3), but 444.0, 627.2, and 1391.2, the selenacyclopentane **8.18** ([M+Na] *m/z* = 444.1), dehydronorvaline ([M+Na] *m/z* = 627.3), and diselenide ([M+Na] *m/z* = 1393.5), were also seen. The subsequent heating of **8.11** went smoothly and the final ESI-MS showed *m/z* ratios of 444.0, 627.2, and 862.9, corresponding to the selenacyclopentane **8.18** ([M+Na] *m/z* = 444.1), dehydronorvaline ([M+Na] *m/z* = 627.3), and noncovalent dimer of the selenacyclopentane ([2M+Na] *m/z* = 865.3), respectively. The reaction was considered complete since the abundances of the *m/z* ratios for the selenol and diselenide, the two products that could be driven to S_N2 cleave the peptide backbone, were baseline. The three *m/z* ratios reported above were of similar high abundances in the ESI-MS after heating, although after irradiation and prior to heating the abundance of the *m/z* ratio for the dehydronorvaline had been low. ESI-MS is not

quantitative, but the shift in the abundance of the dehydronorvaline from low to high suggested that either the elimination reaction continued to occur during heating or the quantities of all of the final products were much reduced after heating. Either situation would predict a decrease in the absolute quantity of the desired selenacyclopentane product present. Purification of selenacyclopentane **8.18** was difficult due to the large amount of DTT present in the reaction. After two successive purifications using flash column chromatography, pure **8.18** was obtained in 29% yield.

Initially, irradiation of **8.17** was performed using the same immersion lamp and filter as was used for depsipeptide **8.11**. The reaction took place in a solution of equal volumes of acetonitrile and pH 8 water with 10 equivalents of DTT. A surprising side product that formed after photolysis was the depsipeptide in which the original nitrobenzylselenyl α-hydroxy acid had been replaced by its phenylalanine analog. While this work was in progress, however, Kitahara and co-workers reported that short wavelength photolysis of arylalkyl selenides can lead to carbon-selenium bond cleavage.[49] As suggested by that study, changing the photolysis wavelength from >280 nm to >330 nm (uranium filter) eliminated this side reaction. When reaction conditions were fully optimized for the photolysis reaction of depsipeptide **8.17**, a 72% yield was obtained of the aryl selenacyclopentane **8.19** without the need for the additional heating step (scheme 8.11). The greater stability to oxidative damage, higher yield of cleavage product, and ability to efficiently cleave without heat proved that the addition of the aryl group in **8.2** created an improved α-hydroxy acid capable of SNIPP.

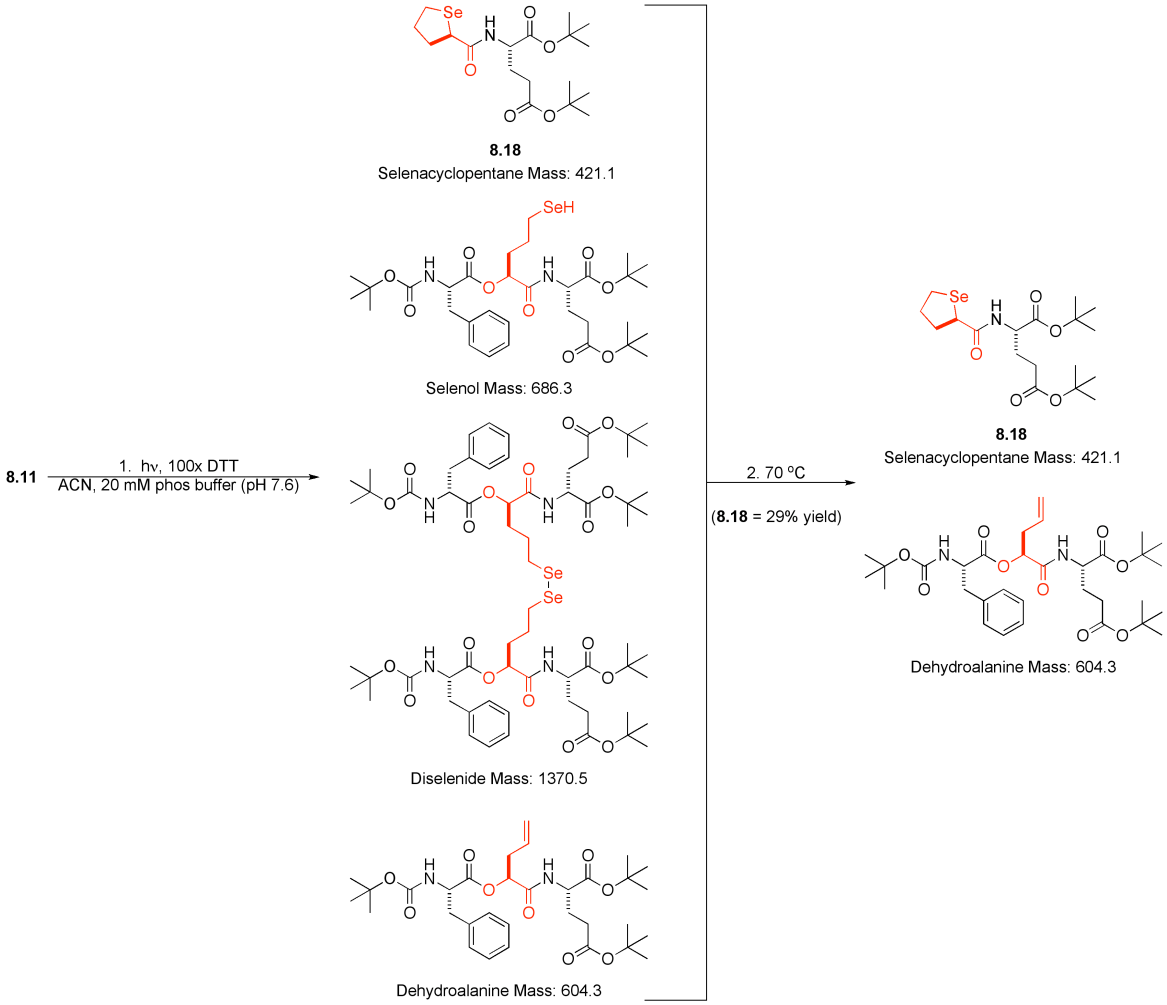

Scheme 8.10. The progress of the large-scale photolysis and heating reaction on depsipeptide **8.11** as followed by ESI-MS. Selenacyclopentane **8.18** was isolated in 29% yield. Only relevant products are shown.

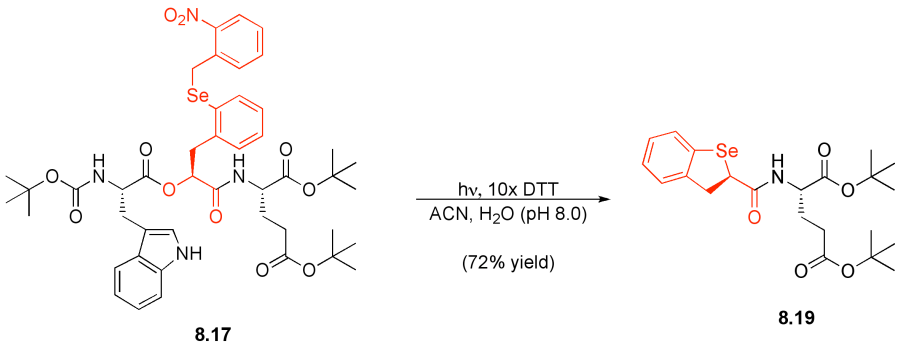

8.17 **8.19**

Scheme 8.11. The large-scale photolysis and heating reaction on depsipeptide **8.17**. Aryl selenacyclopentane **8.19** was isolated in 72% yield. Only the relevant product is shown.

*Preparing **8.1** and **8.2** for Nonsense-Suppression Studies*

Since isolation and characterization of the predicted cleavage fragment proved that the proposed mechanism of the photoinduced proteolysis was correct, **8.1** and **8.2** could now be studied in full proteins. To prepare **8.1** for both *in vitro* and *in vivo* nonsense-suppression experiments, it was activated as the cyanomethyl ester, coupled to dCA, and ligated to both THG73 tRNA (CUA anticodon) and YFaFS tRNA (ACCC anticodon) (scheme 8.12). The same was repeated for **8.2**. Typically, amino acids are also protected on their α-amino group due to the instability induced by the electron withdrawing effects of the amine. Neither **8.1** nor **8.2** needed to be protected on its α-hydroxy group because the hydroxyl does not have the same inductive effect as the amine.

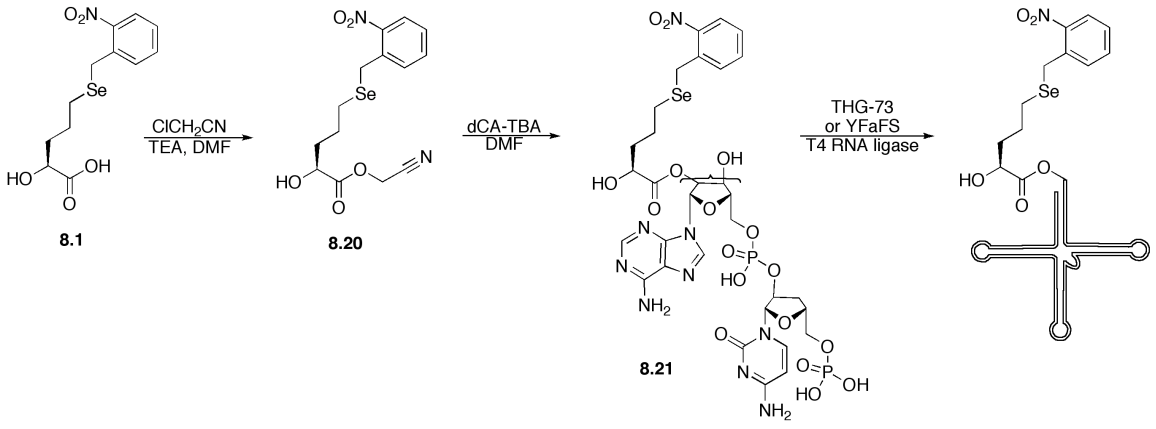

Scheme 8.12. The activation, coupling, and ligation reactions performed on **8.1** in preparation for *in vitro* and *in vivo* nonsense-suppression experiments. The same were repeated for **8.2**.

Attempts to Visualize Proteolysis Using Western Blotting Techniques

Western blotting was anticipated to produce a clear visual result if photolysis of either **8.1** or **8.2** led to proteolysis of a large protein. Proteins made using the *in vitro* nonsense-suppression methodology will separate by polyacrylamide gel electrophoresis (PAGE) based on their mass, and visualization through Western blotting techniques will identify if irradiated samples contain the smaller protein fragment predicted for SNIPP. Earlier studies performed by Zacharias using rabbit reticulocyte lysate to incorporate **8.1** at Leu250 in the α1 nAChR subunit showed that **8.1** was ribosomally competent and was susceptible to base hydrolysis of the backbone ester, but irradiation-induced proteolysis was never seen.[31] Rabbit reticulocyte lysate is the preferred system for *in vitro* nonsense suppression because it is readily available; because it is also a eukaryotic system like *Xenopus laevis*, the traditional system for *in vivo* nonsense suppression; and because it is much higher yielding than other *in vitro* transcription methods. The drawback for using

this lysate in these experiments is that this lysate contains a high level of heme, which makes it deep red in color and may stifle the photolysis reaction.

Zacharias tried to isolate the *in vitro* transcribed protein from the lysate and the negative effects of the heme prior to irradiation using a seven-histidine tag that had been incorporated into the C-terminal sequence of the protein. This short sequence enables the protein to bind to a column of Ni^{2+} agarose beads, isolating it from the rest of the lysate mixture.[50-52] Elution with 300 mM imidazole followed by irradiation resulted in a complete loss of protein, not only in the experiment but also in the positive controls. Potentially, the high levels of imidazole were aggregating the protein during photolysis.

Enantiopure **8.1** was incorporated into two sites in the nAChR α1 subunit, α1Leu253 and α1Ile247, using *in vitro* nonsense-suppression techniques and rabbit reticulocyte lysate. The histidine tag was again used to purify the transcribed protein, but unlike the previous experiments performed by Zacharias, the protein was eluted from the column of Ni^{2+} agarose beads using an eluant with a pH of 4.5,[53] removing the potential for imidazole-related protein loss upon photolysis. The eluate's pH was raised, and then it was split into equal portions, one of which was irradiated by the same 1000 W Hg/Xe arc lamp used in the small-scale depsipeptide reactions, and one of which was left untreated. Unfortunately, though photolyzed protein was now present in the Western blot, proteolysis was never seen and the quantitiy of photolyzed protein was much less than the untreated portion (figure 8.13). Neither dilution nor the addition of TCEP encouraged proteolysis. The same loss of protein was not seen when the same techniques were used to visualize caged phosphoproteins.[53] Due to these inconsistencies, another *in vitro*

transcription system was sought that would eliminate the need to purify the transcribed protein prior to photolysis.

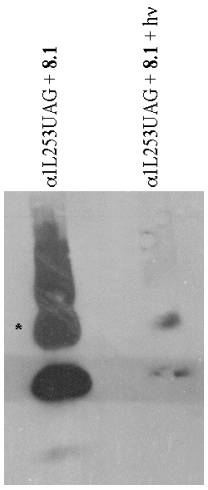

Figure 8.13. Western blot of rabbit reticulocyte lysate *in vitro* nonsense suppressed proteins. The asterisk marks the full-length protein. Control reactions are not shown. A reduction in the quantity of protein was seen upon exposure to UV light. Proteolysis was not seen.

Wheat germ lysate is another commonly used *in vitro* translation system, and its translucent white color made it a better choice for photolysis experiments than the rabbit reticulocyte lysate system. Several different commercially available wheat germ lysate translation systems were compared to determine which system was most proficient at nonsense suppression. The TNT T7 Coupled Wheat Germ Extract System (Promega, Madison, WI) and the Wheat Germ Extract Plus (Promega, Madison, WI) gave inefficient or no suppression, but the wheat germ extract from the Rabbit Reticulocyte Lysate/Wheat Germ Extract Combination System (Promega, Madison, WI) gave reliably consistent suppression. This system successfully incorporated **8.1** but not **8.2** into

proteins using *in vitro* nonsense suppression (figure 8.14). Potentially, **8.2** was too large to be compatible with the yeast ribosome. Protein containing **8.1** was found to be susceptible to base cleavage of the backbone ester, but irradiation-induced cleavage was never observed. Attempts to optimize photolysis by using different UV light sources (the 1000 W Hg/Xe arc lamp described above and a 288 W Hg lamp), by increasing the pH of the protein-solubilizing solutions, by the addition of TCEP, and by exposing the protein to 70 °C heat for one hour postphotolysis did not encourage proteolysis.

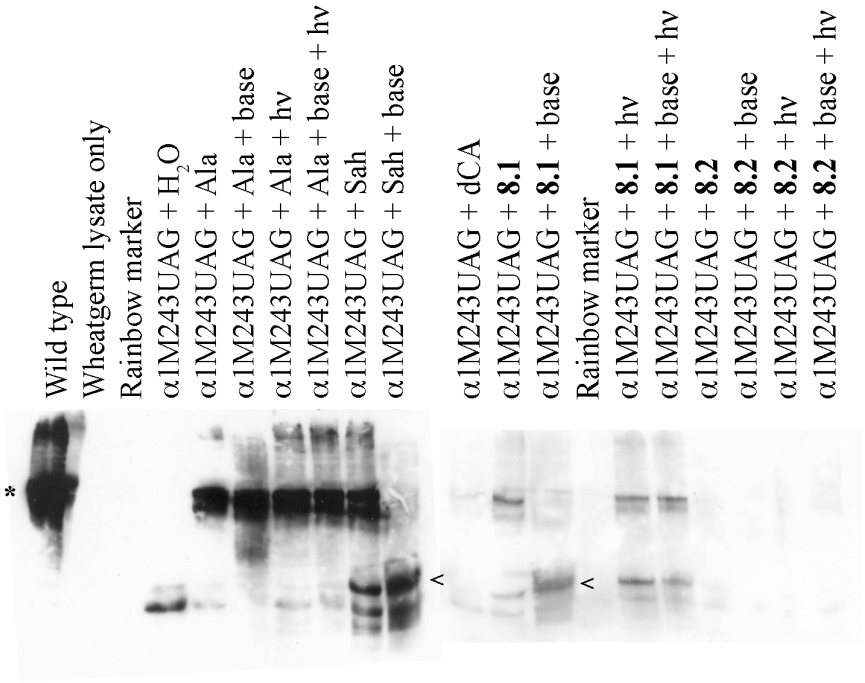

Figure 8.14. Western blot of various wheat germ lysate *in vitro* nonsense suppressed proteins. The asterisk marks the full-length protein. The arrowheads mark the hydrolysis products. Alanine was used as a positive control for efficient suppression and a negative control for the addition of base or UV light. Serine α-hydroxy acid (Sah) was used as a positive control for base hydrolysis of an ester backbone. Proteolysis is only seen upon the addition of base to proteins with an ester in the backbone, not upon irradiation of protein containing **8.1**. No suppression of **8.2** was seen.

A Positive In Vivo *Control for the Efficiency of the UV Light Sources*

Although no successful SNIPP was seen in the *in vitro* photolysis reactions, conditions for successful *in vivo* photolysis reactions were still sought. Several UV light sources were available for irradiating *Xenopus* oocytes in these *in vivo* experiments, including a 500 W Hg arc lamp connected to an electrophysiology rig by a liquid light guide and the 288 W Hg lamp mentioned above. To ensure that these sources of UV light could successfully initiate the *o*-nitrobenzyl deprotection event, the reproduction of the previously published *o*-nitrobenzyl-protected tyrosine (TyrONB) suppression and photoinduced deprotection in the nAChR was sought.[5] The TyrONB markedly differs in size from the natural tyrosine, and its suppression makes a mutant channel that is relatively insensitive to agonist. Upon the addition of 300-350 nm wavelength light, the tyrosine is decaged and a wild-type channel is revealed, increasing the channel's sensitivity to agonist.

Whole-cell recordings were done on an OpusXpress workstation at both 24 and 48 hours after injection of TyrONB-tRNA and the mRNA for the muscle nAChR containing an amber suppression codon at either α1Tyr93 or α1Tyr198. A solution of 250 μM ACh was used to test for channel expression and function. Little to no current was seen prior to photolysis (figure 8.15). After photolyzing the oocytes suppressed at either site for as short as 10 seconds on the 288 W Hg lamp described above, an increase in whole-cell current was seen. The same result was observed with 5 seconds of irradiation from the 500 W Hg lamp on the electrophysiology rig. Thus, the *o*-nitrobenzyl deprotection was efficient with brief exposure to UV light by both UV light sources.

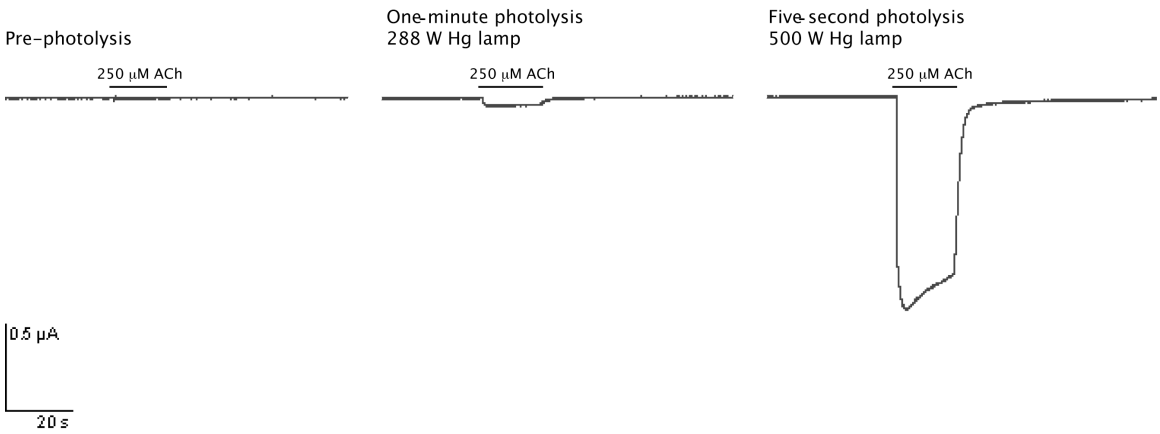

Figure 8.15. Whole-cell currents from the suppression of the nAChR at α1Tyr93 with TyrONB after photolysis. The first trace shows the lack of current prior to photolysis. The second trace shows the increase in current after 1 minute of photolysis on the 288 Hg arc lamp. The third trace shows the increase in current after 5 seconds of photolysis on the 500 W Hg lamp connected to the electrophysiology rig. 250 μM ACh was applied to the oocytes during the time noted by the black bar above the traces.

Attempts to Observe Photolysis-Induced Proteolysis In Vivo

8.1 had previously been incorporated by Zacharias into ShB at Leu47 in the "chain" region of the channel, a site at which England incorporated Npg (figure 8.2).[4,31] Zacharias found that **8.1** suppressed well and that one minute of photolysis resulted in a 33 ± 5% reduction in N-terminal inactivation. This result was extremely promising—one minute was a vast improvement over the 4 hours necessary to remove two of the four N-terminal inactivation domains of ShB with Npg (a 27% reduction in inactivation).[4]

Unfortunately, this same encouraging result was not seen when the photolysis experiments were repeated in these studies, although suppression of the UAG amber nonsense codon with both **8.1** and **8.2** at Leu47 and at Pro64 in ShB was successful. The

read through and reaminoacylation negative controls were always run in conjunction with each experiment to ensure that the current seen in the experiment was at least ten times greater than that seen for mRNA only (a test for read through) and of mRNA and unaminoacylated tRNA (THG73 ligated with dCA, a test for reaminoacylation). Reaminoacylation often led to substantial current with both Leu47UAG and Pro64UAG. Suppression of the GGGU four-base codon with both **8.1** and **8.2** at Pro64 was also successful. The four-base codon suppression method was anticipated to limit the amount of protein made from reaminoacylated tRNA since the YFaFS tRNA has been shown to be more orthogonal to the *Xenopus* oocyte translation system than THG73.[54] In each of the successful suppression experiments, irradiation of *Xenopus* oocytes containing ShB in which either **8.1** or **8.2** had been incorporated did not cause a reduction of N-terminal inactivation. Both of the UV light sources tested above with TyrONB were tried, as well as the 1000 W Hg/Xe arc lamp used in the small-scale depsipeptides studies. Oxidation was not expected to be a problem due to the naturally reducing environment of the cell, but no amount of optimization encouraged **8.1** or **8.2** to cleave the protein backbone at these sites in ShB.

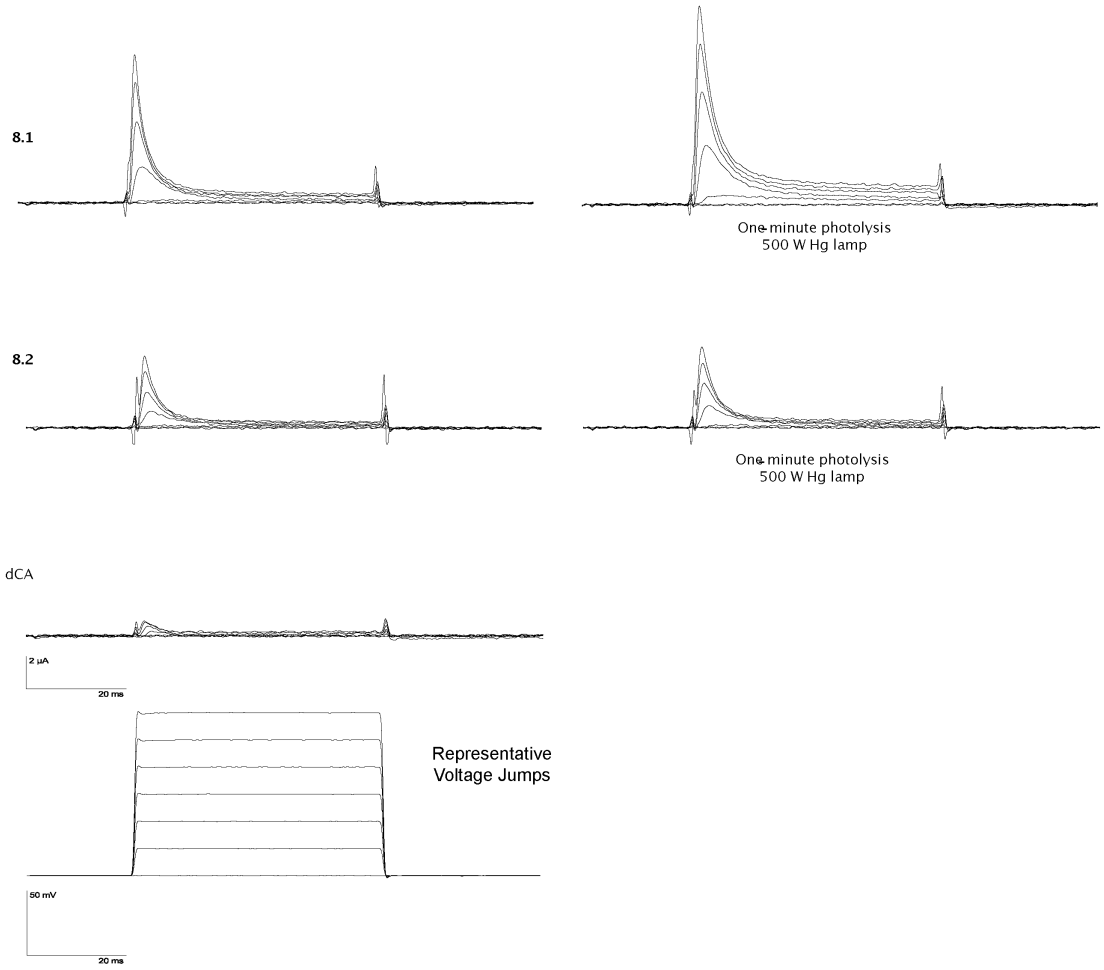

Figure 8.16. Whole-cell currents from the suppression of ShB Pro64GGGU with **8.1**, **8.2**, and dCA (negative control). No decrease in N-terminal inactivation was seen after one minute of photolysis on the 500 W Hg arc lamp connected to the electrophysiology rig for channels containing **8.1** or **8.2**. The membrane voltages of the representative voltage jumps are shown at the bottom of the figure.

Hydrophobic protein environments have been known to increase pKa values.[55] If this effect were occurring here, it would decrease the likelihood that the selenide was anionic. To encourage the formation of a selenide anion, the extracellular site used by England in

the Npg studies was targeted[4] since the pH of the extracellular environment could be controlled. Whole-cell recordings were made on the OpusXpress workstation by applying a high concentration of ACh (1000 μM = 20x wild-type EC_{50}) to each oocyte to test for channel expression. Suppression of α1Val132UAG by either **8.1** or **8.2** was difficult. Triple injections were necessary to get 200 nA of current, although the reaminoacylation negative control (injection of dCA-tRNA) produced 100 nA of current under the same conditions. Oocytes were then irradiated in pH 9.0 ND96 buffer with CHES replacing the HEPES,[56] and then channel expression and function were tested again. Since ACh is not stable at high pH, all whole-cell recordings were run in pH 7.5 ND96 buffer (with HEPES) to ensure any observed decreases in current would be from successful proteolysis. As described by England *et al.*, photolysis of channels with Npg at this site resulted in a dramatic decrease in current.[4] The suppression of neither **8.1** nor **8.2** caused a decrease in whole-cell current after irradiation. Though the negative control showed a substantial amount of current, suggesting that there could be a mixed population of channels—some expressing the desired α-hydroxy acid and some expressing a natural amino acid, proteolysis was still expected to show some decrease in current. None was seen. Thus, the high pH environment did not foster backbone cleavage upon irradiation.

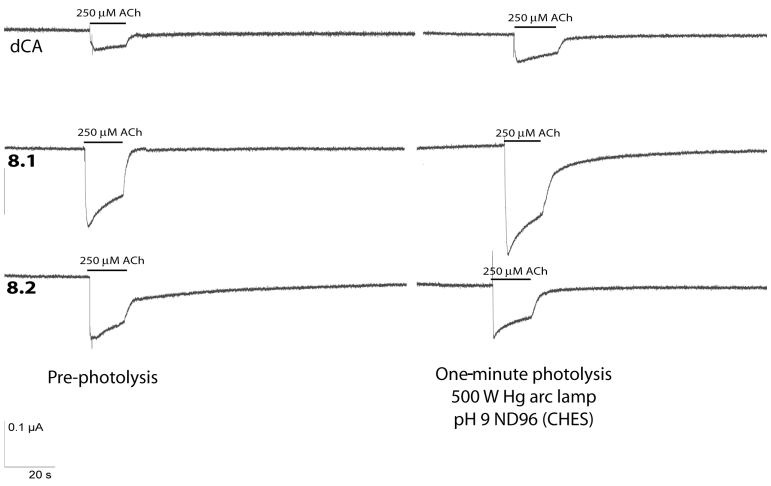

Figure 8.17. Whole-cell currents from the suppression of nAChR at α1Val132 with **8.1**, **8.2**, and dCA (negative control). No decrease in current was seen after one minute of photolysis on the 500 W Hg arc lamp connected to the electrophysiology rig for channels containing **8.1** or **8.2**, though there was a substantial amount of reaminoacylation current.

No further *in vivo* experiments were attempted. Thus, neither **8.1** nor **8.2** were successful at SNIPP in a full protein in these studies even though proteolysis was seen in the depsipeptide model system. Despite the speed of deprotection of **8.1** and **8.2**, Npg remains the superior SNIPP-capable compound due to its *in vivo* success, even with the extended photolysis times needed.

Conclusion

In this study a novel approach to photochemically-induced backbone cleavage of peptides and proteins was described. The two unnatural α-hydroxy acids presented here were

proven to cleave the protein backbone by the anticipated mechanism through the isolation of the cleavage fragment from model studies using depsipeptides. Unfortunately, though photochemical decaging of both selenides was complete in approximately 10 minutes in the model studies as monitored by ESI-MS, proteolysis of a full protein in either an *in vitro* system or an *in vivo* system was never seen.

The model studies provided important information about the selenide compounds. The initial model studies showed the sensitivity of the alkyl selenide **8.1** to oxidative elimination and diselenide formation. Since this sensitivity was minimized in a reducing environment, as seen from the addition of DTT or TCEP, it was not expected to play much of a roll *in vivo* due to the reducing environment of the cell. Selenomethionine would form dehydroalanine if oxidative elimination were rampant in the cell. However, minimizing the possibility of forming these unwanted byproducts was anticipated to strengthen the success of the cleavage reaction, something that was gained through the aryl selenide **8.2**. The initial depsipeptide studies also showed that the alkyl selenide α-hydroxy acid **8.1** was not efficient at cleaving the peptide backbone on its own and that the aryl selenide α-hydroxy acid **8.2** could only cleave the peptide backbone without an outside driving force under extremely optimized conditions. The surrounding pH was very important, and the addition of heat drastically improved the efficiency of the reactions. These two elements did not translate to encourage successful proteolysis in the *in vitro* or the *in vivo* experiments though. Further attempts could be made to incorporate **8.1** or **8.2** into a more exposed extracellular site than nAChR α1Val132.

Ideally, SNIPP would be instantaneous upon irradiation—there would be no lag time between the time of photolysis and the time of proteolysis, and proteolysis would occur

in all of the desired proteins. Unfortunately, neither **8.1** nor **8.2** met the requirements for the speed and efficiency of the ideal SNIPP. Npg still allows for *in vivo* SNIPP, even if irradiation times are prolonged. Other potential solutions include further enhancing the propensity for the ring-closing reaction of **8.2** by incorporating the trimethyl lock elements that made the *o*-nitrobenzyl caged phenol successful.[13] Though successful suppression by *in vitro* transcription reaction with wheat germ lysate of **8.2** was not observed by Western blot, this bulky α-hydroxy acid was successfully incorporated into channels in the *Xenopus* oocyte. Therefore, the rabbit reticulocyte lysate might be a better translation system to test the suppression of any trimethyl lock derivatives that may be developed in the future.

Methods

The work in this chapter was a collaborative effort that included important contributions from Zacharias and Blum. Detailed methods for the experiments discussed in this chapter that were not performed by the author can be found in Zacharias's thesis[31] and in Eastwood *et al.*[57]

Synthesis

All reactions were performed at ambient temperature unless otherwise noted. All reactions involving potentially air-sensitive compounds were conducted under an inert atmosphere using Schlenk techniques. Solvents were purified by passage through

alumina.[58] Unless otherwise noted, all chemicals and reagents were used as received without further purification. Flash chromatography was performed using EMD (Gibbstown, NJ) silica gel 60 (particle size 0.040-0.063 mm). TLC was performed using EMD (Gibbstown, NJ) silica gel 60 F_{254} precoated plates (0.25 mm) and visualized by UV light, potassium permanganate, or ceric ammonium molybdate. NMR spectroscopy was preformed on either a Varian (Palo Alto, CA) Mercury 300 or Inova 500 instrument, and NMR resonances are reported relative to Me_4Si (δ 0.0), CD_3OD (δ 3.31 for ^1H NMR and δ 49.1 for ^{13}C NMR), or D_2O (δ 4.79 for ^1H NMR). Data for ^1H NMR spectra are reported as follows: chemical shift (δ ppm), integration, multiplicity, and coupling constant (Hz). Data for ^{13}C NMR spectra are reported as chemical shift (δ ppm). High-resolution mass spectroscopy (HRMS) spectra were obtained from the Caltech Mass Spectrometry Lab. ESI-MS used to analyze the proteolysis reactions was preformed on an LCQ Classic ion trap (ThermoFinnigan, Waltham, MA) in direct infusion mode. HPLC was preformed using Waters (Milford, MA) equipment and software (510 HPLC pumps and 996 Photodiode Array Detector) and reverse-phase Nova-Pak ^{18}C columns (3.9 × 150 mm analytical column, 7.8 × 300 mm preparatory column).

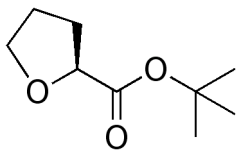

8.3

tert-Butyl ester **8.3**: (S)-(−)-Tetrahydro-2-furoic acid (2.42 mL, 25.0 mmol, 1 eq) was placed in a round-bottom flask under Ar (g) and dissolved in THF (250 mL). To this solution was added 4-(dimethylamino)-pyridine (0.919 g, 7.5 mmol, 0.3 eq) and di-*tert*-

butyl dicarbonate (11.5 mL, 50.0 mmol, 2 eq), at which time the solution turned yellow. The reaction was allowed to stir for 4 hours, and then the solvent was removed under vacuum. The crude product was purified by flash column chromatography (9% EtOAc in hexanes) to afford *tert*-butyl ester **8.3** (4.15 g, 24.1 mmol, 96% yield). R_f = 0.33 (9% EtOAc in hexanes); ^{1}H NMR (300 MHz, $CDCl_3$, 298 K) δ 4.4 (1H, m), 4.0 (2H, m), 2.2 (1H, m), 2.0 (3H, m), 1.5 (9H, s).

Conversion back to (S)-(−)-tetrahydro-2-furoic acid: *tert*-Butyl ester **8.3** (0.045 g, 0.26 mmol, 1 eq) was placed in a round-bottom flask under Ar (g) and dissolved in CH_2Cl_2 (5 mL). This solution was cooled to 0 °C and charged with the dropwise addition of triethylamine (0.010 mL, 0.075 mmol, 0.29 eq). Dimethylboron bromide (2.0 M in CH_2Cl_2, 0.50 mL, 1.0 mmol, 3.8 eq) was added via cannula to the solution. The reaction was allowed to stir at 0 °C for 2 hours. To quench, the reaction mixture was poured over saturated $NaHCO_3$ (aq) and stirred for 20 minutes. An extraction with ether was attempted, but the product remained in the aqueous layer. The pH of the aqueous layer was lowered to 3 with concentrated HCl and then extracted with EtOAc (2×), dried over Na_2SO_4 (s), and concentrated to afford the original acid (0.022 g, 0.19 mmol, 73% yield). ^{1}H NMR (300 MHz, $CDCl_3$, 298 K) δ 4.4 (1H, q), 3.9 (2H, dq), 2.2 (1H, m), 2.0 (3H, m).

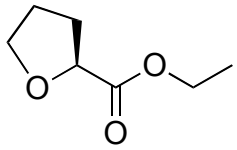

8.4

Ethyl ester **8.4**: (S)-(−)-Tetrahydro-2-furoic acid (25.0 g, 215 mmol) was placed in a round-bottom flask under Ar (g) and dissolved in ethanol (63 mL) and toluene (72 mL). To this solution was added concentrated H_2SO_4 (1.2 mL), and the reaction was allowed to reflux for 6 hours at 80 °C. The reaction was then cooled to room temperature, quenched with concentrated H_2SO_4 (2 mL), diluted with toluene, and washed with saturated $(NH_4)_2SO_4$ (aq), and then H_2O. The aqueous layers were back extracted with toluene (2×). The combined organic layers were washed with saturated $(NH_4)_2SO_4$ (aq) and then saturated $NaHCO_3$ (aq), dried over Na_2SO_4 (s), and concentrated. The crude product was purified by flash chromatography (33% EtOAc in hexanes) to yield ethyl ester **8.3** as a yellow oil (18.3 g, 127 mmol, 61% yield). R_f = 0.35 (33% EtOAc in hexanes). ^{1}H NMR (300 MHz, $CDCl_3$, 298 K) δ 4.43 (1H, dd, *J* = 8.1, 5.1 Hz), 4.19 (2H, qd, *J* = 7.2, 0.9 Hz), 4.01 (1H, m), 3.91 (1H, m), 2.23 (1H, m), 1.95 (3H, m), 1.27 (3H, t, *J* = 7.2 Hz); ^{13}C NMR (75 MHz, $CDCl_3$, 298 K) δ 173.3, 76.7, 69.2, 60.7, 30.1, 25.2, 14.2; HRMS-EI (*m/z*): [M^+] calc'd for $C_7H_{13}O_3$ 145.0865, found 145.0877.

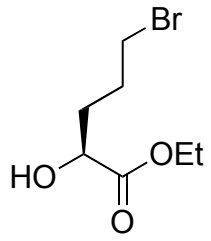

8.5

Bromoalcohol **8.5**: Ethyl ester **8.4** (18.3 g, 127 mmol, 1 eq) was placed in a round-bottom flask under Ar (g) and dissolved in CH_2Cl_2 (450 mL). This solution was cooled to 0 °C and charged with the dropwise addition of triethylamine (2.54 mL, 19.1 mmol, 0.15 eq). Dimethylboron bromide (1.56 M in CH_2Cl_2, 163 mL, 254 mmol, 2 eq) was added via cannula to the solution. The reaction was allowed to stir at 0 °C for 2 hours. To quench, the reaction mixture was poured over saturated $NaHCO_3$ (aq) and stirred for 5 minutes. It was then extracted with ether, washed with brine (2×), dried over Na_2SO_4 (s), and concentrated. The crude product was purified by flash column chromatography (20% EtOAc in hexanes) to afford bromoalcohol **8.5** as an orange oil (20.4 g, 90.6 mmol, 71% yield). R_f = 0.31 (33% EtOAc in hexanes); ^{1}H NMR (300 MHz, $CDCl_3$, 298 K) δ 4.26 (2H, dq, *J* = 7.2, 0.9 Hz), 4.20 (1H, m), 3.45 (2H, m), 2.81 (1H, d, *J* = 5.4 Hz), 2.00 (3H, m), 1.79 (1H, m), 1.31 (3H, t, *J* = 7.2 Hz); ^{13}C NMR (75 MHz, $CDCl_3$, 298 K) δ 174.9, 69.7, 62.0, 33.3, 32.8, 28.2, 14.2; HRMS (EI) *m/z* calc'd for $C_7H_{14}BrO_3$ [M^+]: 225.0126, found 225.0137.

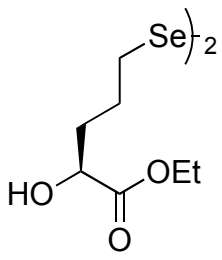

8.6

Diselenide ester **8.6**: Elemental selenium (3.58 g, 45.3 mmol, 0.5 eq) and sodium borohydride (3.43 g, 90.6 mmol, 1 eq) were placed in a round-bottom flask and dissolved in H_2O (265 mL). After stirring for 20 minutes, more elemental selenium (3.58 g, 45.3 mmol, 0.5 eq) was added. The mixture was then stirred over a steam bath for 15 minutes, at which time it turned dark brown suggesting the formation of Na_2Se_2. Bromoalcohol **8.5** (20.4 g, 90.6 mmol, 1 eq) was dissolved in a 1:1 mixture of THF:H_2O (106 mL) and added to the reaction. After stirring overnight, the reaction was quenched with 1 N AcOH (106 mL) and H_2O (264 mL), extracted with CH_2Cl_2 (4×), dried over $MgSO_4$ (s), filtered through a pad of celite, and concentrated. The crude product was purified by flash column chromatography (50% EtOAc in hexanes, dry loaded in CH_2Cl_2) to afford diselenide ester **8.6** as a yellow oil (19.7 g, 43.9 mmol, 97% yield). R_f = 0.17 (33% EtOAc in hexanes); ^{1}H NMR (300 MHz, $CDCl_3$, 298 K) δ 4.26 (4H, q, J = 7.2 Hz), 4.20 (2H, m), 2.91 (4H, m), 1.84 (8H, m), 1.31 (6H, t, J = 7.2 Hz); ^{13}C NMR (75 MHz, $CDCl_3$, 298 K) δ 175.1, 70.0, 61.8, 34.0, 29.3, 26.3, 14.2; HRMS (FAB) *m/z* calc'd for $C_{14}H_{26}O_6Se_2$ [M^+]: 450.0059, found 450.0080.

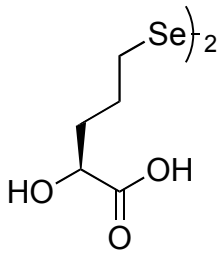

8.7

Diselenide acid **8.7**: Diselenide ester **8.6** (18.6 g, 41.5 mmol) was placed in a round-bottom flask and dissolved in 6 M HCl (240 mL). The reaction was allowed to stir at 75 °C for 12 hours. The solvent was concentrated yielding diselenide acid **8.7** as a yellow solid (15.6 g, 39.8 mmol, 96% yield). R_f = 0.06 (1% formic acid in EtOAc); ^{1}H NMR (300 MHz, $CDCl_3$, 298 K) δ 4.04 (2H, dd, *J* = 7.1, 3.6 Hz), 2.96 (4H, t, *J* = 6.9 Hz), 1.85 (8H, m); ^{13}C NMR (75 MHz, CD_3OD, 298 K) δ 177.9, 71.1, 35.2, 30.4, 27.9; HRMS (TOF) *m/z* calc'd for $C_{10}H_{18}O_6Se_2$ [M−H]: 392.9356, found 392.9360.

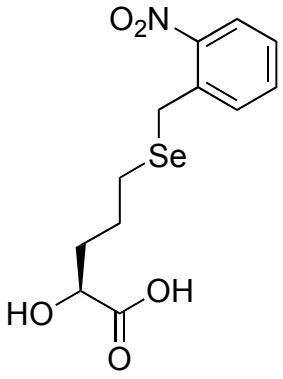

8.1

Alkyl selenide α-hydroxy acid **8.1**: Diselenide acid **8.7** (12.5 g, 31.7 mmol, 1 eq) was placed in a round-bottom flask and dissolved in 0.5 N NaOH (169 mL) and ethanol (42.5 mL) at 0 °C. Slowly $NaBH_4$ (12.0 g, 317 mmol, 10 eq) was added. The dark orange

solution turned white as it was allowed to come to room temperature. The temperature of the reaction was lowered back to 0 °C and then 2 N NaOH (84.3 mL) and *o*-nitrobenzylbromide (27.4 g, 127 mmol, 4 eq) were added. The reaction was allowed to stir for 3 hours as it warmed to room temperature. The mixture was washed with EtOAc (3×), and then the pH of the aqueous layer was lowered to 4. The product was removed from the now cloudy aqueous layer by extraction with EtOAc (3×). The organic solution was filtered through a pad of celite and concentrated to afford alkyl selenide α-hydroxy acid **8.1** as an orange oil (17.9 g, 53.9 mmol, 85%). R_f = 0.11 (1% formic acid and 49.5% EtOAc in hexanes); ^{1}H NMR (500 MHz, $CDCl_3$, 298 K) δ 7.99 (1H, d, *J* = 8.0 Hz), 7.53 (1H, td, *J* = 7.5, 1.5 Hz), 7.38 (2H, t, *J* = 8.0 Hz), 4.25 (1H, m), 4.10 (2H, s), 2.59 (2H, m), 1.92 (1H, m), 1.78 (3H, m); ^{13}C NMR (125 MHz, $CDCl_3$, 298 K) δ 178.6, 148.1, 135.9, 133.2, 131.9, 127.9, 125.6, 76.5, 69.7, 34.1, 25.5, 24.2, 23.8; HRMS (TOF) *m/z* calc'd for $C_{12}H_{15}NO_5Se$ [M−H]: 332.0037, found 332.0050.

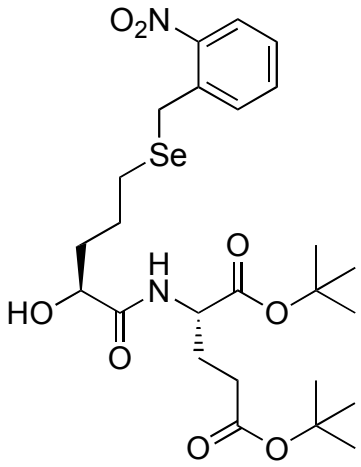

8.8

Alkyl selenide-glutamate dipeptide **8.8**: Method A: Alkyl selenide α-hydroxy acid **8.1** (0.787 g, 2.40 mmol, 1 eq), L-glutamic acid di-*tert*-butyl ester (0.775 g, 0.262 mmol, 1.1

eq), 1,3-dicyclohexylcarbodiimide (0.480 g, 2.33 mmol, 0.97 eq), and 1-hydroxybenzotriazole (0.324 g, 2.40 mmol, 1 eq) were placed in a round-bottom flask under Ar (g) and dissolved in CH_2Cl_2 (20 mL). After stirring for 24 hours, the reaction was diluted with EtOAc. The solution was then washed with 1N HCl, H_2O, saturated $NaHCO_3$ (aq), H_2O, and brine, filtered through a pad of celite, dried over $MgSO_4$ (s), and concentrated. The crude product was purified by flash column chromatography (33% EtOAc in hexanes, dry loaded in CH_2Cl_2) to afford the dipeptide **8.8** as a pale yellow oil (0.373 g, 0.650 mmol, 33% yield).

Method B: Alkyl selenide α-hydroxy acid **8.1** (0.076 g, 0.23 mmol, 1 eq), L-glutamic acid di-*tert*-butyl ester (0.076 g, 0.26 mmol, 1.1 eq), 1,3-dicyclohexylcarbodiimide (0.083 g, 0.40 mmol, 2 eq), and 4-(dimethylamino)pyridine (0.013 g, 0.10 mmol, 0.5 eq) were placed in a round-bottom flask under Ar (g) and dissolved in CH_2Cl_2 (2 mL). After stirring for 24 hours, the reaction was diluted with EtOAc and gravity filtered to remove the solid dicyclohexylurea byproduct. The eluate was washed with saturated $NaHCO_3$ (aq) and brine, filtered through a pad of celite, dried over Na_2SO_4 (s), and concentrated. The crude product was purified by flash column chromatography (33% EtOAc in hexanes, dry loaded in CH_2Cl_2) to afford the dipeptide **8.8** as a pale yellow oil (0.045 g, 0.070 mmol, 34% yield).

Method C: Alkyl selenide α-hydroxy acid **8.1** (0.998 g, 3.00 mmol, 1.1 eq), L-glutamic acid di-*tert*-butyl ester (0.808 g, 2.73 mmol, 1 eq), and benzotriazol-1-yl-oxytripyrrolidinophosphonium hexaflurophosphate (1.56 g, 3.00 mmol, 1.1 eq) were placed in a round-bottom flask under Ar (g) and dissolved in DMF (10 mL). To this was added N-methylmorpholine (0.99 mL, 9.01 mmol, 3.3 eq), and the reaction stirred for 12

hours. The reaction was then diluted with EtOAc, and the solution was washed with 5% $KHSO_4$ (2×), 5% $NaHCO_3$ (2×), and brine, filtered through a pad of celite, dried over Na_2SO_4 (s), and concentrated. The crude product was purified by flash column chromatography (50% EtOAc in hexanes, dry loaded in CH_2Cl_2) to afford the dipeptide **12** as a pale yellow oil (0.698 g, 1.22 mmol, 41% yield). R_f = 0.25 (50% EtOAc in hexanes); ^{1}H NMR (500 MHz, $CDCl_3$, 298 K) δ 7.98 (1H, d, *J* = 7.5 Hz), 7.53 (1H, td, *J* = 7.3, 1.0 Hz), 7.38 (2H, t, *J* = 7.5 Hz), 7.22 (1H, d, *J* = 8.0 Hz), 4.47 (1H, dt, *J* = 8.5, 5.5 Hz), 4.13 (1H, m), 4.09 (1H, s), 2.56 (2H, t, *J* = 6.5 Hz), 2.30 (2H, m), 2.15 (1H, m), 1.92 (1.5H, m), 1.79 (1H, m), 1.71 (0.5H, m), 1.47 (9H, s), 1.44 (9H, s); ^{13}C NMR (125 MHz, $CDCl_3$, 298K) δ 174.0, 172.1, 171.1, 161.0, 148.1, 136.0, 133.1, 131.9, 127.8, 125.6, 82.5, 80.9, 71.3, 52.0, 34.8, 31.5, 28.1, 28.0, 27.5, 25.7, 24.2, 23.7; HRMS (FAB) *m/z* calc'd for $C_{25}H_{38}N_2O_8Se$ [M+H]: 575.1871, found 575.1862.

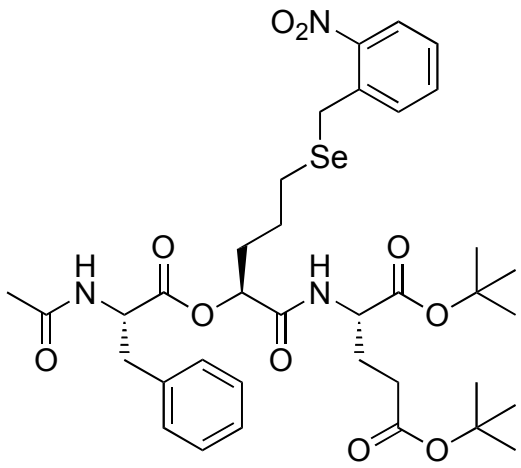

8.9

N-Acetyl-phenylalanine-alkyl selenide-glutamate depsipeptide **8.9**: Dipeptide **8.8** (0.373 g, 0.650 mmol, 1 eq), *N*-acetyl-L-phenylalanine (0.135 g, 0.650 mmol, 1 eq), 4-(dimethylamino)pyridine (0.0794 g, 0.650 mmol, 1 eq), and N,N'-

dicyclohexylcarbodiimide (0.136 g, 0.660 mmol, 1 eq) were placed in a round-bottom flask under Ar (g) and dissolved in CH_2Cl_2 (120 mL). After stirring for 24 hours, the reaction mixture was diluted with EtOAc and gravity filtered to remove the solid dicyclohexylurea by-product. The solution was washed with 1 M $KHSO_4$ (2×), water, and 5% $NaHCO_3$. The organic layer was filtered through a pad of celite, dried over $MgSO_4$ (s), and concentrated. The crude product was purified by flash column chromatography (33% EtOAc in hexanes, dry loaded in CH_2Cl_2) to afford depsipeptide **8.9** as a pale yellow oil (0.330 g, 0.433 mmol, 67% yield). R_f = 0.26 (50% EtOAc in hexanes); ^{1}H NMR (300 MHz, $CDCl_3$, 298 K) δ 8.03 (1H, dd, *J* = 7.95, 1.2 Hz), 7.57 (1H, td, *J* = 7.35, 1.2 Hz), 7.30 (7H, m), 5.13 (1H, t, *J* = 6.3 Hz), 4.77 (1H, q, *J* = 7.2 Hz), 4.38 (1H, m), 4.10 (2H, s), 3.16 (2H, t, *J* = 6.9 Hz), 2.47 (2H, t, *J* = 7.2 Hz), 2.36-1.8 (8H, m), 2.02 (3H, s), 1.48 (9H, s), 1.48 (9H, s); ESI-MS *m/z* calc'd for $C_{36}H_{49}N_3O_{10}Se$ [M+Cl]: 798.8, found 798.2.

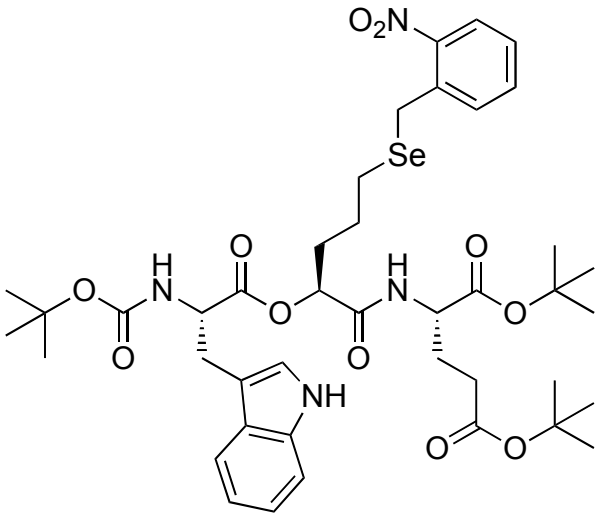

8.10

Tryptophan-alkyl selenide-glutamate depsipeptide **8.10**: Dipeptide **8.8** (5.51 g, 9.60 mmol, 1 eq), *N*-(*tert*-butoxycarbonyl)-L-tryptophan (3.32 g, 10.9 mmol, 1.1 eq), 4-(dimethylamino)pyridine (0.586 g, 4.80 mmol, 0.5 eq), and N,N'-dicyclohexylcarbodiimide (3.98 g, 19.3 mmol, 2 eq) were placed in a round-bottom flask under Ar (g) and dissolved in CH_2Cl_2 (84 mL). After stirring for 48 hours, the reaction mixture was diluted with EtOAc and gravity filtered to remove the solid dicyclohexylurea by-product. The solution was washed with 1 M $KHSO_4$ (2×), water, and 5% $NaHCO_3$ (2×). The organic layer was filtered through a pad of celite, dried over $MgSO_4$ (s), and concentrated. The crude product was purified by flash column chromatography (20% EtOAc in hexanes, dry loaded in CH_2Cl_2) to afford depsipeptide **8.10** as a pale yellow oil (0.989 g, 1.15 mmol, 12% yield). ^{1}H NMR (300 MHz, $CDCl_3$, 298 K) δ 8.1 (1H, d), 7.6 - 6.9 (8H, m), 6.6 (1H, s), 5.1 (1H, m), 4.4 (1H, m), 4.1 (1H, m), 4.0 (2H, s), 3.3 (1H, m), 2.6-1.6 (10H, m), 1.4 (9H, s), 1.4 (9H, s), 1.4 (9H, s); ESI-MS *m/z* calc'd for $C_{41}H_{56}N_4O_{11}Se$ [M+K]: 899.4, found 898.9.

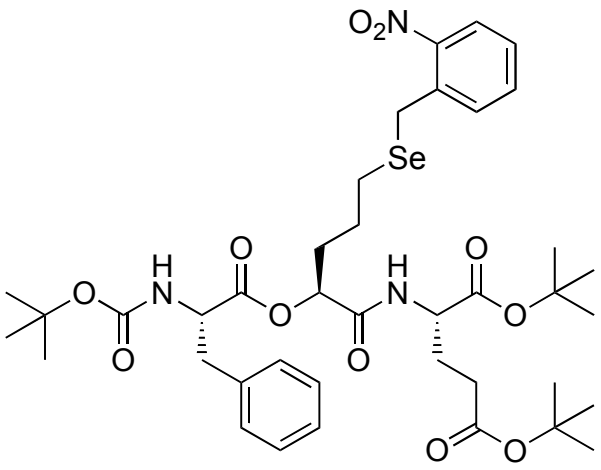

8.11

^{t}Boc-Phenylalanine-alkyl selenide-glutamate depsipeptide **8.11**: Dipeptide **8.8** (0.160 g, 0.280 mmol, 1 eq), *N*-(*tert*-butoxycarbonyl)-L-phenylalanine (0.0891 g, 0.340 mmol, 1.2 eq), 4-(dimethylamino)pyridine (0.0171 g, 0.140 mmol, 0.5 eq), and N,N'-dicyclohexylcarbodiimide (0.1156g, 0.560 mmol, 2 eq) were placed in a round-bottom flask under Ar (g) and dissolved in CH_2Cl_2 (3 mL). After stirring for 45 hours, the reaction mixture was diluted with EtOAc and gravity filtered to removed the solid dicyclohexylurea byproduct. The solution was washed with 1 M $KHSO_4$ (2×), H_2O, and 5% $NaHCO_3$ (2×). The organic layer was filtered through a pad of celite, dried over $MgSO_4$ (s), and concentrated. The crude product was purified by flash column chromatography (50% EtOAc in hexanes, dry loaded in CH_2Cl_2) to afford depsipeptide **8.11** as a pale yellow oil (0.144 g, 0.176 mmol, 63% yield). R_f = 0.53 (50% EtOAc in hexanes); ^{1}H NMR (500 MHz, $CDCl_3$, 298 K) δ 7.99 (1H, dd, *J* = 8.25, 1.0 Hz), 7.53 (1H, td, *J* = 7.5, 1.5 Hz), 7.37 (2H, m), 7.28 (3H, m), 7.19 (3H, m), 5.16 (1H, m), 4.99 (1H, d, *J* = 7.5 Hz), 4.59 (1H, q, *J* = 5.0 Hz), 4.41 (1H, dt, *J* = 8.0, 5.0 Hz), 4.07 (1H, s), 3.24 (1H, dd, *J* = 14.3, 5.0 Hz), 3.12 (1H, m), 2.49 (2H, dt, *J* = 7.5, 2.5 Hz), 2.31 (2H, m),

2.14 (1H, m), 1.92 (3H, m), 1.65 (2H, m), 1.45 (9H, s), 1.44 (9H, s), 1.40 (9H, s); ^{13}C NMR (125 MHz, $CDCl_3$, 298 K) δ 172.1, 170.8, 170.3, 169.3, 155.8, 148.1, 135.9, 135.8, 133.1, 131.9, 129.2, 128.8, 127.8, 127.2, 125.6, 81.1, 80.7, 80.3, 74.2, 54.5, 52.3, 37.2, 32.0, 31.6, 28.3, 28.1, 28.0, 27.1, 25.5, 23.7; HRMS (FAB) *m/z* calc'd for $C_{39}H_{55}N_3O_{11}Se$ [M+H]: 822.3080, found 822.3046.

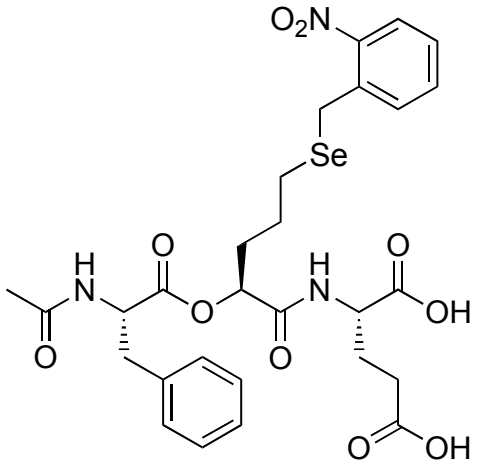

8.12

Deprotected *N*-Acetyl-phenylalanine-alkyl selenide-glutamate depsipeptide **8.12**: Depsipeptide **8.9** (0.076 g, 0.10 mmol) was placed in a round-bottom flask and was dissolved in trifluoroacetic acid (2 mL) and CH_2Cl_2 (2 mL). The reaction was allowed to stir for 45 minutes and then it was concentrated under vacuum. The crude product was purified by reverse-phase semipreparative HPLC using a linear solvent gradient from 5% acetonitrile in 25 mM NH_4OAc buffer pH 4.5 to 100% acetonitrile to afford depsipeptide **8.12**. ^{1}H NMR (300 MHz, D_2O, 298 K) δ 7.92 (1H, d, *J* = 8.1 Hz), 7.51 (1H, t, *J* = 6.6 Hz), 7.34 (2H, t, *J* = 6.6 Hz), 7.19 (5H, m), 4.88 (1H, q, *J* = 6.0 Hz), 4.6 (1H, m), 3.99 (3H, m), 2.9 (2H, m), 2.47 (2H, m), 2.05 (2H, m), 2.0-1.0 (6H, m); ESI-MS *m/z* calc'd for $C_{28}H_{33}N_3O_{10}Se$ [M−H]: 650.1, found 650.0.

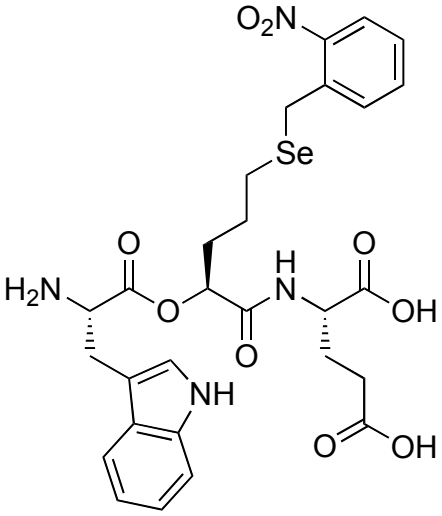

8.13

Deprotected tryptophan-alkyl selenide-glutamate depsipeptide **8.13**: Depsipeptide **8.10** (0.086 g, 0.10 mmol) was placed in a round-bottom flask and was dissolved in trifluoroacetic acid (2 mL) and CH_2Cl_2 (2 mL). The reaction was allowed to stir for 45 minutes and then it was concentrated under vacuum. The crude product was purified by reverse-phase semipreparative HPLC using a linear solvent gradient from 5% acetonitrile in 25 mM NH_4OAc buffer pH 4.5 to 100% acetonitrile to afford depsipeptide **8.13**. ESI-MS *m/z* calc'd for $C_{28}H_{32}N_4O_9Se$ [M−H]: 647.1, found 647.1.

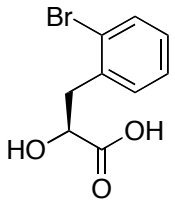

8.14

Bromophenylalanine α-hydroxy acid **8.14**: *o*-Bromophenylalanine (1.0 g, 4.0 mmol, 1 eq) was placed in a round bottom flask and dissolved in 8:2 H_2O:acetic acid (40 mL). This solution was cooled to 0 ºC and charged with the dropwise addition of sodium

nitrate (2 M in H_2O, 8.0 mL, 16 mmol, 4 eq). The reaction was stirred for 3 hours and then quenched with methylamine (2M in THF, 4 mL). The THF was removed under vacuum, and the pH of the resulting aqueous solution was lowered to 2 with concentrated HCl. This solution was extracted with EtOAc (3×), dried over $MgSO_4$ (s), and concentrated to afford bromophenylalanine α-hydroxy acid **8.14** (0.980 g, 4.0 mmol, 100% yield). R_f = 0.47 (50% EtOAc in hexanes); ^{1}H NMR (300 MHz, $CDCl_3$, 298 K) δ 7.6 (1H, d), 7.3 (2H, m), 7.2 (1H, m), 4.6 (1H, m), 3.5 (1H, m), 3.1 (1H, m); ^{13}C NMR (75 MHz, $CDCl_3$, 298 K) δ 178, 136, 133, 132, 129, 128, 125 70, 40; ESI-MS *m/z* calc'd for $C_9H_9BrO_3$ [M−H]: 243.0, found 242.9.

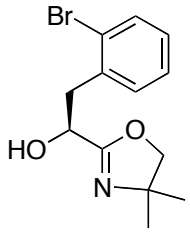

8.15

Oxazoline **8.15**: Bromophenylalanine α-hydroxy acid **8.14** (1.10 g, 4.00 mmol, 1 eq) was placed in a round-bottom flask under Ar (g) and dissolved in 2-amino-2-methyl-1-propanol (0.380 mL, 4.00 mmol, 1 eq) and xylene (5 mL). The reaction was connected to a Dean-Stark trap and allowed to reflux for 4 hours at 160 ºC. The crude product was vacuum distilled on a kugelrohr (Büchi GKR-50, set to 200 ºC) to yield oxazoline **8.15** as a yellow oil (0.149 g, 0.500 mmol, 100% yield). R_f = 0.65 (11% EtOAc in hexanes); ^{1}H NMR (300 MHz, $CDCl_3$, 298 K) δ 7.6 (1H, dd), 7.4 (1H, dd), 7.3 (1H, td), 7.2 (1H, td), 4.6 (1H, m), 4.0 (2H, m), 3.3 (1H, m), 3.1 (1H, m), 1.2 (3H, s), 1.2 (3H, s); ESI-MS *m/z* calc'd for $C_{13}H_{16}BrNO_2$ [M+H]: 298.0, found 297.8.

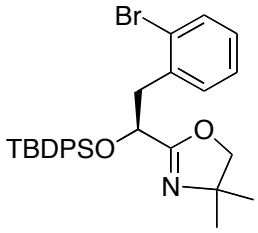

8.16

TBDPS ether **8.16**: Oxazoline **8.15** (2.54 g, 8.50 mmol, 1 eq), imidazole (1.27 g, 18.7 mmol, 2.2 eq), and *tert*-butylchlorodiphenylsilane (2.43 mL, 9.35 mmol, 1.1 eq) were placed in a round-bottom flask under Ar (g) and dissolved in DMF (5 mL). The reaction was allowed to stir for 24 hours, and then the solvent was removed under vacuum. The crude product was purified by flash column chromatography (9% EtOAc in hexanes, then flushed with CH_2Cl_2) to yield TBDPS ether **8.16** as a yellow oil (3.28 g, 6.10 mmol, 72% yield). R_f = 0.83 (50% EtOAc in hexanes); ^{1}H NMR (300 MHz, $CDCl_3$, 298 K) δ 7.8-7.1 (14H, m), 4.3 (1H, m), 4.0-3.0 (4H, m), 1.1 (6H, s) 1.1 (9H, s); ESI-MS *m/z* calc'd for $C_{29}H_{34}BrNO_2Si$ [M+H]: 536.2, found 535.9.

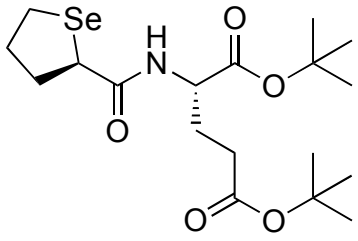

8.18

Selenacyclopentane **8.18**: Depsipeptide **8.11** (0.0722g, 0.088 mmol, 1 eq) was placed in a pyrex photochemical reaction vessel and dissolved in acetonitrile (125 mL). To this was added dithiothreitol (1.36 g, 8.8 mmol, 100 eq) and 20 mM phosphate buffer, pH 7.6 (125 mL). The resulting solution was stirred under N_2 (g), and a 450 W medium-pressure

Hg-vapor UV immersion lamp (ACE Glass), filtered with a pyrex glass absorption sleeve and equipped with a water cooling jacket, was assembled to the reaction vessel. The progress of the reaction was followed by ESI-MS. After 1 hour of photolysis, at which point the temperature of the reaction had increased from 25 to 32 ºC, the two major ratios seen in the mass spectrum of the reaction were the depsipeptide **8.11** ([M+Na] *m/z* = 844) and the nitrobenzyl-deprotected selenol ([M+Na] *m/z* = 709). After 5 hours of photolysis, the *m/z* ratio attributed to **8.11** ([M+Na] *m/z* = 844) had diminished to a negligible level while the *m/z* ratios corresponding to the nitrobenzyl-deprotected selenol ([M+Na] *m/z* = 709), the nitrobenzyl-deprotected diselenide ([M+Na] *m/z* = 1391), the olefin-containing depsipeptide derived from the oxidative elimination of the selenium ([M+Na] *m/z* = 627), and the desired selenacyclopentane **8.18** ([M+Na] *m/z* = 444) persisted. At this time, the reaction was removed from the photoreactor, heated to 70 ºC, and monitored by ESI-MS. After 3 hours of heating at this temperature, both nitrobenzyl-deprotection products (*m/z* ratios 709 and 1391) were no longer detectable, but the *m/z* ratio attributed to the desired selenacyclopentane **8.18** ([M+Na] *m/z* = 444) and a *m/z* ratio corresponding to its dimer ([M+Na] *m/z* = 865) remained. The resulting mixture was extracted with EtOAc (2×), dried over $MgSO_4$ (s), and concentrated. The crude product was purified twice by flash column chromatography (11% EtOAc in hexanes, then 33% EtOAc in hexanes after the DTT eluted, dry loaded in CH_2Cl_2) to afford selenacyclopentane **8.18** as a yellow oil (0.0107 g, 0.0255 mmol, 29% yield). R_f = 0.28 (33% EtOAC in hexanes); ^{1}H NMR (500 MHz, $CDCl_3$, 298 K) δ 7.08 (1H, d, *J* = 13.5 Hz), 4.44 (1H, dt, *J* = 13.5, 8 Hz), 4.08 (1H, m), 3.15 (1H, m), 2.97 (1H, m), 2.37 (1.5H, m), 2.26 (1.5H, m), 2.14 (4H, m), 1.92 (1H, m), 1.47 (9H, s), 1.44 (9H, s); ^{13}C NMR (125 MHz, $CDCl_3$, 298 K) 172.3, 172.1, 170.8,

82.3, 80.7, 52.845.4, 37.4, 32.4, 31.5, 28.1, 28.0, 27.5, 27.1. HRMS (TOF) *m/z* calc'd for $C_{18}H_{31}NO_5Se$ [M+H]: 422.1446, found 422.1465.

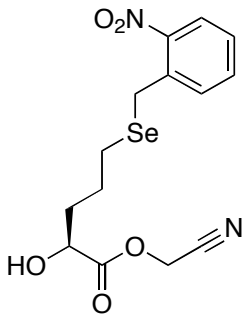

8.20

Cyanomethyl ester **8.20**: Alkyl selenide α-hydroxy acid **8.1** (0.23 g, 0.69 mmol) was added to a round-bottom flask under Ar (g) and dissolved in chloroacetonitrile (2 mL). To this solution was added triethylamine (0.25 mL). The mixture was stirred at room temperature for 75 minutes and then the solvent was removed under vacuum. The residue was purified by flash column chromatography (CH_2Cl_2, then 5% EtOAc in CH_2Cl_2) to afford cyanomethyl ester **8.20** (0.073 g, 0.20 mmol, 29% yield). R_f = 0.45 (17% EtOAC in CH_2Cl_2); ^{1}H NMR (300 MHz, $CDCl_3$, 298 K) δ 7.98 (1H, d, *J* = 8.4 Hz), 7.50 (1H, t, *J* = 7.5 Hz), 7.38 (2H, t, *J* = 7.5 Hz), 4.82 (2H, s), 4.28 (1H, m), 4.09 (2H, s), 2.58 (2H, m), 2.00-1.50 (4H, m); ^{13}C NMR (75 MHz, $CDCl_3$, 298 K) δ 171.1, 133.1, 131.9, 127.9, 125.5, 69.9, 49.0, 33.9, 29.7, 25.3, 23.8.

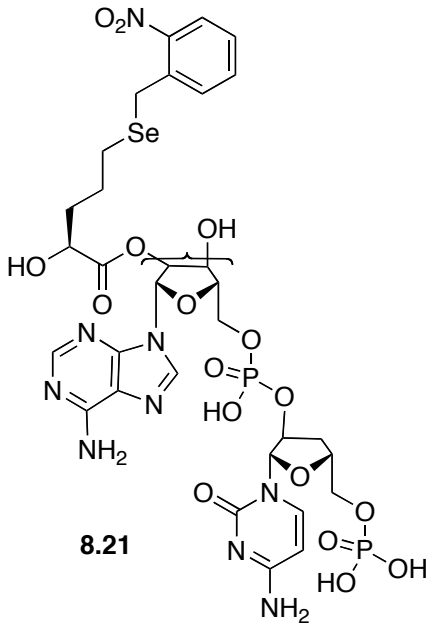

8.21

Alkyl selenide-dCA **8.21**: Cyanomethyl ester **8.20** (0.018 g, 0.048 mmol, 3 eq) was added to a round-bottom flask under Ar (g) and dissolved in DMF (0.5 mL). This solution was transferred to another round-bottom flask under Ar (g), which contained dCA (0.020 g, 0.017 mmol, 1 eq) as a tetrabutylammonium salt (2.4 eq). The reaction was stirred at room temperature for 18 hours while being monitored by reverse-phase analytical HPLC with a linear solvent gradient from 5% acetonitrile in 25 mM NH_4OAc buffer pH 4.5 to 100% acetonitrile. The crude product was purified using reverse-phase semipreparative HPLC with the same linear solvent gradient. The fractions containing the alkyl selenide-dCA **8.21** were combined, and the solvent was removed by lyophilization. The solid was redissolved in 10 mM acetic acid and reconcentrated via lyophilization (3×) to afford alkyl selenide-dCA **8.21** as a white powder (0.014 g, 0.015 mmol, 88% yield). ESI-MS *m/z* calc'd for $C_{12}H_{39}N_9O_{17}P_2Se$ [M−H]: 950.1, found: 950.2.

Small-Scale Depsipeptide Model Reactions

General method: 0.1 μM solution of depsipeptide in a 1:1 mixture of acetonitrile and 20 mM phosphate buffer pH 7.6 (50 μL) was placed in PCR tube and was irradiated for ten minutes with a 1000 W Hg/Xe arc lamp (Oriel, Irvine, CT) operating at 400 W equipped with WG-335 and UG-11 filters (Schott, Elmsford, NY). After photolysis, the reaction was heated to 70 °C for one hour using an iCycler PCR machine (Bio-Rad, Hercules, CA) and then the products were analyzed by ESI-MS.

Many reaction variables were changed during the course of the work presented in this chapter. These factors include the container used to hold the solution of depsipeptide during irradiation, the solvent used during photolysis, the concentration of the depsipeptide in solution, the volume of solution irradiated, the filters used for the arc lamp during photolysis, the addition of a reducing agent (including the point at which the reducing agent was applied to the reaction), the length of time of irradiation, the application of heat after irradiation (including the specific temperature, the length of time of application, and the method of heating), and the addition of high pH water after irradiation. The variables that were found to be important are discussed in the results and discussion section.

Oxidation: 0.1 μM solution of depsipeptide in acetonitrile (50 μL) was placed in a 1.5 mL eppendorf tube, to which was added a solution of 30% H_2O_2 in H_2O (100 μL). After an hour the products of the reaction were analyzed by ESI-MS. As a negative control, double-distilled H_2O (100 μL) replaced the H_2O_2.

Addition of *N*-methyl maleimide: 0.1 μM solution of depsipeptide **8.9** or **8.10** in acetonitrile (50 μL, 1 eq) and DTT (50 eq) were placed in a 1.5 mL eppendorf tube and photolyzed as described above for 10 minutes. ESI-MS was used to analyze the products of the irradiated solution. Excess *N*-methyl maleimide was added to the reaction, and after several minutes the resulting solution was analyzed by ESI-MS. The same procedure was repeated for depsipeptide **8.12** except it was dissolved in double-distilled H_2O instead of acetonitrile.

Nonsense Suppression In Vitro

The site-directed mutagenesis of TAG mutants, gene construction, synthesis of suppressor tRNA, and ligation of aminoacyl-tRNA to tRNA have been described previously.[59-62] Plasmid DNAs were linearized with Not1, and mRNA was transcribed using the Ambion (Austin, TX) T7 mMESSAGE mMACHINE kit.

Method A: Translation was carried out using rabbit reticulocyte lysate translation system (Promega, Madison, WI) according to the manufacturer's protocol. Lysate mix (140 μL), amino acid mix (6 μL), RNAse inhibitor (4 μL), H_2O (18 μL), mRNA (16 μL, 1 μg/μL for suppression experiments and 0.3 μg/μL for wild-type experiments) or H_2O (16 μL, for lysate-only negative control), and either tRNA (16 μL, 1 μg/μL) or H_2O (16 μL, for mRNA-only negative control) were combined and incubated at 30 °C for 106 minutes. Portions of each *in vitro* translation reaction were purified on Ni^{2+}-columns according to the protocol described in Rothman *et al*.[53] The eluted purified protein (30 μL) was

diluted with buffer B (70 μL) from Rothman *et al.*[53] to raise the pH and lower the concentration of the protein in solution. This sample was irradiated on the 1000 W Hg/Xe arc lamp described above for 10 minutes. Samples for sodium dodecyl sulfate (SDS)-PAGE were prepared by mixing the unpurified *in vitro* translation mix (5 μL) with 2× SDS loading buffer (100 mM tris chloride at pH 6.8, 4% SDS, 0.2% bromophenol blue, 20% glycerol) (5 μL), the eluates from the column purification (10 μL) with 2× SDS loading buffer (10 μL), and the photolysis reactions (10 μL) with 2× SDS loading buffer (10 μL). The samples were then kept at −80 °C until further use.

Method B: Translation was carried out using wheat germ lysate translation system (Promega, Madison, WI) according to the manufacturer's protocol. Lysate mix (6.25 μL), amino acid mix (1 μL), RNAse inhibitor (0.25 μL), 1M KOAc (1 μL), water (2.5 μL), mRNA (0.5 μL, 1 μg/μL for suppression experiments and 0.3 μg/μL for wild-type experiments) or H_2O (0.5 μL, for lysate-only negative control), and either tRNA (2 μL, 1 μg/μL) or H_2O (2 μL, for mRNA-only negative control) were combined and incubated at 30 °C for 4 hours. Portions of the *in vitro* translation reactions were subjected to base to test for ester hydrolysis following the protocol described in England *et al.*[63] Portions of the *in vitro* reactions were irradiated to test for SNIPP. For the photolysis, the *in vitro* translation reaction (2.5 μL) was irradiated for 10 minutes on the 1000 W Hg/Xe arc lamp described above or for 30 minutes at 4 °C on the 288 W Hg lamp (BLAK-RAY Longwave Ultraviolet Lamp, Ultraviolet Products, San Gabriel, CA) equipped with a 360 nm band-pass filter at a distance of 15-30 cm. Other photolysis reactions had pH 10.4 H_2O (5 μL) added prior to irradiation. In certain cases, the reactions were heated to up to 90 °C after irradiation. Samples for SDS-PAGE of the hydrolysis reactions were

prepared according to protocol.[63] Samples for SDS-PAGE of the photolysis reactions were prepared by mixing the volume of the reaction (2.5 μL for photolysis reaction with base, 7.5 μL for the photolysis reaction with base) with an equivalent volume of 2× SDS loading buffer. The samples were then kept at −80 °C until further use.

Western blot analysis: Samples were loaded into prepoured 12% tris chloride gels (Bio-Rad, Hercules, CA) for SDS-PAGE. Western blotting was preformed using nitrocellulose transfer, a mouse anti-hemagglutinin (HA) primary antibody, and a goat anti-mouse secondary antibody conjugated to horseradish-peroxidase. Protein was detected by chemiluminescence.

Nonsense Suppression In Vivo

Oocytes from *Xenopus laevis* were isolated and maintained at 18 °C in ND96 solution (96 mM sodium chloride, 2 mM potassium chloride, 1.8 mM calcium chloride, 1 mM magnesium chloride, 5 mM HEPES, 2.5 mM sodium pyruvate, 0.5 mM theophyline, 10 μg/mL gentamycin at pH 7.5) according to published procedures.[64] Each oocyte was microinjected with 50 nL of a 1:1 mixture of mRNA (0.04 ng/nL for ShB and 0.5 ng/nL of a 20:1:1:1 α:β:γ:δ for nAChR) and tRNA (1 μg/μL) or unaminoacylated dCA-tRNA (1 μg/μL). 4PO-protected aminoacylated tRNA was deprotected prior to injection by incubating the sample for 15 minutes in saturated I_2 (aq). This saturated I_2 solution was made by adding an excess of I_2 to H_2O, then sonicating the mixture for 5 minutes, and then heating the mixture to 60 °C for 5 minutes.

Electrophysiology

Electrophysiological recordings were carried out 24 to 72 hours after injection. Whole-cell currents from oocytes were measured using a Geneclamp 500 amplifier (ShB) or an OpusXpress (nAChR) and pCLAMP software (Axon Instruments, Foster City, CA) in the two-electrode voltage-clamp configuration. Microelectrodes were filled with 3 M potassium chloride and had resistances ranging from 0.5 to 1.5 MΩ. Oocytes were continuously perfused with a nominally calcium-free bath solution consisting of 96 mM sodium chloride, 2 mM potassium chloride, 1 mM magnesium chloride, and 5 mM HEPES at pH 7.5. In the ShB experiments, the currents from ShB expressing oocytes were measured during depolarizing jumps from the holding potential to +70 mV in 25 mV increments. In the nAChR experiments, microscopic ACh-induced currents were recorded in response to bath application of ACh at a holding potential of −80 mV.

Acknowledgements

We thank Rick Gerhart for the gift of the uranium glass filter, Mona Shahgholi for her assistance with the mass spectrometers, Michael Krout for sharing his knowledge about the immersion lamp, and Nyssa Puskar for thoughtful discussions. This work was supported by the NIH (NS 34407) and an NIH training grant for A.E. (NRSA 5-T32-GM07616).

References

(1) Haass, C. *EMBO J.* **2004**, *23*, 483-8.

(2) Reed, K. E., and C. M. Rice *Curr. Top. Microbiol. Immunol.* **1999**, *242*, 55-84.

(3) Alnemri, E. S.; Livingston, D. J.; Nicholson, D. W.; Salvesen, G.; Thornberry, N. A.; Wong, W. W.; Yuan, J. *Cell* **1996**, *87*, 171.

(4) England, P. M.; Lester, H. A.; Davidson, N.; Dougherty, D. A. *Proc. Natl. Acad. Sci. USA* **1997**, *94*, 11025-30.

(5) Miller, J. C.; Silverman, S. K.; England, P. M.; Dougherty, D. A.; Lester, H. A. *Neuron* **1998**, *20*, 619-24.

(6) Tong, Y.; Brandt, G. S.; Li, M.; Shapovalov, G.; Slimko, E.; Karschin, A.; Dougherty, D. A.; Lester, H. A. *J. Gen. Physiol.* **2001**, *117*, 103-18.

(7) Petersson, E. J.; Brandt, G. S.; Zacharias, N. M.; Dougherty, D. A.; Lester, H. A. *Methods Enzymol.* **2003**, *360*, 258-73.

(8) Philipson, K. D.; Gallivan, J. P.; Brandt, G. S.; Dougherty, D. A.; Lester, H. A. *Am. J. Physiol. Cell. Physiol.* **2001**, *281*, C195-206.

(9) Endo, M.; Nakayama, K.; Kaida, Y.; Majima, T. *Angew. Chem. Int. Ed. Engl.* **2004**, *43*, 5643-5.

(10) Bosques, C. J.; Imperiali, B. *J. Am. Chem. Soc.* **2003**, *125*, 7530-1.

(11) Parker, L. L.; Kurutz, J. W.; Kent, S. B.; Kron, S. J. *Angew. Chem. Int. Ed. Engl.* **2006**, *45*, 6322-5.

(12) Pellois, J. P.; Muir, T. W. *Angew. Chem. Int. Ed. Engl.* **2005**, *44*, 5713-7.

(13) Shigenaga, A.; Tsuji, D.; Nishioka, N.; Tsuda, S.; Itoh, K.; Otaka, A. *Chembiochem* **2007**, *8*, 1929-31.

(14) Koide, T.; Itoh, H.; Otaka, A.; Yasui, H.; Kuroda, M.; Esaki, N.; Soda, K.; Fujii, N. *Chem. Pharm. Bull. (Tokyo)* **1993**, *41*, 502-6.

(15) Leinfelder, W.; Zehelein, E.; Mandrand-Berthelot, M. A.; Bock, A. *Nature* **1988**, *331*, 723-5.

(16) Ellman, J. A.; Mendel, D.; Schultz, P. G. *Science* **1992**, *255*, 197-200.

(17) Koh, J. T.; Cornish, V. W.; Schultz, P. G. *Biochemistry* **1997**, *36*, 11314-22.

(18) Bain, J.; Wacker, D. A.; Kuo, E. E.; Chamberlain, R. *Tetrahedron* **1991**, *47*, 2389-2400.

(19) Fahnestock, S.; Rich, A. *Science* **1971**, *173*, 340-3.

(20) England, P. M.; Zhang, Y.; Dougherty, D. A.; Lester, H. A. *Cell* **1999**, *96*, 89-98.

(21) Blankenship, J. W.; Balambika, R.; Dawson, P. E. *Biochemistry* **2002**, *41*, 15676-84.

(22) Beligere, G. S.; Dawson, P. E. *Biopolymers* **1999**, *51*, 363-9.

(23) Liotta, D.; Sunay, U.; Santiesteban, H.; Markiewicz, W. *J. Org. Chem.* **1981**, *46*, 2605-2610.

(24) Pearson, R. G.; Sobel, H.; Songstad, J. *J. Am. Chem. Soc.* **1968**, *90*, 319-26.

(25) Best, W. M.; Harrowfield, J. M.; Shand, T. M.; Stick, R. V. *Australian J. Chem.* **1994**, *47*, 2023-2031.

(26) Koch, T.; Buchardt, O. *Synthesis-Stuttgart* **1993**, 1065-1067.

(27) Shah, V. J.; Kuntz, I. D.; Kenyon, G. L. *Bioorganic Chemistry* **1996**, *24*, 194-200.

(28) Klayman, D. L.; Griffin, T. S. *J. Am. Chem. Soc.* **1973**, *95*, 197-200.

(29) Andreadou, I.; Menge, W. M.; Commandeur, J. N.; Worthington, E. A.; Vermeulen, N. P. *J. Med. Chem.* **1996**, *39*, 2040-6.

(30) Rooseboom, M.; Vermeulen, N. P.; Andreadou, I.; Commandeur, J. N. *J Pharmacol. Exp. Ther.* **2000**, *294*, 762-9.

(31) Zacharias, N. M., California Institute of Technology, 2004.

(32) Guindon, Y.; Therien, M.; Girard, Y.; Yoakim, C. *J. Org. Chem.* **1987**, *52*, 1680-6.

(33) Fujima, Y.; Hirayama, Y.; Ikunaka, M.; Nishimoto, Y. *Tet.: Asymm.* **2003**, *14*, 1385-91.

(34) Stocking, E. M.; Schwarz, J. W.; Senn, H.; Salzmann, M.; Silks, L. A. *J. Chem. Soc. Perkin Trans. 1* **1997**, 2443-2447.

(35) Widmer, U. *Synthesis* **1983**, 135-136.

(36) Meroueh, S. O.; Minasov, G.; Lee, W.; Shoichet, B. K.; Mobashery, S. *J. Am. Chem. Soc.* **2003**, *125*, 9612-8.

(37) Patino, N.; Frerot, E.; Galeotti, N.; Poncet, J.; Coste, J.; Dufour, M.; Jouin, P. *Tetrahedron* **1992**, *48*, 4115-4122.

(38) Conrad, P. G., 2nd; Givens, R. S.; Weber, J. F.; Kandler, K. *Org. Lett.* **2000**, *2*, 1545-7.

(39) Sharpless, K. B.; Lauer, R. F. *J. Am. Chem. Soc.* **1973**, *95*, 2697-2699.

(40) Kell, G.; Steinhart, H. *J. Food Sci.* **1990**, *55*, 1120-1132.

(41) Besse, D.; Siedler, F.; Diercks, T.; Kessler, H.; Moroder, L. *Angew. Chem. Int. Ed. Engl.* **1997**, *36*, 883-885.

(42) Liotta, D.; Markiewicz, W.; Santiesteban, H. *Tet. Lett.* **1977**, *18*, 4365-7.

(43) Liotta, D.; Santiesteban, H. *Tet. Lett.* **1977**, *18*, 4369-72.

(44) Deechongkit, S.; You, S. L.; Kelly, J. W. *Org. Lett.* **2004**, *6*, 497-500.

(45) Wehrmeister, H. L. *J. Org. Chem.* **1961**, *26*, 3821-3824.

(46) Hanessian, S.; Lavallee, P. *Canadian J. Chem.* **1975**, *53*, 2975-2977.

(47) Greene, T. W.; Wuts, P. G. M. *Protective Groups in Organic Synthesis*; New York: John Wiley & Sons, Inc., 1999.

(48) Wang, Z.; Brittany, L. A.; Fortunak, J. M. *Tet. Lett.* **1998**, *39*, 5501-5504.

(49) Ouchi, A.; Liu, S.; Li, Z.; Kumar, S. A.; Suzuki, T.; Hyugano, T.; Kitahara, H. *J. Org. Chem.* **2007**, *72*, 8700-6.

(50) Shapovalov, G.; Bass, R.; Rees, D. C.; Lester, H. A. *Biophys. J.* **2003**, *84*, 2357-65.

(51) Nicke, A.; Baumert, H. G.; Rettinger, J.; Eichele, A.; Lambrecht, G.; Mutschler, E.; Schmalzing, G. *EMBO J.* **1998**, *17*, 3016-28.

(52) Janknecht, R.; de Martynoff, G.; Lou, J.; Hipskind, R. A.; Nordheim, A.; Stunnenberg, H. G. *Proc. Natl. Acad. Sci. USA* **1991**, *88*, 8972-6.

(53) Rothman, D. M.; Petersson, E. J.; Vazquez, M. E.; Brandt, G. S.; Dougherty, D. A.; Imperiali, B. *J. Am. Chem. Soc.* **2005**, *127*, 846-7.

(54) Rodriguez, E. A.; Lester, H. A.; Dougherty, D. A. *Proc. Natl. Acad. Sci. USA* **2006**, *103*, 8650-5.

(55) Urry, D. W.; Peng, S.; Parker, T. *J. Am. Chem. Soc.* **1993**, *115*, 7509-7510.

(56) Petersson, E. J.; Choi, A.; Dahan, D. S.; Lester, H. A.; Dougherty, D. A. *J. Am. Chem. Soc.* **2002**, *124*, 12662-3.

(57) Eastwood, A. L.; Blum, A. P.; Zacharias, N. M.; Dougherty, D. A., unpublished manuscript.

(58) Pangborn, A. B.; Giardello, M. A.; Grubbs, R. H.; Rosen, R. K.; Timmers, F. J. *Organometallics* **1996**, *15*, 1518-1520.

(59) England, P. M.; Lester, H. A.; Davidson, N.; Dougherty, D. A. *Proc. Natl. Acad. Sci. USA* **1997**, *94*, 11025-11030.

(60) Nowak, M. W.; Kearney, P. C.; Sampson, J. R.; Saks, M. E.; Labarca, C. G.; Silverman, S. K.; Zhong, W.; Thorson, J.; Abelson, J. N.; Davidson, N.; Schultz, P. G.; Dougherty, D. A.; Lester, H. A. *Science* **1995**, *268*, 439-442.

(61) Nowak, M. W.; Gallivan, J. P.; Silverman, S. K.; Labarca, C. G.; Dougherty, D. A.; Lester, H. A. *Methods Enzymol.* **1998**, *293*, 504-529.

(62) Kearney, P. C.; Nowak, M. W.; Zhong, W.; Silverman, S. K.; Lester, H. A.; Dougherty, D. A. *Mol. Pharm.* **1996**, *50*, 1401-1412.

(63) England, P. M.; Lester, H. A.; Dougherty, D. A. *Biochemistry* **1999**, *38*, 14409-15.

(64) Quick, M.; Lester, H. A. In *Ion Channels of Excitable Cells*; Narahashi, T., Ed.; Academic Press: San Diego, CA, 1994, p 261-279.